

Experimental and Numerical Study of Cemented Clays

by

Mohammad Ibrahim Khalil Ullah

A Thesis Submitted in Partial Fulfillment of the Requirements for the Degree of  
MASTER OF SCIENCE IN CIVIL ENGINEERING (Geotechnical)



DEPARTMENT OF CIVIL ENGINEERING



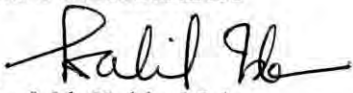
BANGLADESH UNIVERSITY OF ENGINEERING AND TECHNOLOGY, DHAKA

2007



The thesis titled "Experimental and Numerical Study of Cemented Clays" submitted by Mohammad Ibrahim Khalil Ullah, Roll No. 040304210F, session April, 2003 has been accepted as satisfactory in partial fulfillment of the requirement for the degree of Master of Science in Civil Engineering (Geotechnical) on 04-04-2007.

**Board of Examiners**



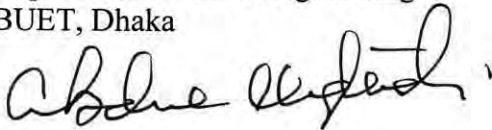
Dr. Md. Kabirul Islam  
Associate Professor,  
Department of Civil Engineering  
BUET, Dhaka

Chairman  
(Supervisor)



Dr. Md. Mazharul Hoque  
Professor and Head,  
Department of Civil Engineering  
BUET, Dhaka

Member



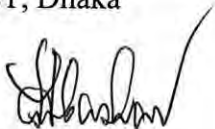
Dr. Abdul Muqtadir  
Professor, Department of Civil Engineering  
BUET, Dhaka

Member



Dr. Abu Siddique  
Professor, Department of Civil Engineering  
BUET, Dhaka

Member



Dr. Md. Abul Bashar  
Professor, Department of Civil Engineering  
KUET, Khulna

Member  
(External)

## CANDIDATE'S DECLARATION

It is hereby declared that this thesis or any part of it has not been submitted elsewhere for the award of any degree or diploma.

MD. IBRAHIM KHALIL ULLAH

Mohammad Ibrahim Khalil Ullah

## TABLE OF CONTENT

<b>CHAPTER 1 INTRODUCTION</b>	<b>1</b>
1.1 Introduction	1
1.2 Aims and Objectives of Proposed Study	2
1.3 Limitations of the Proposed Study	3
1.4 Outline of the Thesis	4
<b>CHAPTER 2 LITERATURE REVIEW</b>	<b>6</b>
2.1 Introduction	6
2.2 Mechanical Properties of Clay	6
2.2.1 Index Properties	7
2.2.2 Drained Behaviour	8
2.2.3 Undrained Behaviour	9
2.2.4 Consolidation Behaviour	10
2.3 Cementation	10
2.3.1 Effect on Index Properties	11
2.3.2 Effect on Drained Response	11
2.3.3 Effect on Undrained Response	11
2.3.4 Effect on Consolidation Response	12
2.4 Review of the Stress-Strain Behaviour of Dhaka Clay	12
2.4.1 Index Properties	12
2.4.2 Stress-Strain Behaviour	13
2.4.3 Consolidation Behaviour	13
2.4.4 Effect of Lime and Cement	13
2.5 Constitutive Modeling	14
2.5.1 Traditional Approach	14
2.5.2 Modern Approach	15
2.5.3 Stress-Strain Response of Cemented Clays	15

2.6	Boundary Value Problems	15
2.6.1	Experimental Modeling	16
2.6.2	Numerical Modeling	16
2.6.3	Finite Element Method	16
2.7	Conclusion	17
 <b>CHAPTER 3 EQUIPMENT, INSTRUMENTATION AND METHODOLOGY</b>		 44
3.1	Introduction	44
3.2	Equipment Used	44
3.2.1	The Rotary Laboratory Mixer	45
3.2.2	Apparatus for $K_o$ consolidation of slurry	45
3.2.3	Unconfined compressive strength apparatus	46
3.2.4	Direct shear apparatus	46
3.2.5	Apparatus for one-dimensional Consolidation test	47
3.2.6	Model Steel Circular Footing and Pile	48
 <b>CHAPTER 4 DETERMINATION OF SOIL PARAMETERS</b>		 55
4.1	Introduction	55
4.2	Soil used	55
4.3	Geological Aspects of Savar Clay	56
4.4	Engineering Properties of Savar Clay	57
4.5	Preparation of Reconstituted Soil	58
4.5.1	General	58
4.5.2	Preparation of Soil Slurry	59
4.5.3	Consolidation of Slurry	59
4.6	Selection of Overburden Pressure	60
4.7	$k_o$ Value of Soil Samples	61
4.8	Preparation of Test Sample	61

4.9 Unconfined Compression Test	62
4.10 Direct Shear Test	62
4.11 One-Dimensional Consolidation Test	62
<b>CHAPTER 5 UNDRAINED PREDICTIONS USING THE MCC MODEL</b>	<b>69</b>
5.1 Introduction	69
5.2 Modified Cam Clay (MCC) Model	69
5.2.1 Defining the Critical State	70
5.2.2 Yield Function	70
5.2.3 Strain Hardening	71
5.2.4 Plastic Potential Function	72
5.2.5 Elastic behavior	73
5.3 Suitability of the Modified Cam Clay Model for Savar Clays	73
5.4 Modified Cam Clay Parameters for Savar Clays	74
5.4.1 Elastic parameters	74
5.4.2 Plastic Parameters	75
5.4.3 Critical State Parameters	76
5.4.4 Modified Cam Clay Parameters for Savar clay	77
5.6 Numerical Modeling of Triaxial Shear	77
5.7 Numerical Predictions of Undrained Tests	78
5.8 Prediction of CIU Response of Savar Clays	78
5. 8.1 Stress-Strain	78
5. 8.2 Stress Path	79
5.9 Comparison of Cemented and Uncemented behavior	80
5.9.1 Stress-Strain	80
5.9.2 Stress Path	81
5.9.3 Pore Pressure	82
5.10 Summary and Conclusions	83

<b>CHAPTER 6 DRAINED PREDICTIONS: MODIFIED CAM CLAY MODEL</b>	<b>103</b>
6.1 Introduction	103
6.2 Approach in Drained Analysis	103
6.3 Drained MCC parameters	104
6.4 Drained MCC Predictions	104
6.4.1 Stress-Strain	104
6.4.2 Stress Path and volume response	105
6.5 Comparison of Cemented and Uncemented behavior	106
6.5.1 Stress Strain	106
6.5.2 Stress Path	107
6.5.3 Volume Change Responses	107
6.6 Comparison of Drained and Undrained Predictions	108
6.7 Limitations of the Modified Cam Clay Model	109
6.9 Summary and Conclusion	109
<b>CHAPTER 7 MODIFIED MODIFIED CAM CLAY MODEL (MMCC MODEL)</b>	<b>128</b>
7.1 Introduction	128
7.2 The Modified Modified Cam Clay (MMCC) Model	128
7.2.1 The MMCC Yield Locus and Plastic Flow Rule	128
7.2.2 Tensile Strength and Unconfined Compression Strength	130
7.3 Prediction of Drained Response Using MCC and MMCC	131
7.3.1 Model Parameters	131
7.3.2 Stress Strain	131
7.3.3 Stress Path	132
7.3.4 Volume Change Response	132
7.4 Prediction of Undrained Response Using MCC and MMCC	133
7.4.1 Model Parameters	133
7.4.2 Stress Strain	133

7.4.3	Stress Path	134
7.4.4	Pore Pressure Response	134
7.5	Summary and Conclusion	135

**CHAPTER 8 EMMCC MODEL INCORPORATING CEMENTATION BREAKDOWN 172**

8.1	Introduction	172
8.2	Extended MMCC (EMMCC) Model	172
8.2.1	Tensile Strength Breakdown	173
8.2.2	Consolidation Strength Breakdown	174
8.2.3	Yield Locus and Flow Rule	174
8.3	Prediction of Drained Response	176
8.3.1	Drained Model Parameters	176
8.3.2	Stress-Strain	176
8.3.3	Stress Path	177
8.3.4	Volume Change Response	177
8.4	Prediction of Undrained Response	178
8.4.1	Model Parameters	178
8.4.2	Stress-Strain	179
8.4.3	Stress Path	180
8.4.4	Pore Pressure Response	181
8.5	Summary and Conclusion	182

**CHAPTER 9 EXPERIMENTAL AND NUMERICAL INVESTIGATION OF MODEL SCALE FOOTINGS AND PILES 219**

9.1	Introduction	219
9.2	Sample Preparation	219
9.3	Experimental Setup	220
9.4	Finite Element Modeling	221
9.5	Comparison of Numerical Predictions with Experimental data	222



9.6 Comparison of MCC and MMCC Model Predictions	222
9.7 Conclusion	223
<b>CHAPTER 10 CONCLUSIONS AND RECOMMENDATIONS</b>	<b>230</b>
10.1 Introduction	230
10.2 Concluding Observations	230
10.3 Recommendations for Further Research	232
REFERENCE	
APPENDIX- I	
APPENDIX- I I	
APPENDIX- I I I	

## LIST OF TABLES

<b>Table No.</b>	<b>Caption</b>	<b>Page No.</b>
5.1	The MCC model parameters of reconstituted Savar area clay	77
7.1	The MMCC model parameters of reconstituted Savar area clay	131
8.1	The EMMCC model parameters of reconstituted Savar area clay	177
A1.1	Index and other properties of Dhaka clay	242
A1.2	Geotechnical parameter of Dhaka clay	242
A1.3	Effect of cement treatment on engineering properties of the clay	243
A1.4	Index and shrinkage properties of cement treated Dhaka clay	244
A1.5	Index and shrinkage properties of lime treated Dhaka clay	244
A1.6	Unconfined compressive strength test result of untreated and cement treated Dhaka clay	245
A1.7	Unconfined compressive strength test result of untreated and lime treated Dhaka clay	246
A2.1	The index properties and classification of uncemented remolded Savar area clay	248
A2.2	The index properties of the cemented Savar area clay	248
A2.3	Unconfined compression strength and elastic modulus of uncemented and 7% and 14% cemented reconstituted Savar clay	248
A2.4	Unconsolidated direct shear test result of uncemented and 7% and 14% cemented reconstituted Savar clay	249
A2.5	The critical state parameters from consolidation test of uncemented and 7% and 14% cemented reconstituted Savar clay	249

## LIST OF FIGURES

Figure No.	Caption	Page No.
2.1	Idealized microscopic view of the structure of a clay soil	18
2.2	Index properties of clay in a layered stratum	18
2.3	Index and related engineering properties of a clay stratum	19
2.4	Relationship between water content and liquid limit of a clay stratum	19
2.5	Variation of plasticity index (PI) with liquid limit	20
2.6	Variation of unconfined shear strength with plasticity index (PI)	20
2.7	Variation of preconsolidation pressure with plasticity index (PI) in normally consolidated clays	21
2.8	Relationship between drained friction angle and plasticity index (PI) of a normally consolidated clays	21
2.9	Variation of void ratio or water content with mean overburden pressure for a normally consolidated sedimented clay	22
2.10	Effective stress path from consolidated drained (CD) tests on a normally consolidated clay	22
2.11	Effective stress path from consolidated drained (CD) tests on a overconsolidated clay	23
2.12	Drained stress-strain curves (CD tests) for undisturbed Leda clay	23
2.13	Strength envelop for unweathered London clay	24
2.14	Mohr-Coulomb strength envelop, Mohr-Coulomb parameters and relation between peak and ultimate parameters	24
2.15	Effective Stress path in consolidation undrained (CU) test on normally consolidated Weald	25
2.16	Effective Stress path in consolidation undrained (CU) test on overconsolidated Weald clay	25
2.17	Qualitative stress-strain and excess pore pressure curves in consolidated undrained (CU) test on normally and overconsolidated weald clay	26

2.18	Stress- strain curves from triaxial test on five normally consolidated clay in undrained conditions	27
2.19	Typical consolidation curve for Bangkok clay from Bangpli	27
2.20	Effect of removal of cementing agents on consolidated curve of a clay	28
2.21	Yield or preconsolidation pressure of drained consolidation tests on clay	28
2.22	Time-settlement curves for different magnitudes of stress increment	29
2.23	a. Effect of lime addition on clay structure	29
	b. Effect of lime addition on compression strength of silt and clays	30
2.24	Effect of cement on unconfined compression strength and stress-strain behaviour of clays	30
2.25	Effect of curing period on unconfined strength of cemented clay	31
2.26	Effect of cement on the Atterberg Limits of clay	31
2.27	Effect of cement on the water content of clay	32
2.28	Effect of cement on the unit weight of clay	32
2.29	Effect of cement content on stress-strain curve during drained triaxial shearing of cemented clay at relatively low cell pressure	33
2.30	Effect of cement content on stress-strain curve during drained triaxial shearing of cemented clay at relatively high cell pressure	33
2.31	Effect of cement content on volume change response during drained triaxial shearing of cemented clay at relatively low cell pressure	34
2.32	Effect of cement content on undrained stress path during triaxial shearing of cemented clay	34
2.33	Effect of cement content on stress-strain during consolidated undrained (CU) test of cemented clay	35
2.34	Effect of cement content on pore pressure response during consolidated undrained (CU) test of cemented clay	35
2.35	Effect of cement content on consolidation response of clay	36
2.36	Void ratio vs log (Vertical Effective stress) plot for one –dimensional consolidation test on block sample of soft Dhaka clay	36
2.37	Coefficient of consolidation vs vertical effective stress plot for block	37

	sample of soft Dhaka clay	
2.38	Effect of cement content and duration on compressive strength of cement treated Dhaka clay	37
2.39	Effect of cement content and curing age on compressive strength of cement treated Dhaka clay	38
2.40	Effect of Lime content on compressive strength of cement treated Dhaka clay	38
2.41	Effect of curing age on unconfined compression strength of lime treated Dhaka clay	39
2.42	The Mohr-Coulomb model in generalized and $I_1 - J_2$ space	39
2.43	The Drucker-Prager model in principal stress space	40
2.44	State Boundary surface in $p', q, e$ space	40
2.45	Cam Clay and Modified Cam Clay yield surface	41
2.46	Settlement of model footing at ultimate failure	41
2.47	Finite element analysis of plate load test	42
2.48	Finite element analysis of surface heave caused by pile driving	42
2.49	Result of finite element analysis of a single pile	43
3.1	Hobert laboratory mixer machine: (a) Photograph of the machine, (b) Photograph of attachment and bowl	49
3.2	Apparatus for $K_o$ -consolidation of soil slurry	50
3.3	Unconfined compression test Apparatus	51
3.4	Line Details of the Direct Shear Test	52
3.5	Direct Shear Machine Showing shear Box, Loading Arrangement and Frame	52
3.6	One Dimensional Consolidation Test Apparatus	53
4.1	Axial stress vs axial strain curve of uncemented Savar clay	64
4.2	Axial stress vs axial strain curve of 7 % cemented Savar clay	64
4.3	Axial stress vs axial strain curve of 14 % cemented Savar clay	65
4.4	Peak shear stress vs total normal stress curve of uncemented Savar clay	65
4.5	Peak shear stress vs total normal stress curve of 7 % cemented Savar clay	66
4.6	Peak shear stress vs total normal stress curve of 14% cemented Savar	66

	clay	
4.7	e-log p curves for uncemented Savar clay	67
4.8	E-log p curve for 7% cemented Savar clay	67
4.9	E-log p curve for 14% cemented Savar clay	68
5.1	MCC model yield locus and plastic potential function	84
5.2	MCC model critical state line and normal consolidation line	84
5.3	MCC prediction of undrained stress-strain response for normally consolidated and low OCR uncemented Savar clay	85
5.4	MCC prediction of undrained stress-strain response of highly overconsolidated uncemented Savar clay	85
5.5	MCC prediction of undrained stress-strain response of normally consolidated and low OCR 7% cemented Savar clay	86
5.6	MCC prediction of undrained stress-strain response of highly overconsolidated 7% cemented Savar clay	86
5.7	MCC prediction of undrained stress-strain response of normally consolidated and low OCR 14% cemented Savar clay	87
5.8	MCC prediction of undrained stress-strain response of highly overconsolidated 14% cemented Savar clay	87
5.9	MCC prediction of undrained stress path of normally consolidated and low OCR uncemented Savar clay	88
5.10	MCC prediction of undrained stress path of highly overconsolidated uncemented Savar clay	88
5.11	MCC prediction of undrained stress path of normally consolidated and low OCR 7% cemented Savar clay	89
5.12	MCC prediction of undrained stress path of highly overconsolidated 7% cemented Savar clay	89
5.13	MCC prediction of undrained stress path of normally consolidated and low OCR 14% cemented Savar clay	90
5.14	MCC prediction of undrained stress path of highly overconsolidated 14% cemented Savar clay	90
5.15	MCC prediction of excess pore pressure response of normally consolidated and low OCR uncemented Savar clay	91

5.16	MCC prediction of excess pore pressure response of highly overconsolidated uncemented Savar clay	91
5.17	MCC prediction of excess pore pressure response of normally consolidated and low OCR 7% cemented Savar clay	92
5.18	MCC prediction of excess pore pressure response of highly overconsolidated 7% cemented Savar clay	92
5.19	MCC prediction of excess pore pressure response of normally consolidated and low OCR 14% cemented Savar clay	93
5.20	MCC prediction of excess pore pressure response of highly overconsolidated 14% cemented Savar clay	93
5.21	MCC prediction of undrained stress-strain response of normally consolidated reconstituted Savar clay (CCR=1) for varying degrees of cementation	94
5.22	MCC prediction of undrained stress-strain response of low OCR (OCR=2) reconstituted Savar clay for varying degrees of cementation	94
5.23	MCC prediction of undrained stress-strain response of moderately overconsolidated (OCR=5) reconstituted Savar clay for varying degrees of cementation	95
5.24	MCC prediction of undrained stress-strain response of highly overconsolidated (OCR=10) reconstituted Savar clay for varying degrees of cementation	95
5.25	MCC prediction of undrained stress-strain response of highly overconsolidated (OCR=20) reconstituted Savar clay for varying degrees of cementation	96
5.26	MCC prediction of undrained stress-strain response of highly overconsolidated (OCR=30) reconstituted Savar clay for varying degrees of cementation	96
5.27	MCC prediction of undrained stress path of normally consolidated (OCR=1) reconstituted Savar clay for varying degrees of cementation	97
5.28	MCC prediction of undrained stress path of low overconsolidated	97

	(OCR=2) reconstituted Savar clay for varying degrees of cementation	
5.29	MCC prediction of undrained stress path of moderately overconsolidated (OCR=5) reconstituted Savar clay for varying degrees of cementation	98
5.30	MCC prediction of undrained stress path of highly overconsolidated (OCR=10) reconstituted Savar clay for varying degrees of cementation	98
5.31	MCC prediction of undrained stress path of highly overconsolidated (OCR=20) reconstituted Savar clay for varying degrees of cementation	99
5.32	MCC prediction of undrained stress path of highly overconsolidated (OCR=30) reconstituted Savar clay for varying degrees of cementation	99
5.33	MCC prediction of excess pore pressure response of normally consolidated (OCR=1) reconstituted Savar clay for varying degrees of cementation	100
5.34	MCC prediction of excess pore pressure response of low over consolidated (OCR=2) reconstituted Savar clay for varying degrees of cementation	100
5.35	MCC prediction of excess pore pressure response of moderately overconsolidated (OCR=5) reconstituted Savar clay for varying degrees of cementation	101
5.36	MCC prediction of excess pore pressure response of highly overconsolidated (OCR=10) reconstituted Savar clay for varying degrees of cementation	101
5.37	MCC prediction of excess pore pressure response of highly overconsolidated (OCR=20) reconstituted Savar clay for varying degrees of cementation	102
5.38	MCC prediction of excess pore pressure response of highly overconsolidated (OCR=30) reconstituted Savar clay for varying degrees of cementation	102



6.1	MCC prediction of drained stress-strain response of normal, low, and moderately overconsolidated uncemented Savar clay	110
6.2	MCC prediction of drained stress-strain response of highly overconsolidated uncemented Savar clay	110
6.3	MCC prediction of drained stress-strain response of normal, low, and moderately overconsolidated 7% cemented Savar clay	111
6.4	MCC prediction of drained stress-strain response of highly overconsolidated 7% cemented Savar clay	111
6.5	MCC prediction of drained stress-strain response of normal, low, and moderately overconsolidated 14% cemented Savar clay	112
6.6	MCC prediction of drained stress-strain response of highly overconsolidated 14% cemented Savar clay	112
6.7	MCC drained stress path of normal, low, and moderately overconsolidated uncemented Savar clay	113
6.8	MCC drained stress path of highly overconsolidated uncemented Savar clay	113
6.9	MCC drained stress path of normal, low, and moderately overconsolidated 7% cemented Savar clay	114
6.10	MCC drained stress path of highly overconsolidated 7% cemented Savar clay	114
6.11	MCC drained stress path of normal, low, and moderately overconsolidated 14% cemented Savar clay	115
6.12	MCC drained stress path of highly overconsolidated 14% cemented Savar clay	115
6.13	MCC drained test prediction of volume strain response of normal, low, and moderately overconsolidated uncemented Savar clay	116
6.14	MCC drained test prediction of volume strain response of highly overconsolidated uncemented Savar clay	116
6.15	MCC drained prediction of volume strain response of normal, low, and moderately overconsolidated 7% cemented Savar clay	117
6.16	MCC drained prediction of volume strain response of highly overconsolidated 7% cemented Savar clay	117

6.17	MCC drained prediction of volume strain response of normal, low, and moderately overconsolidated 14% cemented Savar clay	118
6.18	MCC drained prediction of volume strain response of highly overconsolidated 14% cemented Savar clay	118
6.19	MCC prediction of drained stress-strain response of normally consolidated (OCR=1) remolded Savar clay for varying degrees of cementation	119
6.20	MCC prediction of drained stress-strain response of low over consolidated (OCR=2) reconstituted Savar clay for varying degrees of cementation	119
6.21	MCC prediction of drained stress-strain response of moderately overconsolidated (OCR=5) remolded Savar clay for varying degrees of cementation	120
6.22	MCC prediction of drained stress-strain response of highly overconsolidated (OCR=10) remolded Savar clay for varying degrees of cementation	120
6.23	MCC prediction of drained stress-strain response of highly overconsolidated (OCR=20) remolded Savar clay for varying degrees of cementation	121
6.24	MCC prediction of drained stress-strain response of highly overconsolidated (OCR=30) remolded Savar clay for varying degrees of cementation	121
6.25	MCC prediction of undrained stress path of normally consolidated (OCR=1) remolded Savar clay for varying degrees of cementation	122
6.26	MCC prediction of undrained stress path of low overconsolidated (OCR=2) remolded Savar clay for varying degrees of cementation	122
6.27	MCC prediction of undrained stress path of moderately overconsolidated (OCR=5) remolded Savar clay for varying degrees of cementation	123
6.28	MCC prediction of undrained stress path of highly overconsolidated (OCR=10) remolded Savar clay for varying degrees of cementation	123
6.29	MCC prediction of undrained stress path of highly overconsolidated	124

	(OCR=20) remolded Savar clay for varying degrees of cementation	
6.30	MCC prediction of undrained stress path of highly overconsolidated	124
	(OCR=30) remolded Savar clay for varying degrees of cementation	
6.31	MCC prediction of volume change response of normally consolidated (OCR=1) remolded Savar clay for varying degrees of cementation	125
6.32	MCC prediction of volume change response of low overconsolidated (OCR=2) remolded Savar clay for varying degrees of cementation	125
6.33	MCC prediction of volume change response of moderately overconsolidated (OCR=5) remolded Savar clay for varying degrees of cementation	126
6.34	MCC prediction of volume change response of highly overconsolidated (OCR=10) remolded Savar clay for varying degrees of cementation	126
6.35	MCC prediction of volume change response of highly overconsolidated (OCR=20) remolded Savar clay for varying degrees of cementation	127
6.36	MCC prediction of volume change response of highly overconsolidated (OCR=30) remolded Savar clay for varying degrees of cementation	127
7.1	MCC and MMCC prediction of drained stress-strain response of 7% cemented Savar clay (OCR=1)	136
7.2	MCC and MMCC prediction of drained stress-strain response of 7% cemented Savar clay (OCR=2)	136
7.3	MCC and MMCC prediction of drained stress-strain response of 7% cemented Savar clay (OCR=5)	137
7.4	MCC and MMCC prediction of drained stress-strain response of 7% cemented Savar clay (OCR=10)	137
7.5	MCC and MMCC prediction of drained stress-strain response of 7% cemented Savar clay (OCR=20)	138
7.6	MCC and MMCC prediction of drained stress-strain response of 7% cemented Savar clay (OCR=30)	138

7.7	MCC and MMCC prediction of drained stress-strain response of 14% cemented Savar clay (OCR=1)	139
7.8	MCC and MMCC prediction of drained stress-strain response of 14% cemented Savar clay (OCR=2)	139
7.9	MCC and MMCC prediction of drained stress-strain response of 14% cemented Savar clay (OCR=5)	140
7.10	MCC and MMCC prediction of drained stress-strain response of 14% cemented Savar clay (OCR=10)	10
7.11	MCC and MMCC prediction of drained stress-strain response of 14% cemented Savar clay (OCR=20)	141
7.12	MCC and MMCC prediction of drained stress-strain response of 14% cemented Savar clay (OCR=30)	141
7.13	MCC and MMCC prediction of drained triaxial stress path for 7% cemented Savar clay (OCR=1)	142
7.14	MCC and MMCC prediction of drained triaxial stress path for 7% cemented Savar clay (OCR=2)	142
7.15	MCC and MMCC prediction of drained triaxial stress path for 7% cemented Savar clay (OCR=5)	143
7.16	MCC and MMCC prediction of drained triaxial stress path for 7% cemented Savarelay (OCR=10)	143
7.17	MCC and MMCC prediction of drained triaxial stress path for 7% cemented Savar clay (OCR=20)	144
7.18	MCC and MMCC prediction of drained triaxial stress path for 7% cemented Savar clay (OCR=30)	144
7.19	MCC and MMCC prediction of drained triaxial stress path for 14% cemented Savar clay (OCR=1)	145
7.20	MCC and MMCC prediction of drained triaxial stress path for 14% cemented Savar clay (OCR=2)	145
7.21	MCC and MMCC prediction of drained triaxial stress path for 14% cemented Savar clay (OCR=5)	146
7.22	MCC and MMCC prediction of drained triaxial stress path for 14% cemented Savar clay (OCR=10)	146

7.23	MCC and MMCC prediction of drained triaxial stress path for 14% cemented Savar clay (OCR=20)	147
7.24	MCC and MMCC prediction of drained triaxial stress path for 14% cemented Savar clay (OCR=30)	147
7.25	MCC and MMCC prediction of volume change response for 7% cemented Savar clay (OCR=1)	148
7.26	MCC and MMCC prediction of volume change response for 7% cemented Savar clay (OCR=2)	148
7.27	MCC and MMCC prediction of volume change response for 7% cemented Savar clay (OCR=5)	149
7.28	MCC and MMCC prediction of volume change response for 7% cemented Savar clay (OCR=10)	149
7.29	MCC and MMCC prediction of volume change response for 7% cemented Savar clay (OCR=20)	150
7.30	MCC and MMCC prediction of volume change response for 7% cemented Savar clay (OCR=30)	150
7.31	MCC and MMCC prediction of volume change response for 14% cemented Savar clay (OCR=1)	151
7.32	MCC and MMCC prediction of volume change response for 14% cemented Savar clay (OCR=2)	151
7.33	MCC and MMCC prediction of volume change response for 14% cemented Savar clay (OCR=5)	152
7.34	MCC and MMCC prediction of volume change response for 14% cemented Savar clay (OCR=10)	152
7.35	MCC and MMCC prediction of volume change response for 14% cemented Savar clay (OCR=20)	153
7.36	MCC and MMCC prediction of volume change response for 14% cemented Savar clay (OCR=30)	153
7.37	MCC and MMCC prediction of undrained stress-strain response for 7% cemented Savar clay (OCR=1)	154
7.38	MCC and MMCC prediction of undrained stress-strain response for 7% cemented Savar clay (OCR=2)	154

7.39	MCC and MMCC prediction of undrained stress-strain response for 7% cemented Savar clay (OCR=5)	155
7.40	MCC and MMCC prediction of undrained stress-strain response for 7% cemented Savar clay (OCR=10)	155
7.41	MCC and MMCC prediction of undrained stress-strain response for 7% cemented Savar clay (OCR=20)	156
7.42	MCC and MMCC prediction of undrained stress-strain response for 7% cemented Savar clay (OCR=30)	156
7.43	MCC and MMCC prediction of undrained stress-strain response for 14% cemented Savar clay (OCR=1)	157
7.44	MCC and MMCC prediction of undrained stress-strain response for 14% cemented Savar clay (OCR=2)	157
7.45	MCC and MMCC prediction of undrained stress-strain response for 14% cemented Savar clay (OCR=5)	158
7.46	MCC and MMCC prediction of undrained stress-strain response for 14% cemented Savar clay (OCR=10)	158
7.47	MCC and MMCC prediction of undrained stress-strain response for 14% cemented Savar clay (OCR=20)	159
7.48	MCC and MMCC prediction of undrained stress-strain response for 14% cemented Savar clay (OCR=30)	159
7.49	MCC and MMCC prediction of undrained triaxial stress path for 7% cemented Savar clay (OCR=1)	160
7.50	MCC and MMCC prediction of undrained triaxial stress path for 7% cemented Savar clay (OCR=2)	160
7.51	MCC and MMCC prediction of undrained triaxial stress path for 7% cemented Savar clay (OCR=5)	161
7.52	MCC and MMCC prediction of undrained triaxial stress path for 7% cemented Savar clay (OCR=10)	161
7.53	MCC and MMCC prediction of undrained triaxial stress path for 7% cemented Savar clay (OCR=20)	162
7.54	MCC and MMCC prediction of undrained triaxial stress path for 7% cemented Savar clay (OCR=30)	162

7.55	MCC and MMCC prediction of undrained triaxial stress path for 14% cemented Savar clay (OCR=1)	163
7.56	MCC and MMCC prediction of undrained triaxial stress path for 14% cemented Savar clay (OCR=2)	163
7.57	MCC and MMCC prediction of undrained triaxial stress path for 14% cemented Savar clay (OCR=5)	164
7.58	MCC and MMCC prediction of undrained triaxial stress path for 14% cemented Savar clay (OCR=10)	164
7.59	MCC and MMCC prediction of undrained triaxial stress path for 14% cemented Savar clay (OCR=20)	165
7.60	MCC and MMCC prediction of undrained triaxial stress path for 14% cemented Savar clay (OCR=30)	165
7.61	MCC and MMCC prediction of excess pore pressure response for 7% cemented Savar clay (OCR=1)	166
7.62	MCC and MMCC prediction of excess pore pressure response for 7% cemented Savar clay (OCR=2)	166
7.63	MCC and MMCC prediction of eExcess pore pressure response for 7% cemented Savar clay (OCR=5)	167
7.64	MCC and MMCC prediction of excess pore pressure response for 7% cemented Savar clay (OCR=10)	167
7.65	MCC and MMCC prediction of excess pore pressure response for 7% cemented Savar clay (OCR=20)	168
7.66	MCC and MMCC prediction of excess pore pressure response for 7% cemented Savar clay (OCR=30)	168
7.67	MCC and MMCC prediction of excess pore pressure response for 14% cemented Savar clay (OCR=1)	169
7.68	MCC and MMCC prediction of excess pore pressure response for 14% cemented Savar clay (OCR=2)	169
7.69	MCC and MMCC prediction of excess pore pressure response for 14% cemented Savar clay (OCR=5)	170
7.70	MCC and MMCC prediction of excess pore pressure response for 14% cemented Savar clay (OCR=10)	170

7.71	MCC and MMCC prediction of excess pore pressure response for 14% cemented Savar clay (OCR=20)	171
7.72	MCC and MMCC prediction of excess pore pressure response for 14% cemented Savar clay (OCR=30)	171
8.1	EMMCC model prediction of drained triaxial stress-strain response of 7% cemented Savar clay (OCR=1)	183
8.2	EMMCC model prediction of drained triaxial stress-strain response of 7% cemented Savar clay (OCR=2)	183
8.3	EMMCC model prediction of drained triaxial stress-strain response of 7% cemented Savar clay (OCR=5)	184
8.4	EMMCC model prediction of drained triaxial stress-strain response of 7% cemented Savar clay (OCR=10)	184
8.5	EMMCC model prediction of drained triaxial stress-strain response of 7% cemented Savar clay (OCR=20)	185
8.6	EMMCC model prediction of drained triaxial stress-strain response of 7% cemented Savar clay (OCR=30)	185
8.7	EMMCC model prediction of drained triaxial stress-strain response of 14% cemented Savar clay (OCR=1)	186
8.8	EMMCC model prediction of drained triaxial stress-strain response of 14% cemented Savar clay (OCR=2)	186
8.9	EMMCC model prediction of drained triaxial stress-strain response of 14% cemented Savar clay (OCR=5)	187
8.10	EMMCC model prediction of drained triaxial stress-strain response of 14% cemented Savar clay (OCR=10)	187
8.11	EMMCC model prediction of drained triaxial stress-strain response of 14% cemented Savar clay (OCR=20)	188
8.12	EMMCC model prediction of drained triaxial stress-strain response of 14% cemented Savar clay (OCR=30)	188
8.13	EMMCC model prediction of drained triaxial stress path of 7% cemented Savar clay (OCR=1)	189
8.14	EMMCC model prediction of drained triaxial stress path of 7% cemented Savar clay (OCR=2)	189



8.15	EMMCC model prediction of drained triaxial stress path of 7% cemented Savar clay (OCR=5)	190
8.16	EMMCC model prediction of drained triaxial stress path of 7% cemented Savarclay (OCR=10)	190
8.17	EMMCC model prediction of drained triaxial stress path of 7% cemented Savar clay (OCR=20)	191
8.18	EMMCC model prediction of drained triaxial stress path of 7% cemented Savar clay (OCR=30)	191
8.19	EMMCC model prediction of drained triaxial stress path of 14% cemented Savar clay (OCR=1)	192
8.20	EMMCC model prediction of drained triaxial stress path of 14% cemented Savar clay (OCR=2)	192
8.21	EMMCC model prediction of drained triaxial stress path of 14% cemented Savar clay (OCR=5)	193
8.22	EMMCC model prediction of drained triaxial stress path of 14% cemented Savar clay (OCR=10)	193
8.23	EMMCC model prediction of drained triaxial stress path of 14% cemented Savar clay (OCR=20)	194
8.24	EMMCC model prediction of drained triaxial stress path of 14% cemented Savar clay (OCR=30)	194
8.25	EMMCC model prediction of drained volume-strain response of 7% cemented Savar clay (OCR=1)	195
8.26	EMMCC model prediction of drained volume-strain response of 7% cemented Savar clay (OCR=2)	195
8.27	EMMCC model prediction of drained volume-strain response of 7% cemented Savar clay (OCR=5)	196
8.28	EMMCC model prediction of drained volume-strain response of 7% cemented Savar clay (OCR=10)	196
8.29	EMMCC model prediction of drained volume-strain response of 7% cemented Savar clay (OCR=20)	197
8.30	EMMCC model prediction of drained volume-strain response of 7% cemented Savar clay (OCR=30)	197

8.31	EMMCC model prediction of drained volume-strain response of 14% cemented Savar clay (OCR=1)	198
8.32	EMMCC model prediction of drained volume-strain response of 14% cemented Savar clay (OCR=2)	198
8.33	EMMCC model prediction of drained volume-strain response of 14% cemented Savar clay (OCR=5)	199
8.34	EMMCC model prediction of drained volume-strain response of 14% cemented Savar clay (OCR=10)	199
8.35	EMMCC model prediction of drained volume-strain response of 14% cemented Savar clay (OCR=20)	200
8.36	EMMCC model prediction of drained volume-strain response of 14% cemented Savar clay (OCR=30)	200
8.37	EMMCC model prediction of undrained triaxial stress-strain response of 7% cemented Savar clay (OCR=1)	201
8.38	EMMCC model prediction of undrained triaxial stress-strain response of 7% cemented Savar clay (OCR=2)	201
8.39	EMMCC model prediction of undrained triaxial stress-strain response of 7% cemented Savar clay (OCR=5)	202
8.40	EMMCC model prediction of undrained triaxial stress-strain response of 7% cemented Savar clay (OCR=10)	202
8.41	EMMCC model prediction of undrained triaxial stress-strain response of 7% cemented Savar clay (OCR=20)	203
8.42	EMMCC model prediction of undrained triaxial stress-strain response of 7% cemented Savar clay (OCR=30)	203
8.43	EMMCC model prediction of undrained triaxial stress-strain response of 14% cemented Savar clay (OCR=1)	204
8.44	EMMCC model prediction of undrained triaxial stress-strain response of 14% cemented Savar clay (OCR=2)	204
8.45	EMMCC model prediction of undrained triaxial stress-strain response of 14% cemented Savar clay (OCR=5)	205
8.46	EMMCC model prediction of undrained triaxial stress-strain response of 14% cemented Savar clay (OCR=10)	205

8.47	EMMCC model prediction of undrained triaxial stress-strain response of 14% cemented Savar clay (OCR=20)	206
8.48	EMMCC model prediction of undrained triaxial stress-strain response of 14% cemented Savar clay (OCR=30)	206
8.49	EMMCC model prediction of undrained triaxial stress path of 7% cemented Savar clay (OCR=1)	207
8.50	EMMCC model prediction of undrained triaxial stress path of 7% cemented Savar clay (OCR=2)	207
8.51	EMMCC model prediction of undrained triaxial stress path of 7% cemented Savar clay (OCR=5)	208
8.52	EMMCC model prediction of undrained triaxial stress path of 7% cemented Savar clay (OCR=10)	208
8.53	EMMCC model prediction of undrained triaxial stress path of 7% cemented Savar clay (OCR=20)	209
8.54	EMMCC model prediction of undrained triaxial stress path of 7% cemented Savar clay (OCR=30)	209
8.55	EMMCC model prediction of undrained triaxial stress path of 14% cemented Savar clay (OCR=1)	210
8.56	EMMCC model prediction of undrained triaxial stress path of 14% cemented Savar clay (OCR=2)	210
8.57	EMMCC model prediction of undrained triaxial stress path of 14% cemented Savar clay (OCR=5)	211
8.58	EMMCC model prediction of undrained triaxial stress path of 14% cemented Savar clay (OCR=10)	211
8.59	EMMCC model prediction of undrained triaxial stress path of 14% cemented Savar clay (OCR=20)	212
8.60	EMMCC model prediction of undrained triaxial stress path of 14% cemented Savar clay (OCR=30)	212
8.61	EMMCC model prediction of excess pore pressure response of 7% cemented Savar clay (OCR=1)	213
8.62	EMMCC model prediction of excess pore pressure response of 7% cemented Savar clay (OCR=2)	213

8.63	EMMCC model prediction of excess pore pressure response of 7% cemented Savar clay (OCR=5)	214
8.64	EMMCC model prediction of excess pore pressure response of 7% cemented Savar clay (OCR=10)	214
8.65	EMMCC model prediction of excess pore pressure response of 7% cemented Savar clay (OCR=20)	215
8.66	EMMCC model prediction of excess pore pressure response of 7% cemented Savar clay (OCR=30)	215
8.67	EMMCC model prediction of excess pore pressure response of 14% cemented Savar clay (OCR=1)	216
8.68	EMMCC model prediction of excess pore pressure response of 14% cemented Savar clay (OCR=2)	216
8.69	EMMCC model prediction of excess pore pressure response of 14% cemented Savar clay (OCR=5)	217
8.70	EMMCC model prediction of excess pore pressure response of 14% cemented Savar clay (OCR=10)	217
8.71	EMMCC model prediction of excess pore pressure response of 14% cemented Savar clay (OCR=20)	218
8.72	EMMCC model prediction of excess pore pressure response of 14% cemented Savar clay (OCR=30)	218
9.1	Model scale footing on consolidation mold	224
9.2	Model scale pile on consolidation mold	224
9.3	Finite element mesh for model footing using 8-noded quadrilateral elements	225
9.4	An 8-noded quadrilateral element	225
9.5	Comparison of MCC model predictions with the test data (T.D) of model scale footing on uncemented Savar clay.	226
9.6	Comparison of MCC model predictions with the test data (T.D) of model scale piles on uncemented Savar clay.	226
9.7	Comparison of MCC & MMCC model prediction for model scale footing resting on 7 % cemented remolded Savar clay	227
9.8	Comparison of MCC & MMCC model prediction for model scale	227

	footing resting on 14 % cemented remolded Savar clay	
9.9	Comparison of MCC & MMCC model prediction for model scale pile test on 7 % cemented remolded Savar clay	228
9.10	Comparison of MCC & MMCC model prediction for model scale pile test on 14 % cemented remolded Savar clay	228
9.11	Comparison of MMCC model prediction of load displacement response of model scale footing resting on 7 % & 14 % cemented remolded Savar clay	229
9.12	Comparison of MMCC model prediction of load displacement response of model scale piles resting on 7 % & 14 % cemented remolded Savar clay	229
A2.50	Comparison of experimental data of model scale footing test ( $\sigma'_v=50\text{kPa}$ ) with numerical predictions using the Modified Cam Clay model	
A2.51	Comparison of experimental data of model scale footing test ( $\sigma'_v=150\text{kPa}$ ) with numerical predictions using the Modified Cam Clay model	
A2.52	Comparison of experimental data of model scale pile test ( $\sigma'_v=150\text{kPa}$ ) with numerical predictions using the Modified Cam Clay model	
A2.53	Comparison of experimental data of model scale footing test ( $\sigma'_v=50\text{kPa}$ ) with numerical predictions using the Mohr-Coulomb model	
A2.54	Comparison of experimental data of model scale footing test ( $\sigma'_v=150\text{kPa}$ ) with numerical predictions using the Mohr-Coulomb model	
A2.55	Comparison of experimental data of model scale pile test ( $\sigma'_v=150\text{kPa}$ ) with numerical predictions using the Mohr-Coulomb model	
A4.10	Shear stress vs shear displacement curve of uncemented Savar clay	
A4.11	Shear stress vs shear displacement curve of 7% cemented Savar clay	
A4.12	Shear stress vs shear displacement curve of 14% cemented Savar clay	

## NOTATIONS

A	pore pressure parameter
$A_p$	area of pile point
$b_c, b_q, b_\gamma$	base factors
$c$	soil cohesion
CD	consolidated drained
CSL	critical state line
CU	consolidated un-drained
$c_u, s_u$	un-drained shear strength
D	depth of embedment of foundation
$d_c, d_q, d_\gamma$	depth factors
$E_i$	initial modulus of elasticity
$E_{50}$	secant modulus of elasticity
$e$	void ratio
G	elastic shear modulus
$g_c, g_q, g_\gamma$	ground factors
$I_1$	the first invariant of the effective stress tensor and it is proportional to the effective mean pressure.
$J_2$	the second invariant of the deviatoric stress tensor
LL, $w_L$	liquid limit
$M$	critical stress ratio
MC	Mohr-Coulomb model
MCC	Modified Cam Clay model
NC	normally consolidated
NCL	normally consolidated line
$N_c, N_q, N_\gamma$	traditional bearing capacity factors
$P_{pu}$	ultimate static point load capacity of the pile
OC	over consolidated
OCR	over consolidation ratio
PI, $I_p$	plasticity index

PL, $w_p$	plastic limit
$p'$	mean effective pressure= $(\sigma'_a + 2\sigma'_r)/3$
$p'_o$	hardening parameter
$Q_{ult}$	ultimate bearing capacity
$q$	deviator stress
$\bar{q}$	uniform pressure on the soil surface
$s_c, s_g, s_\gamma$	shape factors
$u$	pore pressure
UU	unconsolidated un-drained test
$w$	water content
$\gamma$	unit weight of the soil
$\sigma'_v, p'_o$	pre-consolidation pressure
$\sigma'_1$	major principal effective stress
$\sigma'_2, \sigma'_3$	minor principal effective stresses
$\Delta\sigma_v$	change of vertical total stress
$\theta$	lode angle
$\lambda, \kappa$	slope of the normal consolidation line and the elastic rebound line
$\rho_l, \rho_m$	Degradation parameter of $p'_{l_o}$ and $p_{m_o}$
$\tau_{ff}$	peak or ultimate shear resistance
$\mu$	Poisson's ratio
$\phi'$	Angle of internal friction (peak or ultimate).
$\psi'$	dilation angle
$p'_l, p_{m_o}$	Tensile strength and Consolidation strength parameter
$\epsilon_v, \epsilon_a$	volumetric strain, axial strain
$d\epsilon_v^p$	incremental plastic deviator strain
$d\epsilon_q^p$	incremental plastic volumetric strain
$\eta$	stress ratio

## ACKNOWLEDGEMENT

Thanks to Almighty Allah for his graciousness and unlimited kindness.

The author wishes to express his profound gratefulness and indebtedness to his supervisor Associate Professor Dr. Md. Kabirul Islam for his unfailing guidance, constant supervision, helpful criticisms and encouragement offered throughout the course of this research work. The author recognizes and acknowledges his unstinted help in both academic and personal concerns, throughout the years of the author's graduate studies at the Bangladesh University of Engineering and Technology, Dhaka.

The author expresses his profound gratitude to the Head of the Department of Civil Engineering, Bangladesh University of Engineering and Technology, Dhaka for providing laboratory facilities and necessary co-operation during the research. The financial support provided by the authority of BUET, Dhaka is also gratefully acknowledged.

The author is interested to expresses his sincere thanks to the research colleagues of the Department of Civil Engineering, namely, Sajjad, Anis, Noman, Arif, and Muktar for their encouragement and friendship during his study at BUET, Dhaka.

Mr. Habibur Rahman and Mr. Alimuddin who are the staff of Geotechnical Engineering Laboratory, are liable to get thanks due to their helps when needed in the experimental works.

Finally, the author proud of his beloved Parents along with his family members, who are always a constant source of inspiration throughout this research.



## ABSTRACT

This thesis deals with the numerical and experimental investigations of Savar area clays of Dhaka city. Three critical state soil models were used to numerically simulate the drained and undrained stress-stress response under triaxial condition of Savar area clays, with and without cementation. The models used were the Modified Cam Clay (MCC) model, Modified Modified Cam Clay (MMCC) model which incorporates cementation strength and the Extended MMCC model or EMMCC model incorporating cementation breakdown effects. The numerical study provides an in-depth understanding of the strengths and limitations of critical state models to simulate the stress-strain behaviour of Savar area clays, with and without cementation, and in drained and undrained condition. In particular, it was observed that the MCC model could simulate the effect of cementation on clays. However, the MMCC model which explicitly incorporated the effect of tensile strength in the MCC model, significantly improved the predictions expected for the effect of cementation on clays. Finally, it was shown with the EMMCC model, that cementation breakdown effects could also be incorporated in the MCC model and simulated with this model. Such analysis may be necessary in particular situations or cases of soil behaviour.

Finally, experimental model-scale footing and pile tests were carried out in a consolidation mold containing Savar area clays, with and without cementation. The experimental data clearly indicated that cementation of clays significantly increases the bearing capacity mobilised by footings resting on such soils. The results of the tests were numerically simulated using elasto-plastic finite element analysis and the Modified Cam Clay model. The experimental data was subsequently compared with numerical predictions. The comparison of the results of finite element analysis for footings resting on cemented and uncemented Savar area clays, with experimental data showed that, using the MCC model for such analysis could predict the effect of cementation of clays on footing behaviour. Finally, the strengths and limitations of the MCC model in predicting the load-displacement response of model-scale footings and piles resting on Savar area clays, with and without cementation, were critically evaluated.

# CHAPTER 1

## INTRODUCTION



### 1.1 Introduction

Dhaka city and its surrounding zones such as Savar are undergoing rapid development. Low lying areas, marshy land, fill areas etc. are increasingly being utilized for building structures and other civic amenities. Due to the critical sub-soil conditions in many areas, it is becoming important to consider the safety of the foundation for structures to be built in these soils. For this purpose, it has become essential to understand the stress-strain characteristics of the sub-soil of Dhaka city and its surrounding suburbs.

In this thesis, the focus of research is typical clay collected from Savar area nearby Dhaka city. The clay soil was tested in the laboratory to determine its engineering properties. Particularly, the critical state parameters of Savar area clay were determined. In the next phase, the Savar clay was cemented to various degrees using ordinary Portland cement and cured for 7 days. Numerical predictions of the triaxial stress-strain response of Savar area clays, both cemented and uncemented, were then carried out using the Modified Cam Clay (MCC) model, Modified MCC (MMCC) model (MCC incorporating cementation) and MMCC model incorporating cementation break down assumptions.

As of now, no detailed numerical investigation of the stress-strain behavior of cemented and uncemented Savar area clays under triaxial conditions have been carried out. This thesis attempts to use three advanced constitutive models within the critical state framework and a finite element program, to numerically simulate the stress-strain response of cemented and uncemented Savar area clays. The predictions have been carried out assuming both drained and undrained conditions. Some experiments were also carried out to investigate the load-displacement response of

model-scale footings and piles resting on remolded Savar area clays. The numerically simulated load-displacement response of model scale footings and piles using elasto-plastic finite element analysis were then compared with the experimental data.

In summary, in these research investigation critical state parameters of Savar area clay was experimentally determined. Detailed numerical analysis of these clays was then carried out, both in cemented and uncemented condition, and under drained and undrained assumptions. Experiments on model-scale footings and piles resting on remolded Savar area clays were also performed as part of this study. The load-displacement response of model-scale footings and piles on cemented and uncemented Savar area clays was carried out using elasto-plastic finite element analysis.

## **1.2 Aims and Objectives of Proposed Study**

The present study has been undertaken to achieve the following principal aims and objectives:

- Experimental determination of the engineering properties and critical state parameters of uncemented and cemented Savar area clay.
- Prediction of the stress-strain response, excess pore pressure and effective stress path of Savar area clays at various cell pressures and different degrees of cementation during triaxial shear under undrained condition using the Modified Cam Clay model
- Prediction of the stress-strain and volume strain response of Savar area clays at various cell pressures and different degrees of cementation during triaxial shear under drained conditions using the Modified Cam Clay model.
- Prediction of the stress-strain response, excess pore pressure and effective stress path of Savar area clays at various cell pressures and different degrees of cementation during triaxial shear under undrained condition using the Modified Modified Cam

Clay model i.e. MCC model incorporating cementation and with and without cementation breakdown assumption.

- Prediction of the stress-strain and volume strain response of Savar area clays at various cell pressures and different degrees of cementation during triaxial shear under drained conditions using the Modified Modified Cam Clay model i.e. Modified Cam Clay model incorporating cementation and Extended Modified Modified Cam Clay (EMMCC) model incorporating cementation breakdown assumption
- Investigate experimentally the load-displacement response of model-scale footings and piles resting on remolded Savar area clays under undrained conditions.
- Use the MCC and MMCC model and elasto-plastic finite element analysis for numerical prediction of the experimentally determined load-displacement response of model-scale footings and piles resting on cemented and uncemented Savar area clays.
- Comparison of the load-displacement predictions of elasto-plastic finite element analysis with experimental data of model scale footing and pile.

### **1.3 Limitations of the Proposed Study**

Following limitations were necessarily applicable to the scope of the present study are described:

- Experimental data of Savar area clays in triaxial shearing were not available. So the numerical predictions could not be compared with actual experimental data of triaxial shearing under drained and undrained condition.
- Simulation of the load-displacement response of model-scale footings and piles resting on remolded Savar area clays were for undrained conditions and axial loading only conducted in a consolidation mold. The specific conditions of the model-scale experiment may not be truly representative of field conditions.

#### **1.4 Outline of the Thesis**

In Chapter 1, the aims, objectives and limitations of the current research work have been described.

In Chapter 2, a literature review of clay and Dhaka clays behavior, constitutive modeling of soils and elasto-plastic finite element analysis is presented. This chapter also outlines the rationale for carrying out the present research study.

In Chapter 3, the Methodology and Equipment used in the current research work are described.

In Chapter 4, laboratory test procedure and the corresponding results, namely the determination of engineering properties and critical state parameters of cemented and uncemented Savar area clays are presented.

In Chapter 5, the Modified Cam Clay model is described. Numerical predictions of the stress-strain response, excess pore pressure and effective stress path of Savar area clays using the MCC model during triaxial shearing and undrained conditions are presented.

In Chapter 6, numerical prediction of Savar area clays during drained triaxial shear using the Modified Cam Clay model are presented. Comparisons of drained and undrained predictions using the Modified Cam Clay model are also discussed here. Finally, the limitations of the Modified Cam Clay model prediction of the stress-strain and volume strain response of Savar area clays are discussed.

In Chapter 7, the Modified Cam Clay model incorporating cementation termed in this thesis as the Modified Modified Cam Clay model (MMCC) is described. It is then used to predict both the drained and undrained stress-strain response of Savar area

clays during triaxial shearing. MMCC model predictions are compared with the predictions of the MCC model.

In Chapter 8, the Extended Modified Modified Cam Clay (EMMCC) model with cementation break down assumption is described. The EMMCC model is then used to predict both the drained and undrained stress-strain response of cemented and uncemented Savar area clays during triaxial shearing.

In Chapter 9, details of the experimental investigation of the load-displacement response of a model-scale footing and pile resting on remolded Savar area clays under undrained conditions is discussed. Numerical predictions of the load-displacement response of model-scale footing and pile resting on Savar area clays carried out using elasto-plastic finite element analysis were compared with experimental data.

Chapter 10 presents the main findings and conclusions of this study. Recommendations for further research are also included in this chapter.

## CHAPTER 2

### LITERATURE REVIEW

#### 2.1 Introduction

Clay soils are found all over the world. Innumerable varieties of clay soils are spread across different geographic areas and regions. They occur at various depths and extend to large areas both horizontally and vertically. Structures are built on clay and sometimes built with clay. Clays are thus one of the most important types of soils from the geotechnical perspective. Earth dams, road embankments, retaining structures, tunnels, pipes, various types of shallow and deep foundations are built on clay soils. The current research deals with the experimental and numerical study of Savar area clays, and the effect of cementation on such clays.

All clays exhibit some common characteristics. However, in spite of such a classification, clay soils show wide variation in their response to applied loads. These include stress-strain and settlement behaviour, failure behaviour and consolidation behavior. In addition, understanding the slope-stability, permeability, stiffness, sensitivity, plasticity etc. of clays is also important. Each of the above mentioned clay characteristics and behaviour has been the subject of intensive study and research in geotechnical literature (Bjerrum L., 1955, Casagrande A. and Wilson S. D., 1949, Casagrande A., 1944, Glossop R., 1968, Terzaghi K., 1943, Tschebotarioff G. P., 1951). The following sections present a detailed literature review of the properties and behaviors of clays

#### 2.2 Mechanical Properties of Clay

The study of the mechanical properties of clay primarily implies the study of its stress-strain behaviour. From geotechnical engineering considerations, the stress-strain response of clays is the one of the most important aspect of its behaviour. The stress-strain behaviour of clays has been extensively studied by many researchers

(Balasubramaniam, A.S., 1969, Mitchell, R.J., 1970, Nadarajah, V., 1973, Roscoe, K.H. and Burland, J.B., 1968, Roscoe, K.H. and Schofield, A.N., 1963). The mechanical behaviour of clay is determined by its microscopic or molecular structure. Figure 2.1 shows an idealized microscopic view of the structure of a clay soil. However, from geotechnical engineering considerations, it is considered more relevant and simpler to study and model the stress-strain response of clays from macroscopic considerations.

Superstructure loads are transferred relatively rapidly or almost immediately on the clay stratum. Because of the fineness of individual clay particles and its consequent low permeability, these loads are first and immediately transferred to the water trapped within the clay pores, rather than to the clay particle contacts. This results in the so called undrained condition. However, over relatively longer periods of time, these pore waters gradually seep or drain out of the pores as a response to the imposed loads. The superimposed loads are then transferred to the clay particle contacts. Hence over the longer term, the drained condition is attained. Thus, from the geotechnical perspective, it is important to understand both the short and long term response of clays to imposed loads i.e. the stress-strain behaviour of clays both under drained and undrained conditions.

### 2.2.1 Index Properties

There is a large body of geotechnical literature on the index properties of clays (Bjerrum, L., 1954a, Casagrande, A., 1932a, 1948, Foster, C.R., 1962, Lambe, T.W. and Martin, R.T., 1953-1957, Wagner, A.A., 1957). These studies include classification of clays based on grain size and hydrometer analysis as well as the tests involving natural moisture content and the Atterberg limits namely the liquid, plastic and the shrinkage limit. The advantage of index properties is that these are very simple and easy to determine, and interpret. Figures 2.2 and 2.3 show index properties of a typical clay stratum and some corresponding engineering properties. Properties such as the degree of over consolidation, undrained or cohesion strength, coefficient of consolidation have been correlated with plasticity index, natural moisture content,



liquid limit etc. Figures 2.4 to 2.9 show some typical relationships between index and engineering properties of clay soils.

### 2.2.2 Drained Behaviour

The stress-strain behaviour of clays under drained conditions have been extensively studied by various researchers (Henkel, D.J., 1959, 1960, Terzaghi, K. 1943. The drained stress-strain behaviour of clays have been found to be dependent both on the type of clay, as well as it's degree of overconsolidation or history of loading, structure and the degree of cementation of the clay. The effective stress principle enunciated by Karl Terzaghi (1943), provides the framework to rationally explain the stress-strain behaviour of clays under drained conditions.

In the laboratory, the drained stress-strain responses of clays are obtained either by the direct shear test or the triaxial test under very slow rate of load application. This allows the assumption of drained condition to be satisfied for the clay specimen's during shear. Results of drained direct shear tests in various clays have been widely reported in the literature (Bjerrum, L., 1954b, 1961, Bjerrum, L. and Landva, A., 1966, Henkel, D. J., 1956, Hermann, H. G. and Wolfskill, L. A., 1966, O'Neill, H. M. 1962). A drawback of the direct shear test is that the field conditions of stress are not replicated in the direct shear box. The more standard triaxial test overcomes this limitation by approximating the triaxial states of stress observed in the field. Drained tests show both friction angle and cohesion for clays. Drained triaxial tests have been carried out on various types of clays by Bishop A.W. and Henkel, D. J., 1962, Cadling, L. and Odenstad, S., 1958., Lambe T.W., 1951, Mitchell, J. K. and Gardener, W.S., 1975, Tavenas, F.A., 1975a.

Figures 2.10 and 2.11 represent the effective stress path in drained triaxial tests conducted on normally consolidated and overconsolidated clay respectively. Figure 2.12 represents the stress-strain curve in drained test. Figure 2.13 and 2.14 shows the Mohr-Coulomb strength envelop and the relation between peak and ultimate strength parameters of clay.

### 2.2.3 Undrained Behavior

The shear stress arising in the clay stratum as a consequence of the superimposed load has to be resisted by the intrinsic cohesion or undrained shear strength of the clay (Skempton, A. W., 1948, Skempton, A.W. and Golder, H. Q., 1948). The maximum load that can be imposed on a foundation overlying a clay stratum is defined to be the bearing capacity of the foundation in geotechnical literature. It is directly dependent on the undrained strength of the underlying clay stratum. When the ultimate bearing load of the foundation is exceeded, the stress on the slip plane in the underlying clay stratum exceeds the undrained shear strength of the clay. Once this happens, catastrophic failure and total collapse of the foundation and the superstructure may occur.

The bearing capacity of shallow and deep foundations resting on a clay stratum is dependent on the compressive strength of the clay under undrained conditions. Studies of bearing capacity of foundations have been carried out among many others by Casagrande, A., and Fadum, R.E., 1944, Chellis, R. D., 1962, Kerisel, J. L., 1967, Leonards, G. A., 1962, Skempton, A. W. 1942, Sowers, G.F., 1963.

The undrained stress-strain response of clays is obtained in the laboratory from direct shear or triaxial test under relatively rapid rate of load application. If pore water pressure measurements are made in an undrained triaxial test, stress-strain response may also be reported in terms of effective stresses. Generally, the direct shear test has no provision for measuring pore water pressure generated within the test specimen during shearing. Figures 2.15 and 2.16 show the effective stress paths from a consolidated undrained (CU) tests conducted on normally consolidated and over consolidated Weald clay respectively. Figure 2.17 show the qualitative stress-strain curves from the undrained triaxial tests conducted on normally consolidated clays. Figure 2.18 shows the actual stress-strain curves from triaxial tests on normally consolidated clays. Unconfined compression tests are undrained test of clays at zero

cell pressure. These tests are widely used as a simple and easy method to determine the unconfined compression strength and cohesion of the clay soil.

#### **2.2.4 Consolidation Behavior**

The consolidation behaviour of clays measures the time dependent settlement characteristics of clay. Foundations or structures on clay stratum frequently encounter large time dependent settlement behaviour, which if not properly accounted for, may cause severe cracks in as well as failure of the superstructure. The consolidation behaviour of clays have been extensively studied by Barden, L.,(1969); Biot, M.A., (1941); Ladd, C.C., (1973); Lambe, T.W. (1964); Newland, P.L. and Alley, B.H., (1960).

The consolidation characteristic of clay is determined by performing consolidation test on clay specimens and plotting the normal consolidation curve or the so called  $e$ -log $p$  curve or void ratio by log of mean effective stress curve of the clay. The consolidation test is used to obtain the coefficient of primary and secondary consolidation from the normal consolidation curve. Figures 2.19 to 2.21 show some typical consolidation curves of clay. Figure 2.22 shows time-settlement curves of clay for various magnitude of stress increment.

### **2.3 Cementation**

A problem frequently encountered during construction of structures or foundations on clay stratum is the lack of adequate cohesive or shear strength of clays. One approach, that is employed by many researchers and engineers, is to add chemical additives such as lime or cement to improve the strength or compressibility characteristics of clay. The effect of cement or lime on clay properties have been well studied by Ingles, O.G. and Metcalf, J. B., 1972; Kamon, M. & Bergado, D.T., 1992; Uddin, M.K. & Buensuceso, B. R., 2001, 2002; Wissa, A.E.Z. , Ladd, C.C. and lambe, T.W., 1965. Figures 2.23 to 2.25 show the effect of addition of lime or cement

and curing period on the unconfined compression strength of clays. These effects are described in detail in the subsections given below

### **2.3.1 Effect on Index Properties**

The effect of addition of lime and cement on the index properties of clays has been studied. It has been observed that water content or void ratio decrease as a result of addition of cement, while there is an increase in the unit weight and degree of saturation. Among the Atterberg limits, the plastic limit and plasticity index increase with cement content, with small or no reduction in the liquid limit. Significant increase of the unconfined compression strength and preconsolidation pressure is observed to occur as cement is added to clays. Figures 2.26 to 2.28 show the effect of cement treatment on some engineering properties of clay.

### **2.3.2 Effect on Drained Response**

The drained shear behaviour of cemented clays shows significant increase of shear strength. However, due to increased stiffness due to cementation, the shear strain at failure, in case of cemented clays, is observed to be significantly lower than that of uncemented clays. Figures 2.29 and 2.30 show the effect of cement content on the drained shear strength. Figure 2.31 shows the volume strain response of clays with various cement content.

### **2.3.3 Effect on Undrained Response**

Cementation of clays increases the undrained shear strength as well as shear stiffness. In undrained shear, the pore pressure response at a given cell pressure is generally lower for cemented clays as compared to uncemented clays. Figure 2.32 shows the effect of cement content on the effective stress path during undrained shearing. Figures 2.33 and 2.34 show the effect of cement content on the undrained stress-strain and pore pressure response.

### **2.3.4 Effect on Consolidation Response**

Cementation increases the apparent preconsolidation pressure of clay soils. It however decrease the slope of elastic rebound modulus i.e. it increase the elastic stiffness. The consolidation response beyond the preconsolidation pressure is however observed to be quite similar to that of uncemented clays. Figure 2.35 shows the effect of cement content on the isotropic consolidation response of cement treated clays

## **2.4 Review of the Stress-Strain Behaviour of Dhaka Clay**

It will be useful to briefly review the properties of Dhaka clay. Such an investigation helps us to identify the salient features that might be expected in Savar clays. The general characteristics of Dhaka clay has been described in the work of several authors (Siddique,A. and Safiullah, A.M.M, 1995, Siddique,A. and Sarker, J.K, 1998, Rahman, M.M 2000, Hasan, K.A, 2002, M.J, 2003 Hasan). Dhaka clay is generally identified as the clay located in depths of 25 ft to 30 ft above the sand layer in different areas of Dhaka region. The geologic and formation history of Dhaka clay is generally described to be as follows. These are clays from the Pleistocene Terrace Sediments and some smaller part of recent alluvium period.

### **2.4.1 Index Properties**

Index properties of Dhaka clay as obtained from the literature are as follows. The natural moisture content of Dhaka clays is observed to vary between 17 % to 37 %, the unit weight between 90 kPa to 115 kPa, liquid limit between 39 % to 50 %, and plasticity index ranges from 18 to 29. The unconfined compressive strength of Dhaka clays vary between 3 ksf to 10 ksf, Table A1.1 of Appendix1 lists some of the index properties (Uddin, 1990) and Table A1.2 of Appendix1 lists some of the geotechnical parameters of Dhaka clay (Ameen, 1986). Table A1.3 of Appendix1 shows the effect of cement treatment on engineering properties of Dhaka clay (Uddin. K, 2004)

#### **2.4.2 Stress-Strain Behaviour**

The drained and undrained stress-strain behaviour of Dhaka clays has been studied by the following authors (Islam, M.J, 2003, Rahman, M.M, 2000). These tests indicate that the stress -strain behaviour of Dhaka clay is similar to that of overconsolidated clays.

#### **2.4.3 Consolidation Behaviour**

The consolidation behaviour of Dhaka clays have also been studied by various authors (Islam, M.J, 2003). Figures 2.36 & 2.37 give some typical consolidation plots of Dhaka clays. These plots show that Dhaka clays generally have a medium value of void ratio, and the value of coefficient of consolidation indicates these are clays of medium compressibility. The overconsolidation ratios computed for Dhaka clays indicate them to be from lightly to heavily overconsolidated.

#### **2.4.4 Effect of Lime and Cement**

There has been a significant study on the effect of addition of lime and cement on Dhaka clays (Hasan, K.A, 2002, Hasan, K.A, 2002). These studies include the effect of percent of lime and cement added, and the curing period primarily on the unconfined compressive strength and cohesion, and less frequently on the Atterberg limits of clay. The tests conducted were generally the direct shear test or the unconfined compressive strength. Figures 2.38 and 2.39 give the results of some plots of the effect of addition of cement on the unconfined compression strength and cohesion of Dhaka clays. Figures 2.40 and 2.41 give the results of some plots of the effect of addition of lime of the unconfined compression strength and cohesion of Dhaka clays. Table A1.4 of Appendix1 summarizes the effect of cement content on the index properties of Dhaka clay, Table A1.5 of Appendix1 the effect of lime content on the index properties, Tables A1.6 and A1.7 of Appendix1 shows the effect

of cement and lime content respectively on the unconfined compressive strength of Dhaka clay.

## 2.5 Constitutive Modeling

Constitutive models are used to describe the relationship between the stress and strain of the soil. There are a variety of constitutive models describing the stress-strain relationships for various soils such as sand, or clays (Atkinson, J.H. and Bransby, P.L., 1978, Chen, W.F. and Mizuno, E., 1990, Dimaggio, F.L, and Sandler, I. S., 1971, Drucker, D.C. and Prager, W., 1952, Gens, A. and Potts, D.M., 1988, Lade, P.V. and Duncan, J.M., 1975, Lagioia, R. and Nova, R., 1993, Roscoe, K.H. and Burland, J.B., 1968, Schofield, A. and wroth, C.P., 1968, Yu, H.S., 1995). In some instances, these constitutive models have been modified to give the stress-strain relationship of cemented clays and sands (Lagioia,R. and Nova, R.1993). The following subsections describe some commonly used constitutive models to model the stress-strain relationship of clays.

### 2.5.1 Traditional Approach

The traditional approaches to model clay behaviour are given by the Tresca model, Von Mises model or the Mohr-Coulomb model. Figures 2.42 show the Mohr-Coulomb model in generalized as well  $I_1$ - $J_2$  space.

The drained stress-strain response of clays is generally obtained using the traditional Mohr-Coulomb model or the Drucker-Prager model. Figure 2.43 show the Drucker-Prager model in principal stress space. These models are of the elastic, perfectly plastic type and with few parameters. The advantages of these models are their relative simplicity, and routine implementation in finite element codes.

### **2.5.2 Modern Approach**

The real behaviour of clays is neither elastic, nor perfectly plastic. Rather clay behaviour is strain hardening, elasto-plastic with ultimate failure at critical state line. A framework based on these realities, was developed in the late sixties, came to be known as the Modified Cam Clay model. Two and three dimensional plots of the various aspects of the Modified Cam Clay behaviour are shown in Figures 2.44 to 2.45. The Modified Cam Clay model have been shown to give qualitatively good simulation of the stress-strain response of normally consolidated and lightly overconsolidated clays.

### **2.5.3 Stress-Strain Response of Cemented Clays**

The modeling of the stress strain response of cemented and structured clays has been receiving increasing attention in recent times. Models by Lagioia and Nova 1993, structured Cam Clay model by Liu and Carter, 2000 have incorporated cementation and structure effects.

## **2.6 Boundary Value Problems**

Engineering problems of structures interacting with soils are modeled with finite domains and boundaries. These problems are often termed as boundary value of problems in engineering. A suitable numerical approach is devised to predict the response of both the boundary and the domain to the boundary forces and restraints. The numeral methods used are the finite element, finite difference or boundary element type of method. Experimental model tests conducted on clay domains may be simulated using the finite element technique and constitutive or stress-strain models of clay. The qualitative and quantitative agreements between the experimental model test results and numerical predictions often allow us to make indirect judgments regarding the applicability of these models for describing clay behaviour.



### 2.6.1 Experimental Modeling

Many kinds of geotechnical engineering problems have been modeled experimentally in laboratories. A common boundary value problem is the experimental modeling of the load-displacement response of surface circular footings and single piles in clays (Barden, L. and Monkton, M.F., 1970, Hanna, A.M. and Meyerhoff, C.G., 1981, Tate, A.P.K. 1963, van Weele, A.F. 1957). A.K.M Anisur Rahman Siddiquee has completed his M.Sc reaserch on coastal clays of Bangladesh in BUET laboratory in 2006 by doing experimental investigation on model scale footing and pile. This allows a greater understanding of the relationship of the footing or pile load-displacement relationship with underlying clay properties. Figure 2.46 shows the settlement of model footing of various shapes at ultimate failure and Figure 2.50, 251 & 252 in Appendix III shows the experimental model scale footing and pile test on coastal clays of Bangladesh by Siddiquee 2006.

### 2.6.2 Numerical Modeling

The finite element method, coupled with an appropriate constitutive relationships to model boundary value problems. The stress-strain models commonly used for boundary value problems of surface circular footings and piles in clays is either the Mohr-Coulomb or Modified Cam Clay model. The Modified Cam Clay model appears to predict reasonably well qualitatively and to some extent quantitatively the load-displacement response of surface circular footing and piles on clays. Figure 253, 254 & 255 in Appendix III shows the numerical prediction of model scale footing and pile on coastal clays of Bangladesh by Siddiquee 2006.

### 2.6.3 Finite Element Method

The finite element method is widely used numerical method for civil engineering problems. The finite element techniques used for various problems has been

extensively described in the literature (de Borst, R. and Vermeer, P.A., 1984, Griffiths, D.V., 1982, Smith, I.M., 1982, Wroth, C.P. 1977, Zienkiewicz, D.C. and Naylor, D.J., 1971). The methods of discretization, numerical integration techniques, generation of element and global stiffness techniques, iterative solution techniques for elasto-plastic problems etc are all discussed in the finite element literature. Figures 2.47 through 2.49 show the domain modeling of footing and pile problems for finite element analysis.

## 2.7 Conclusion

The stress-strain properties of clays have been widely investigated in geotechnical engineering. The material properties of clays strongly influence the response of structures resting on clay strata. As clays in each region have distinctive characteristics, it is important to undertake serious investigation of the stress-strain behavior of clays in different regions. In this thesis, the properties of Savar area clays, in remolded condition and with the addition of cement, will be investigated in detail. The stress-strain behaviour of Savar area clays, both cemented and uncemented, will be simulated numerically under various conditions of drainage. Boundary value problem of model surface circular footings and piles in Savar area clays will also be experimentally and numerically modeled. These detailed investigations of the stress-strain behaviour of cemented and uncemented Savar area clays is expected to help in having a greater understanding of the clay soils of this area. The study is also expected to help assess the feasibility of soil improvement in this area using grouting or cementation techniques.

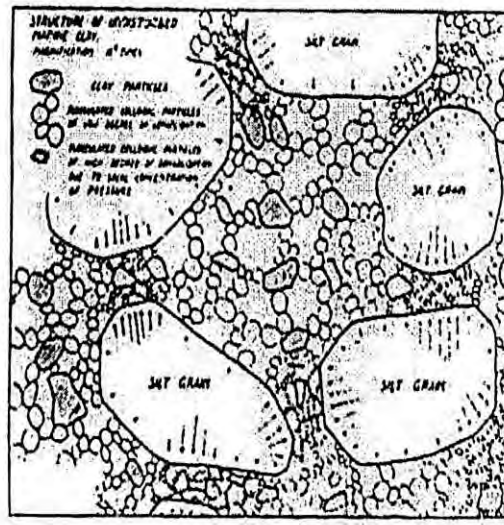


Figure 2.1 Idealized microscopic view of the structure of a clay soil (Casagrande A., 1932b)

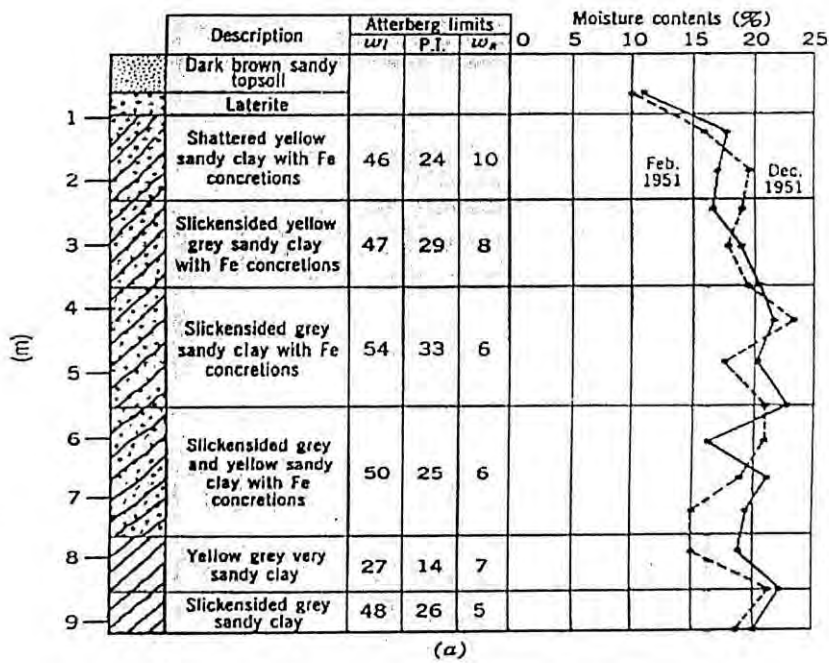


Figure 2.2 Index properties of clay in a layered stratum (Jennings, 1953)

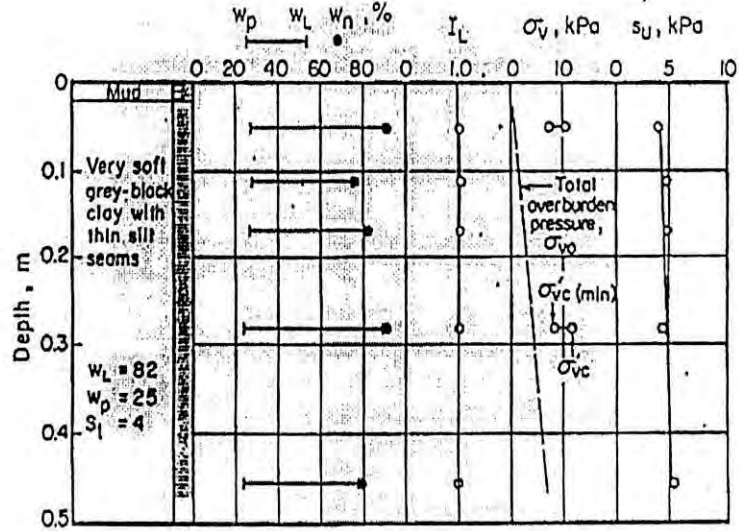


Figure 2.3 Index and related engineering properties of a clay stratum (Skempton, 1970)

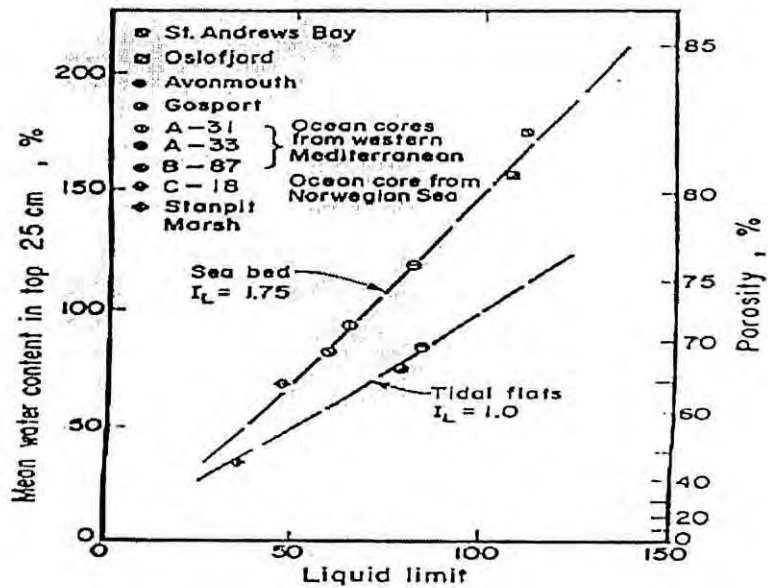


Figure 2.4 Relationship between water content and liquid limit a clay stratum (Skempton, 1970)

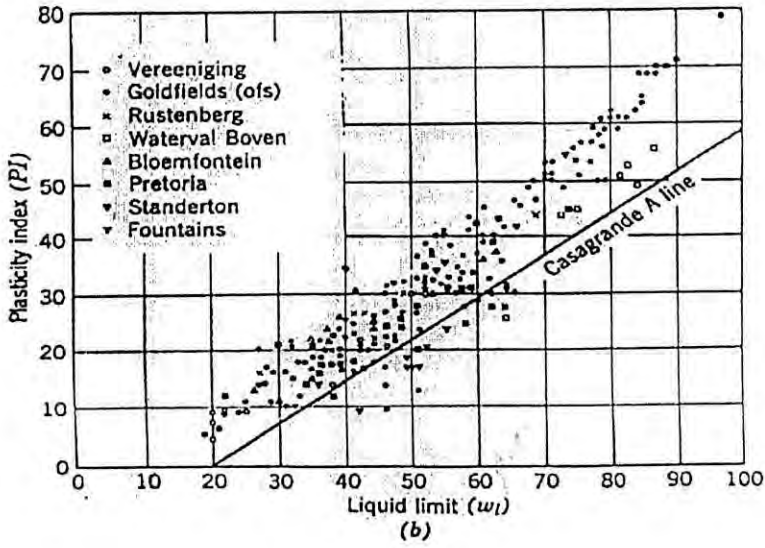


Figure 2.5 Variation of plasticity index (PI) with liquid limit (Jennings, 1953)

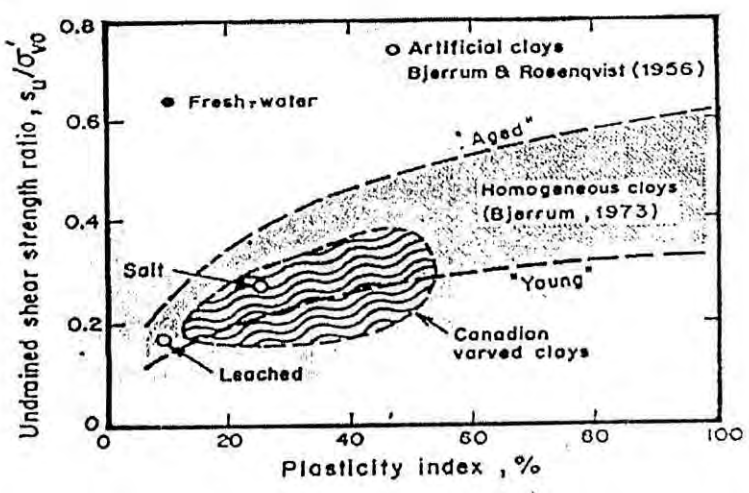


Figure 2.6 Variation of unconfined shear strength with plasticity index (PI) (Kenney, 1976)

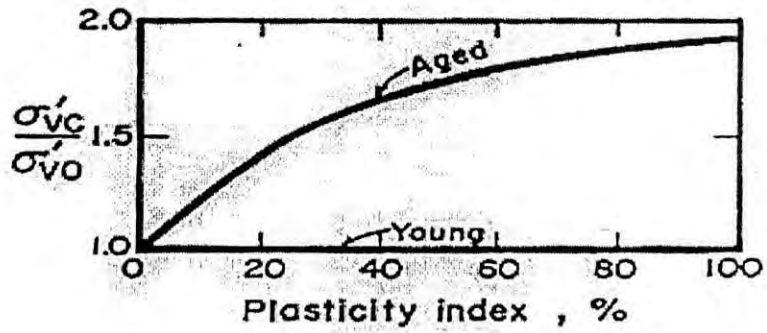


Figure 2.7 Variation of preconsolidation pressure with plasticity index (PI) in normally consolidated clays (Bjerrum, 1972)

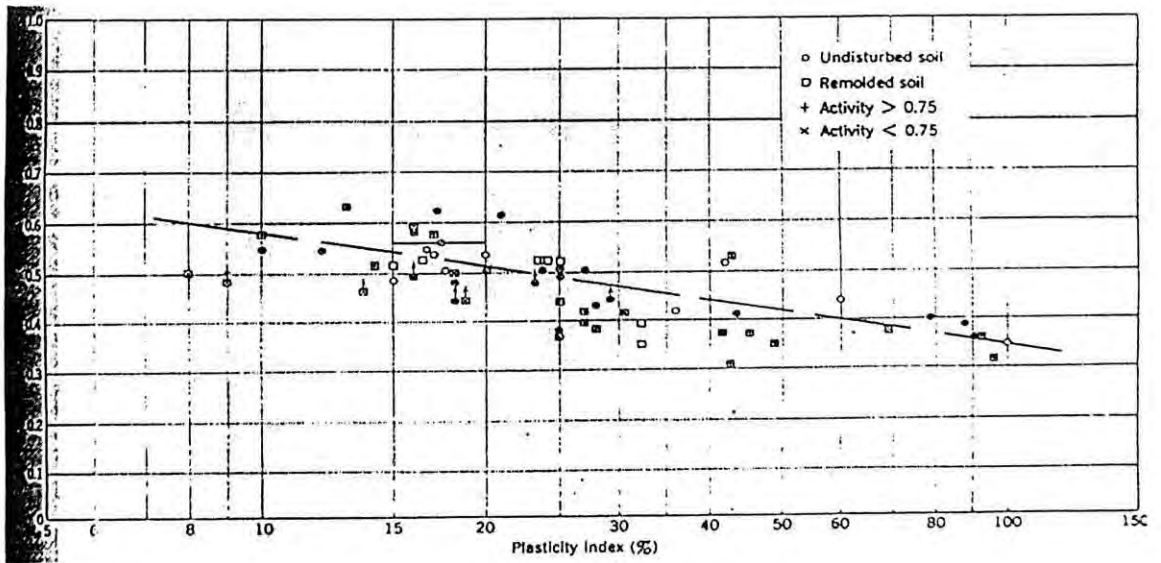


Figure 2.8 Relationship between drained friction angle and plasticity index (PI) of normally consolidated clays (Kenney, 1959)

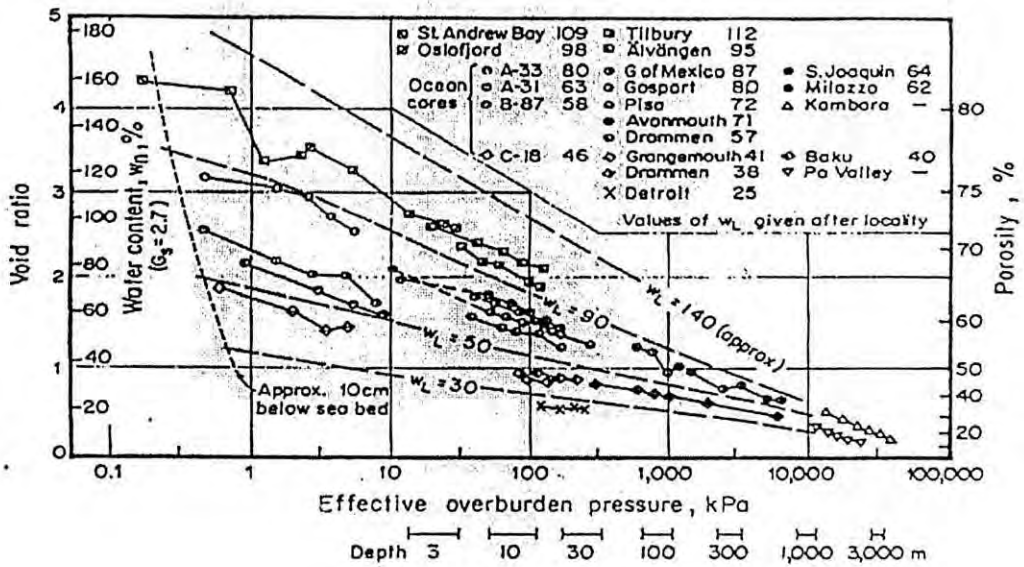


Figure 2.9 Variation of void ratio or water content with mean overburden pressure for normally consolidated sedimented clay (Skempton, 1970)

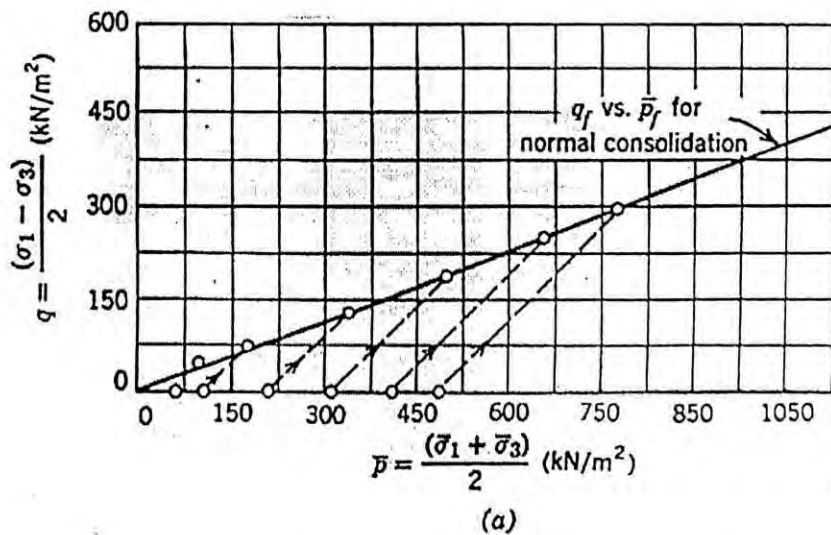


Figure 2.10 Effective stress paths from consolidated drained (CD) tests on normally consolidated clay (Lambe and Whitman, soil mechanics, 1979)

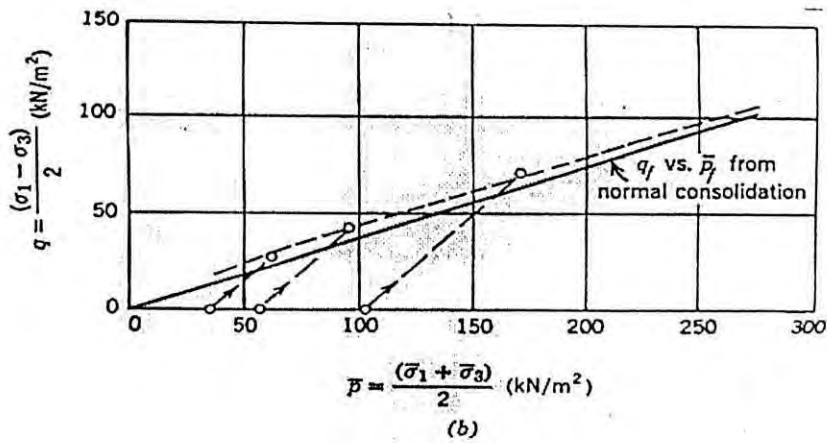


Figure 2.11 Effective stress path from consolidated drained (CD) tests on overconsolidated clay (Lambe and Whitman, soil mechanics, 1979)

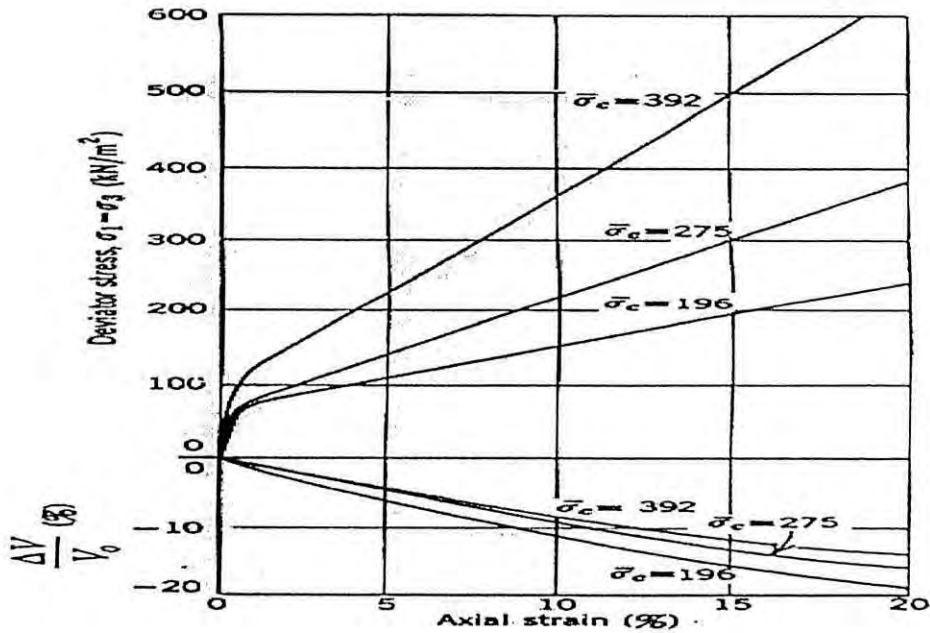


Figure 2.12 Drained stress-strain curves (CD tests) for undisturbed Leda clay (Crawford, 1959)



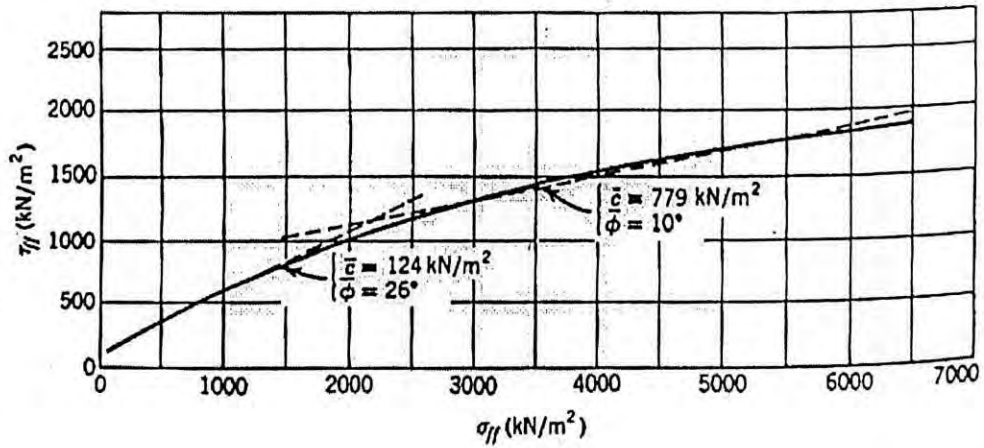


Figure 2.13 Strength envelop for unweathered London clay (Bishop et al, 1965)

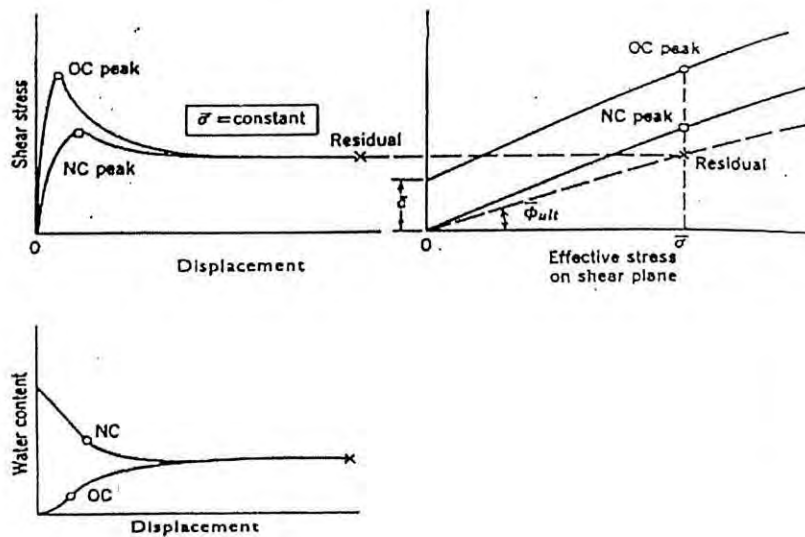


Figure 2.14 Mohr-Coulomb strength envelope, Mohr-Coulomb parameters and relation between peak and ultimate parameters (Lambe and Whitman, soil Mechanics, Jhon Wiley and Sons 1979)

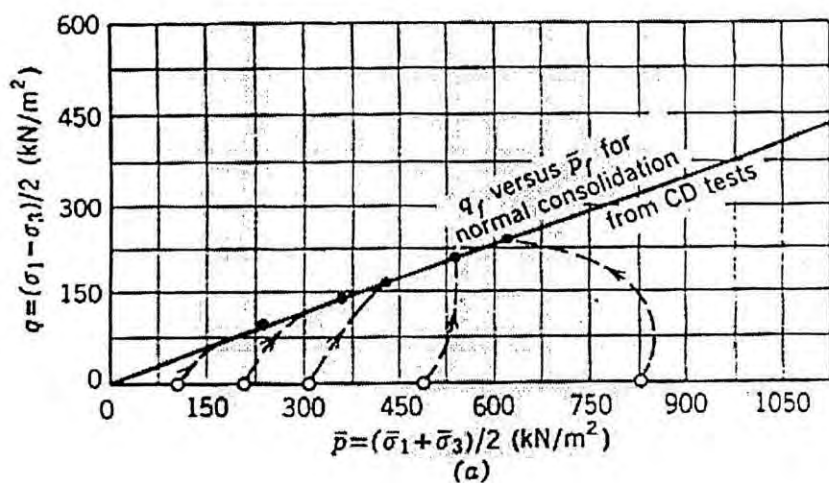


Figure 2.15 Effective Stress path in consolidation undrained (CU) test on normally consolidated Weald (Lambe and Whitman, soil Mechanics, Jhon Wiley and Sons 1979)

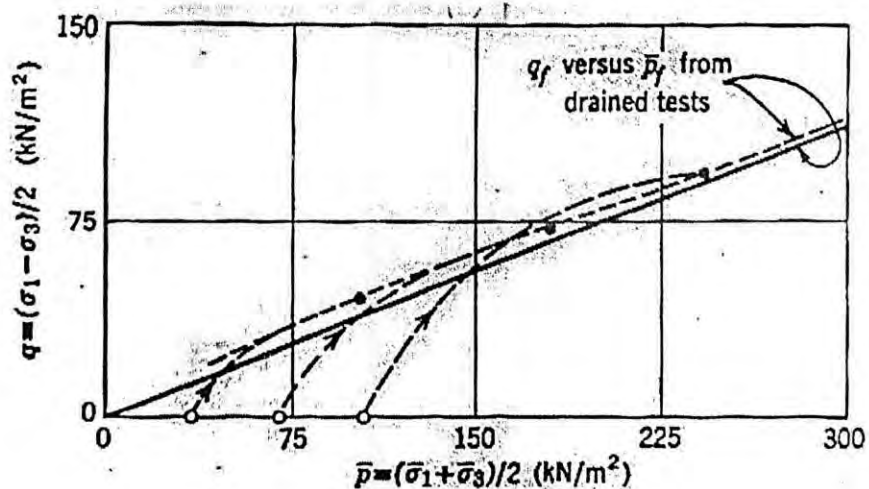


Figure 2.16 Effective stress path in consolidation undrained (CU) test on overconsolidated Weald clay (Lambe and Whitman, soil Mechanics, Jhon Wiley and Sons 1979)

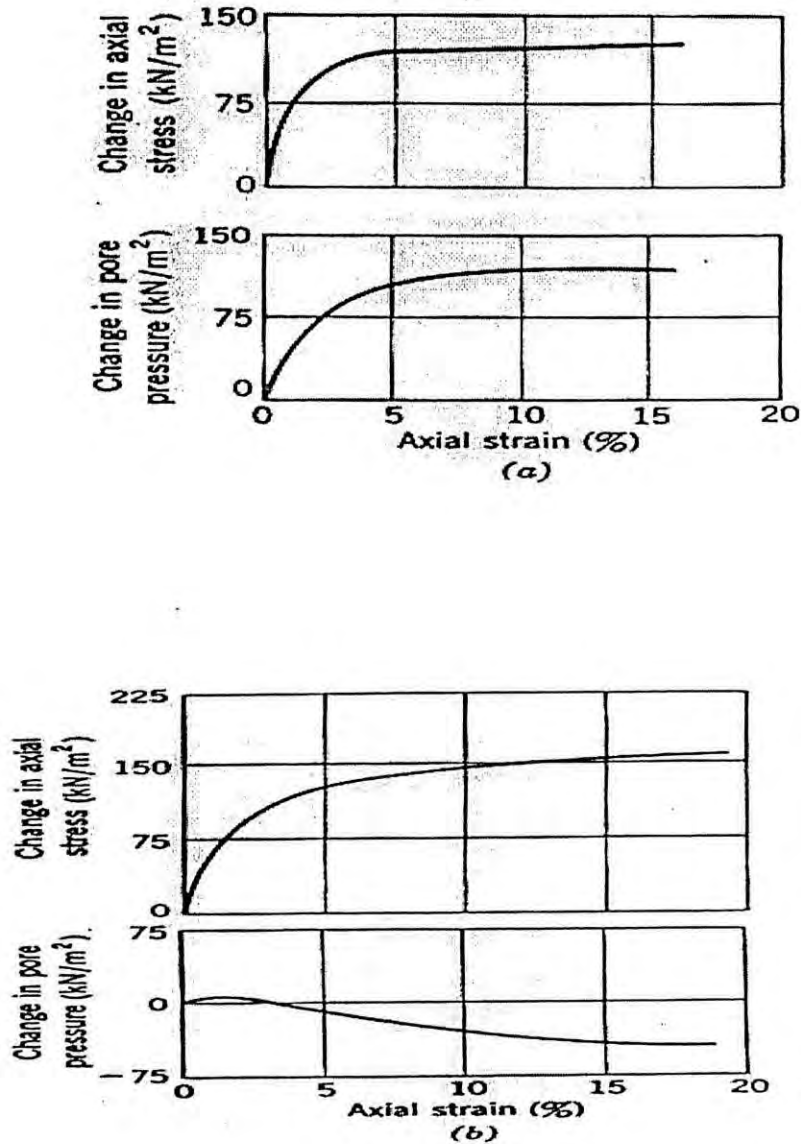


Figure 2.17 Qualitative stress-strain and excess pore pressure curves in consolidated undrained (CU) test on normally and overconsolidated Weald clay (Lambe and Whitman, soil Mechanics, Jhon Wiley and Sons 1979)

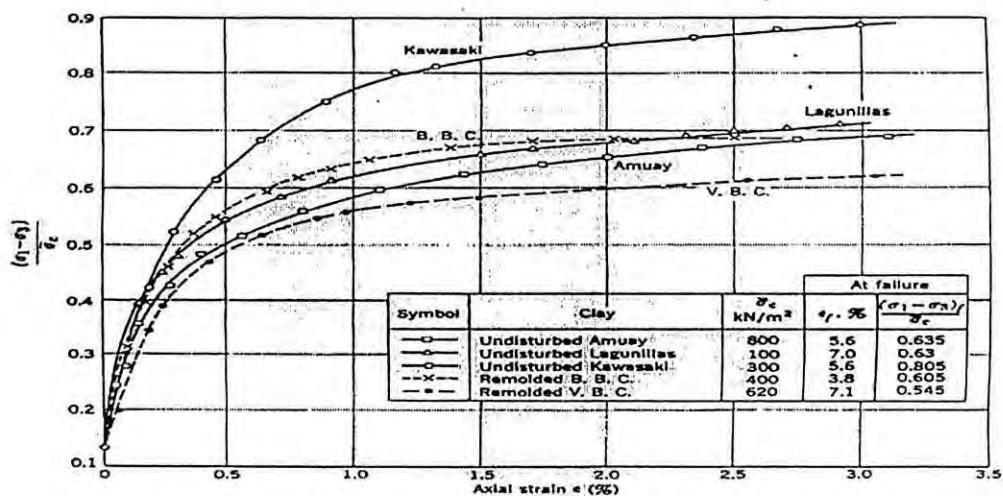


Figure 2.18 Stress- strain curves from triaxial test on five normally consolidated clay in undrained conditions (Ladd, 1964)

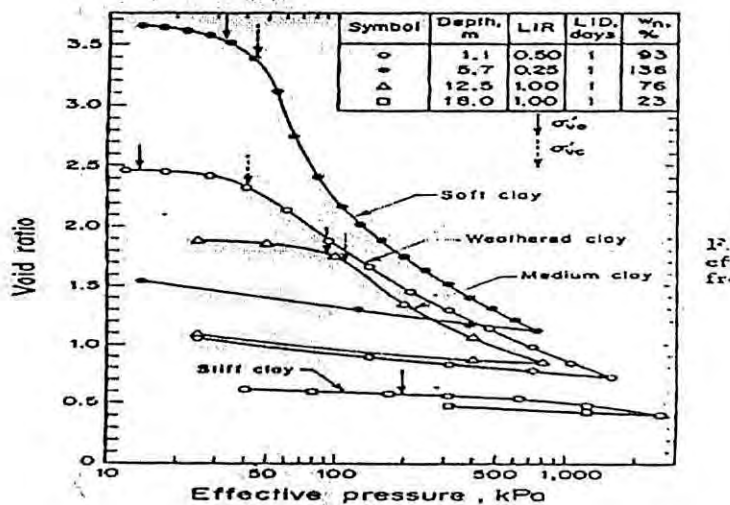


Figure 2.19 Typical consolidation curves for Bangkok clay from Bangpli (Balasubramaniam and Brenner, Soft Clay Engineering, Elsevier Scientific Publishing Company, 1981)

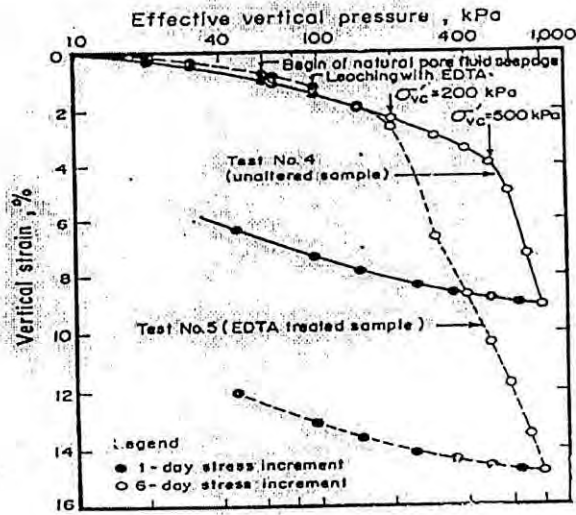


Figure 2.20 Effect of removal of cementing agents on consolidated curve of clay (Kenney et al, 1967)

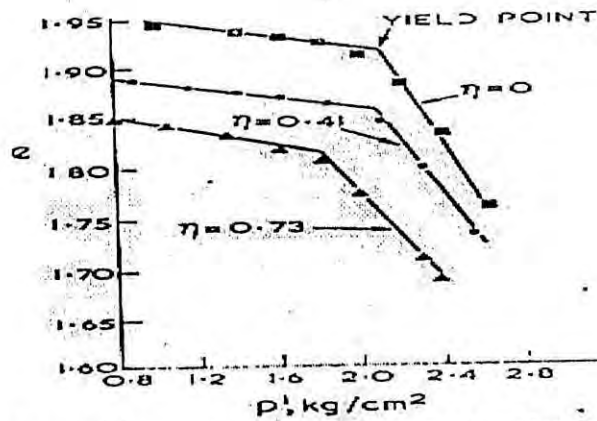


Fig. 4.14. Yield points in drained tests on Leda Clay (Mitchell, 1970).

Figure 2.21 Yield or preconsolidation pressure of drained consolidation tests on clay (Mitchell, 1970)

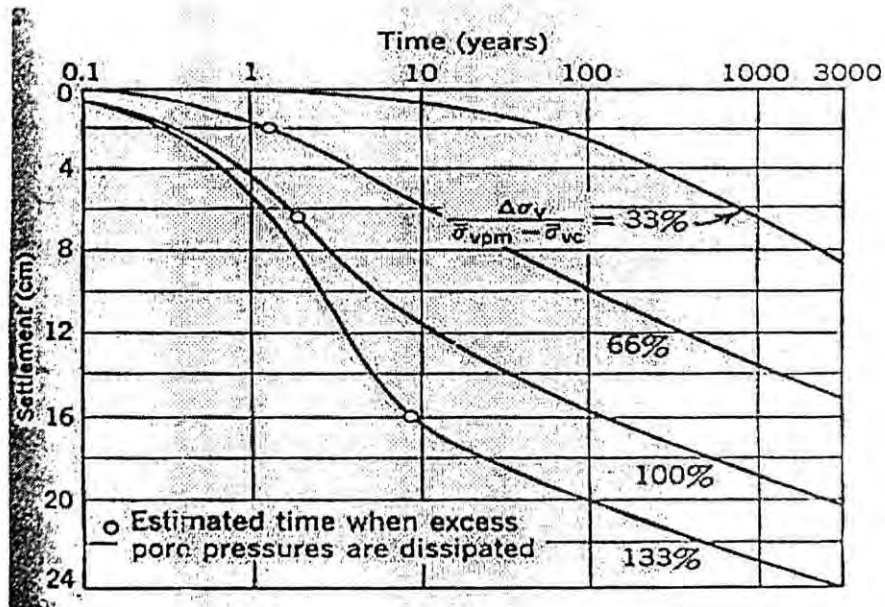


Figure 2.22 Time-settlement curves for different magnitudes of stress increment (Bjerrum, 1967)

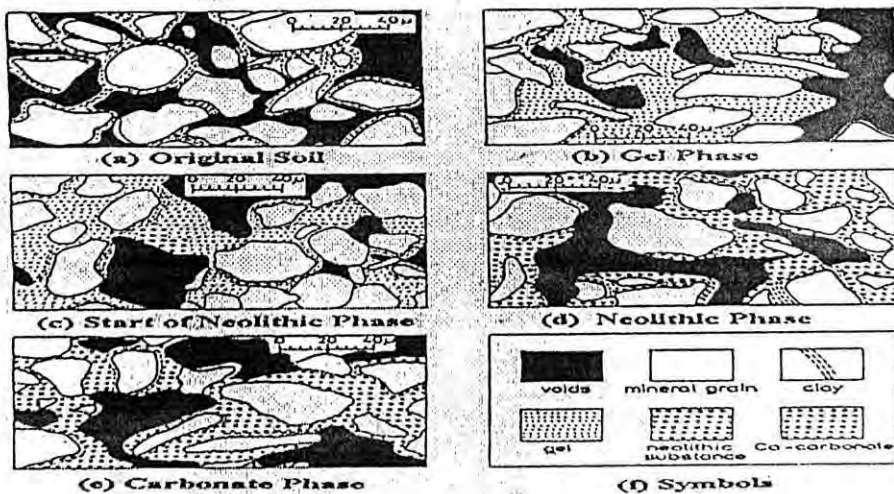


Figure 2.23.a. Effect of lime addition on clay structure (Kezdi, 1979)

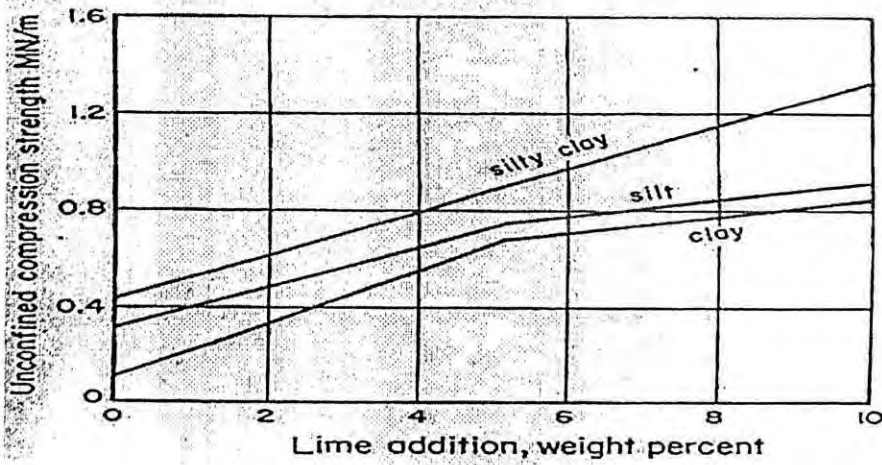


Figure 2.23.b. Effect of lime addition on compression strength of silt and clays (Kezdi, 1979)

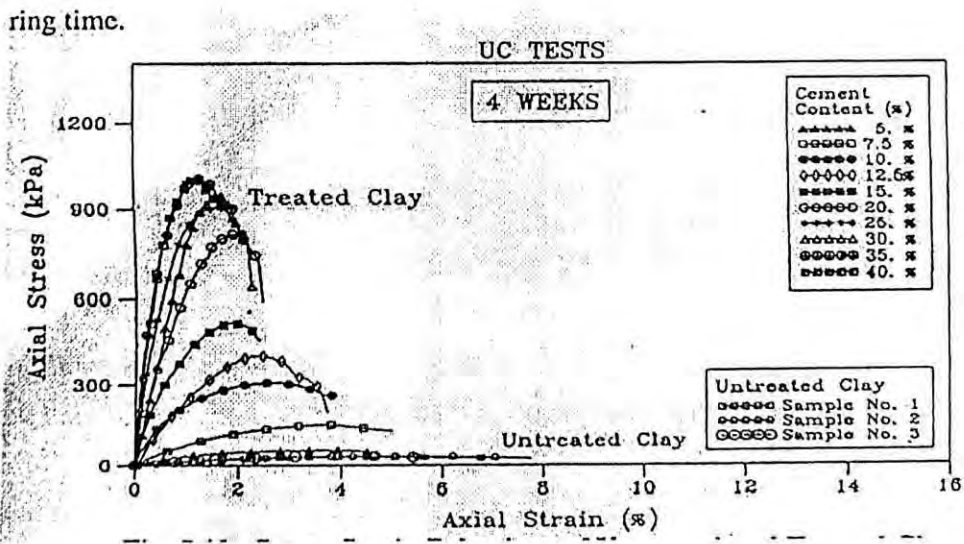


Figure 2.24 Effect of cement on unconfined compression strength and stress-strain behaviour of clays (Kamaluddin, Advanced Ground Improvement Techniques by cement and lime Treatment, 2004)

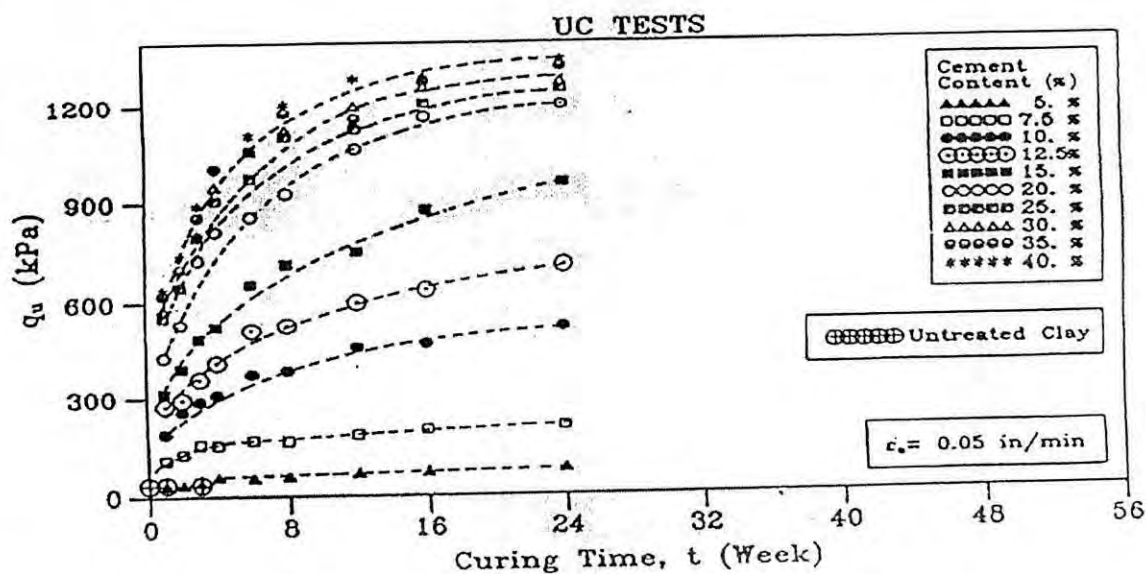


Figure 2.25 Effect of curing period on unconfined strength of cemented clay (Kamaluddin, Advanced Ground Improvement Techniques by cement and lime Treatment, 2004)

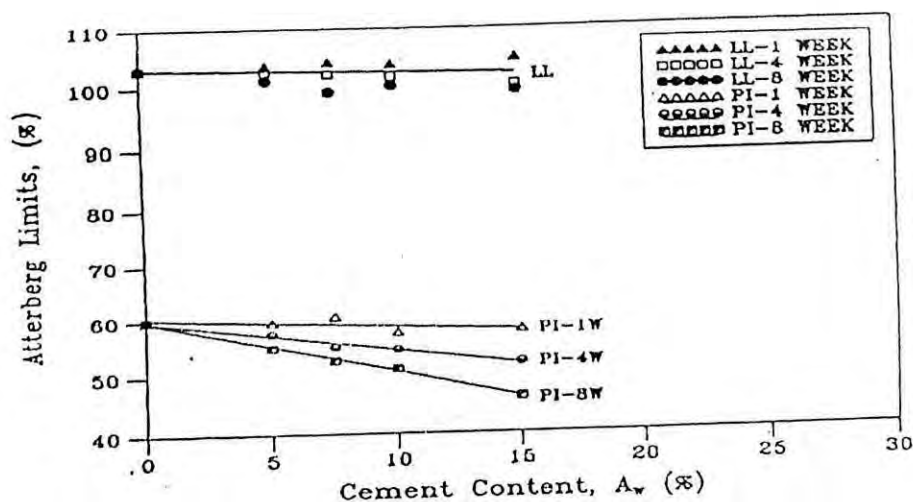


Figure 2.26 Effect of cement on the Atterberg limits of clay (Kamaluddin, Advanced Ground Improvement Techniques by cement and Lime Treatment, 2004)



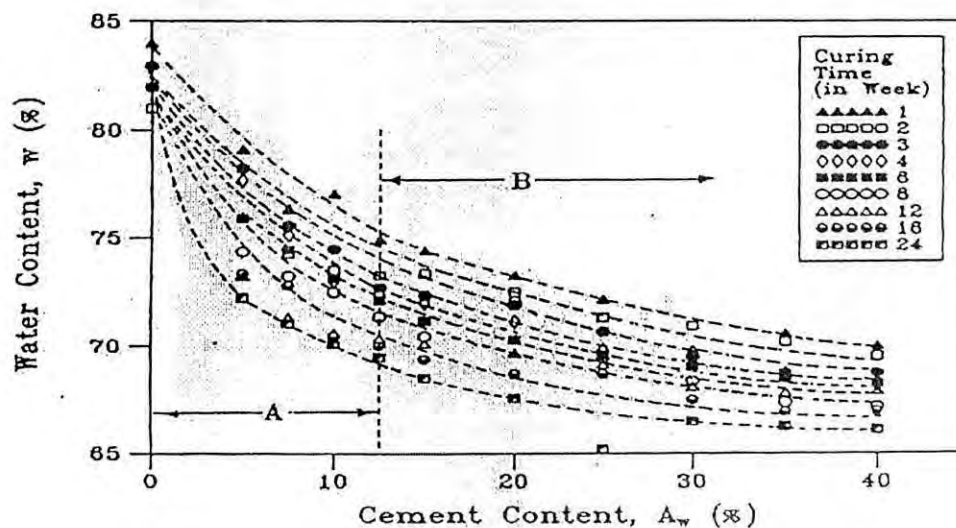


Figure 2.27 Effect of cement on the water content of clay (Kamaluddin, Advanced Ground Improvement Techniques by cement and Lime Treatment, 2004)

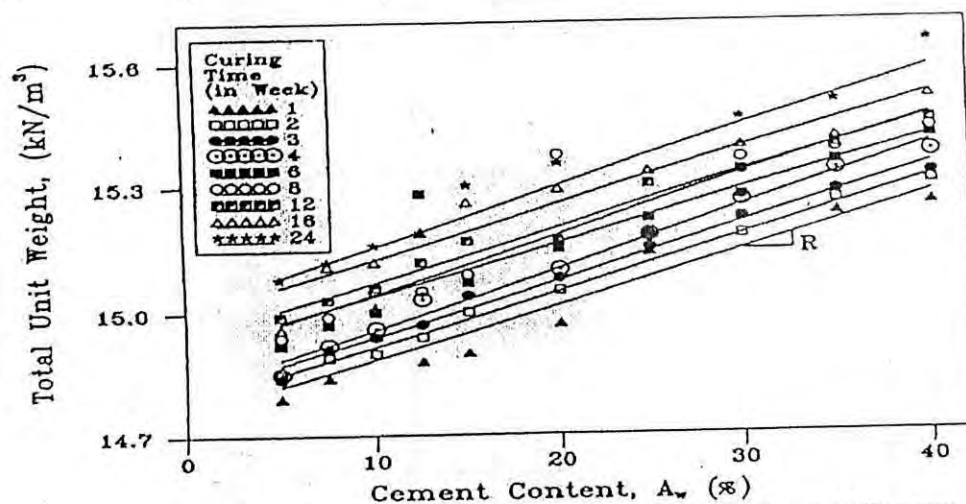


Figure 2.28 Effect of cement on the unit weight of clay (Kamaluddin, Advanced Ground Improvement Techniques by cement and Lime Treatment, 2004)

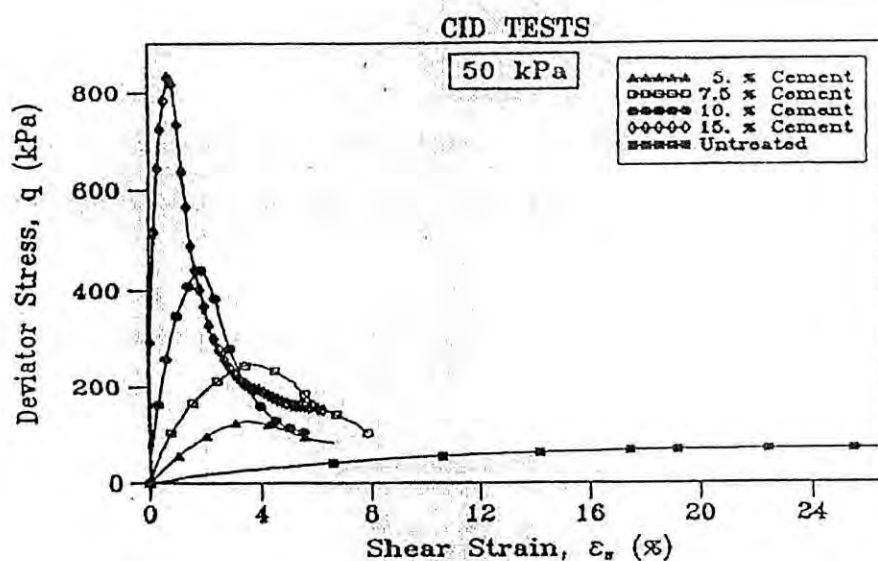


Figure 2.29 Effect of cement content on stress-strain curve during drained triaxial shearing of cemented clay at relatively low cell pressure (Kamaluddin, Advanced Ground Improvement Techniques by cement and Lime Treatment, 2004)

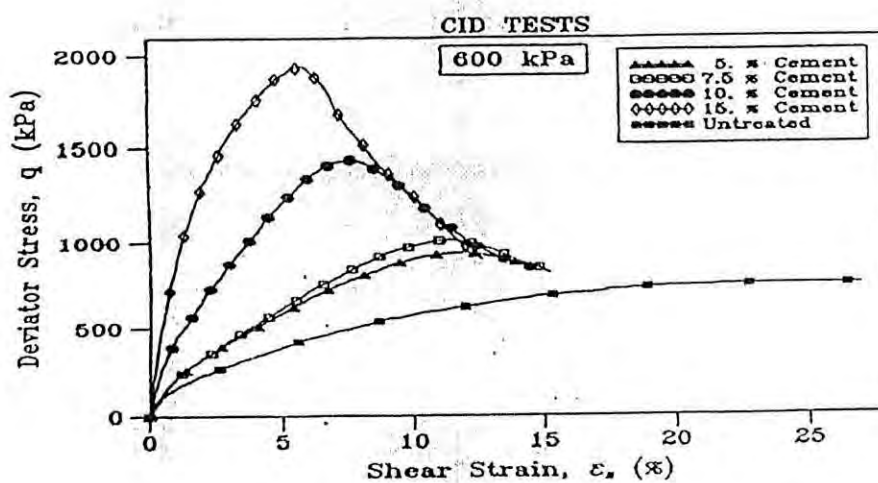


Figure 2.30 Effect of cement content on stress-strain curve during drained triaxial shearing of cemented clay at relatively high cell pressure (Kamaluddin, Advanced Ground Improvement Techniques by cement and Lime Treatment, 2004)

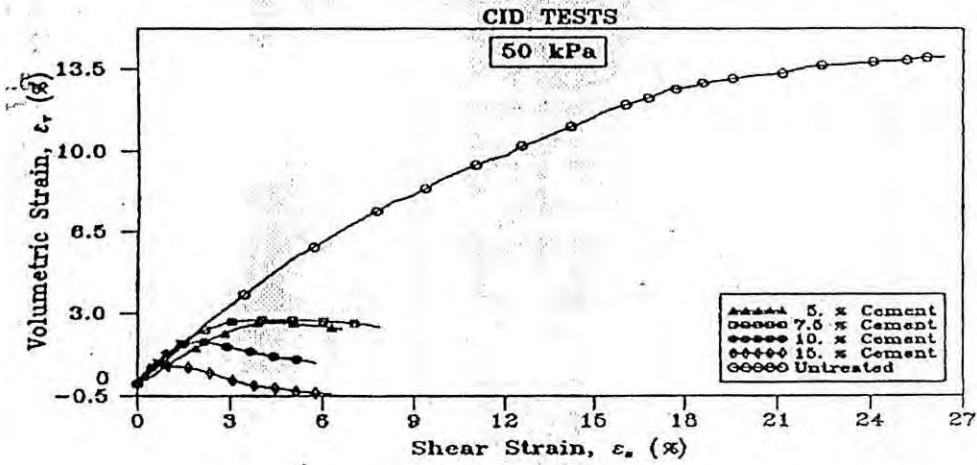


Figure 2.31 Effect of cement content on volume change response during drained triaxial shearing of cemented clay (Kamaluddin, Advanced Ground Improvement Techniques by cement and Lime Treatment, 2004)

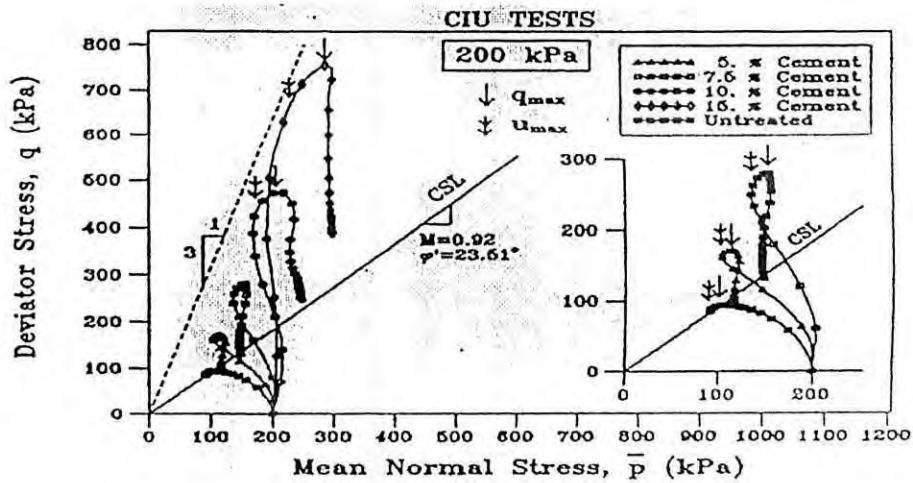


Figure 2.32 Effect of cement content on undrained stress path during triaxial shearing of cemented clay (Kamaluddin, Advanced Ground Improvement Techniques by cement and Lime Treatment, 2004)

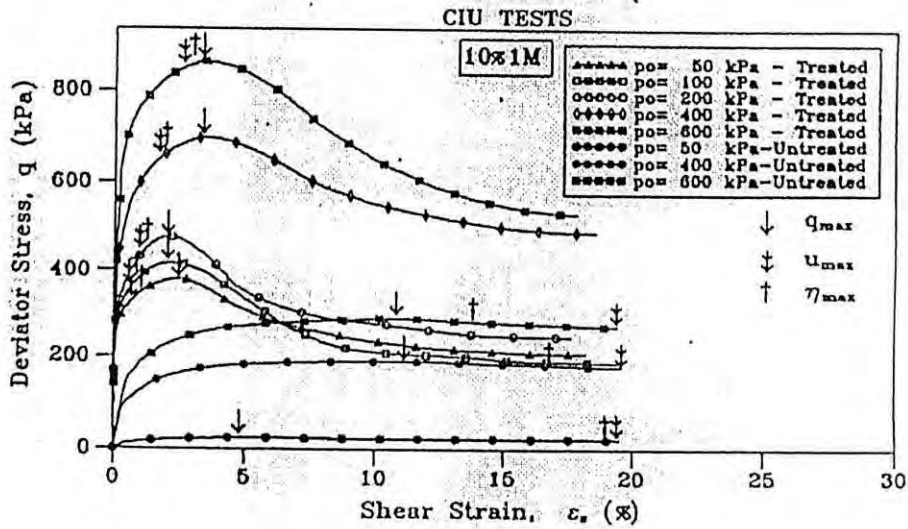


Figure 2.33 Effect of cement content on stress-strain during consolidated undrained (CU) test of cemented clay (Kamaluddin, Advanced Ground Improvement Techniques by cement and Lime Treatment, 2004)

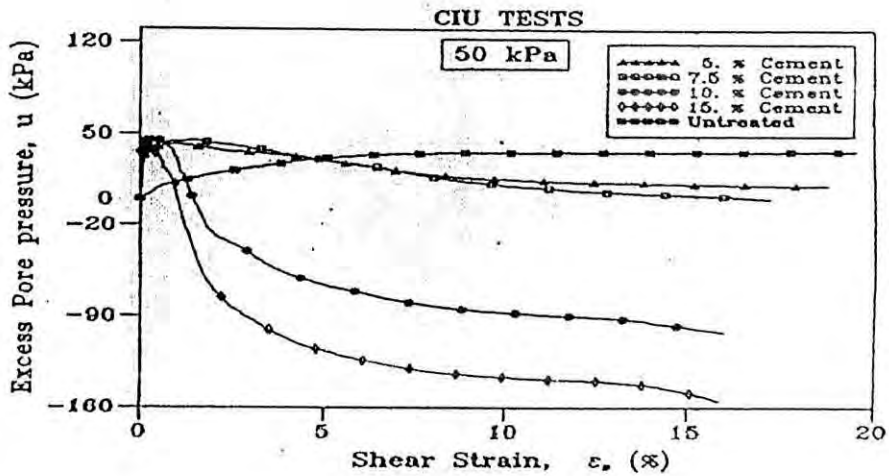


Figure 2.34 Effect of cement content on pore pressure response during consolidated undrained (CU) test of cemented clay (Kamaluddin, Advanced Ground Improvement Techniques by cement and Lime Treatment, 2004)

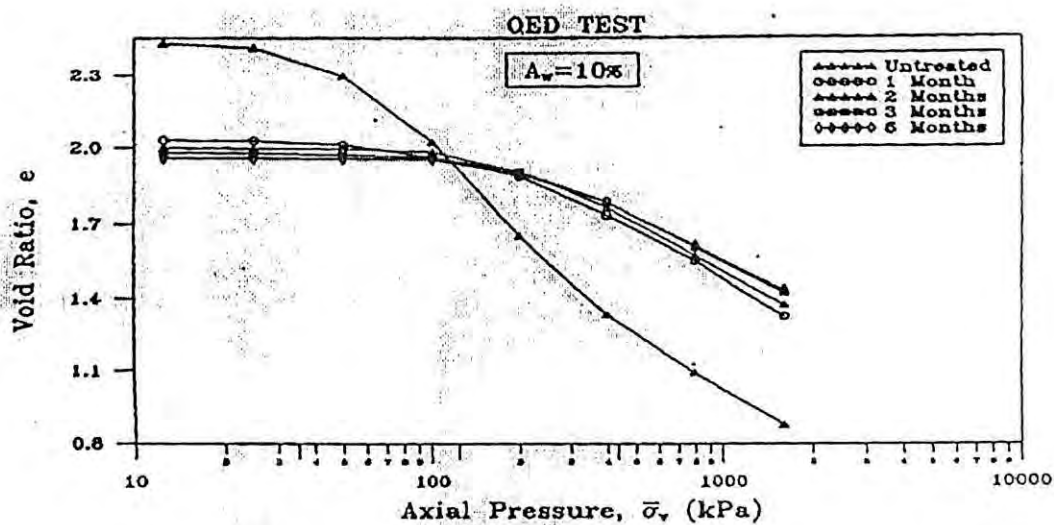


Figure 2.35 Effect of cement content on consolidation response of clay (Kamaluddin, Advanced Ground Improvement Techniques by cement and Lime Treatment, 2004)

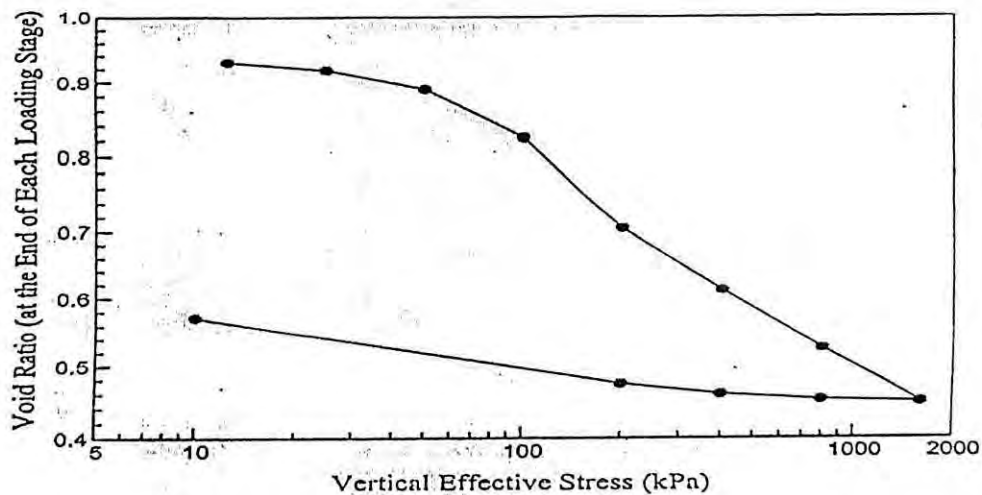


Figure 2.36 Void ratio vs log (Vertical Effective stress) Plot for one-dimensional consolidation test on Block sample of soft Dhaka clay (Islam, 2003)

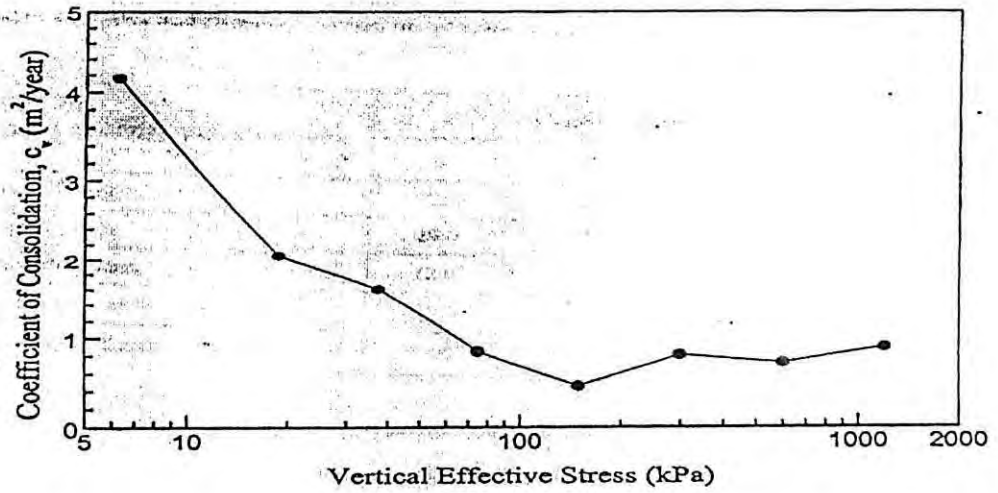


Figure 2.37 Coefficient of consolidation vs vertical effective stress plot for block sample of soft Dhaka clay (Islam, 2003)

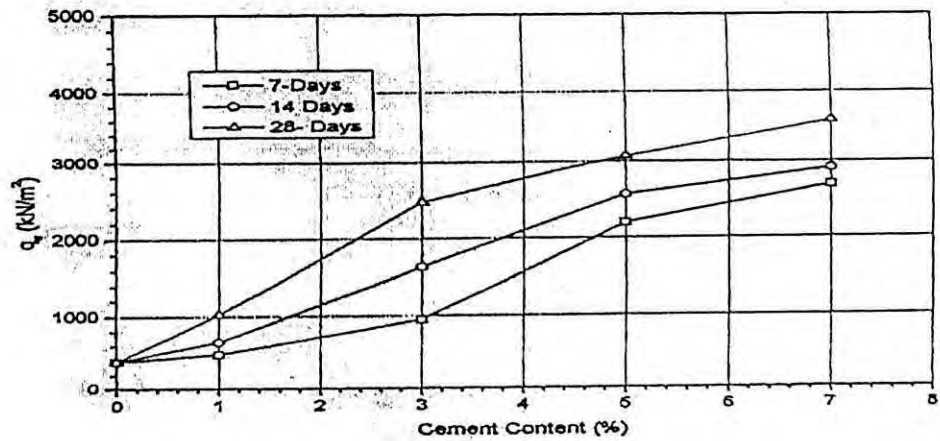


Figure 2.38 Effect of cement content on compressive strength of cement treated Dhaka clay (Hasan, 2002)

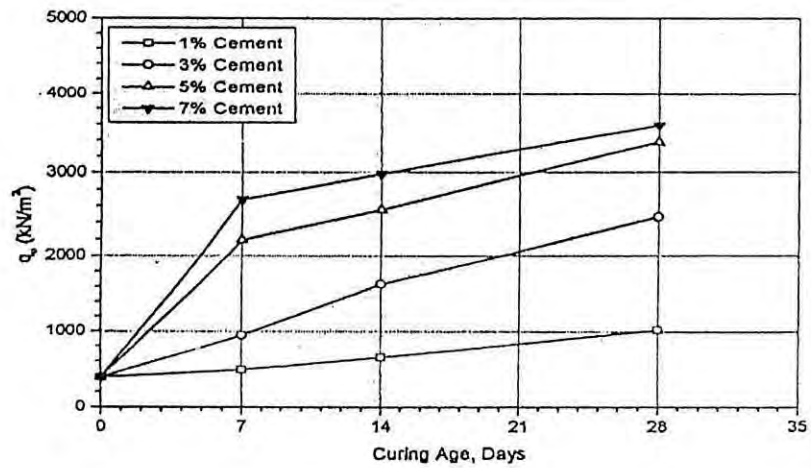


Figure 2.39 Effect of cement content on compressive strength of cement treated Dhaka clay (Hasan, 2002)

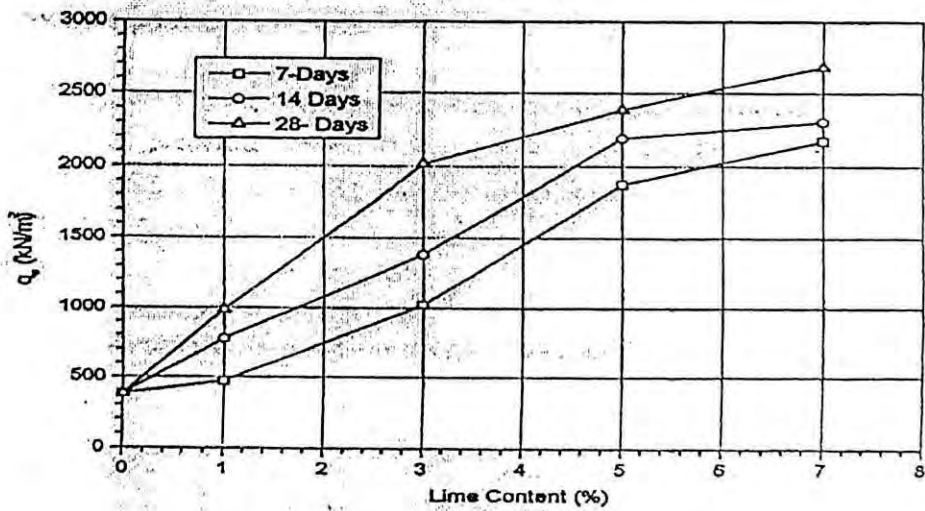


Figure 2.40 Effect of lime content on compressive strength of lime treated Dhaka clay (Hasan, 2002)

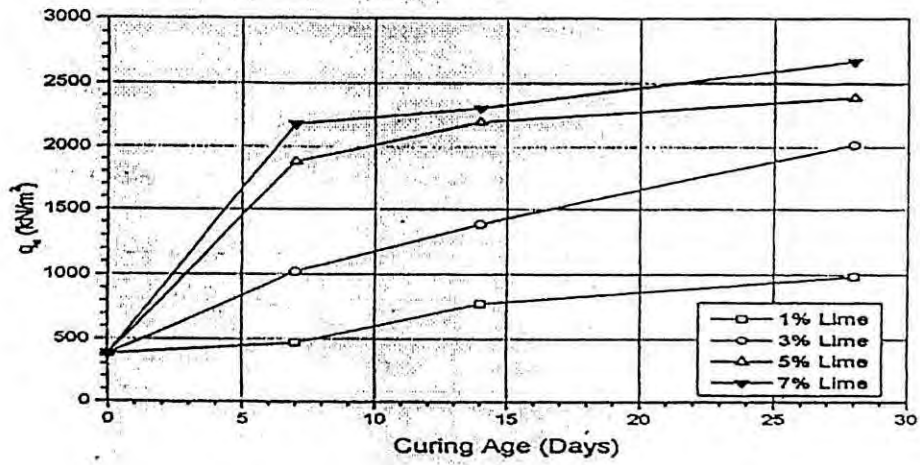


Figure 2.41 Effect of curing age on unconfined compression strength of lime treated Dhaka clay (Hasan, 2002)

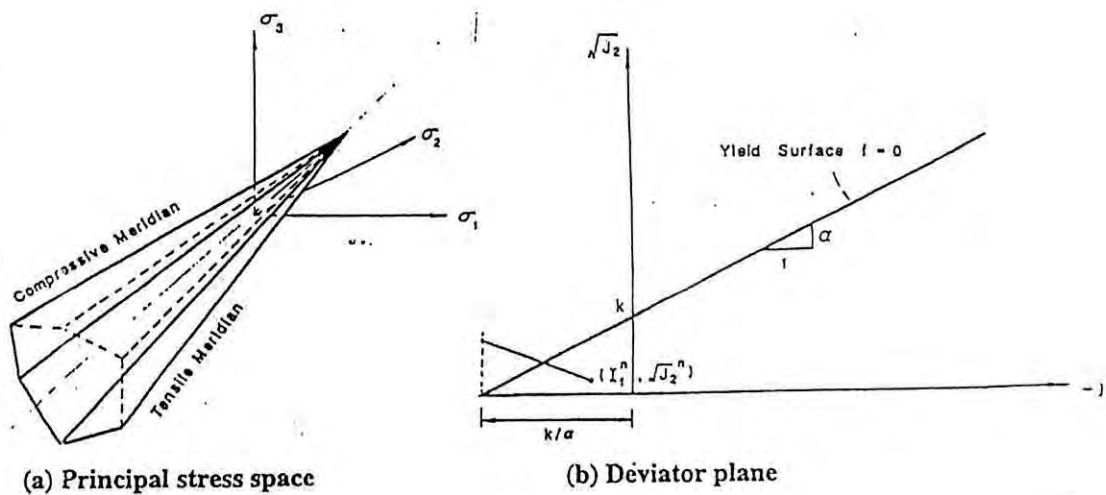




Figure 2.42 Mohr-Coulomb model in generalized and  $I_1 - J_2$  space (Chen and Mizuno, 1990)

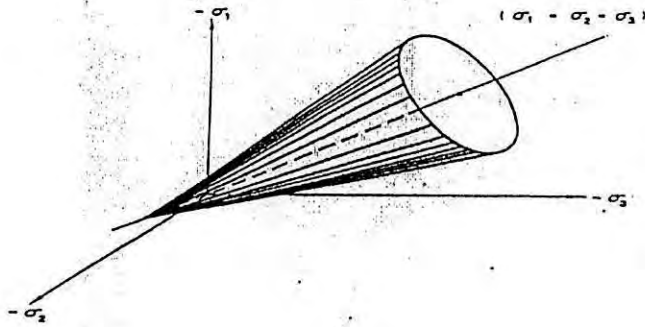


Figure 2.43 Drucker-Prager models in principal stress space (Chen and Mizuno, 1990)

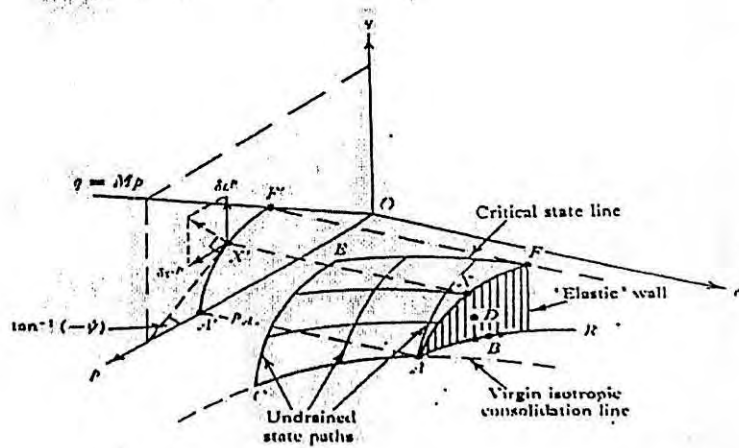


Figure 2.44 State Boundary surface in  $p', q, e$  space (Roscoe and Burland, 1968)

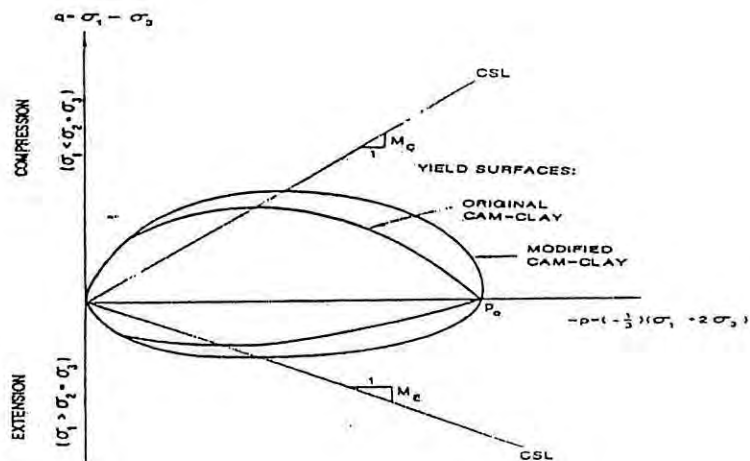


Figure 2.45 Cam Clay and Modified Cam Clay yield surface (Chen and Mizuno)

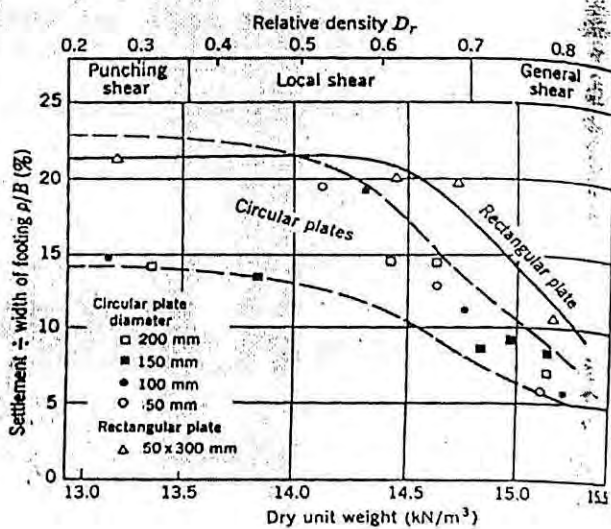


Figure 2.46 Settlement of model footing at ultimate failure (Vesic, 1963)

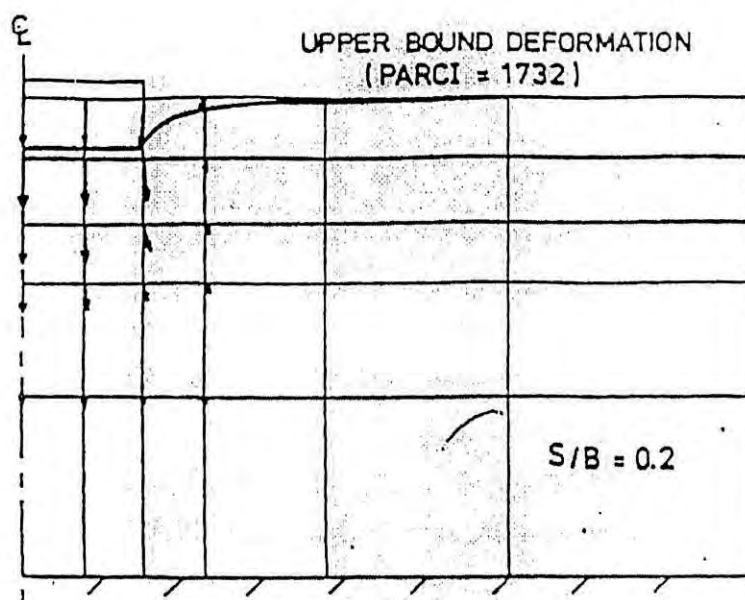


Figure 2.47 Finite element analysis of plate load test (Smith et al, 1968)

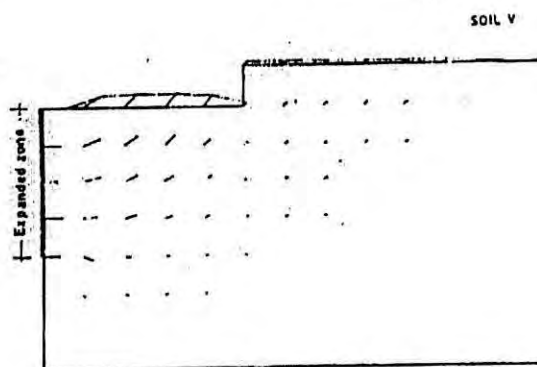


Figure 2.48 Finite element analysis of surface heave caused by pile driving (Massarsch, 1976)

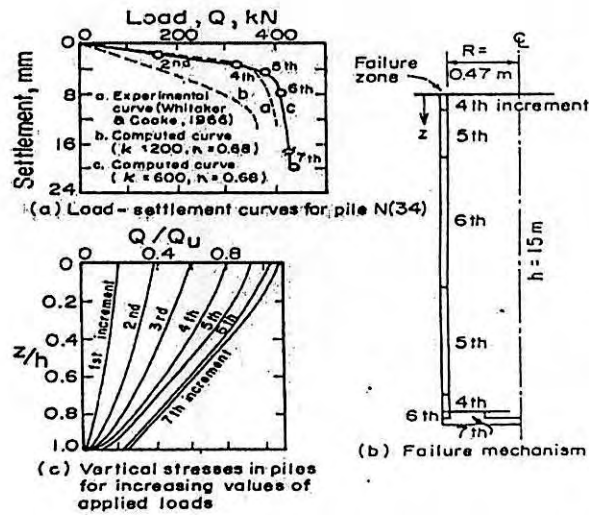


Figure 2.49 Result of finite element analysis of a single pile (Essu & Ottaviani, 1975)

## CHAPTER -3

### EQUIPMENT, INSTRUMENTATION AND METHODOLOGY

#### 3.1 Introduction

One of the major objectives of this work is to simulate the stress-strain behaviors of uncemented and cemented Savar area clays using critical state soil models. For this purpose, it is necessary to determine appropriate soil parameters to be used as input in these soil models. A series of laboratory tests was carried out to determine the input soil parameters. In this chapter, the equipments used for the determination of geotechnical parameters are described in detail for the sake of completeness. The basic equipments and instruments used are described below in different articles. In addition, a simple setup used for performing model footing and steel piles in cemented clays under  $K_0$  consolidation condition is also described here.

#### 3.2 Equipment Used

The equipment that was used for determining the various soil parameters of Savar clay are described below. An unconfined compression device was used to determine the undrained shear strength of the remolded Savar clay as well as the remolded clay cemented artificially by ordinary Portland cement to 7 % and 14 % of the weight of the clay. The direct shear apparatus was used to determine the friction angle of the remolded and artificially cemented Savar clay. This friction angle was used to compute the critical state parameter  $M$  for the Modified Cam Clay model and its variations used in this thesis. Soil slurry was prepared for preparing quality remolded samples. For this purpose, a rotary mixer was used. A consolidation cell was used for consolidation of the soil slurry under  $K_0$  consolidation condition. The one-dimensional consolidation apparatus was used

to determine the elastic and plastic compressibility parameters ( $\lambda$  and  $\kappa$ ) of the remolded Savar area clay.

### 3.2.1 The Rotary Laboratory Mixer

For producing uniform soil slurry, a Hobart mixer machine was used. A photograph of the Hobart rotary mixer machine, bowl and attachment is shown in Figures 3.1. The rotary blades of this machine ensure proper mixing of soil particles with water over a short period of time at the required moisture content. The mixture machine used has dimensions of 738mm x 406mm x 489mm and includes a three speed gear box driven by a fully enclosed and ventilated motor. The shift handle is connected mechanically with the switch, giving definite gear location. It is necessary to switch off the motor before changing gears. The beater shaft is carried on ball bearings. The bowl used to prepare the slurry, locks at the top and bottom of lift travel. The lift travel is controlled by a convenient hand lever.

### 3.2.2 Apparatus for $K_0$ Consolidation of Slurry

For  $K_0$  consolidation of slurry, a consolidation mold attached to a loading frame was used as shown in Figure 3.2. The dimension of the consolidation mold was as follows: 210 mm internal diameter and 180 mm in height. The cylindrical consolidation cell, containing the soil slurry was placed on a rigid platform. The platform was raised manually by rotating a wheel. In this way, the loading of the soil sample was achieved using a loading ram and proving ring. In this process, continuous manual operation was required to adjust position of the consolidation mold with deformation of the soil to maintain required pressure on the sample. The proving ring was calibrated. The dial gauge attached with the proving ring could be used measure the deformation of the proving ring. The load imposed on the soil sample could be computed at any stage of consolidation from the proving ring dial reading using the calibration constant of the ring.

### 3.2.3 Unconfined Compressive Strength Apparatus

The unconfined compression apparatus was used to measure the unconfined compressive strength of the remolded and cemented Savar clay. The unconfined compressive apparatus consists of a compression type-loading ram. A screw-jack-activated loading yoke was used to apply the load to the soil. The axial load applied to the soil was measured by means of deformation of a proving ring dial gauge. The deformation of this dial gauge may be used with the calibration constant of the proving ring to compute the load applied to the cylindrical soil specimen used to measure the unconfined compressive strength. Loading rate is usually controlled manually by turning a hand lever. In this way, axial strains of 0.5% to 2% per minute may be applied. A photograph of the unconfined compression test apparatus with its various parts is shown in Figure 3.3.

### 3.2.4 Direct Shear Apparatus

The direct shear test was used to determine the ultimate friction angle of remolded and artificially cemented Savar clay. The friction angle of the remolded and artificially cemented clay was then used to compute the critical state parameter  $M$  for the soil. The shear box of the shear testing equipment used was of standard size (63.5mm in diameter and 25.4mm high). The shear box is split into two halves. The shear box was filled with remolded clay and the top half of the box was slowly and gradually moved over the bottom part of the box, shearing the soil specimen at the interface. A photograph showing the shear box, loading arrangement and frame of the direct shear apparatus is shown in Figure 3.4. The box is circular in section and it is split horizontally at the center level of the soil specimen. The lower half of the box is rigidly held in position in a container. The container as well as the lower part of shear box slides forward at a constant rate by a geared jack. The jack is driven by an electric motor. The shear force applied on the upper half of the box is indicated by a calibrated steel-proving ring through a proving ring dial

gauge. The movement of the lower part of the box is transmitted through the specimen to the upper part and hence, on to the proving ring. The resulting deformation of the proving ring dial gauge may be used to compute the applied shear force on the soil specimen. Metal grids and porous stones are used both at the top as well as the bottom side of the soil specimen. Normal load is applied on the specimen from a loading yoke, which applies pressure on a metal pad through a steel ball. The volume change during consolidation of the soil as well as during the shearing process is measured by a dial gauge mounted at the top of the box. The test is thus of a strain-controlled type. The rate of shear displacement or strain within the specimen could be controlled precisely using appropriate gears of the motor controlling the movement of the shear box. The soil specimen and the shear box may be submerged in water and the drainage of water from or to the soil (as the case may be for either normally consolidated or over consolidated specimens) through the porous stones may also be allowed for drained shearing of the soil specimens.

### **3.2.5 Apparatus for One-Dimensional Consolidation Test**

A one-dimensional consolidation apparatus was used to measure the elastic rebound and plastic consolidation parameter of the remolded and cemented Savar clays. A specified pressure was applied on the soil specimen by a jack, which is measured by a balance scale. The ring used for the sample soil specimen was 63.5mm in internal diameter and 25.4mm high. Two porous stones with filter paper were used to provide drainage from both top and bottom of the sample. A dial gauge was used to measure axial deformation during consolidation. A photograph of the one-dimensional consolidation apparatus is shown in Figure 3.6



### 3.2.6 Model Steel Circular Footing and Pile

A model steel circular footing 20 mm in diameter and a model steel pile 75 mm in length and 20 mm diameter with a pile cap was manufactured in the machine tools laboratory. Soil slurry consisting of Savar clay was  $K_0$  consolidated at a given pressure on the consolidation of 210 mm internal diameter and 180 mm height as described in section 3.2.2. The model steel footing was then rested at the center of this circular consolidation mold. The loading frame of the consolidation mold was used to gradually apply steady pressure on the model steel footing and the pressure applied to the footing as well as the displacement of the model footing was recorded. Similar experiments to obtain the pressure-displacement response of model footings were conducted by consolidating a mixture of ordinary portland cement and Savar clay slurry in the consolidation mold at various proportions. In the same way, the model steel pile with circular pile cap was pushed into consolidation mold containing remolded Savar clay and artificially cemented Savar clay respectively. Similar pressure-displacement response test of the model piles were then carried out.

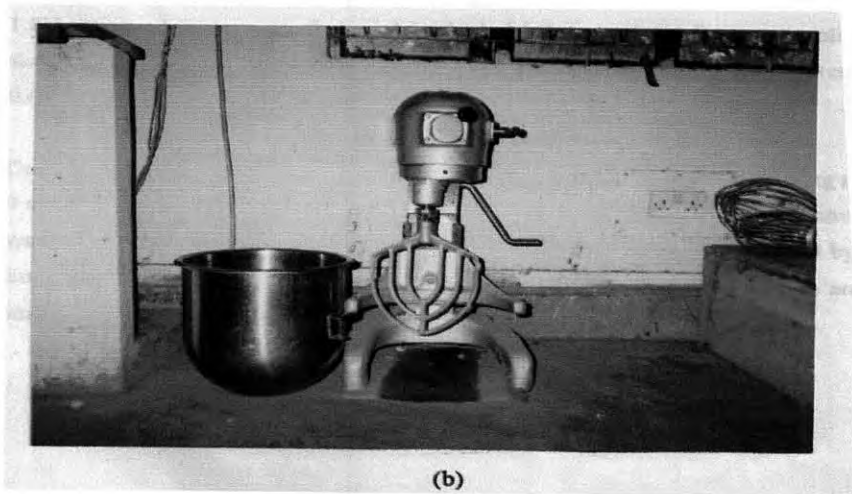
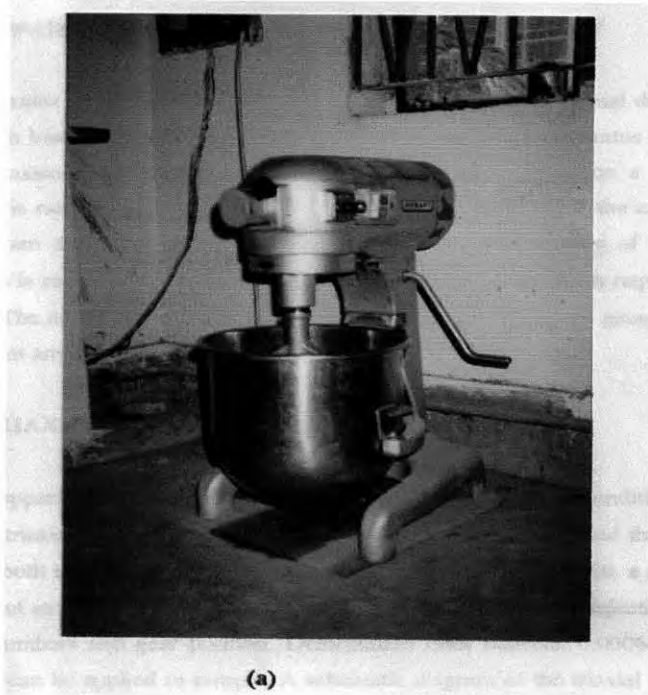


Figure 3.1 Hobart laboratory mixer machine: (a) Photograph of the machine, (b) Photograph of attachment and bowl

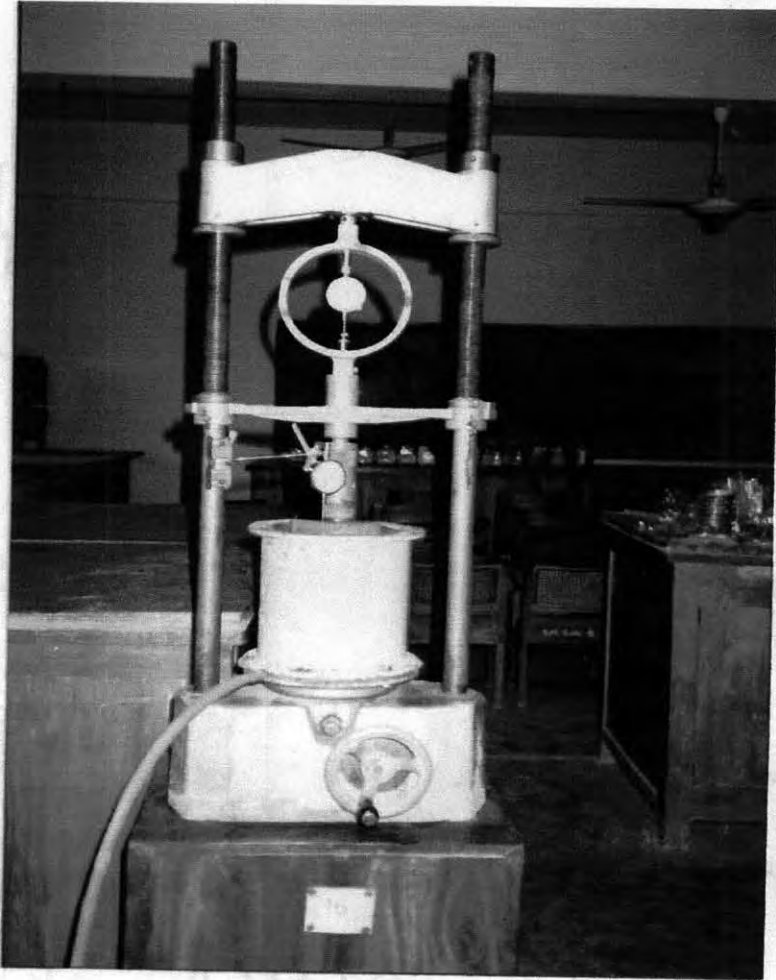


Figure 3.2 Apparatus for  $K_0$ -consolidation of soil slurry

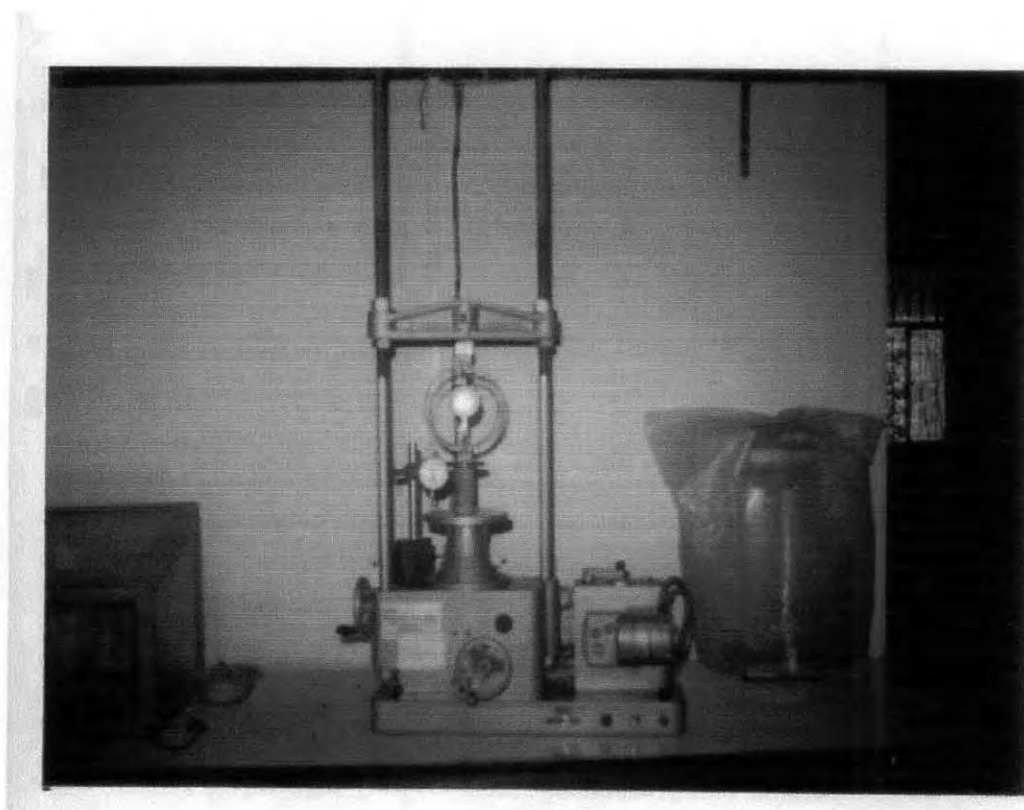


Figure 3.3 Unconfined Compression Test Apparatus

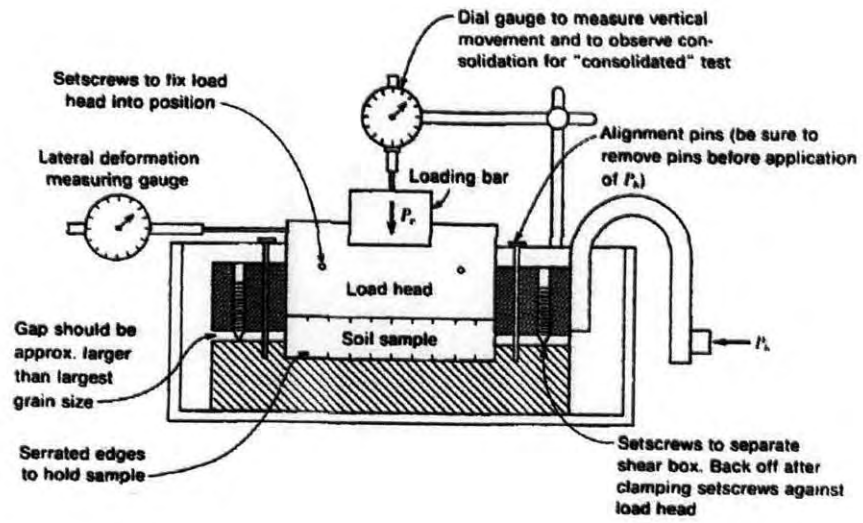


Figure 3.4 Line Details of the Direct-Shear Test



Figure 3.5 Direct Shear Machine Showing shear Box, Loading Arrangement and Frame

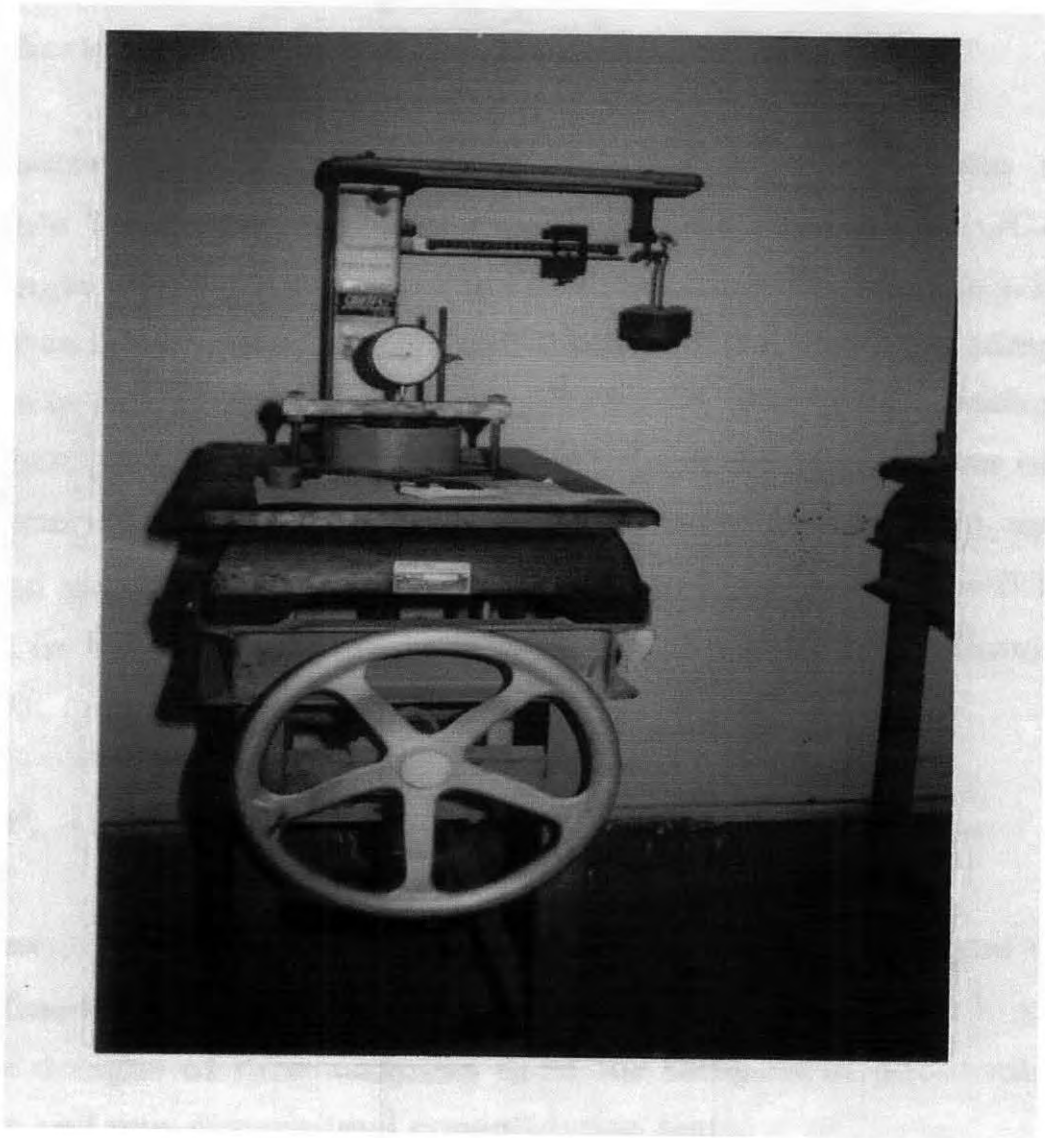


Figure 3.6 One Dimensional Consolidation Test Apparatus

## CHAPTER – 4

### DETERMINATION OF SOIL PARAMETERS

#### 4.1 Introduction

The use of undisturbed samples of soil for testing is desirable for the study of field behavior of structures constructed on such soils. However, such samples are seldom uniform due to complex geological conditions under which they form over a long period of time. Thus from results of test on such soil samples, it is rather difficult to generalize the effect of soil parameters on the stress-strain behavior of soils. For a systematic study of the effect of various soil parameters on the stress-strain behavior of soils, it is essential to use uniform reconstituted samples prepared under controlled conditions in the laboratory (Hvorslev, 1960). In this chapter, the process of obtaining critical state parameters of reconstituted Savar clay determined from selected laboratory tests are presented. The laboratory investigations made on the soil sample are described in detail in this chapter.

#### 4.2 Soil Used

For the present study, disturbed soil samples were collected from Habib Tower area, Bank-Colony, B-Block, beside the Dhaka-Aricha high way at Savar, Dhaka, Bangladesh. The soil samples were collected from the area of excavation for foundation of Habib Tower. Disturbed samples were collected from the bottom of the excavation pit by using hand shovels. The samples were packed in large polythene bags and then measurements were taken to transport them to the Geotechnical Engineering Laboratory of Bangladesh University of Engineering and Technology (BUET), Dhaka. After collection of the

samples, any debris, coarse aggregates and vegetations that were present in the soil samples were removed by visual inspection

### 4.3 Geological Aspects of Savar Clay

The geological aspect of Savar clay, which is located in Dhaka district, is expected to be similar to that of Dhaka clay, which has been extensively studied and investigated. The city of Dhaka is situated on the southern part of Modhupurgor, which was formed by older Pleistocene Terrace sediments according to geological literature. Dhaka soil belongs mainly to the category of Pleistocene Terraces. Some smaller parts of the soil of this district belong to recent alluvium. Pleistocene and recent samples do not appear to differ in maximum grain size. However, an excess of very fine-grained material is observed in the Pleistocene samples (Morgan et. Al., 1959). Pleistocene sediments are generally well oxidized and are consequently typically reddish, brown or tan in colour and are mottled. A description of the geological soil profile over Dhaka is provided by Eusufzai (1967) and Ameen (1985).

Most Dhaka soils belong to Dihing formation of Pleistocene age. These formations generally have a thickness ranging between 8 to 9 meters. It generally consists of clay, more specifically red clay, fine sand and pebbles, which are mostly mottled. Dupi-Tila formation underlies the Modhupur clay residuum, which is locally called Dhaka clay. Dupi-Tila formation consists of clay, fine sands, medium sands, clayey lenses, subordinate shale and poorly consolidated sand stone. It is massive and thick bedded, and it is yellow to yellow brownish in color.

A part of the area to the east and west side of Dhaka consists of recent Alluvium. These alluvium deposits consists of stream deposits, natural levee and back slope deposits, swamp deposits and inter-stream deposits. Although some part of Dhaka is covered by recent alluvium, most of Dhaka soil is of older Pleistocene deposits.



The state of over consolidation of most of the natural Dhaka soil deposits may be characterized as slightly too heavily over consolidated. The city of Dhaka is at an elevation ranging from 6 to 8 meters above the mean sea level. The top layer of Dhaka soil generally consists of a mixture of clay and silt. The depth of this top layer varies from 6 meters to 7.5 meters from the surface of the ground. Clay layer at this depth of the Savar zone of Dhaka district is currently under research. Layer of coarser materials such as sand and gravel exists at the lower levels and layers of finer particles such as clay and silt dominates the top surface.

#### 4.4 Engineering Properties of Savar Clay

In order to characterize the soil from a geotechnical point of view, it is necessary to determine index properties of soil samples. This section describes the procedures followed to determine the index properties of Savar area clay. After collecting disturbed soil samples, these were first air dried and then any soil lumps found were broken carefully with a wooden hammer to bring it in powder form. The soil samples were then sieved through a number 40 ASTM sieve. The following tests were performed to determine index properties of the Savar area clay as prepared above:

- (i) Specific gravity
- (ii) Atterberg limits and
- (iii) Grain size distribution

The specific gravity (ASTM D854 ), liquid limit (BS1377 ), plastic limit (BS1377 ), plasticity index (BS1377 ), and grain size distribution (ASTM D1140 ) of the soil samples were then determined. Using MIT Classification System (1931), the percentage of sand, silt and clay in the soil samples were determined. The soil was also classified according to Unified Soil Classification System (Casagrande, 1948). Table A2.1 of

Appendix II shows the index properties and classification of the soil used. Also Table A2.2 of Appendix II Shows the index properties of different percent of cemented Savar area clay.

## 4.5 Preparation of Reconstituted Soil

### 4.5.1 General

Reconstituted Savar clay was prepared by mechanically breaking down the excavated Savar clay in the laboratory, mixing it with water and different percent of cement (uncemented and 7%, and 14% cement) for cementation to prepare soil slurry and finally reconsolidating the soil slurry with a selected overburden pressure under  $K_0$  condition. Reconstituted soil enables a general pattern of behavior to be established. These behaviors may be correlated with index properties of clay and other laboratory obtained soil parameters. Additionally, comparisons with the response of intact samples may be used to identify any special features associated with fabric, stress history, bonding or cementation. The major advantages of using data from reconstituted soils are that the effect of sampling of natural soils and the effect of inhomogeneity inherently present in natural soils can be eliminated. On the other hand, the effects of stress history and composition of soils may be reproduced in the laboratory and thus can be represented and can be correlated with laboratory obtained soil parameters. However, the important effects of post depositional processes, such as ageing, leaching, etc. and of variations of composition and fabric are generally not included in remolded soils. Thus the stress-strain behavior of reconstituted Savar clay as will be discussed in the following chapters will represent the stress-strain behaviors of young or un-aged soils, without cementation or structure, in which no post-depositional processes is assumed to have operated.

#### 4.5.2 Preparation of Soil Slurry

For preparing remolded soil samples, clay slurry with an initial water content well beyond the liquid limit is commonly used (Siddique, 1990, Hopper, 1992). Initial water content higher than the liquid limit provides several advantages. It provides a higher degree of saturation and thus a higher freedom of particle orientation. However, this requires larger initial volumes of soil-water mixture and longer consolidation periods. In this study, an initial water content which was just sufficient to yield uniform and homogeneous slurry was used. This was done to reduce the volume of clay-water mixture and also to reduce the consolidation time required for consolidation of the soil samples. The samples were first air dried and powdered with the help of a wooden hammer. The powdered samples were then sieved through No. 40 sieve and the sieved samples were mixed with water and different percent cement for cementation at approximately 1.5 times the liquid limit to form soil slurry. The soil and water were thoroughly mixed by hand kneading to form slurry to ensure full saturation. The product was then further remixed uniformly by using rotary laboratory mixer for about 30 minutes.

#### 4.5.3 Consolidation of Slurry

The soil slurry was  $K_0$ -consolidated in a cylindrical consolidation cell of 210 mm diameter and 180 mm in height. At the bottom of the consolidation mold, a geotextile and a 6 mm thick perforated steel disc were placed for bottom drainage. The inner wall of the cylindrical consolidation mold was coated with a thin layer of silicon grease. This would minimize the side friction during consolidation of the clay sample. The prepared slurry was gradually poured into the  $K_0$ -consolidation cell and stirred with a steel rod to remove any entrapped air from the slurry. After removing the air bubble, the top surface of the soil sample was leveled properly. At the top of the slurry, a geotextile filter followed by a perforated steel discs was placed to permit top drainage. There was a clearance of a few

millimeters in between the perforated discs and inside edge of the cell. This would eliminate any side friction during consolidation of soil slurry.

The required axial load of  $150 \text{ kN/m}^2$  was gradually applied to the soil sample in the consolidation mold using a loading frame with proving ring. Initially the slurry was allowed to consolidate by the self-weight of the sample and the weight of the porous discs for about 24 hours. Initially, a pressure of  $14 \text{ kN/m}^2$  was applied to the sample for the every 24 hours. Subsequently, the pressure was increased gradually; until at the end of one week the consolidation pressure was brought to the target value of  $150 \text{ kN/m}^2$ . This pressure ( $150 \text{ kN/m}^2$ ) was maintained until the end of primary consolidation, which was indicated by the constant reading of the compression dial gauge. It took about fourteen to fifteen days for the completion of primary consolidation. Rate of compression was very rapid at the initial stages of consolidation. However, this rate gradually decreased with time. After the completion of consolidation, the top and bottom part of the cell were separated. The consolidated soil sample or soil cake was then extruded using a mechanical extruder. A soil cake was obtained by the above procedure. The uniformity in density and moisture content of the consolidated soil cake was checked from moisture and density of specimens from two to three locations within the cake. The average water content of the reconstituted normally consolidated Savar area clay sample was computed to be  $42.5 \pm 1\%$ . The average water content of the cemented Savar area clay samples were  $40.5 \pm 1\%$ .

#### 4.6 Selection of Overburden Pressure

Early researchers considered a consolidation pressure ( $\sigma'_{vc}$ ) of  $276 \text{ kN/m}^2$  was the minimum consolidation pressure necessary to prepare remolded clay samples which are stiff enough to prepare soil specimens for testing. However, Kirkpatrick and Khan, 1984 after subsequent studies with remolded samples concluded that remolded samples consolidation to consolidation pressures of  $\sigma'_{vc} = 150 \text{ kN/m}^2$  could be used to prepare

soil specimens for testing. It was also observed that this produced insignificant difference in undrained stress-strain behavior. Similar results were observed by Bashar, 2002 in his research investigation. So in the present study the reconstituted samples were prepared in by consolidation pressure equal to  $150 \text{ kN/m}^2$

#### 4.7 $k_o$ Value of Soil Samples

The determinations of the exact value of  $k_o$  for clay samples is difficult and still the subject of study and research. Some empirical formulas are available for determination of the value of  $k_o$  for clays. Bashar (2002) used a stress path approach in triaxial tests to determine the  $k_o$  value of coastal clays of Bangladesh. Based on research evidence and experimental results of Bashar (2002) the  $k_o$  value of reconstituted Savar clay was assumed to be 0.50 in this study.

#### 4.8 Preparation of Test Sample

After consolidation of the soil slurry, the reconstituted normally consolidated Savar area clay with or without cementation block sample was extruded from the consolidation cell. The extruded block sample was then sliced into small blocks by a wire knife. The small block samples were subsequently trimmed by using a piano wire. A split mould was then used to prepare samples of nominal dimensions of 38 mm diameter by 76 mm high. Unconfined compression test were then performed on these samples.

Block samples were also prepared for unconsolidated slow direct shear test and one dimensional consolidation test. For performing these tests, small slabs of clay were obtained out of reconstituted samples from large consolidation cell. Then a sample ring of 63.5 mm diameter by 25.4 mm high having its internal surface well covered with silicon grease was gradually and in stages pushed into the clay, which was continuously being

trimmed away from the cutting edge of the ring with a knife. These soil samples were then used to perform slow direct shear test and one dimensional consolidation tests.

#### **4.9 Unconfined Compression Test**

Unconfined compression tests were conducted on the prepared samples of remolded Savar area clays, with and without cementation. Table A2.3 of Appendix II tabulates the test results of the unconfined compression test. Figures 4.1 to 4.3 show the axial stress vs axial strain relationship in unconfined compression test of reconstituted Savar area clay without cementation and with 7% and 14% cementation. It was observed that cementation significantly increases the undrained compression strength of remolded Savar area clays.

#### **4.10 Direct Shear Test**

Direct shear tests were performed on prepared samples of reconsolidated Savar area clay with and without cementation. Table A2.4 of Appendix II summarizes the direct shear test results. Figures 4.4 to 4.6 show the shear stress vs shear displacement relationship of reconstituted Savar area clay without and with cementation. It was observed that although cementation significantly increased the failure shear stress of Savar area clay. However it was observed that the friction angle of the remolded Savar area clay was not significantly affected by the degree of cementation.

#### **4.11 One-Dimensional Consolidation Test**

One dimensional consolidation tests were performed on prepared samples of reconsolidated Savar area clay with and without cementation. The plastic parameter  $\lambda$  was determined from the slope of the normal consolidation line and the elastic

parameter  $\kappa$  was determined from the slope of the elastic rebound line. Table A2.5 of Appendix II summarizes the two consolidation parameters for reconstituted Savar area clay, with and without cementation. Figures 4.7 to 4.9 show the  $e$ -log  $p$  curve of reconstituted Savar clay with and without cementation. It is observed that the plastic consolidated curve and elastic rebound curve of Savar area clay with and without cementation are similar to typical consolidation curves generally observed for clays

104285

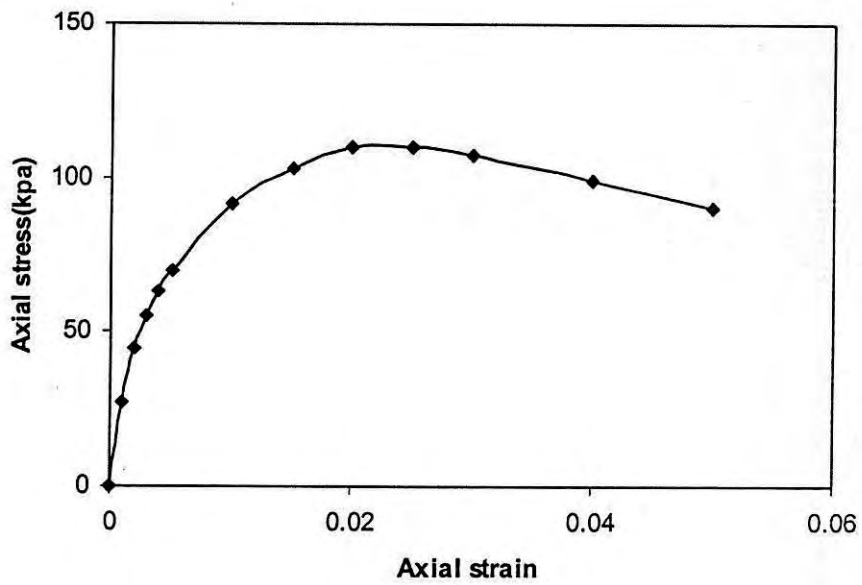


Figure 4.1 Axial stress vs axial strain curve of uncemented Savar clay

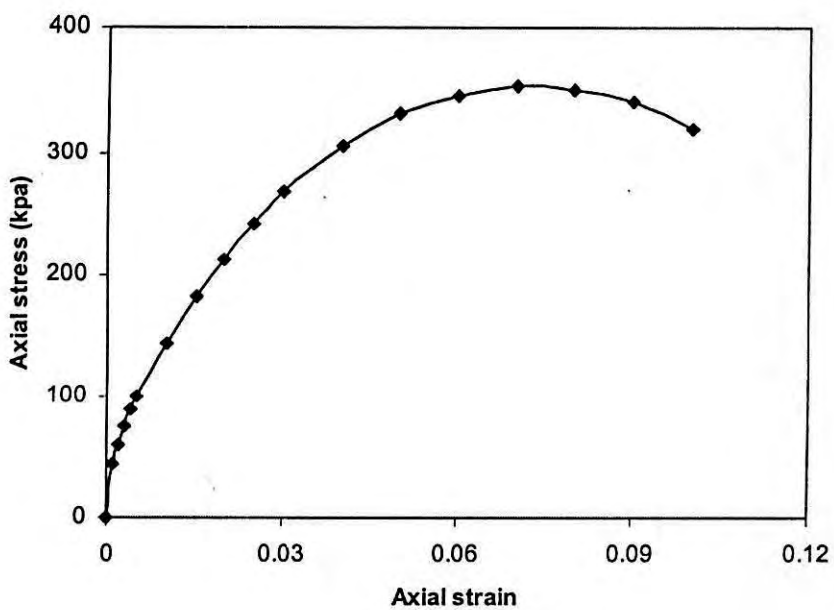


Figure 4.2 Axial stress vs axial strain curve of 7 % cemented Savar clay



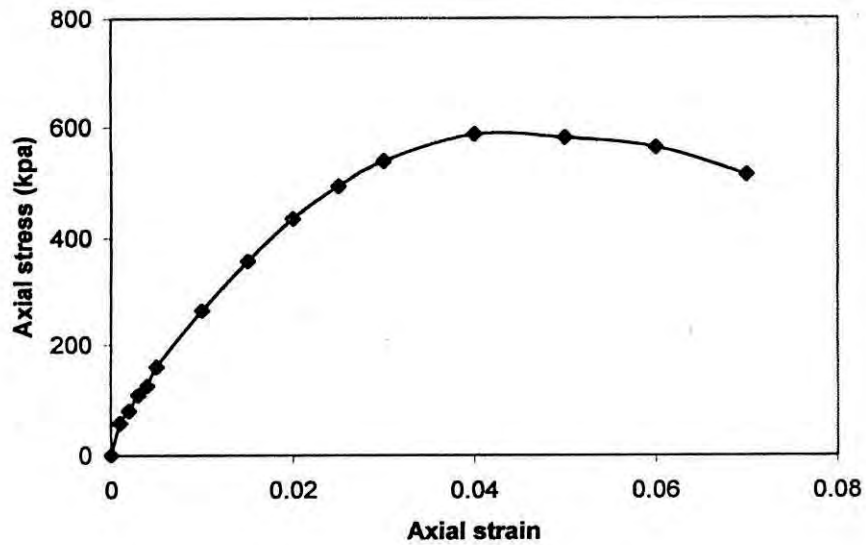


Figure 4.3 Axial stress vs axial strain curve of 14 % cemented Savar clay

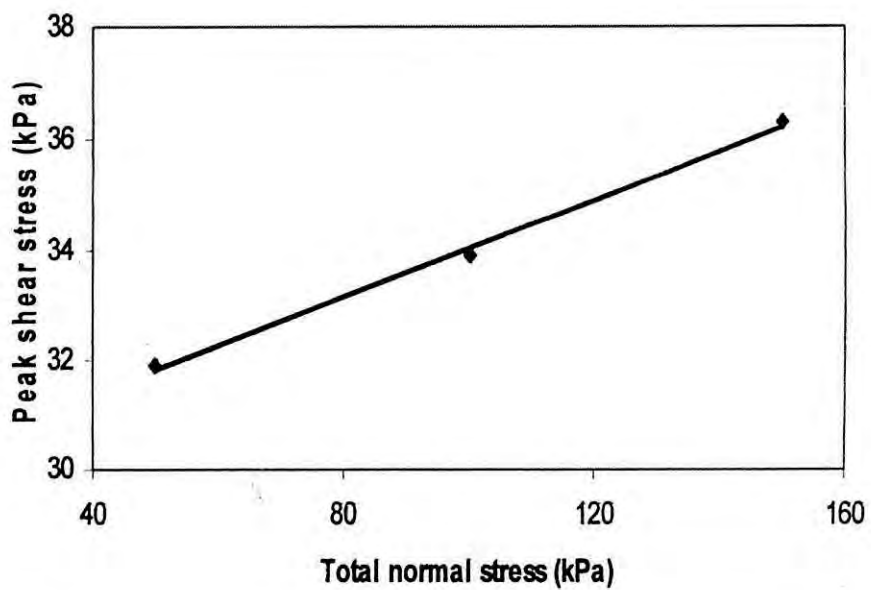


Figure 4.4 Shear stress vs shear displacement curve of uncemented Savar clay

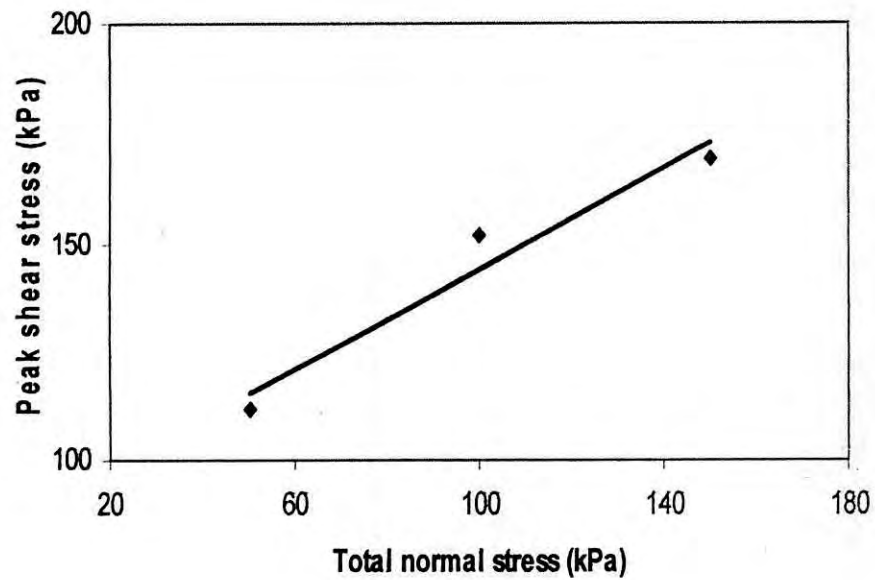


Figure 4.5 Shear stress vs shear displacement curve of 7% cemented Savar clay

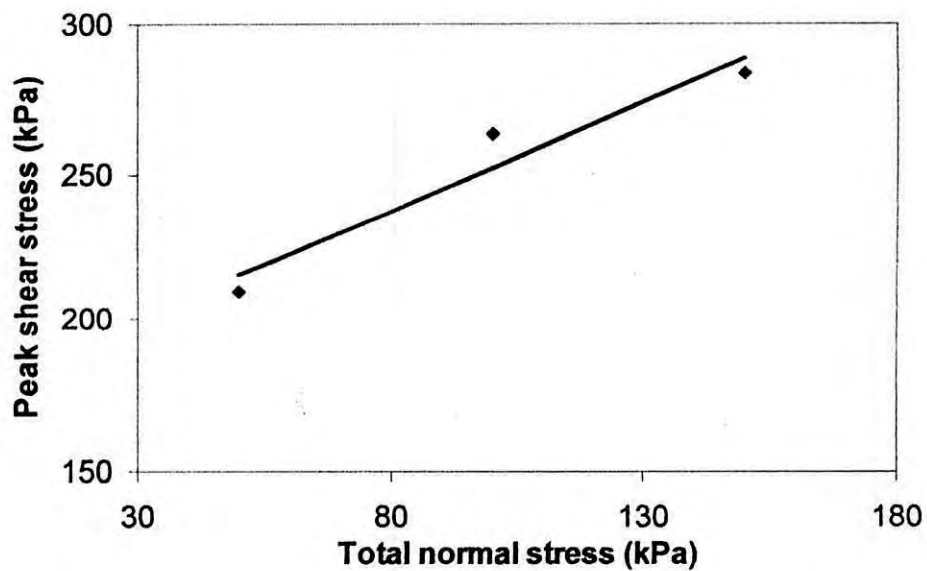


Figure 4.6 Shear stress vs shear displacement curve of 14% cemented Savar clay

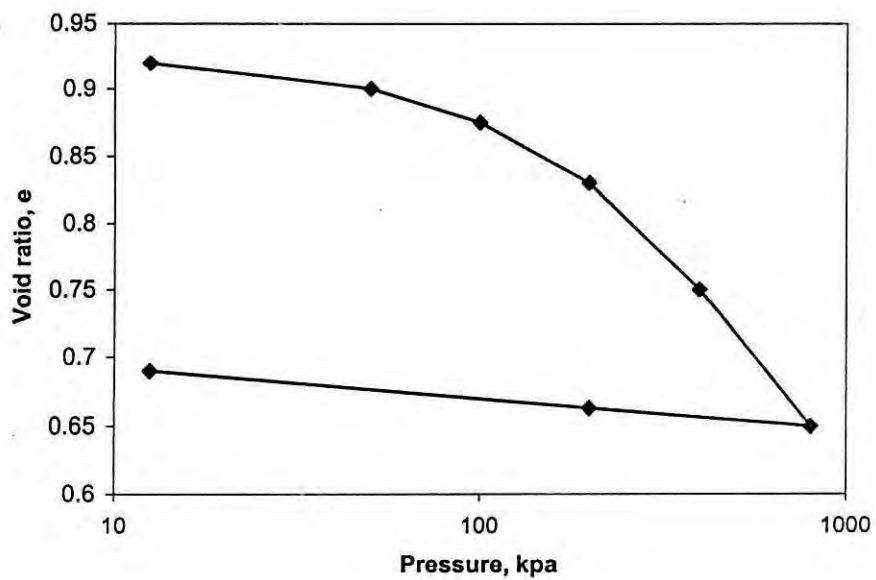


Figure 4.7 e-log p curves for uncemented Savar area clay

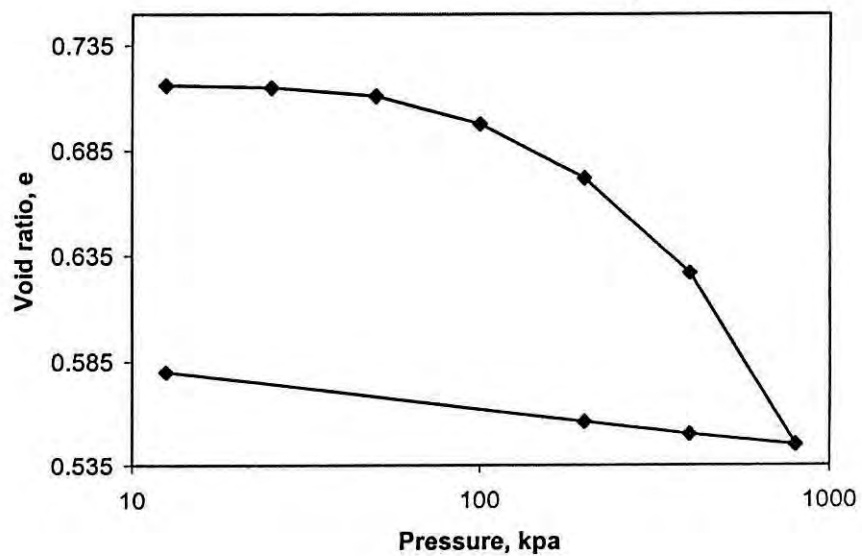


Figure 4.8 e-log p curve for 7% cemented Savar area clay

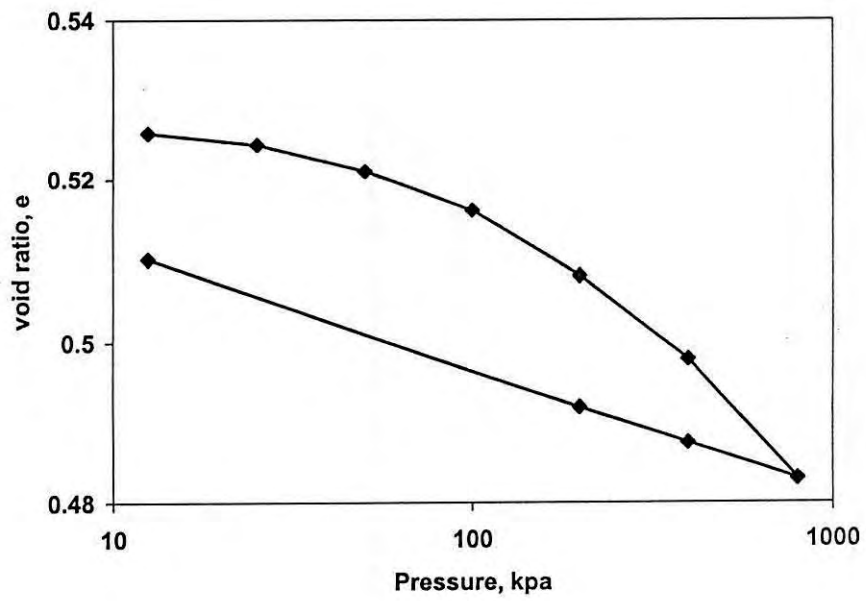


Figure 4.9 e-log p curve for 14% cemented Savar area clay

## CHAPTER 5

### UNDRAINED PREDICTIONS USING THE MCC MODEL

#### 5.1 Introduction

A model originally devised in Cambridge and termed as the "Modified Cam Clay Model" (MCC), is generally used to simulate the stress-strain response for clays. In this chapter, the Modified Cam Clay model was used to numerically simulate the stress-strain and pore pressure response of Savar clays, with and without cementation, and for different over consolidation ratios (OCR). The model parameters for the MCC model relevant for undrained analysis of remolded Savar clays, with and without cementation, was obtained from laboratory tests of reconstituted Savar clay samples. The undrained stress-strain response, effective stress paths and pore pressures predicted by the MCC model, for various OCR's was compared, both for the uncemented and cemented cases. Finally, conclusions were drawn regarding the capabilities of the MCC model to predict the undrained response of reconstituted Savar clays for various OCR's, and with and without cementation.

#### 5.2 Modified Cam Clay (MCC) Model

The Modified Cam Clay Model (MCC) is a critical state model incorporating volumetric strain hardening assumptions. The model has been generally observed to predict, with reasonable accuracy, the stress-strain response of normally consolidated reconstituted clays. The prediction of the qualitative response for reconstituted over consolidated clays is also generally observed to be quite satisfactory. The significant aspects of the MCC model are described below.

### 5.2.1 The Critical State

The MCC model is based on the critical state concept. The critical state is defined to be that condition of the soil at which the soil shears continuously at constant stress and at constant volume. Such a condition is observed at failure of the soil at its ultimate state. The critical state occurs at a certain ratio of the mean effective stress  $p'$  and the shear or deviator stress  $q$ . The critical states may be defined by a straight line in  $(p', q)$  space. This straight line is termed as the critical state line. The slope of this line is termed as the critical state ratio generally identified by the parameter  $M$ . The mean pressure  $p'$  and the deviator or shear stress  $q$  at the octahedral plane is given in terms of the effective principal stresses  $\sigma'_1, \sigma'_2, \sigma'_3$  as below:

$$p' = (\sigma'_1 + \sigma'_2 + \sigma'_3)/3 \quad (5.1)$$

$$q = \frac{1}{\sqrt{2}} \sqrt{(\sigma'_1 - \sigma'_2)^2 + (\sigma'_2 - \sigma'_3)^2 + (\sigma'_3 - \sigma'_1)^2} \quad (5.2)$$

$$M = \frac{q'_f}{p'_f} \quad (5.3)$$

In the above equations  $\sigma'_1$  is the major principal effective stress and  $\sigma'_2, \sigma'_3$  are minor principal effective stresses.  $M$  is the critical stress ratio.  $p'_f$  and  $q'_f$  are respectively the mean effective stress and deviator stress at the ultimate or failure state.

### 5.2.2 Yield Function

The combination of mean and effective stresses  $(p', q)$  at which the soil starts to have irrecoverable or plastic deformations may be represented by a convex function in  $(p', q)$  space. This function may be represented as follows:

$$f(p', q, p'_o) = 0 \quad (5.4)$$

Equation (5.4) is called the yield function, where  $p'_o$  is the preconsolidation pressure of the soil. In the Modified Cam Clay model, preconsolidation pressure  $p'_o$  is the soil parameter which determines the size of the yield locus in the effective stress space. Once the stress state touches the yield locus, the stress-strain response becomes elasto-plastic.  $p'_o$  is also termed as the hardening parameter in elasto-plasticity. For stress states within the yield function, the stress-strain response of the soil is assumed to be elastic.

### 5.2.3 Strain Hardening

At stress states on the yield function, an increment of stress applied outside of the yield function, results in incremental plastic strains. At the same time the value of the hardening parameter  $p'_o$  increases. Consequently the yield function expands and the current stress state lies on the new expanded yield surface. The elastic region is permanently expanded. This is observed as an apparent hardening effect if the soil is unloaded and then reloaded. The hardening parameter  $p'_o$  is related to the plastic volumetric deformation of the soil. This may be derived from the  $e - \log p'$  or void ratio by log of mean effective stress relation of a soil. It is given as follows:

$$\frac{dp'_o}{d\varepsilon_v^p} = \frac{p'_o(1+e)}{(\lambda - \kappa)} \quad (5.5)$$

In equation (5.5),  $p'_o$  is the preconsolidation pressure,  $dp'_o$  is the increment of preconsolidation pressure,  $e$  is the void ratio, and  $\lambda$  and  $\kappa$  are respectively the slope of the normal consolidation line and elastic rebound line of the  $e - \log p'$  line.

### 5.2.4 Plastic Potential Function

At the yield or plastic condition, the Modified Cam Clay model assumes the ratio of incremental plastic volumetric strains to incremental plastic deviator or shear strains to be related to the stress ratio  $\eta$  as follows:

$$\frac{d\varepsilon_q^p}{d\varepsilon_v^p} = \frac{M^2 - \eta^2}{2n} \quad (5.6)$$

$$\text{where } \eta = \frac{q}{p'}$$

In equation (5.6),  $M$  is the critical stress ratio. At stress ratios  $\eta > M$ , the soils undergo expansive volume strain and soften. At stress ratios  $\eta < M$ , the soil goes compressive plastic volume strain and hardens. At the critical state ratio  $M$ , the incremental plastic volumetric strain is zero and the soil becomes perfectly plastic.

Assuming associated flow rule and integrating equation (5.6), the yield and the plastic potential function for the Modified Cam Clay model may be obtained as below:

$$\left( \frac{q}{Mp'} \right)^2 = \frac{p'_0}{p'} - 1 \quad (5.7)$$

Figure 5.1 shows the MCC yield locus and plastic potential function in  $p'$ - $q$  space and Figure 5.2 shows the position of the normal consolidation line (NCC) and critical state line (CSL) in  $e$ - $\log p'$  space.



### 5.2.5 Elastic Behavior

The MCC model assumes elastic stress-strain response for stress states within the yield locus. The MCC model defines a pressure dependent non-linear stress-strain response defined by the elastic bulk modulus and elastic shear modulus. The elastic bulk modulus of the MCC model is given as below:

$$\frac{dp'}{d\varepsilon_v^e} = \frac{p'(1+e)}{\kappa} \quad (5.8)$$

Generally, a constant value of the Poisson's ratio  $\mu$  is assumed in the MCC model. The elastic shear modulus  $G$  is then obtained as below:

$$G = \frac{3k(1-2\mu)}{2(1+\mu)} \quad (5.9)$$

### 5.3 Suitability of the Modified Cam Clay Model for Savar Clays

The Modified Cam Clay model has been used by many researchers to successfully predict the stress-strain response of many types of clay under triaxial stress states, both for drained and undrained conditions. From observations of physical characteristics, and from the results of basic index and other laboratory tests conducted in remolded Savar clays, it is reasonable to assume that the Modified Cam Clay model is likely to be appropriate for predicting the undrained stress-strain response of remolded Savar clays under triaxial conditions.

## 5.4 Modified Cam Clay Parameters for Savar Clays

There are five parameters used for the Modified Cam Clay model. Two of them are elastic parameters. These are the slope  $\kappa$  of the elastic unload-reload line plotted in the  $e - \ln p'$  space, and the elastic Poisson's ratio  $\mu$ . The remaining three are plastic parameters. These are the slope of the normal consolidation line  $\lambda$ , preconsolidation pressure  $p'_o$  and the critical stress ratio  $M$ . The MCC model parameters may be obtained from conventional laboratory tests. These parameters may be directly related with the physical and mechanical properties of the soil. The selection of the Modified Cam Clay model parameters for reconstituted Savar clay (with and without cementation) from laboratory test are described in the following sections. The laboratory tests conducted on reconstituted Savar clays, with and without cementation, have been already discussed in Chapter 3.

### 5.4.1 Elastic Parameters

$\kappa$  is the elastic parameter of the Modified Cam Clay model. It was obtained by computing the slope of the unload-reload part of the consolidation curve of reconstituted Savar clay. It was observed that although there is little change of the value of  $\kappa$  for relatively lower degrees of cementation (7%), a significant decrease of the value of the elastic rebound parameter  $\kappa$  occurs, for relatively higher degrees of cementation (14%).

The undrained elastic Poisson's ratio for remolded Savar clays was assumed to be close to 0.49. From the theory of elasticity it can be shown that a value of elastic Poisson's ratio of 0.5 implies volume incompressibility. This is the basic assumption for undrained condition. In this research study, an elastic Poisson's ratio of 0.49 was assumed for numerical stability.

#### 5.4.2 Plastic Parameters

The plastic parameter  $\lambda$  of reconstituted Savar clay, with and without cementation, was obtained by computing the slope of the virgin portion of the normal consolidation line of the reconstituted Savar clay, with and without cementation, and drawn in  $e - \log \sigma'_v$  space. The normal consolidation lines for Savar clays were plotted by conducting  $K_0$  consolidation tests on reconstituted Savar clay samples (with and without cementation). The parameter  $\sigma'_v$  is the pressure at which the slope of the consolidation line of the remolded Savar clay, with and without cementation, is observed to change from elastic (low) to plastic (high). No abrupt change was observed for reconstituted Savar clays without cementation. Rather the change was smooth and gradual. The value of  $\lambda$  changed significantly with cementation of the remolded Savar clay. An empirical approach was used to make an estimate of the preconsolidation pressure  $p'_o$  from the  $K_0$  consolidation curve. Such approaches are described in standard soil mechanics text. The parameter  $N$  is generally used to define the void ratio at unit pressure on the normal consolidation line.  $N$  is used as a parameter of the Modified Cam Clay model. The value of  $N$  is dependent on the unit of the mean effective pressure  $p'$ .  $N$  defines the position of the virgin or normal consolidation line in  $e - \log p'$  space. Once the value of  $\lambda$ ,  $p'_o$  and  $N$  are determined, then the normal consolidation line is defined uniquely at  $e - \log p'$  space. The method for obtaining  $\lambda$ ,  $p'_o$  and  $N$  is further elaborated below.

Reconstituted Savar clays, with or without cementation, undergo consolidation or time dependent stress-strain response. From  $K_0$  consolidation tests on reconstituted Savar clay samples, void ratio by effective stress ( $e - \log \sigma'_v$ ) curves or  $K_0$  consolidation curves, were obtained. From the consolidation curve of reconstituted Savar clays (with and without cementation), the slope  $\kappa$  of the elastic rebound curve, the slope  $\lambda$  of the normal consolidation line was obtained. The preconsolidation pressure  $p'_o$  was computed from

the empirically determined vertical consolidation pressure  $\sigma'_v$ . The vertical preconsolidation pressure  $\sigma'_v$  was identified for Savar clays from the break of elastic rebound and plastic consolidation part of the  $e - \log \sigma'_v$  curve. This gives three of the 6 MCC model parameters. The initial void ratio of the reconstituted Savar clay, another parameter of the MCC model, was also obtained from the  $e - \log \sigma'_v$  curve.

### 5.4.3 Critical State Parameters

The critical stress ratio ( $M = \frac{q_f}{p'_f}$ ) at the ultimate stress state gives the value of the critical state parameter,  $M$  of the MCC model. The ultimate stress state is the condition, at which soil shears at constant stress and constant excess pore pressure (undrained case) or constant volume strain (drained case). The locus of ultimate stress states is generally a straight line passing through the origin in  $(p', q)$  space. This line is termed as the critical state line. The slope of the critical state line gives the critical state ratio  $M$ . For reconstituted Savar clay with 7% and 14% cementation, and without cementation, the ultimate friction angle was obtained by performing drained or slow direct shear tests and plotting the ultimate Mohr-Coulomb line in  $\tau - \sigma'_n$  Or shear stress versus effective normal stress space. The critical state parameter  $M$  was then indirectly determined from the drained friction angle using the following relation:

$$M = \frac{6 \sin \phi}{3 - \sin \phi} \quad (5.10)$$

#### 5.4.4 Modified Cam Clay Parameters for Savar clay

The Modified Cam Clay model parameters obtained for reconstituted Savar clay, without cementation, and with 7% and 14% cementation, are summarized in Table 5.1. It can be clearly shown from Table 5.1 that as cementation of the reconstituted Savar clay is increased from 0% to 14%, the plastic slope of the normal consolidation line decreases approximately 200% (from about 0.197 to 0.1). The slope of the elastic rebound line or elastic stiffness of reconstituted Savar clay also decreases by about 300% (from about 0.033 to 0.01). On the other hand, the apparent preconsolidation pressure  $p'_o$  was observed to increase as cementation was increased in the reconstituted Savar clay. A small apparent increase of the critical state ratio  $M$  (approximately 12%) was also observed to occur with increase of cementation of the reconstituted Savar clay from 0% to 14%.

Table 5.1 The MCC model parameters

Modified Cam Clay Parameters	Normal Savar Clay	7%Cemented Savar Clay	14% Cemented Savar Clay
$\lambda$	.29	.197	.1
$\kappa$	0.033	0.03	0.01
$M$	1.16	1.25	1.3
$p'_o$ (kPa)	133	375	400
$\mu$	0.49	0.49	0.49

#### 5.6 Numerical Modeling of Triaxial Shear

A numerical analysis was undertaken to predict the stress-strain and pore pressure response of reconstituted Savar clays, with and without cementation, using the Modified

Cam Clay model. For this purpose, the finite element program AFENA (Carter and Balaam, 1995) was used. The consolidation and triaxial shearing test of reconstituted Savar clay (with and without cementation) was simulated using a single element finite element model. An 8-noded axisymmetric, quadrilateral and isoparametric element with reduced Gaussian integration was used. The MCC model was used as the constitutive model. The MCC model parameters for the reconstituted Savar clays, with and without cementation, were input in finite element program. A constant all round cell pressure was numerically generated in the element model and the response of the soil element to isotropic load was first computed. Vertically downward displacement was subsequently applied at the top boundary nodes of the single finite element. The bottom boundary was fixed in the vertical direction. The lateral boundaries were allowed to move freely both vertically and in the radial direction. An incremental iterative analysis with stress scaling and drift correction was employed.

### **5.7 Numerical Prediction of Undrained Tests**

In the procedure described above, a numerical simulation of consolidated undrained laboratory shearing of reconstituted Savar clays (with and without cementation) under triaxial states of stress was carried out. A zero volume change condition is simulated in finite element modeling by using a value for the elastic bulk modulus of water several orders of magnitude higher than the elastic bulk modulus of the soil element. This value is then added to each of the diagonal terms of the elasto-plastic stress-strain matrix of the soil element.

### **5.8 Prediction of CIU Response of Savar Clays**

During an undrained triaxial shear, the stress-strain response of reconstituted Savar clay, Savar clay with 7% and 14% cementation were predicted using the MCC model parameters which are given in Table A5.1. Numerical predictions were obtained for over

consolidation ratios (OCR's) of 1, 2, 5, 10, 20 and 30 respectively. The predictions of numerical response of reconstituted Savar clays, using the MCC model are discussed in detail below.

### 5.8.1 Stress-Strain

Figures 5.3 to 5.8 show the predicted behaviour of undrained stress-strain response of reconstituted Savar clays, with and without cementation, at different OCR's in triaxial shear, and using the Modified Cam Clay model. It is observed that in each case, the MCC model predicts non-linear strain hardening behavior. At the ultimate state, the clay undergoes continuous axial strains at constant deviator or shear stress. This, by definition, is the critical state of the clay. It is also observed that the higher value of OCR, the lower the soil stiffness. This is an expected prediction of the Modified Cam Clay model. For a given preconsolidation pressure, a higher OCR implies lower cell or consolidation pressures. As the MCC model assumes the elastic stiffness to be directly proportional to the cell pressure, higher OCR values imply lower elastic stiffness, which has been observed in the numerical predictions.

### 5.8.2 Stress Path

Figures 5.9 through 5.14 show the predicted undrained stress paths for remolded Savar clays with 0%, 7% and 14% cementation at different OCRs. It is observed from the undrained stress paths that for normally consolidated clays, decreasing effective stresses and positive pore pressures are predicted. For over consolidated clays, increasing effective stresses and negative pore pressures are predicted. The stress paths predicted by MCC model for highly over consolidated clays are straight vertical lines initially in  $p' - q$  space. This happens as the Modified Cam Clay model simulates elastic behavior prior to yielding for high OCR clays.

The pore pressure predictions for reconstituted Savar clays without cementation, and with 7% and 14% cementation, are shown in Figures 5.15 through 5.20. The stress-strain and pore pressure predictions for reconstituted Savar clays, with and without cementation, using the Modified Cam Clay model, are observed to be qualitatively similar to the actual stress-strain and pore pressure response typically exhibited by clays. The MCC model predictions for cemented clays are qualitatively similar to that of uncemented clays. However, the predicted quantitative stress-strain and other values of remolded Savar clays, with and without cementation, are observed to be different. This is expected, as the predicted difference of cemented and uncemented Savar clays occur as a result of the different values of the MCC model parameters used for different degrees of cementation.

## **5.9 Comparison of Cemented and Uncemented Behavior**

Numerical predictions were obtained for the stress-strain and pore pressure response of reconstituted Savar clays, with and without cementation, for different degrees of over consolidation ratios. In the following subsections the predictions for reconstituted Savar clays, with and without cementations, for normally and lightly over consolidated clays, as well as those for highly overconsolidated clays, are compared.

### **5.9.1 Stress-Strain**

Figures 5.21 through 5.23 compare the MCC model predictions of stress-strain response under undrained conditions of normally consolidated reconstituted Savar clays and Savar clays of relatively low overconsolidation ratios. The reconstituted Savar clays considered here have 0%, 7% and 14% cementation with overconsolidation ratios (OCR's) of 1, 2 and 5 respectively. It is observed from the figures that the MCC model predicts increased initial shear stiffness and ultimate shear resistance of the soil with increasing degrees of cementation.



Comparison of the predicted stress-strain response using the MCC model for highly overconsolidated reconstituted Savar clays, with and without cementation, and under undrained conditions, are shown in Figures 5.24, 5.25 and 5.26. The OCR values in this case are 10, 20, and 30 respectively. It is observed from the figures that in this case also the Modified Cam Clay predicts increased initial shear stiffness and ultimate shear resistance of the soil with increasing degrees of cementation. It is also observed from the figures that the Modified Cam Clay predicts decreased initial shear stiffness as well as decreased ultimate shear resistance of the soil with increasing OCR values.

### 5.9.2 Stress Path

Figures 5.27, 5.28 and 5.29 compare the undrained stress-paths of the uncemented reconstituted Savar clay and those with 7% and 14% cementation. In this case also, normally consolidated case (OCR value of 1) and the cases of low and moderate overconsolidation ratios (OCR values of 2 and 5), are compared. For normally consolidated Savar clays, increase of deviator stress with decreasing mean effective stress is predicted, until failure occurs at the critical state. Clay samples with higher degrees of cementations show higher initial preconsolidation stresses and failure at higher deviator stresses. A low overconsolidation ratio 2 shows vertical stress paths in  $p' - q$  space, for all degrees of cementation. This implies that there is no change of mean effective stresses and no excess pore pressure development until failure. This is only possible if pure elastic conditions prevail prior to failure. It can be shown, that for undrained conditions, and using the Modified Cam Clay model, this is a reasonable prediction. For moderate overconsolidation ratio 5, for both cemented and uncemented case, a vertical stress path is observed initially. However, negative pore pressure or suction pressure is predicted after a certain deviator stress is reached. This is evidenced by the fact that the stress path rotates to the right, showing increase of mean effective stresses. In all cases, higher

degrees of cementation show increased deviator stress at failure. These predictions are in accordance with those that may actually be expected for clays with higher degrees of cementation.

Figures 5.30, 5.31 and 5.32 compare the undrained stress paths of reconstituted Savar clays with and without cementation (0%, 7%, and 14%), at different OCR values. In all cases (0%, 7%, 14% cementation and OCR values of 10, 20, 30), a vertical stress path is observed initially. However, negative pore pressure or suction pressure is predicted after a certain deviator stress is reached. This is evidenced by the fact that the stress path rotates to the right, showing increase of mean effective stresses. In all case, higher degrees of cementation show increased deviator stress at failure. These predictions are also in accordance with those that may actually be expected for clays with higher degrees of cementation.

### 5.9.3 Pore Pressure

Figures 5.33, 5.34 and 5.35 show the pore pressure response for reconstituted Savar clays for various degrees of cementation and for OCR values of 1, 2 and 5 respectively. For normal consolidation, positive pore pressures are predicted for all degrees of cementation. However, the predicted pore pressures are higher, the higher the degree of cementation. For low overconsolidation ratio (OCR equals 2), the predicted pore pressures are either zero or close to zero, for all degrees of cementation. For moderate consolidation ratio (OCR equals 5), negative pore pressures are predicted in all cases. The predicted suction pressures are higher, the higher the degree of cementation.

Figures 5.36, 5.37 and 5.38 show the pore pressure responses for reconstituted Savar clays for various degrees of cementation and for OCR values of 10, 20 and 30 respectively. In all cases (0%, 7%, 14% cementation and OCR values of 10, 20 and 30

respectively), negative pore pressures are predicted. However, the predicted negative pore pressures are higher, the higher the degree of cementation.

### 5.10 Summary and Conclusions

The MCC model was used to predict the stress-strain, excess pore pressure and effective stress path of reconstituted Savar clays without cementation, and with 7% and 14% cementation, during undrained shearing under triaxial conditions. It was observed that the MCC model is a good qualitative predictor of the undrained shearing response of clays. The MCC model predicts qualitatively similar responses for reconstituted Savar clays, with and without cementation. The quantitative predictions of the model for different degrees of cementation are however different. Modified Cam Clay model predictions were also obtained for various degrees of over consolidation. For highly over consolidated clays, an initial elastic response was observed before the onset of yield. This is more obvious from the observed stress paths for over consolidated clays. The qualitative predictions of Modified Cam Clay model for reconstituted Savar clays, with and without cementation, appear to be similar to those actually observed for typical clays during undrained shear in triaxial condition.

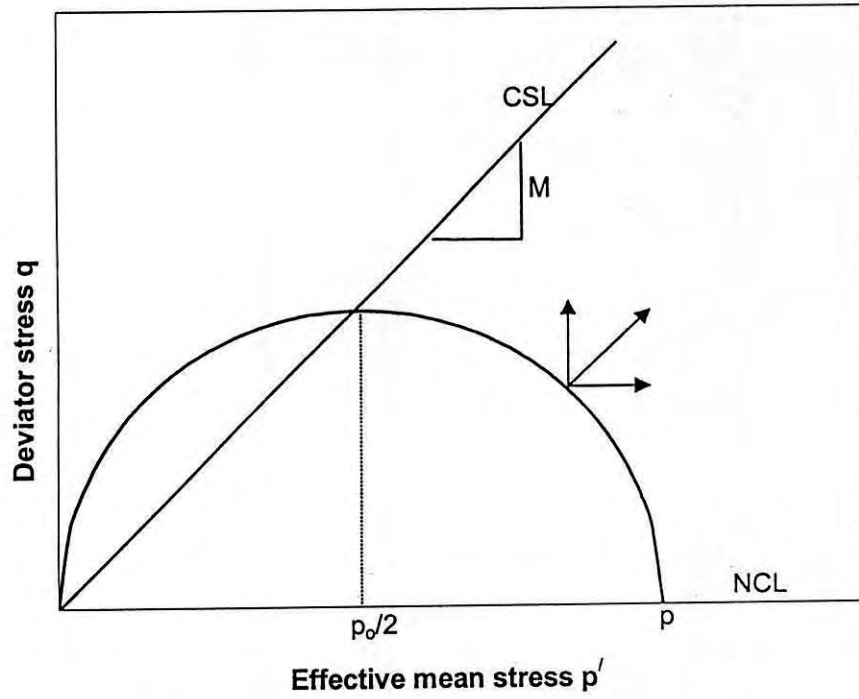


Figure 5.1 MCC model yield locus and plastic potential function

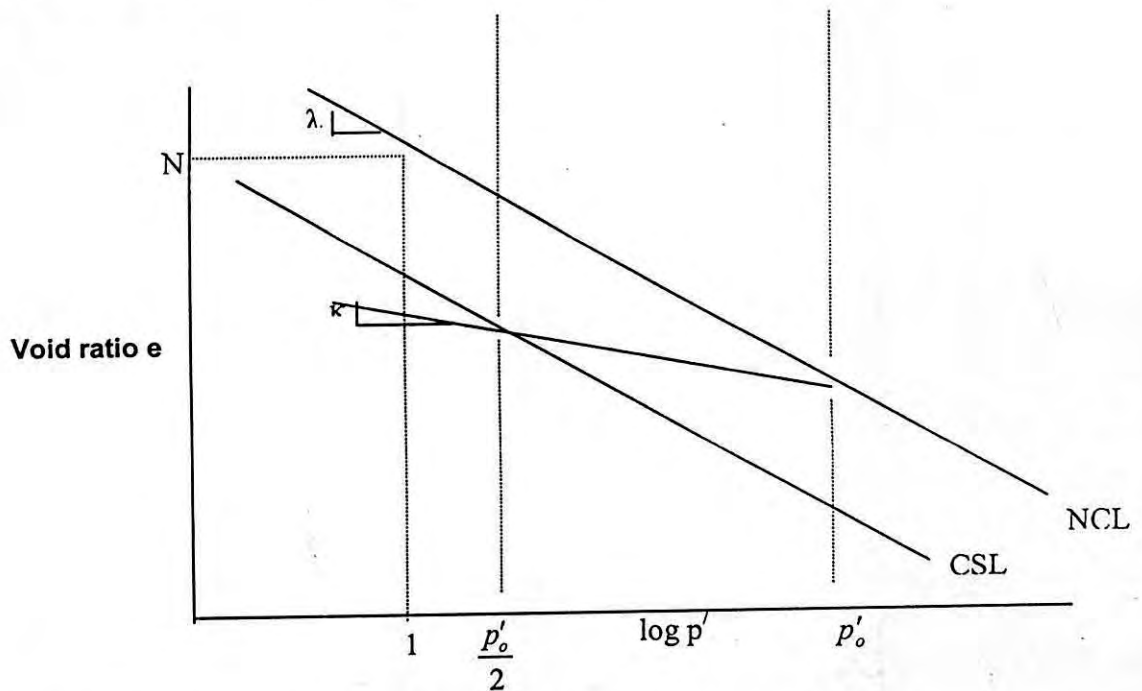


Figure 5.2 MCC model critical state line and normal consolidation line

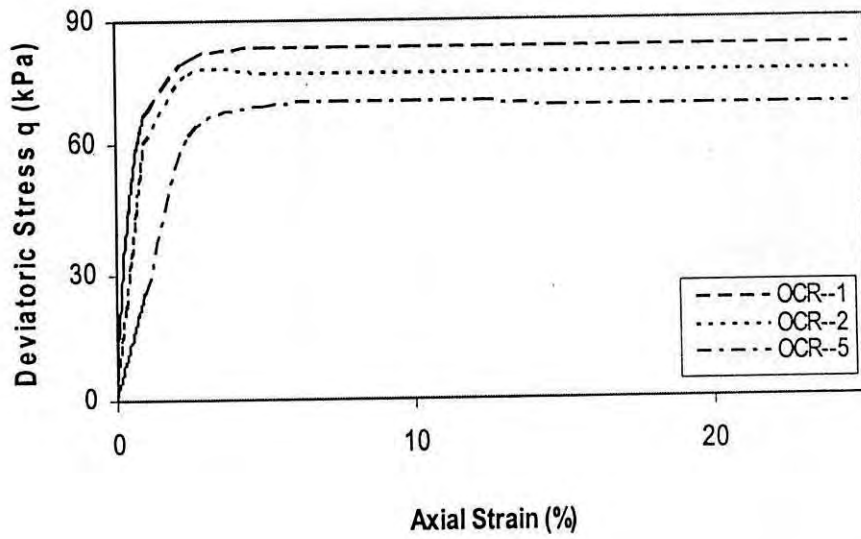


Figure 5.3 MCC prediction of undrained stress-strain response for normally consolidated and low OCR uncemented Savar clay

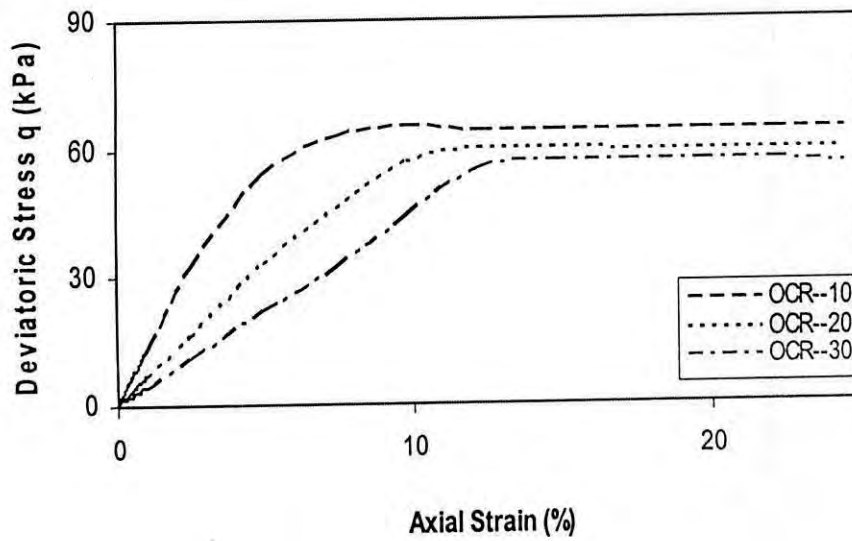


Figure 5.4 MCC prediction of undrained stress-strain response of highly overconsolidated uncemented Savar clay

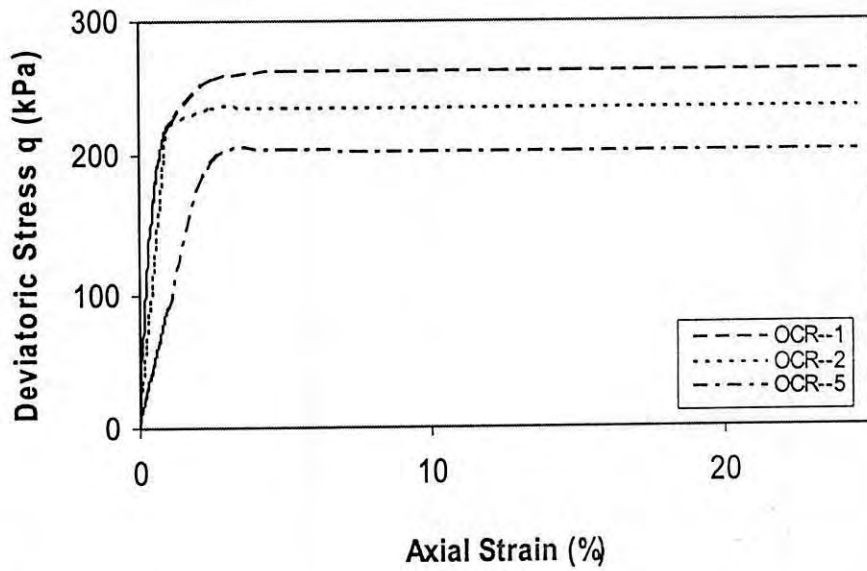


Figure 5.5 MCC prediction of undrained stress-strain response of normally consolidated and low OCR 7% cemented Savar clay

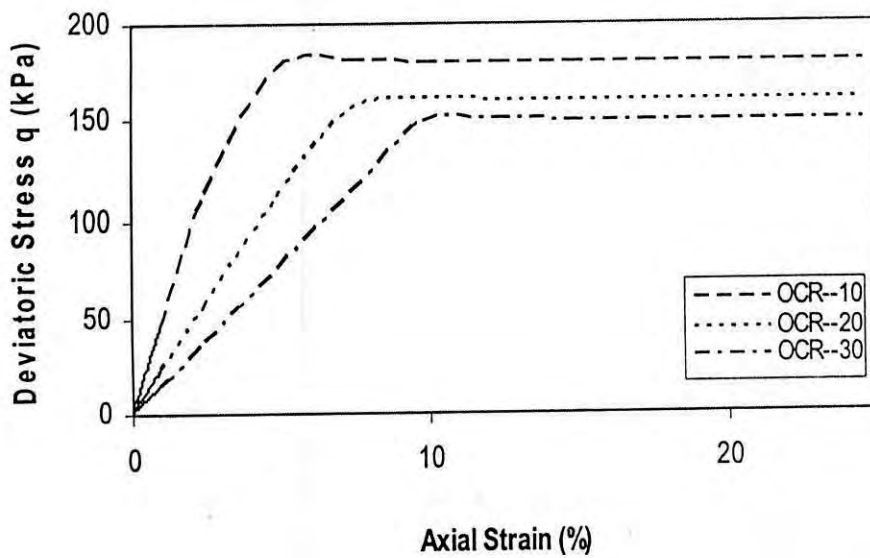


Figure 5.6 MCC prediction of undrained stress-strain response of highly overconsolidated 7% cemented Savar clay

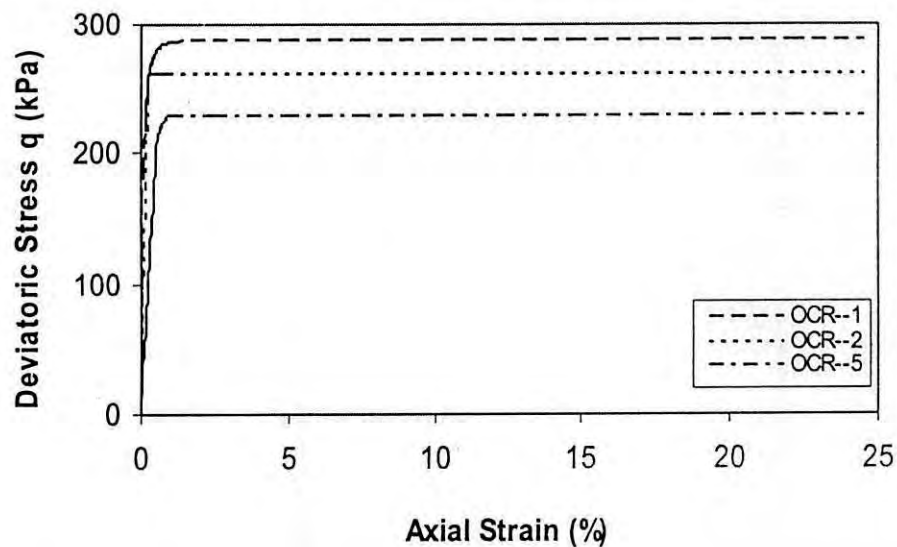


Figure 5.7 MCC prediction of undrained stress-strain response of normally consolidated and low OCR 14% cemented Savar clay

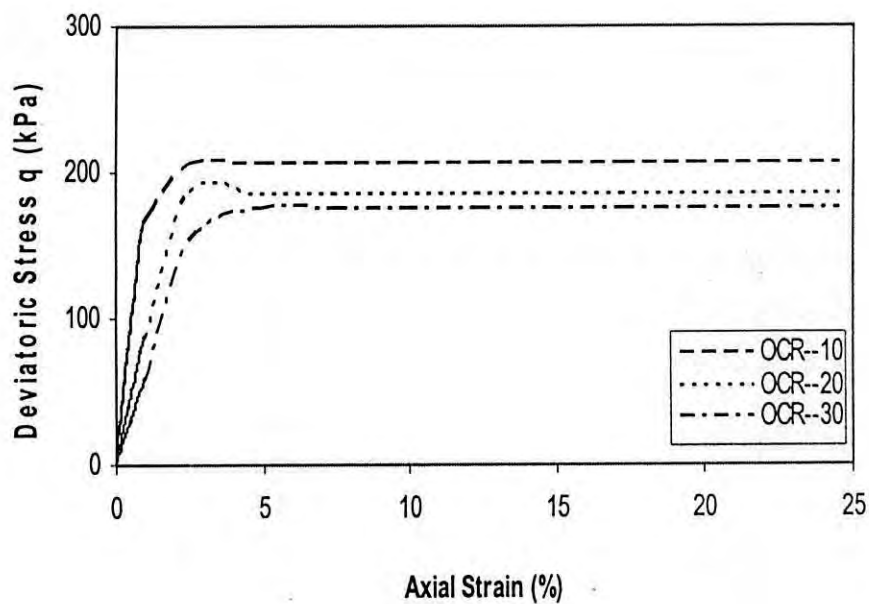


Figure 5.8 MCC prediction of undrained stress-strain response of highly consolidated 14% cemented Savar clay.

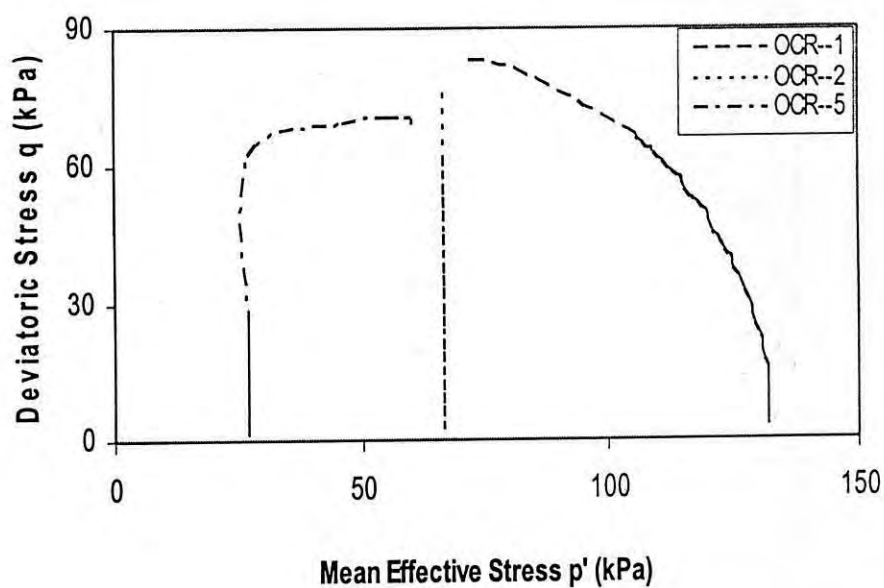


Figure 5.9 MCC prediction of undrained stress path of normally consolidated and low OCR uncemented Savar clay

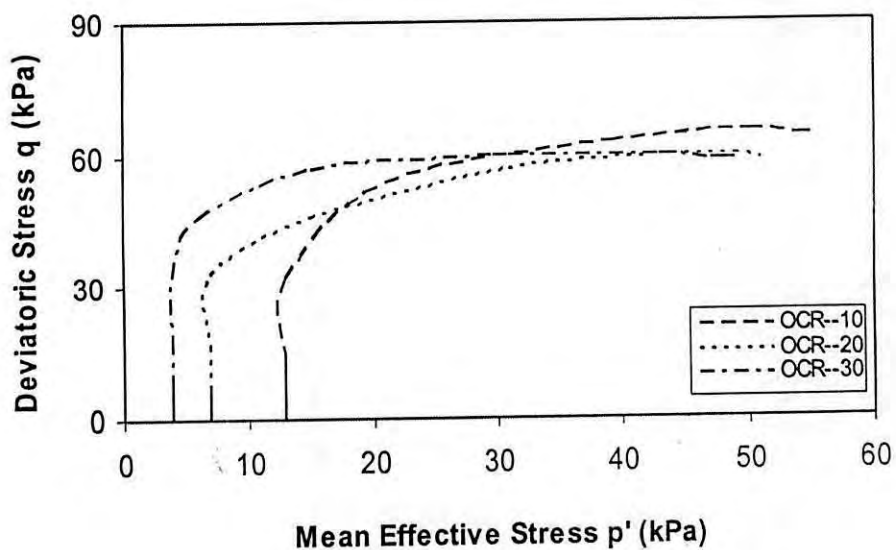


Figure 5.10 MCC prediction of undrained stress path of highly overconsolidated uncemented Savar clay.



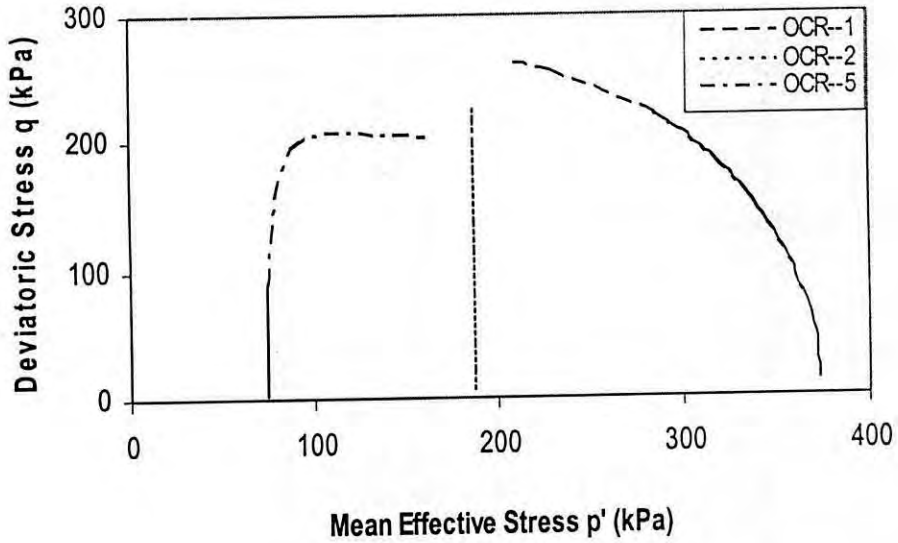


Figure 5.11 MCC prediction of undrained stress path of normally consolidated and low OCR 7% cemented Savar clay

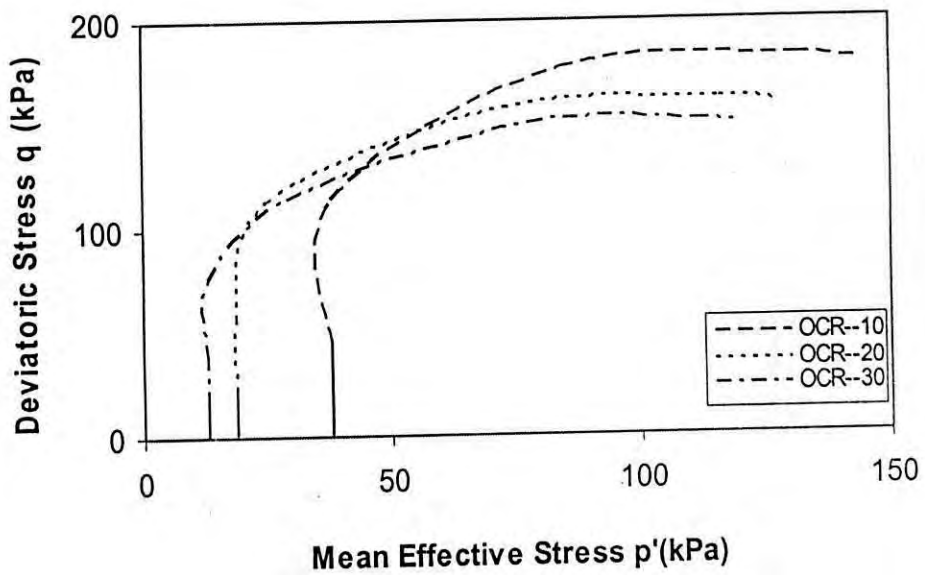


Figure 5.12 MCC prediction of undrained stress path of highly overconsolidated 7% cemented Savar clay.

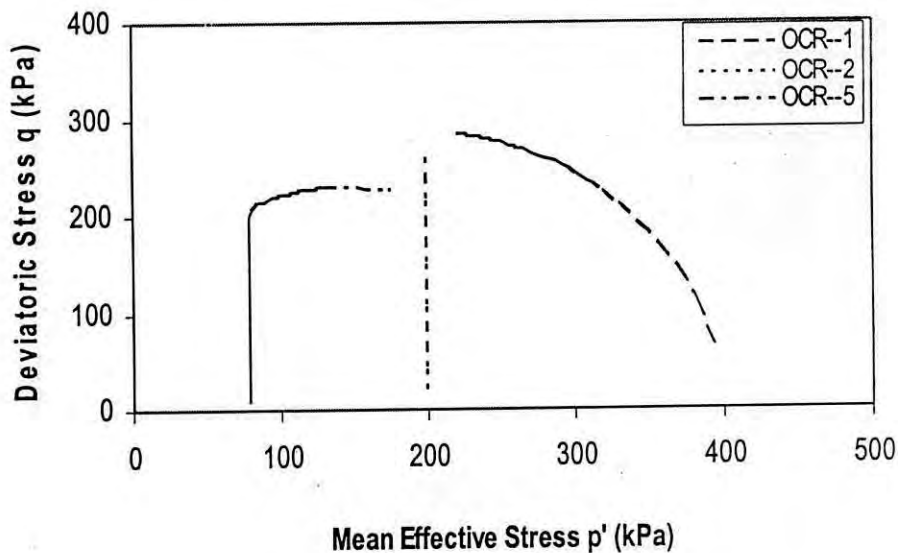


Figure 5.13 MCC prediction of undrained stress path of normally consolidated and low OCR 14% cemented Savar clay

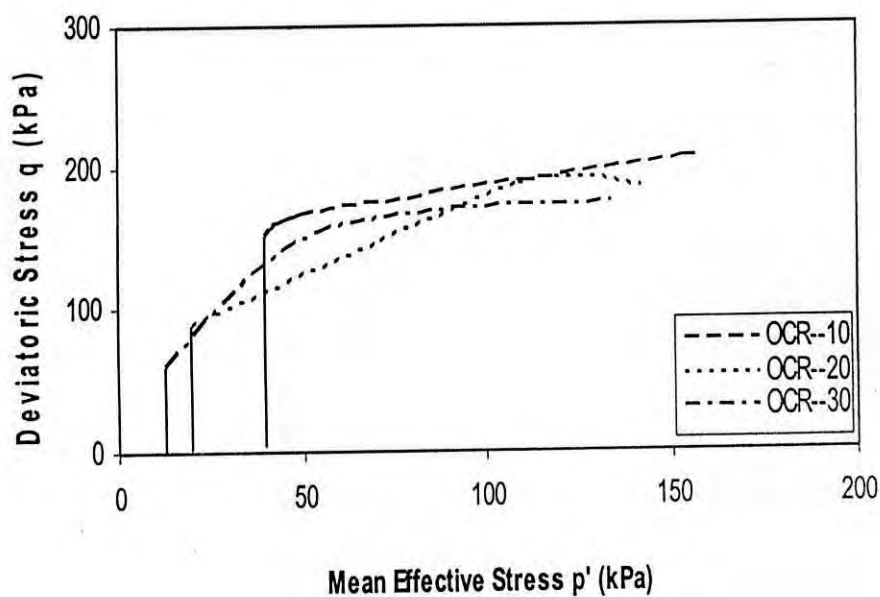


Figure 5.14 MCC prediction of undrained stress path of highly overconsolidated 14% cemented Savar clay.

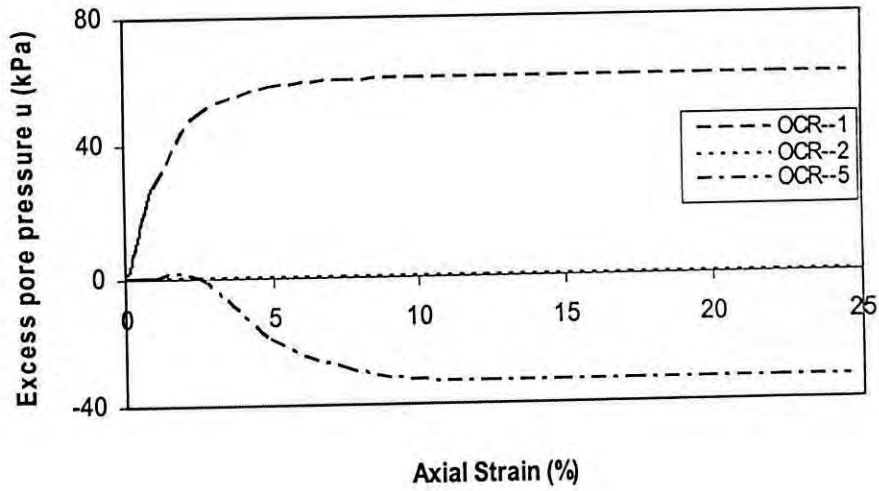


Figure 5.15 MCC prediction of excess pore pressure response of normally consolidated and low OCR uncemented Savar clay.

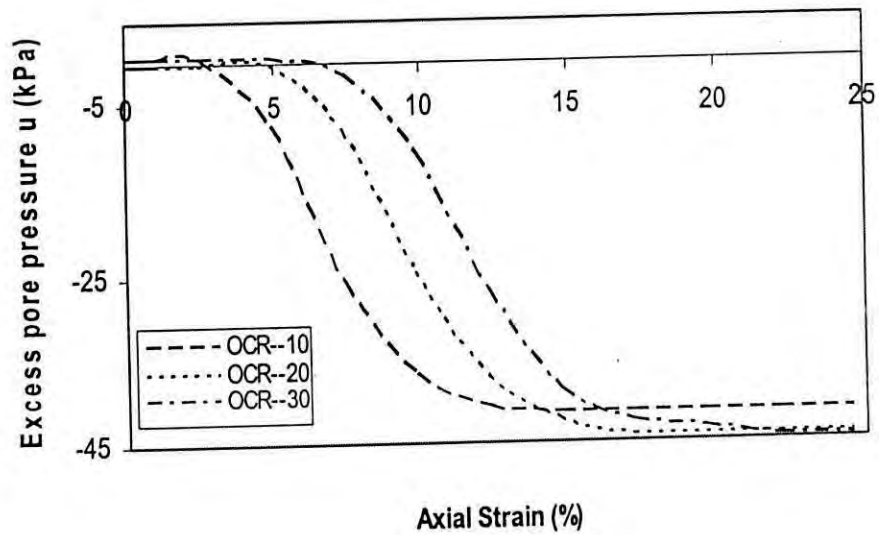


Figure 5.16 MCC prediction of excess pore pressure response of highly overconsolidated uncemented Savar clay.

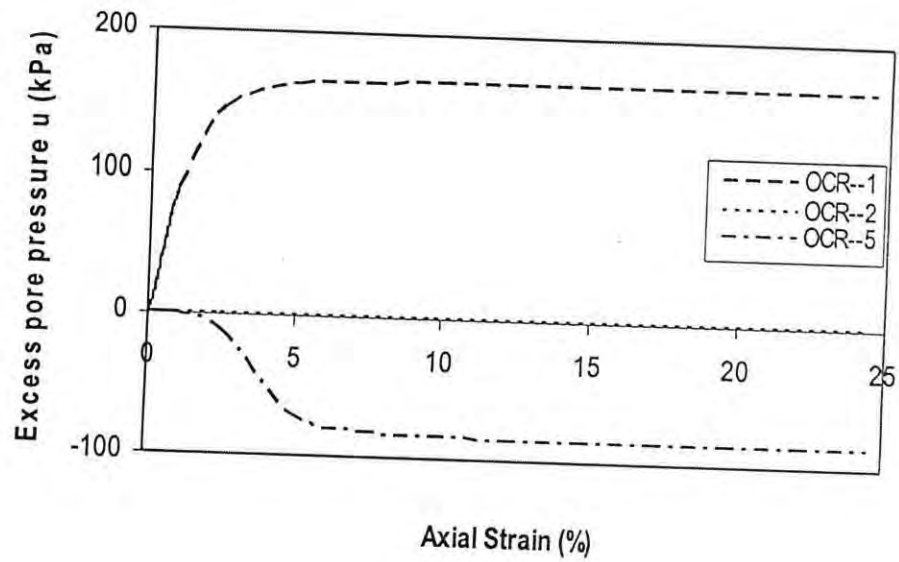


Figure 5.17 MCC prediction of excess pore pressure response of normally consolidated and low OCR 7% cemented Savar clay.

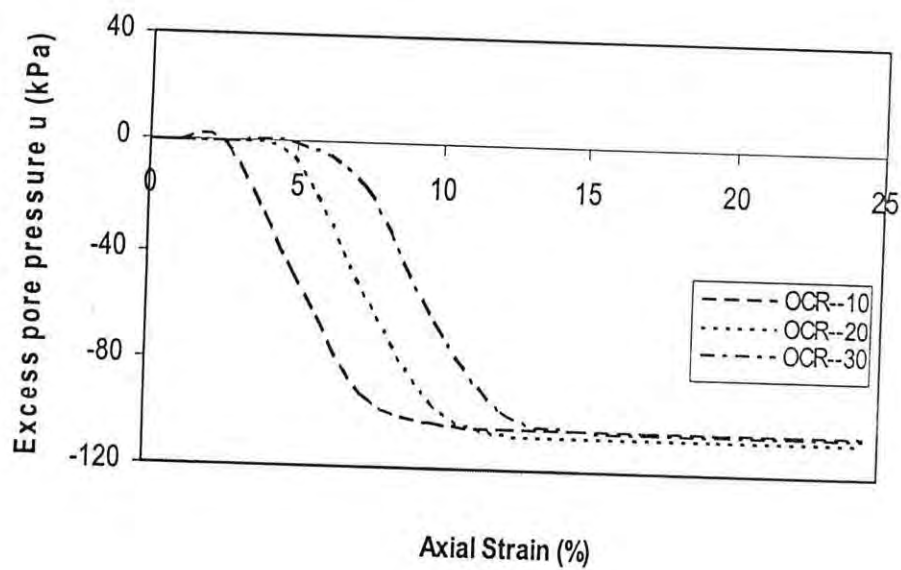


Figure 5.18 MCC prediction of excess pore pressure response of highly overconsolidated 7% cemented Savar clay.

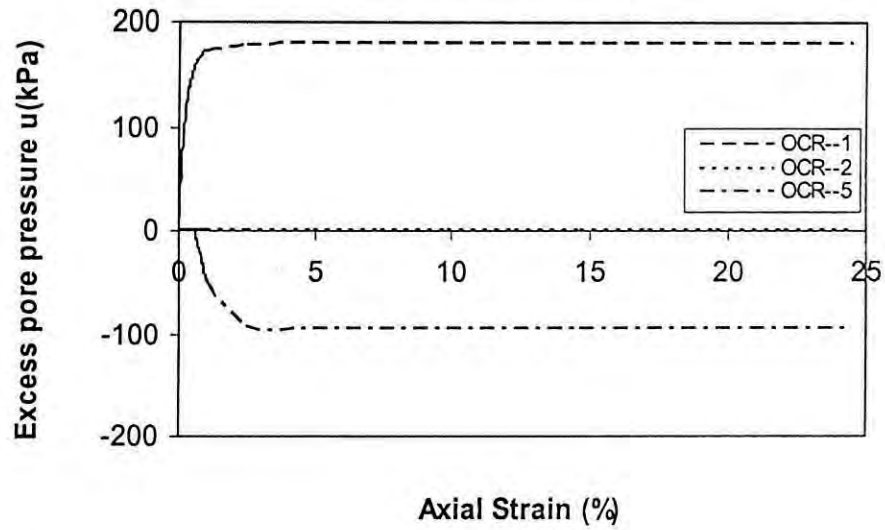


Figure 5.19 MCC prediction of excess pore pressure response of normally consolidated and low OCR 14% cemented Savar clay.

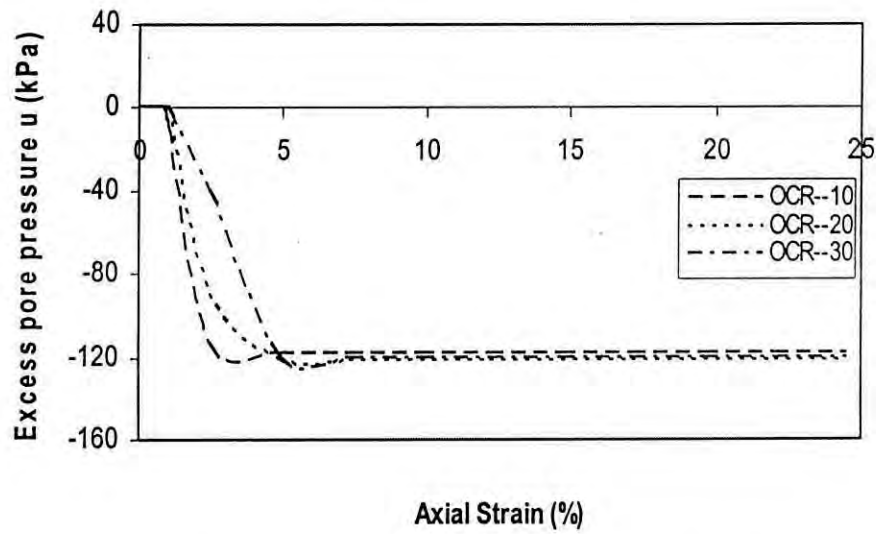


Figure 5.20 MCC prediction of excess pore pressure response of highly overconsolidated 14% cemented Savar clay.

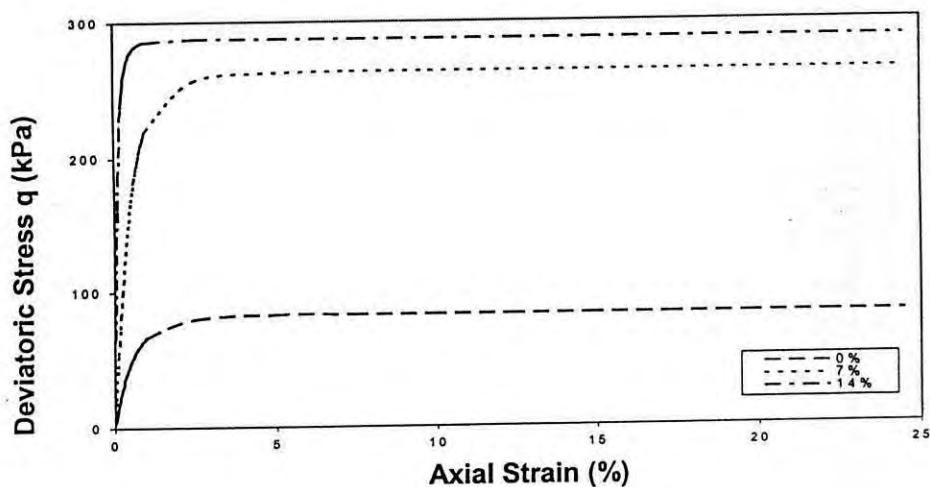


Figure 5.21 MCC prediction of undrained stress-strain response of normally consolidated reconstituted Savar clay (OCR = 1) for varying degrees of cementation.

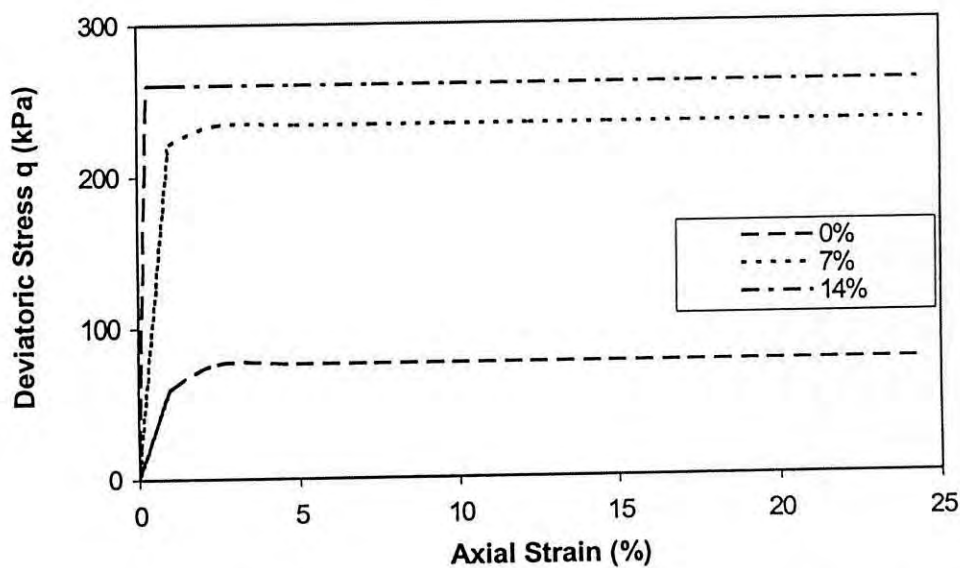


Figure 5.22 MCC prediction of undrained stress-strain response of low OCR (OCR = 2) reconstituted Savar clay for varying degrees of cementation.

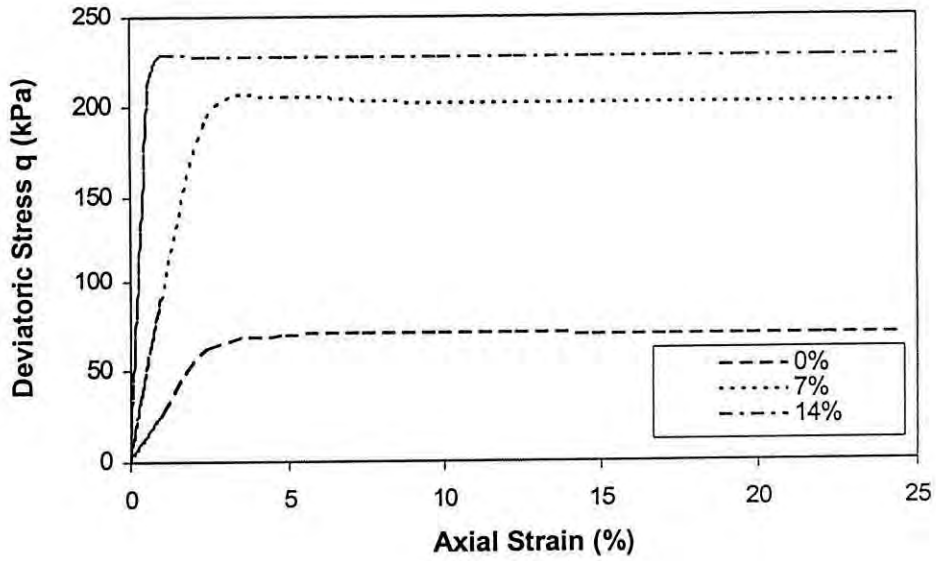


Figure 5.23 MCC prediction of undrained stress-strain response of moderately overconsolidated (OCR =5) reconstituted Savar clay for varying degrees of cementation

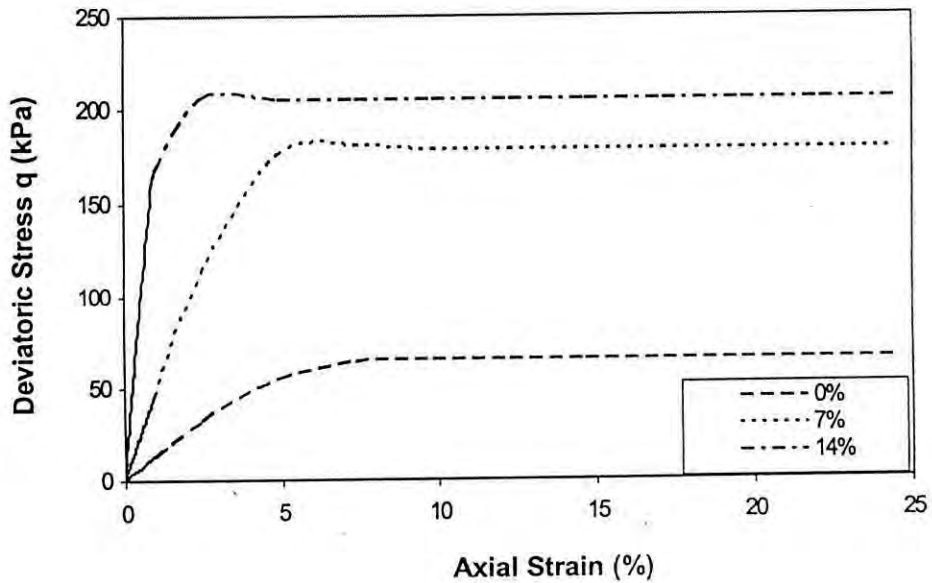


Figure 5.24 MCC prediction of undrained stress-strain response of highly overconsolidated (OCR =10) reconstituted Savar clay for varying degrees of cementation

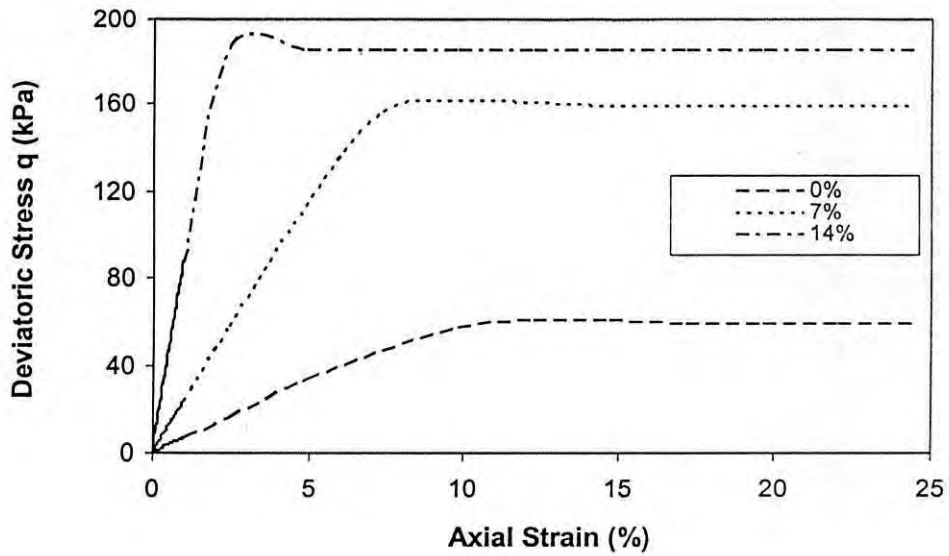


Figure 5.25 MCC prediction of undrained stress-strain response of highly overconsolidated (OCR =20) reconstituted Savar clay for varying degrees of cementation.

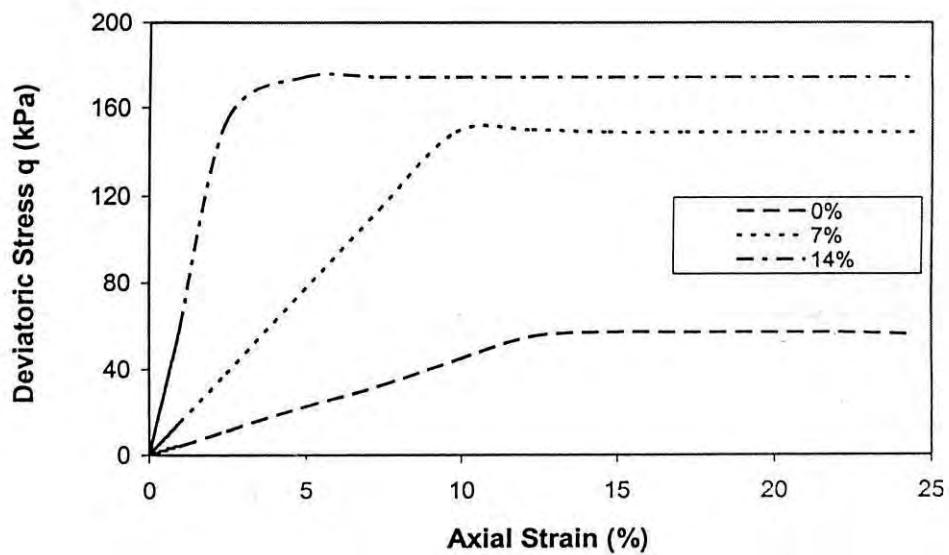


Figure 5.26 MCC prediction of undrained stress-strain response of highly overconsolidated (OCR =30) reconstituted Savar clay for varying degrees of cementation.



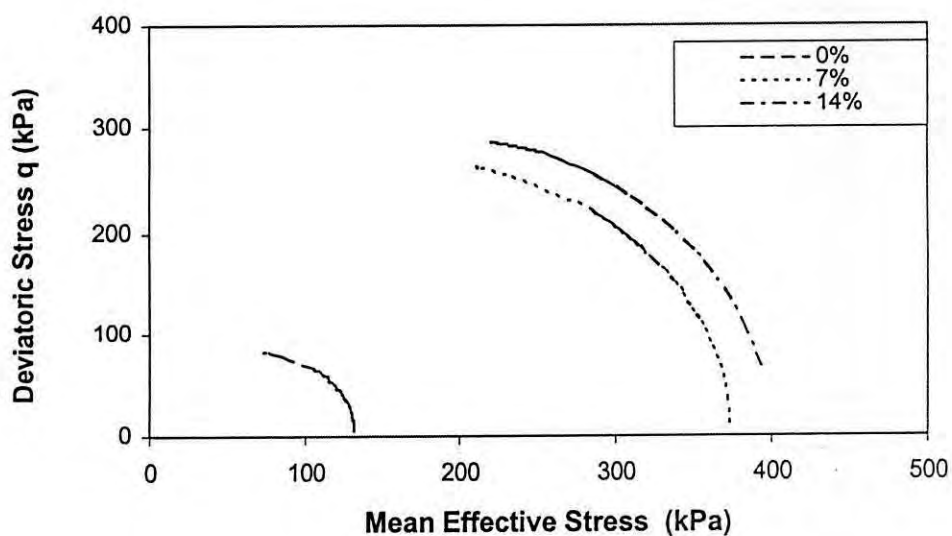


Figure 5.27 MCC prediction of undrained stress path of normally consolidated (OCR = 1) reconstituted Savar clay for varying degrees of cementation.

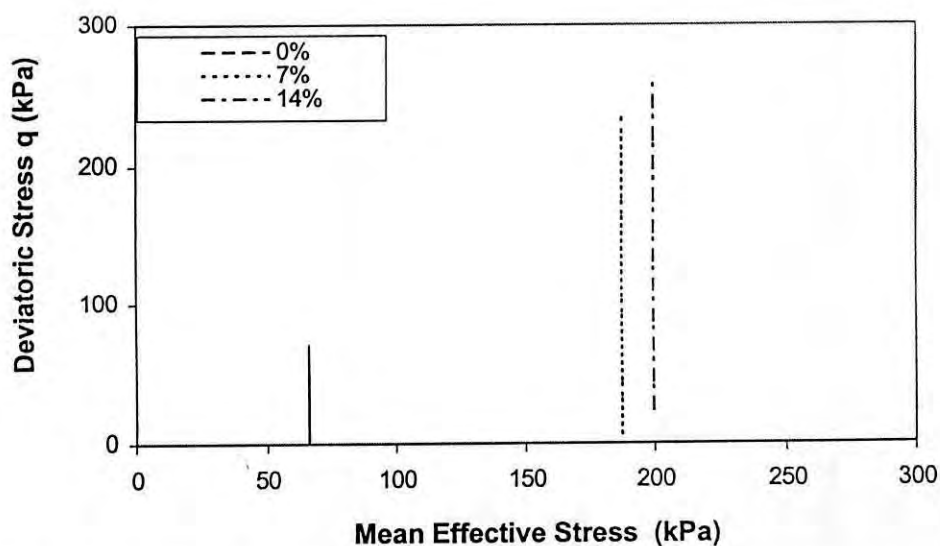


Figure 5.28 MCC prediction of undrained stress path of low overconsolidated (OCR = 2) reconstituted Savar clay for varying degrees of cementation.

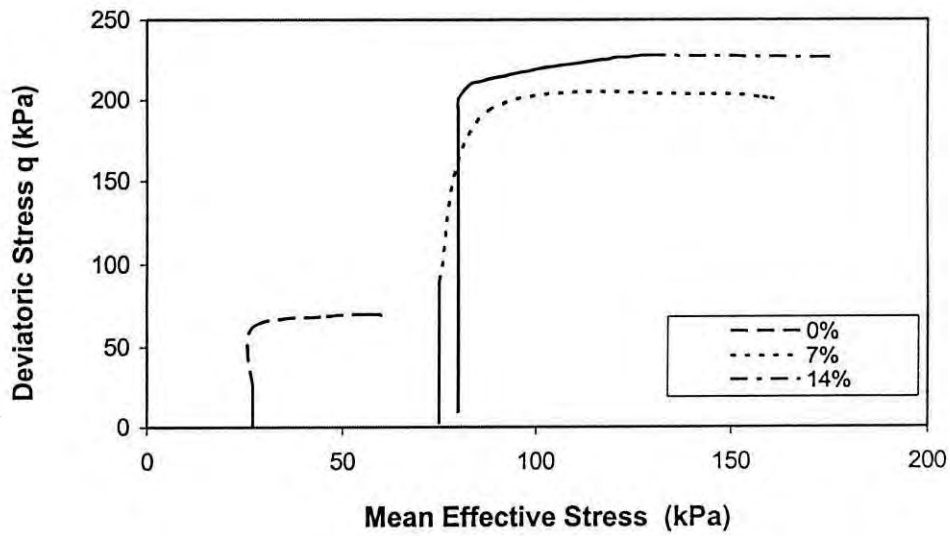


Figure 5.29 MCC prediction of undrained stress path of moderately overconsolidated ( $OCR = 5$ ) reconstituted Savar clay for varying degrees of cementation.

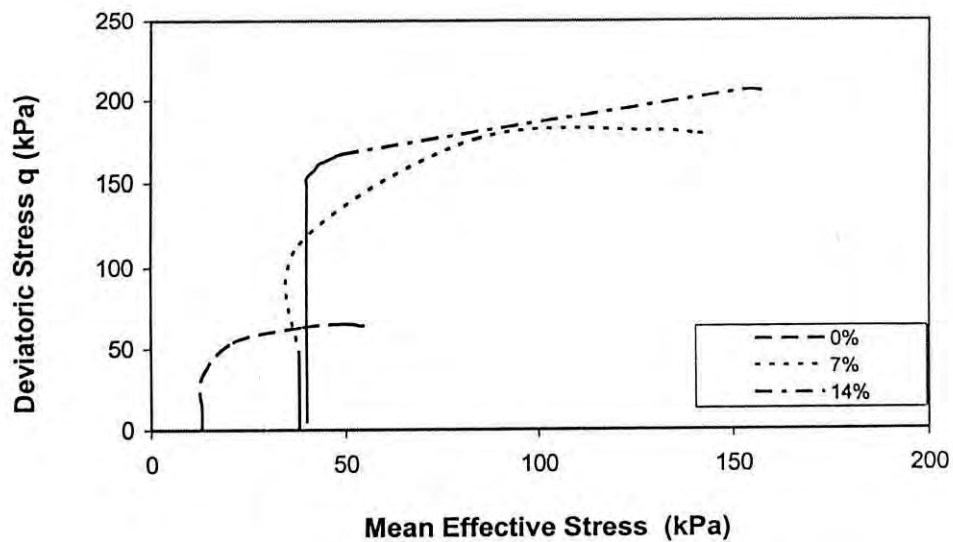


Figure 5.30 MCC prediction of undrained stress path of highly overconsolidated ( $OCR = 10$ ) reconstituted Savar clay for varying degrees of cementation.

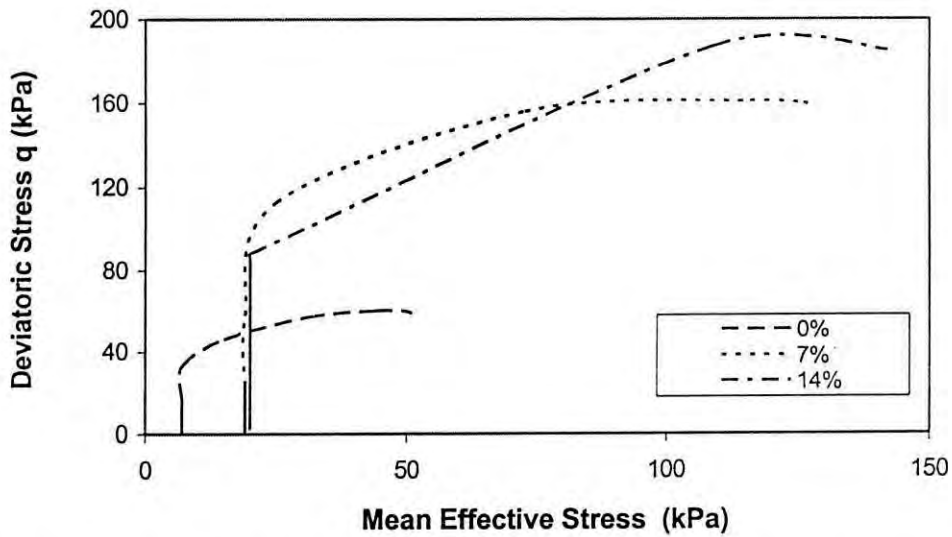


Figure 5.31 MCC prediction of undrained stress path of highly overconsolidated ( $OCR=20$ ) reconstituted Savar clay for varying degrees of cementation.

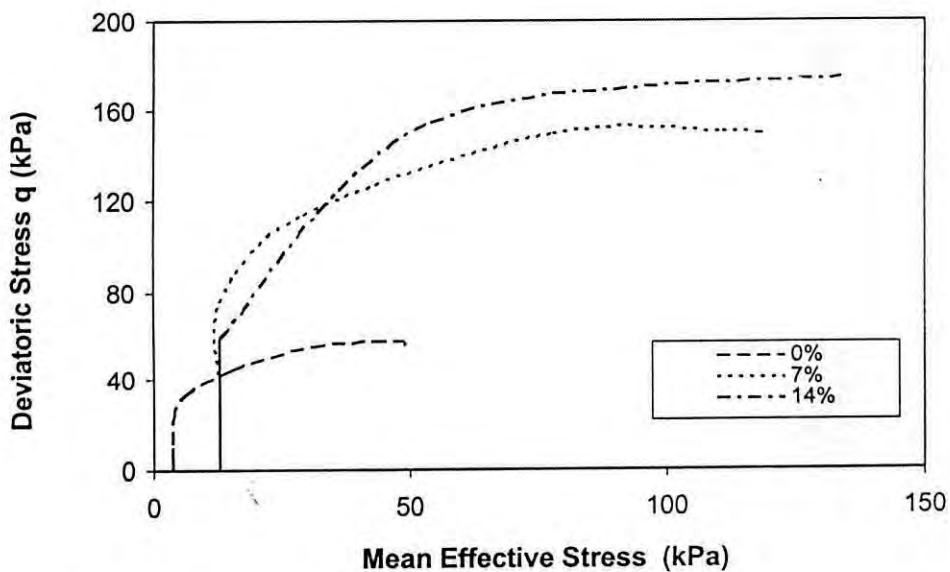


Figure 5.32 MCC prediction of undrained stress path of highly overconsolidated ( $OCR=30$ ) reconstituted Savar clay for varying degrees of cementation.

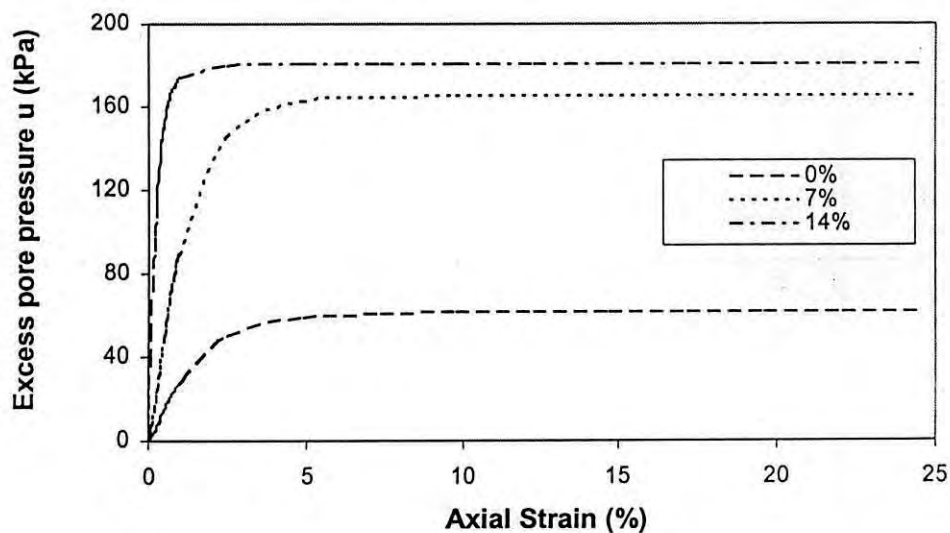


Figure 5.33 MCC prediction of excess pore pressure response of normally consolidated (OCR = 1) reconstituted Savar clay for varying degrees of cementation.

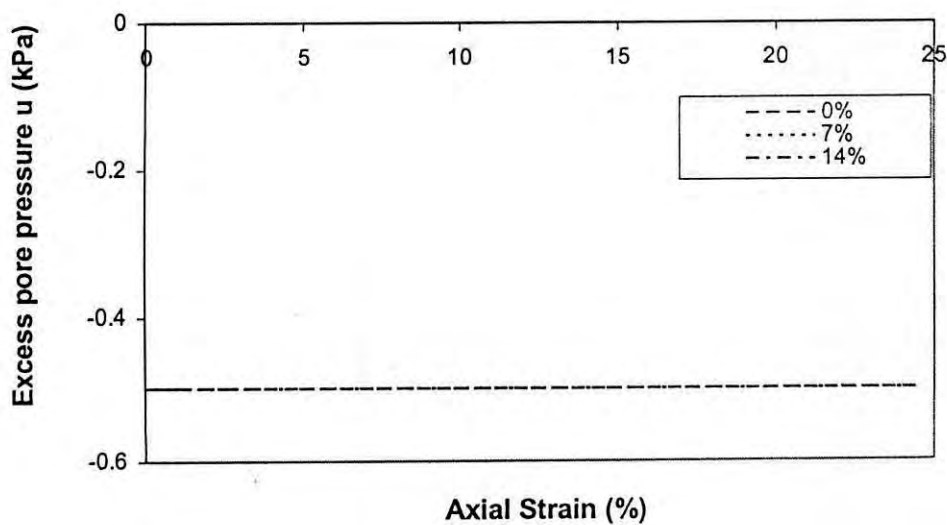


Figure 5.34 MCC prediction of excess pore pressure response of low overconsolidated (OCR = 2) reconstituted Savar clay for varying degrees of cementation.

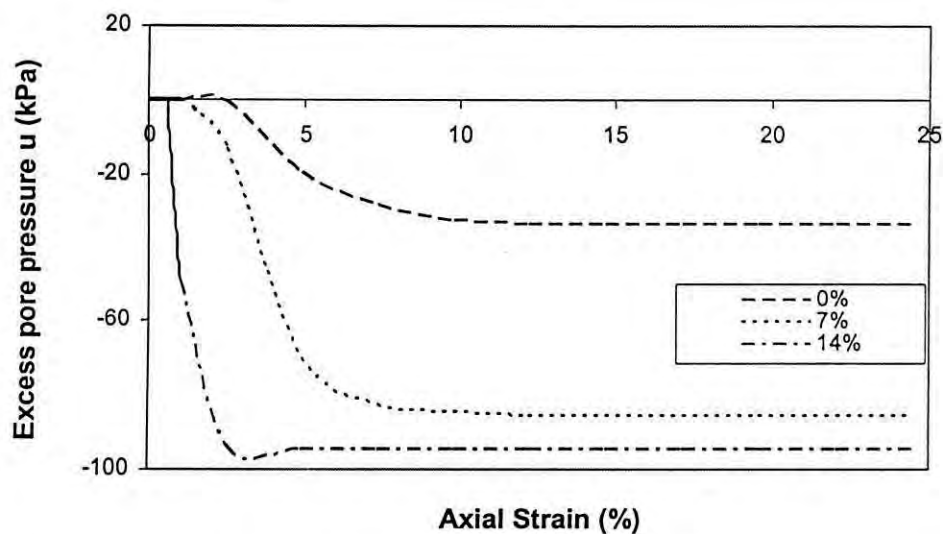


Figure 5.35 MCC prediction of excess pore pressure response of moderately overconsolidated ( $OCR = 5$ ) reconstituted Savar clay for varying degrees of cementation

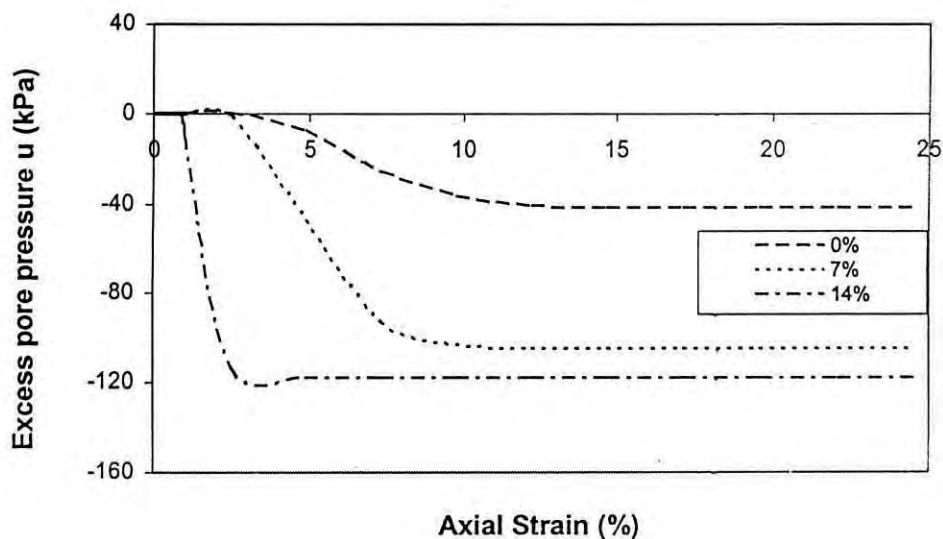


Figure 5.36 MCC prediction of excess pore pressure response of highly overconsolidated ( $OCR = 10$ ) reconstituted Savar clay for varying degrees of cementation.

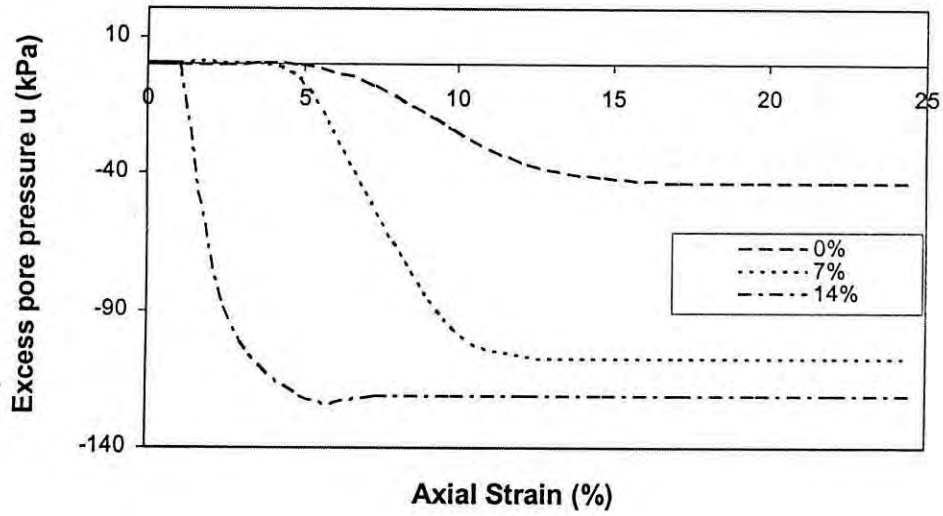


Figure 5.37 MCC prediction of excess pore pressure response of highly overconsolidated (OCR =20) reconstituted Savar clay for varying degrees of cementation.

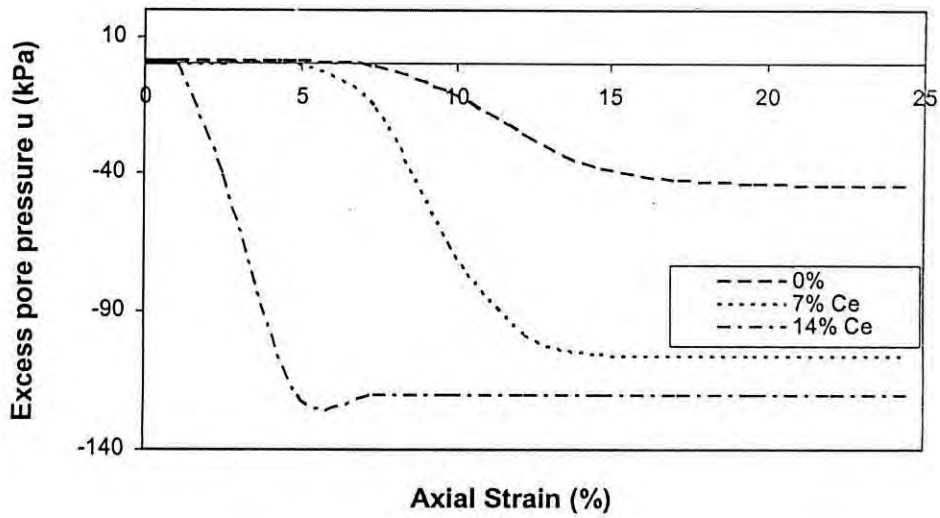


Figure 5.38 MCC prediction of excess pore pressure response of highly overconsolidated (OCR =30) reconstituted Savar clay for varying degrees of cementation

## CHAPTER 6

### DRAINED PREDICTIONS USING MCC MODEL

#### 6.1 Introduction

In this chapter, the Modified Cam Clay model is used to numerically predict the stress-strain and volume change response under triaxial stress states of normally consolidated, low OCR clays and over consolidated reconstituted Savar clays, with and without cementation, and under drained condition. Most of the significant parameters of the Modified Cam Clay model parameters for reconstituted Savar clays, with and without cementation, were obtained experimentally, which have been used to obtain the numerical predictions. The numerical predictions obtained for stress-strain and volume change responses of reconstituted Savar clays for various OCR's and with and without cementation were compared and analyzed. Finally, observations were made regarding the weaknesses, limitations and the capabilities of the MCC model to predict the drained response of reconstituted Savar clays.

#### 6.2 Approaches in Drained Analysis

The excess pore water pressure is zero under drained conditions and the sample changes in volume. Drained conditions are generally assumed to exist in clay layers when the rate of loading is very slow. In undrained condition, there is no volume change. Consequently excess pore pressure develops within the soil sample. This kind of situations occurs in conditions of rapid application of the load. Fully saturated conditions have been assumed both for drained as well as undrained analysis.

The MCC model is a mathematical model giving the response of clays to applied loads. In the undrained analysis, the bulk modulus of water is generally given a very high value

compared to the bulk modulus of soil particles. As a result an incompressibility condition is simulated. On the other hand, in drained conditions, the bulk modulus of water is set equal to zero. Volume change of the soil skeleton is then predicted. No excess pore water pressures are predicted under these circumstances. For clays, the value of the drained elastic Poisson's ratio is generally assumed to be between 0.1 to 0.3.

### 6.3 Drained MCC Parameters

It is observed that the MCC model parameters are identical for both undrained and drained analysis, except for the value of the elastic Poisson's ratio. In the absence of experimental data, the drained Poisson's ratio for reconstituted Savar clays with and without cementation has been assumed to be 0.3.

### 6.4 Drained MCC Predictions

#### 6.4.1 Stress-Strain

Figures 6.1 through 6.6 respectively give the predictions of stress-strain response of reconstituted Savar clays, with and without cementation, at different OCR's under triaxial condition. In each case, the MCC model is observed to predict non-linear strain hardening behavior. However, the initial elastic non-linear effect is observed to be negligible. For normally consolidated, low OCR and moderately overconsolidated clays (OCR's 1, 2 and 5), the predicted elastic shear stiffness under drained conditions increases with increasing OCR. For high OCR clays (OCR values of 10, 20 and 30), the reverse is observed. That is, in these cases, the predicted elastic shear stiffness decreases with increasing OCR. This happens as the MCC model assumes the elastic stiffness of the clay to be directly proportional to the applied mean effective stress. At the ultimate state, continuous axial strains are predicted to occur at constant deviator stress. However, for moderately high OCR clays (OCR's 5, 10, 20 and 30), a peak stress state is first reached. Strain softening or decreasing deviator stress with increasing axial strains is



predicted beyond the peak. These predictions are observed for reconstituted Savar clays both with and without cementation. However, for increasing cementation, sharper peaks at higher deviator stresses are observed. In this case, the strain softening response is observed to be relatively rapid.

#### 6.4.2 Stress Path and Volume Response

Figures 6.7 through 6.12 show the predicted drained stress paths for reconstituted Savar clays, with and without cementation, at different OCR values. Under drained condition and during triaxial shear, the drained total and effective stress paths are identical. The stress path is the total stress path applied under triaxial condition. It is independent of the constitutive model used. The ratio of the increment of deviator stress to the increment of mean effective pressure is 3 under triaxial test conditions. The following condition holds during triaxial shear under drained conditions:

$$\frac{\Delta q}{\Delta p} = \frac{\Delta q}{\Delta p'} = 3$$

Here  $\Delta q$ ,  $\Delta p$ ,  $\Delta p'$  are respectively the increment of deviator stress, increment of mean effective pressure and increment of total effective pressure in the soil sample. The stress paths predicted by MCC model under drained condition are always inclined straight lines in  $p' - q$  space with slope equals to 3 to 1. The stress path starts at the mean isotropic pressure axis at a value of mean effective pressure equal to the cell pressure.

The volume response predictions for reconstituted Savar clays without cementation, and with 7% and 14% cementation, are shown in Figures 6.13 through 6.17 respectively. For normally consolidated and low OCR clays (OCRs 1 and 2 only) positive volume response is predicted. An initially positive volume response is predicted at moderate overconsolidation ratio of 5. However, subsequent to further shearing, negative volume responses are predicted. In case of highly overconsolidated clays (OCR values of 10, 20

and 30), the MCC model predicts a small positive volume response at the initial stage. This is the elastic part of the volume change. On further shearing, high OCR cases predict negative volume change. The higher percentage of cement content in clays, the higher is the negative volume change response predicted.

## **6.5 Comparison of Cemented and Uncemented behavior**

In the following subsections, the prediction of the stress-strain, stress path and volume change response of the reconstituted Savar clays, for normal, light and moderately overconsolidated clays, and those for highly over consolidated clays, are compared and analyzed, for varying degrees of cementation.

### **6.5.1 Stress-Strain**

Figures 6.19, 6.20 and 6.21 compare the predicted stress-strain response under drained conditions, of normally consolidated and low overconsolidated reconstituted Savar clays, using the MCC model under varying degrees of cementation. In these figures, the stress-strain behaviour of reconstituted Savar clays with varying degrees of cementation for over-consolidation ratios of 1, 2 and 5 are shown. It may be clearly observed from the figures that the MCC model predicts increased initial shear stiffness as well as increased ultimate shear resistance of the soil at each OCR with varying degrees of cementation. The reconstituted Savar clays, having OCR values of 10, 20 and 30 respectively are considered here as highly overconsolidated clay. Comparison of the predicted stress-strain response of highly overconsolidated reconstituted Savar clays, under drained conditions and for different degrees of cementation (0%, 7% and 14%) using the Modified Cam Clay model are shown in Figures 6.22, 6.23 and 6.24. It is observed from these figures that in these cases, the MCC model predicts increased initial shear stiffness as well as increased ultimate shear resistance of the soil, with increasing degrees of cementation. It is also observed from the figures that in this case, after

reaching a peak value of deviator stress, strain softening occurs. Thus, in these cases, the deviator stress decreases with increasing axial strain. Decreasing deviator stresses are associated with expansive volume changes. Beyond a certain axial strain, a constant state of shear stress is reached. This is the ultimate or critical state. There is no longer any volume change at this state.

### 6.5.2 Stress Path

Figures 6.25 through 6.30 show the drained stress paths of the uncemented reconstituted Savar clay and those with 7% and 14% cementation. The drained stress paths for all OCR and for all degrees of cementation are qualitatively identical. In all cases, the stress paths are inclined straight lines starting from initial applied mean pressure axis and having an incremental slope equal to 3.

### 6.5.3 Volume change response

Figures 6.31, 6.32 and 6.33 show the volume change response for reconstituted Savar clays at various degrees of cementation for OCR values of 1, 2 and 5 respectively. Positive volume changes are predicted for all degrees of cementation and for OCR values of 1 and 2. However, the predicted volume changes are lower, the higher the degree of cementation. For OCR value of 5, the initial volume changes are positive or compressive. However, with further shearing strains, negative or expansive volume changes are predicted in all cases. In each case, the higher the degree of cementation, the higher are the predicted suction pressures.

Figures 6.34, 6.35 and 6.36 compare the predicted volume change responses for reconstituted Savar clays at various degrees of cementation (0%, 7%, and 14%) and for OCR values of 10, 20 and 30 respectively. In all cases, initially a small positive or compressive volume change response is predicted. This is the elastic volume change. On further shearing, negative or expansive volume change responses are predicted. From the

figures, the predicted expansive volume change are observed to be higher, the lower the degree of cementation.

### 6.6 Comparison of Drained and Undrained Predictions

Initial shear stiffness and shear resistance is observed to be some what higher in drained conditions for normal, low and overconsolidated clays, and in all cases of cementation. But this difference is not significant. Under drained condition, the effective stress path predicted is determined by the condition of the stress states in the test (in this case a triaxial state of stress). The stress paths in  $p' - q$  space are inclined straight lines with an incremental slope of 3. The stress path is independent of constitutive properties of the soil. On the other hand, the effective stress path is dependent on the model used for undrained predictions. The predicted initial effective stress paths under undrained condition in  $p' - q$  space are observed to be gently curved for reconstituted Savar clays with and without cementation.

During undrained shearing of normally consolidated and low OCR Savar clays, positive pore pressure develops. Consequently, the mean effective pressure is predicted to decrease. As a result, the predicted deviator stress at failure is generally lower than that during drained shear, for normally consolidated and low OCR clays. During drained shearing of normally consolidated and low OCR clays, no pore pressure develops. Rather compressive volume change response of the soil is observed. During undrained shear of overconsolidated clays, negative pore pressure develops. Consequently, the mean effective pressure is predicted to increase. As a result, during undrained shearing, the predicted deviator stress at failure is either somewhat higher or very close to that during drained shear, for high OCR clays. During drained shearing of overconsolidated clays, expansive volume change response is predicted and softening response of the clay is observed. Due to the stabilizing effect of suction or negative pore pressure, no such softening response is predicted in undrained test.

### 6.7 Limitations of the Modified Cam Clay Model

The MCC model has generally been observed to give good qualitative predictions of the stress-strain and volume change response of clays. However, it does suffer from limitations. For overconsolidated clays, the initial stress-strain response predicted by the MCC model is non-linear elastic. However, for many types of clays, even the initial stress-strain response has been observed to be elasto-plastic. For high OCR clays, the stress-strain, pore pressure and volume change response prediction is observed to be qualitatively correct. However, no experimental tests were carried out for reconstituted Savar clays as part of this study. In the absence of tests, it is not possible to make specific quantitative observations regarding the limitations of the MCC model to predict the stress-strain response of such clays.

### 6.8 Summary and Conclusion

Under triaxial states of stress and drained conditions, the stress-strain, stress path and volume change response of reconstituted Savar clays, with and without cementation, were predicted using the Modified Cam Clay model. The numerical predictions were made for triaxial stress states under drained conditions, for various values of overconsolidation ratios, simulating drained laboratory triaxial tests. The predictions show the stress-strain and volume change responses of reconstituted Savar clays for various OCR's and for various degrees of cementation, appear to be realistic and typical to the behaviour observed for clays. Cementation increases the drained shear strength and drained shear stiffness of clays. MCC model also predicts higher drained shear strength and stiffness for high overconsolidation ratios.

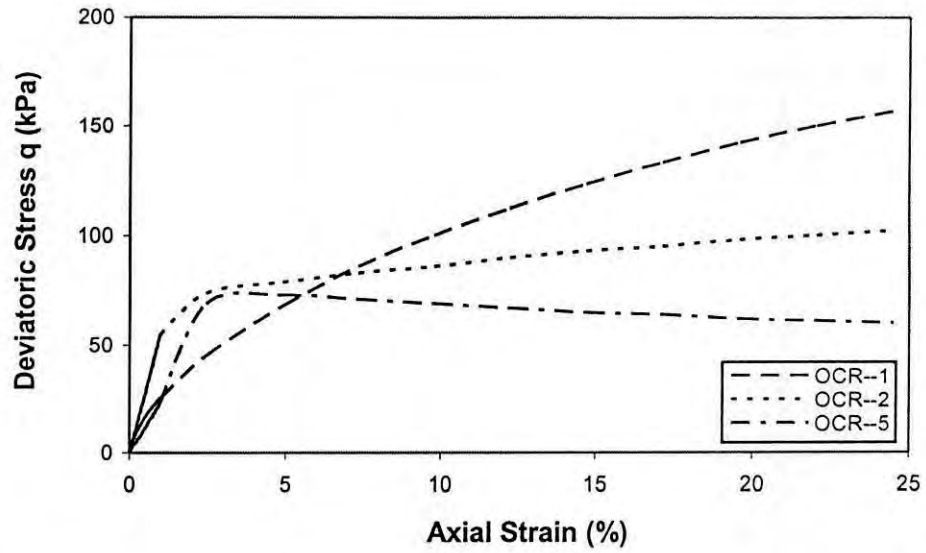


Figure 6.1 MCC prediction of drained stress-strain response of normal, low, and moderately overconsolidated uncemented Savar clay

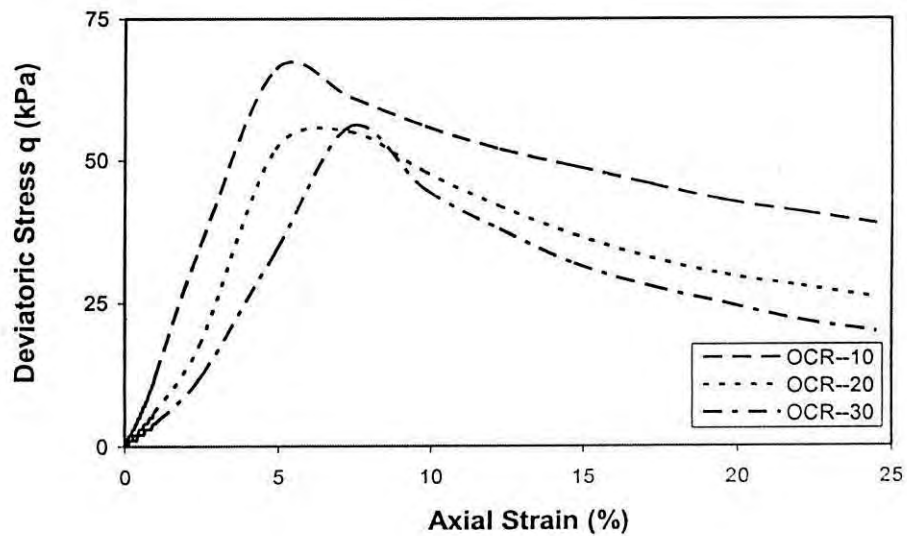


Figure 6.2 MCC prediction of drained stress-strain response of highly overconsolidated uncemented Savar clay

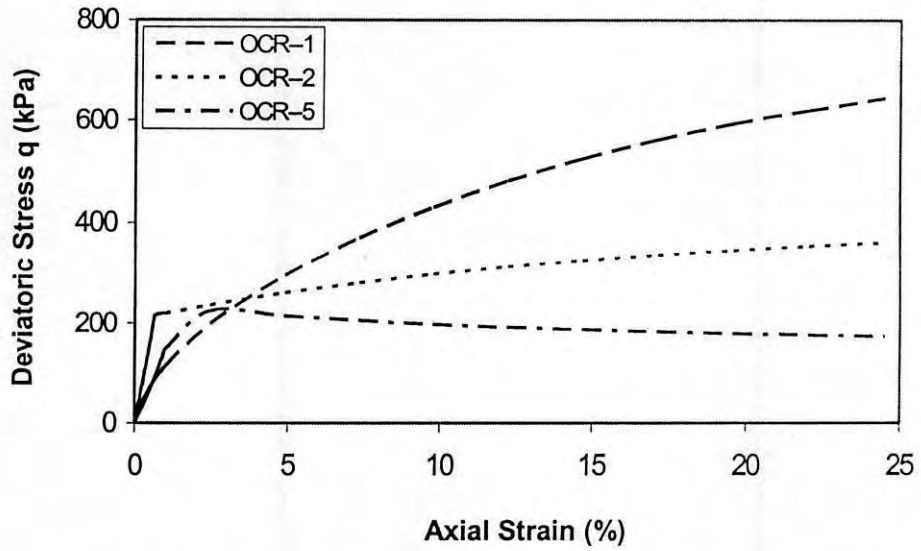


Figure 6.3 MCC prediction of drained stress-strain response of normal, low, and moderately overconsolidated 7% cemented Savar clay

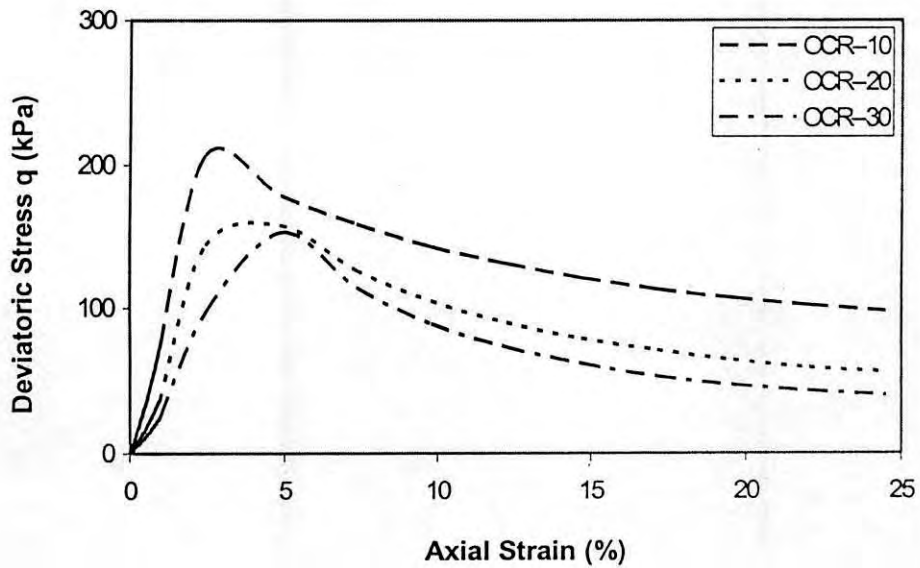


Figure 6.4 MCC prediction of drained stress-strain response of highly overconsolidated 7% cemented Savar clay

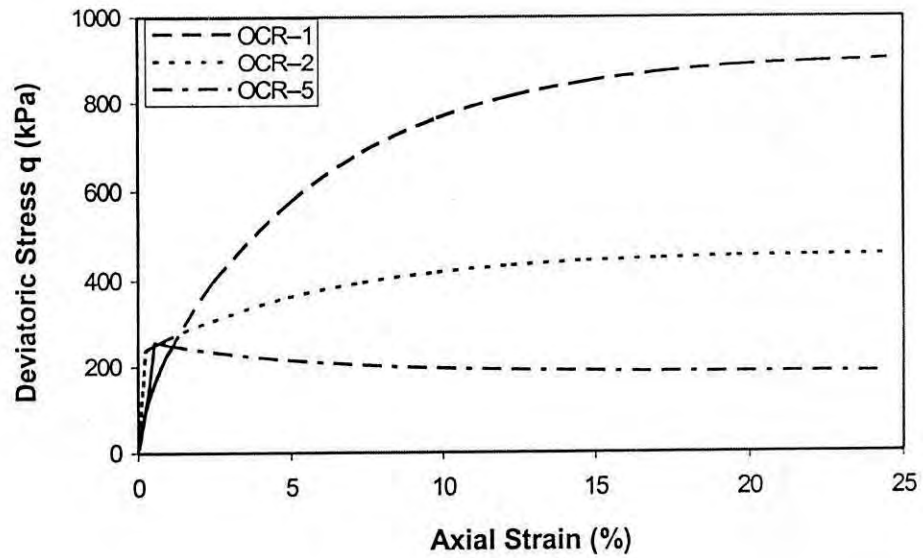


Figure 6.5 MCC prediction of drained stress-strain response of normal, low, and moderately overconsolidated 14% cemented Savar clay

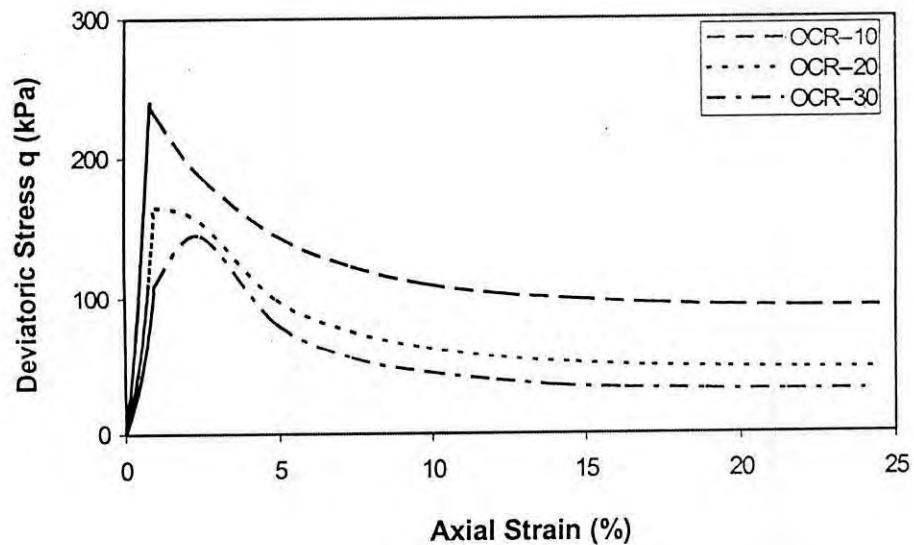


Figure 6.6 MCC prediction of drained stress-strain response of highly overconsolidated 14% cemented Savar clay



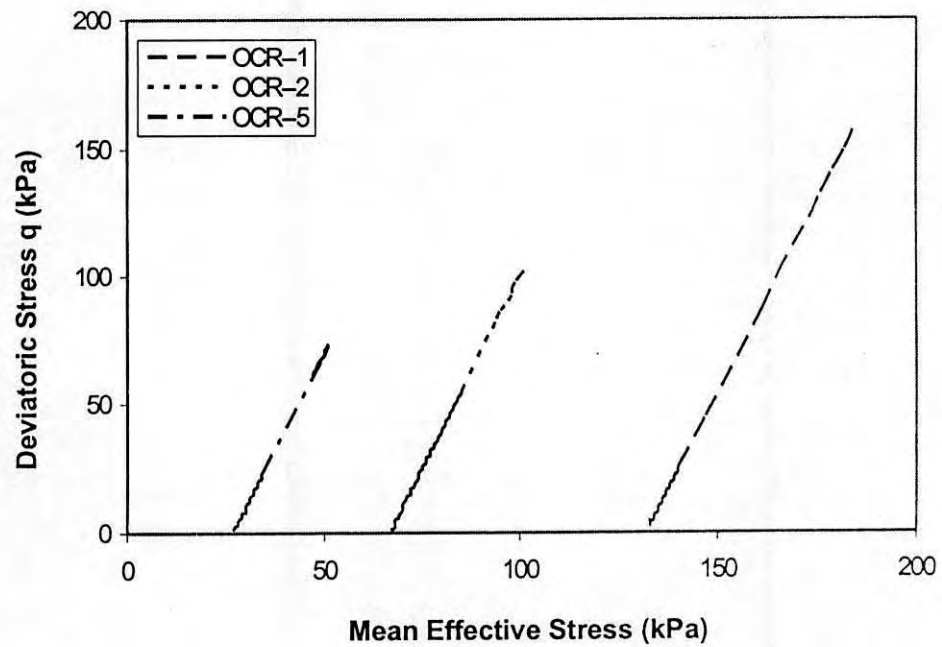


Figure 6.7 MCC drained stress path of normal, low, and moderately overconsolidated uncemented Savar clay

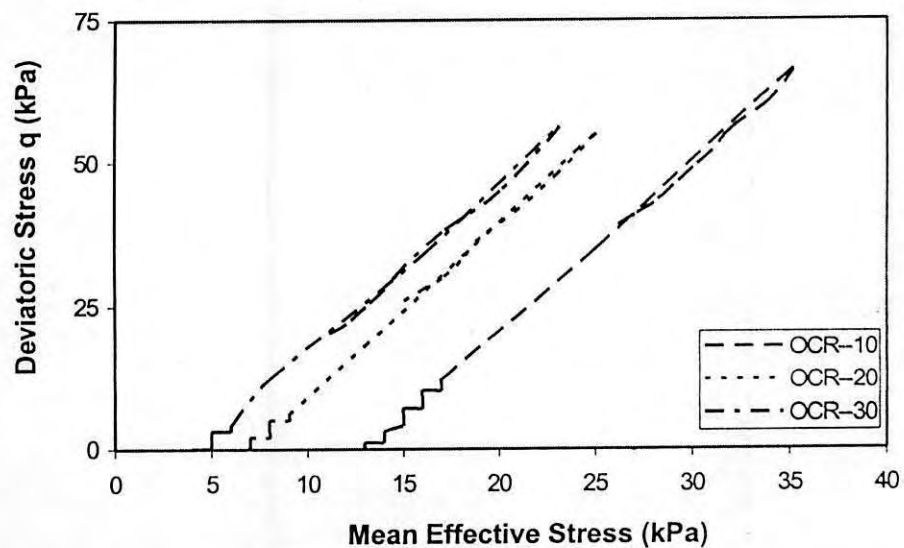


Figure 6.8 MCC drained stress path of highly overconsolidated uncemented Savar clay

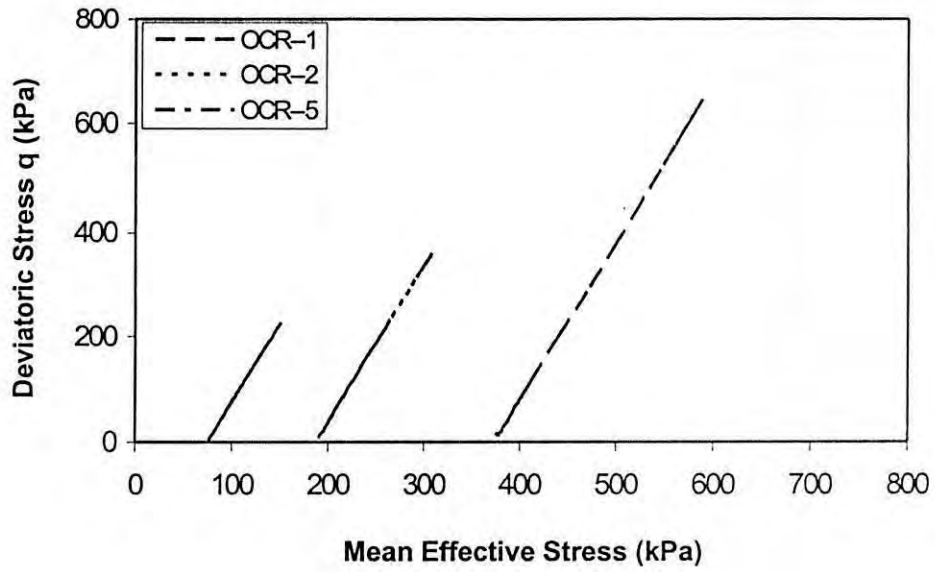


Figure 6.9 MCC drained stress path of normal, low, and moderately overconsolidated 7% cemented Savar clay

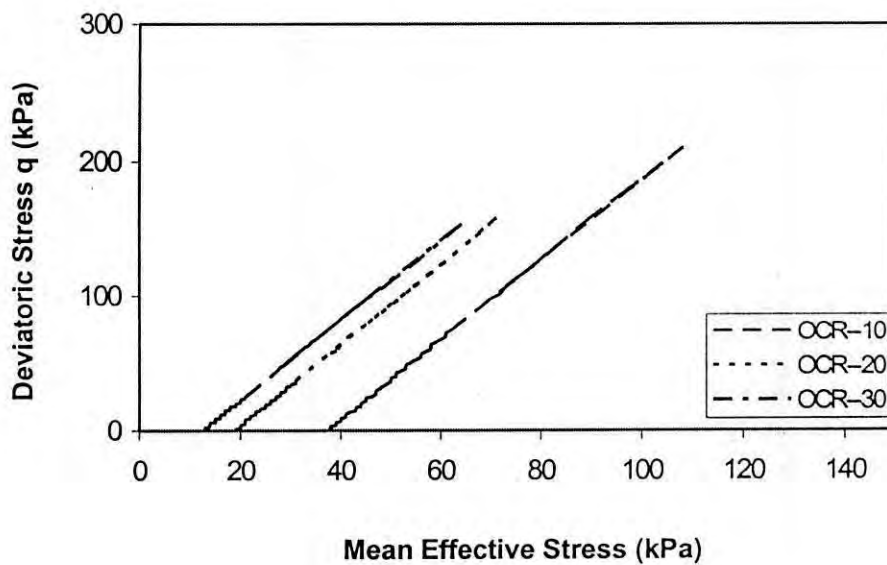


Figure 6.10 MCC drained stress path of highly overconsolidated 7% cemented Savar clay

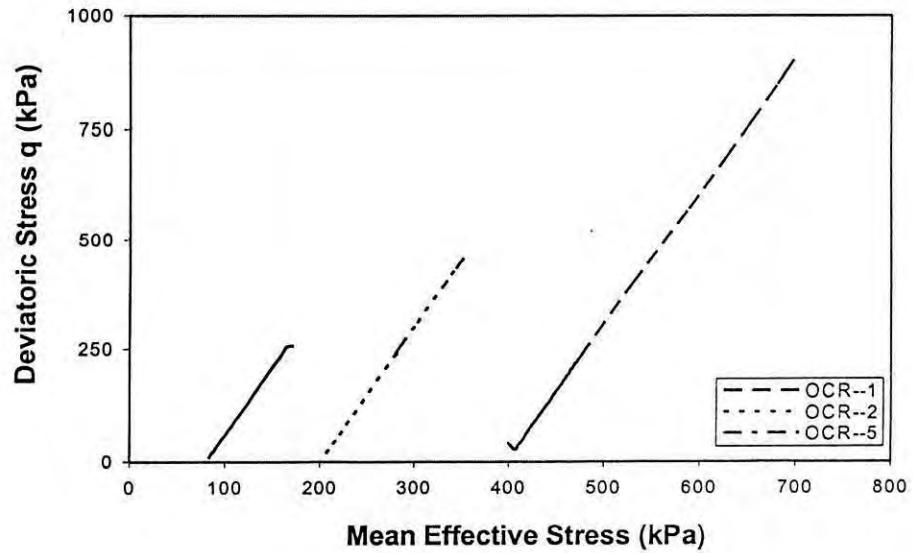


Figure 6.11 MCC drained stress path of normal, low, and moderately overconsolidated 14% cemented Savar clay

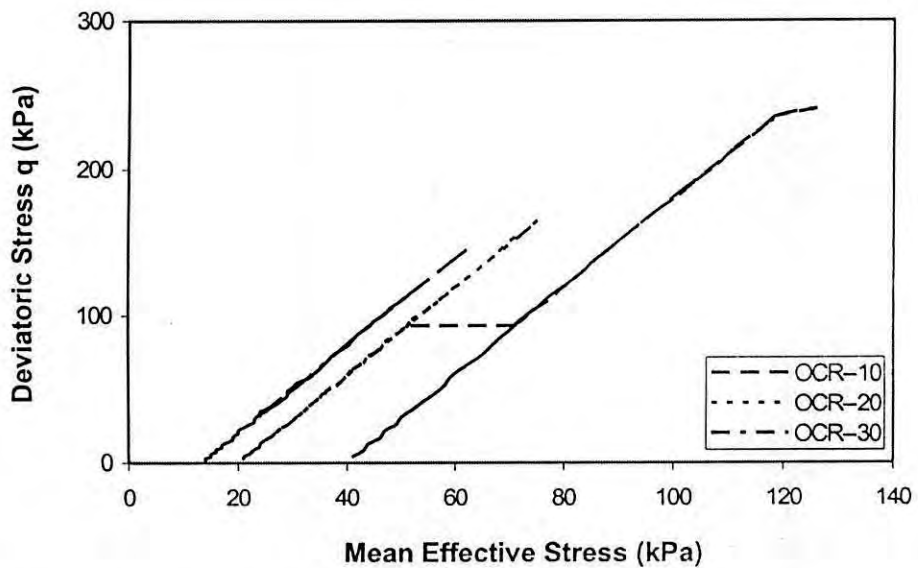


Figure 6.12 MCC drained stress path of highly overconsolidated 14% cemented Savar clay

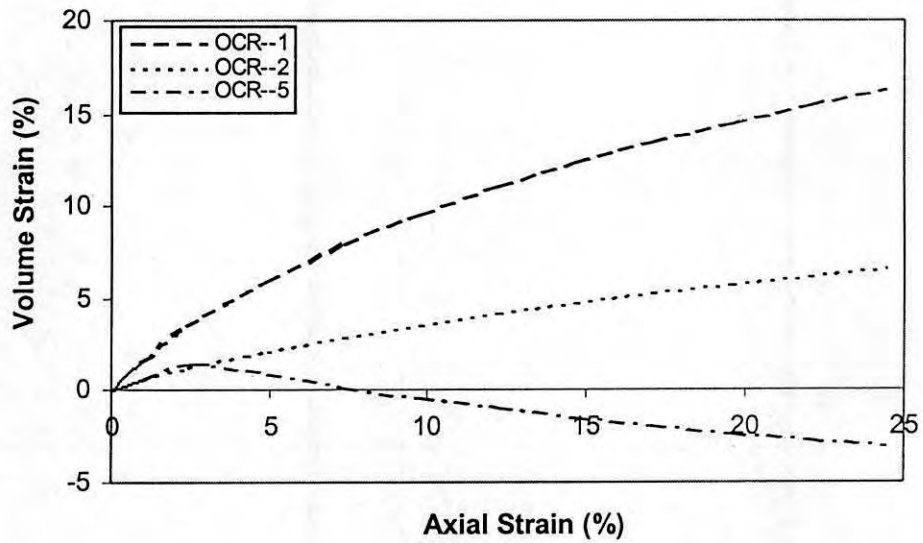


Figure 6.13 MCC predictions of volume strain response of normal, low, and moderately overconsolidated uncemented Savar clay

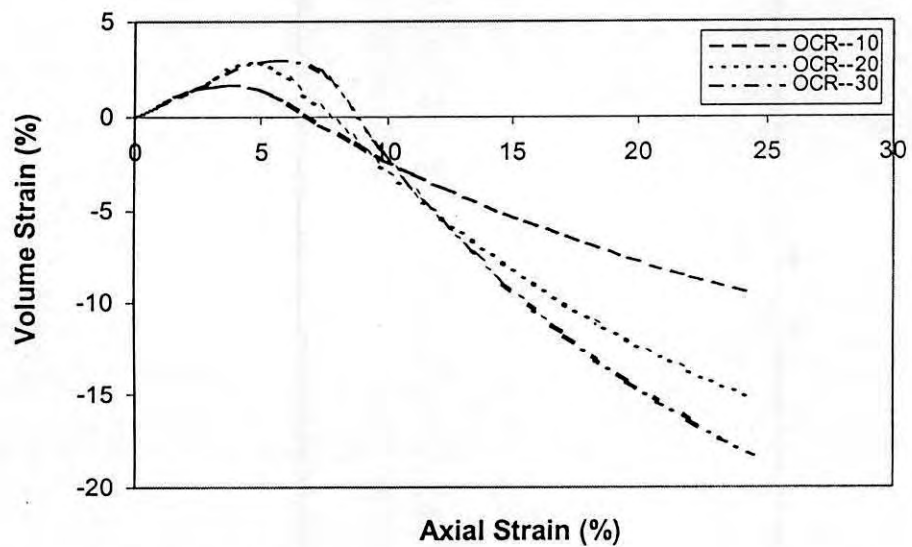


Figure 6.14 MCC predictions of volume strain response of highly overconsolidated uncemented Savar clay

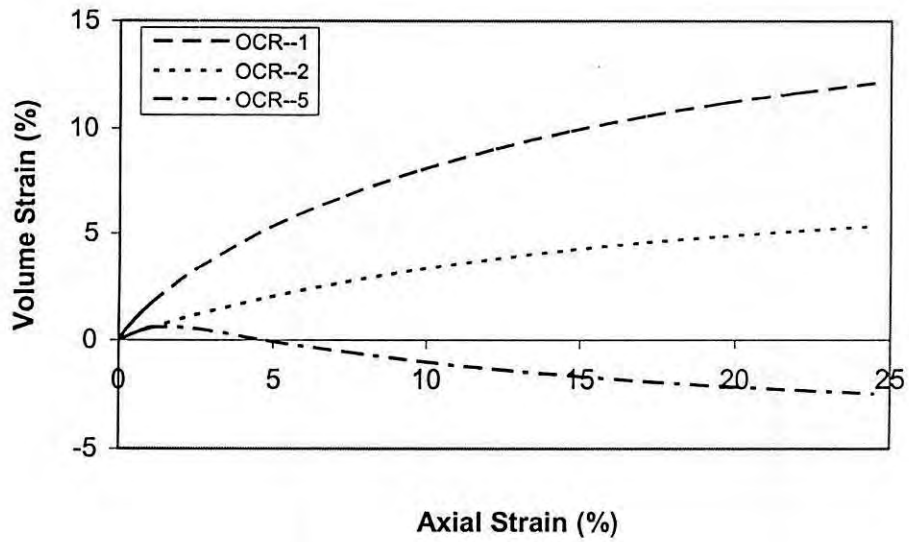


Figure 6.15 MCC predictions of volume strain response of normal, low, and moderately overconsolidated 7% cemented Savar clay

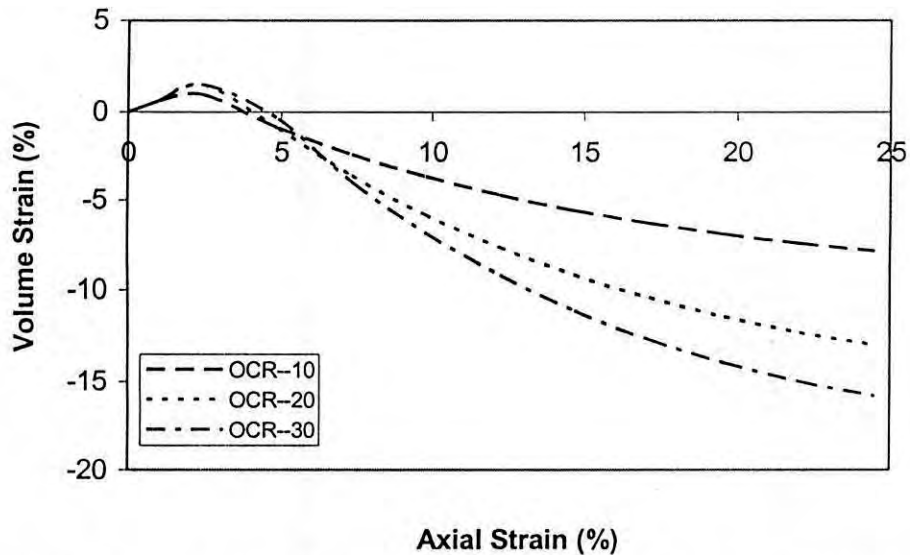


Figure 6.16 MCC predictions of volume strain response of highly overconsolidated 7% cemented Savar clay

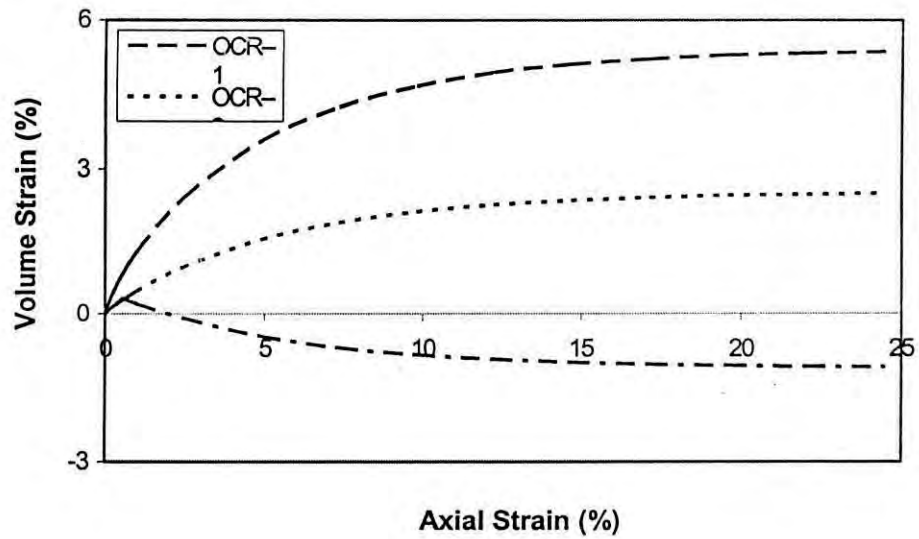


Figure 6.17 MCC drained prediction of volume strain response of normal, low, and moderately overconsolidated 14% cemented Savar clay.

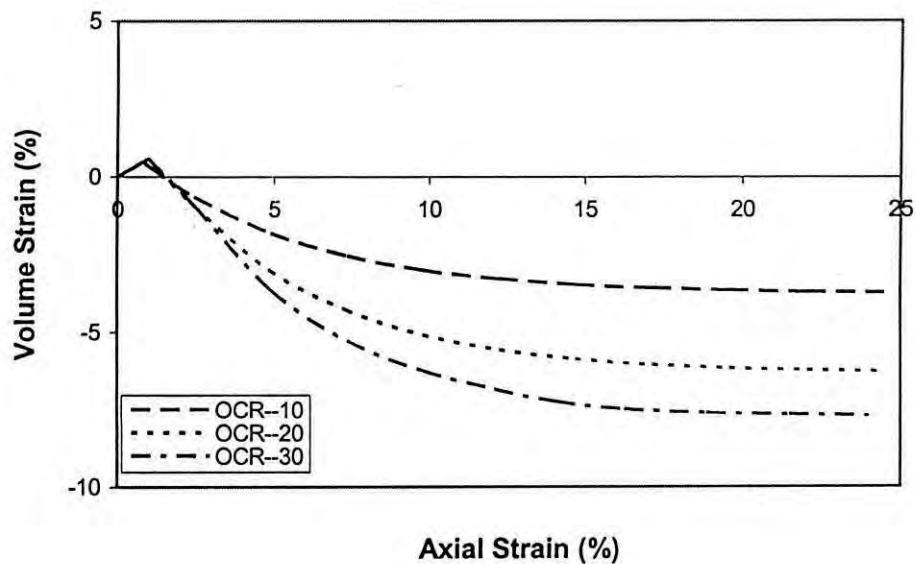


Figure 6.18 MCC predictions of volume strain response of highly overconsolidated 14% cemented Savar clay

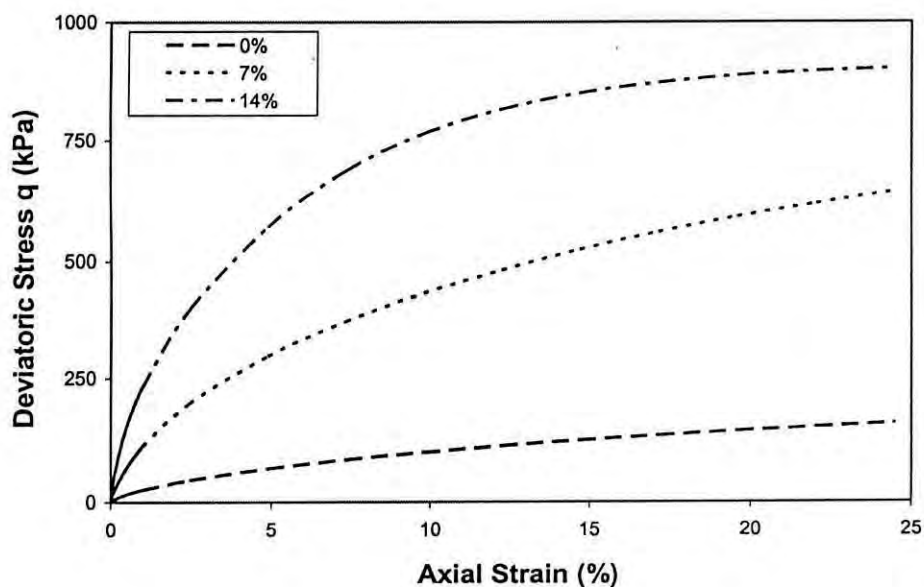


Figure 6.19 MCC predictions of drained stress-strain response of normally consolidated (OCR=1) remolded Savar clay for varying degrees of cementation

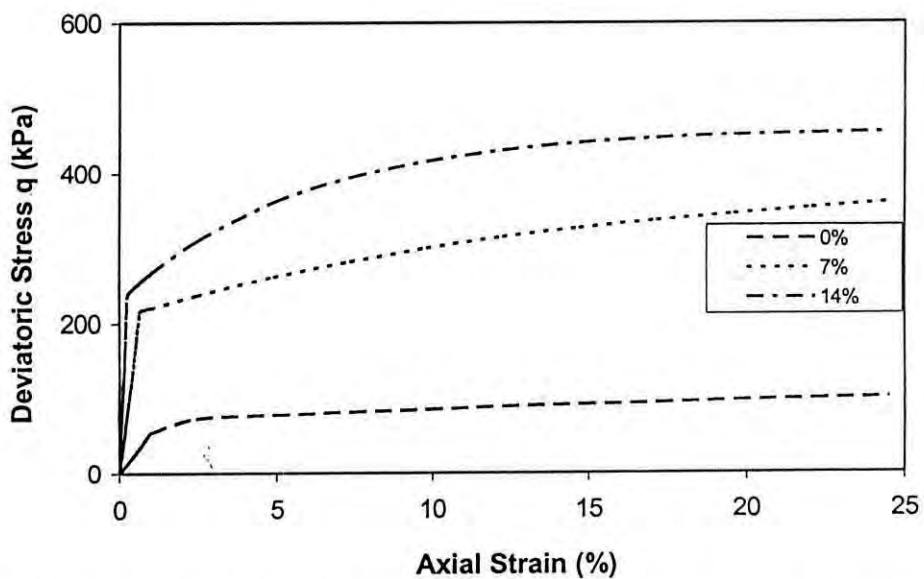


Figure 6.20 MCC predictions of drained stress-strain response of low overconsolidated (OCR=2) remolded Savar clay for varying degrees of cementation

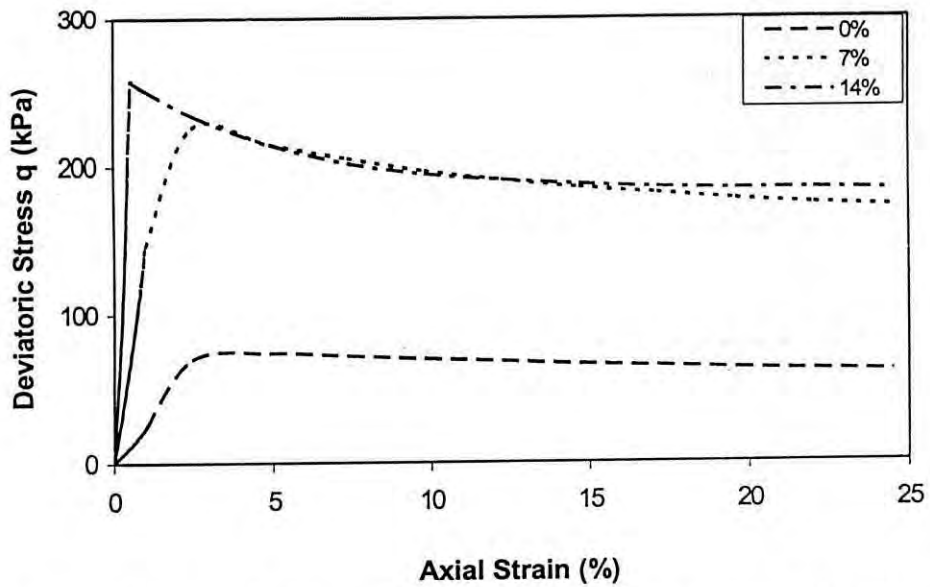


Figure 6.21 MCC predictions of drained stress-strain response of moderately overconsolidated (OCR=5) remolded Savar clay for varying degrees of cementation

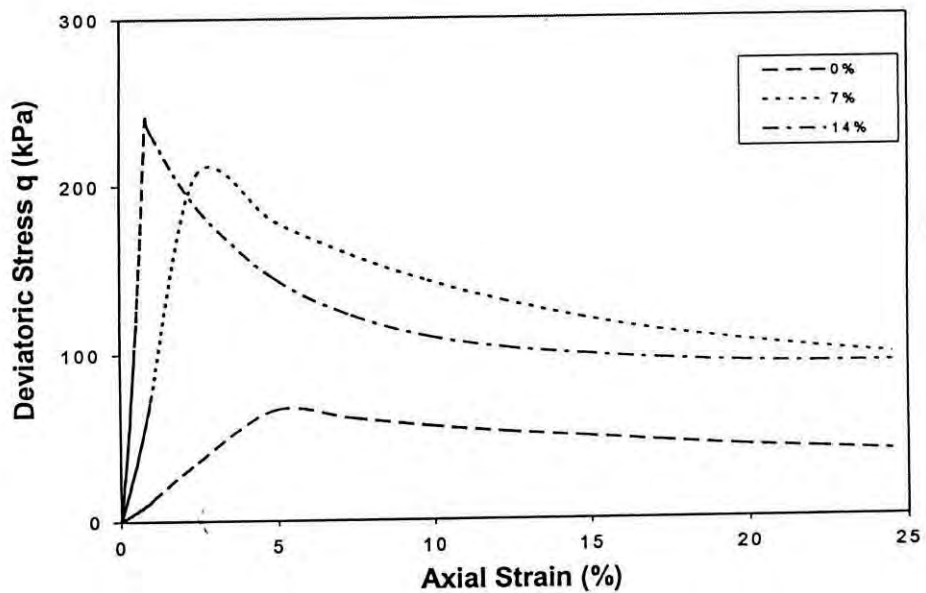


Figure 6.22 MCC prediction of drained stress-strain response of highly overconsolidated (OCR=10) remolded Savar clay for varying degrees of cementation



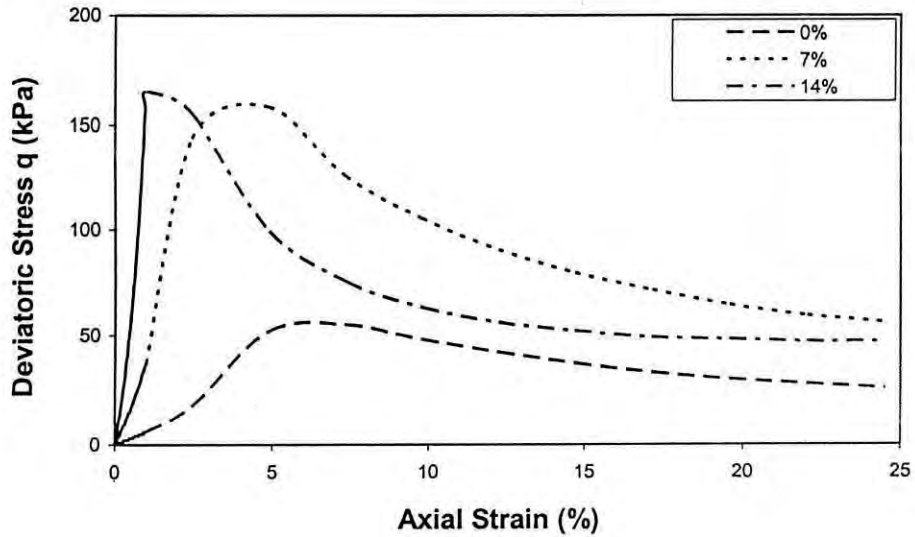


Figure 6.23 MCC predictions of drained stress-strain response highly overconsolidated (OCR=20) remolded Savar clay for varying degrees of cementation

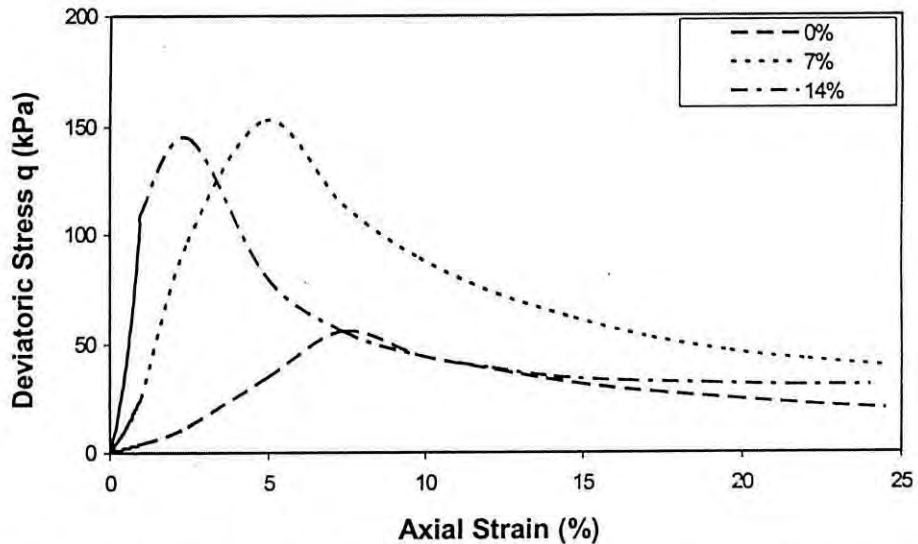


Figure 6.24 MCC prediction of drained stress-strain response highly overconsolidated (OCR= 30) remolded Savar clay for varying degrees of cementation

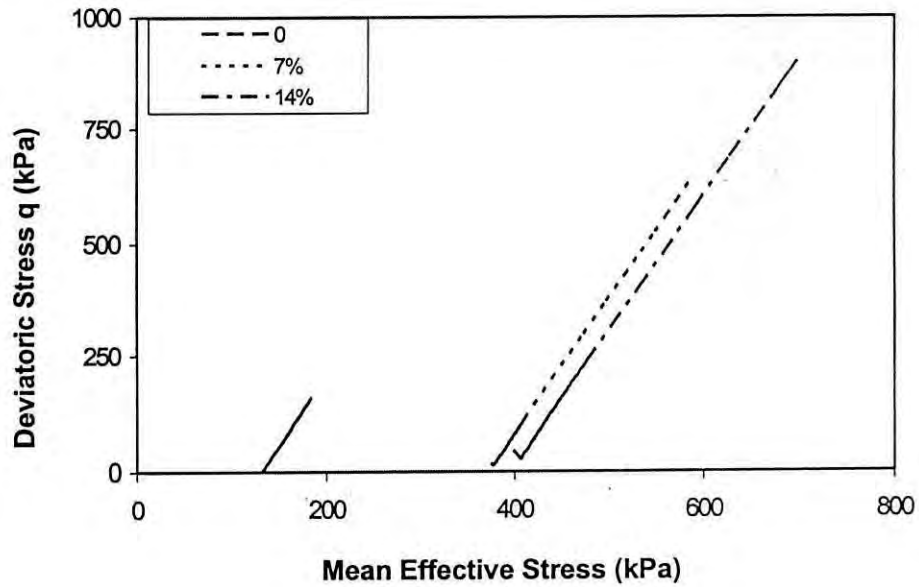


Figure 6.25 MCC predictions of drained stress path of normally consolidated (OCR=1) remolded Savar clay for varying degrees of cementation

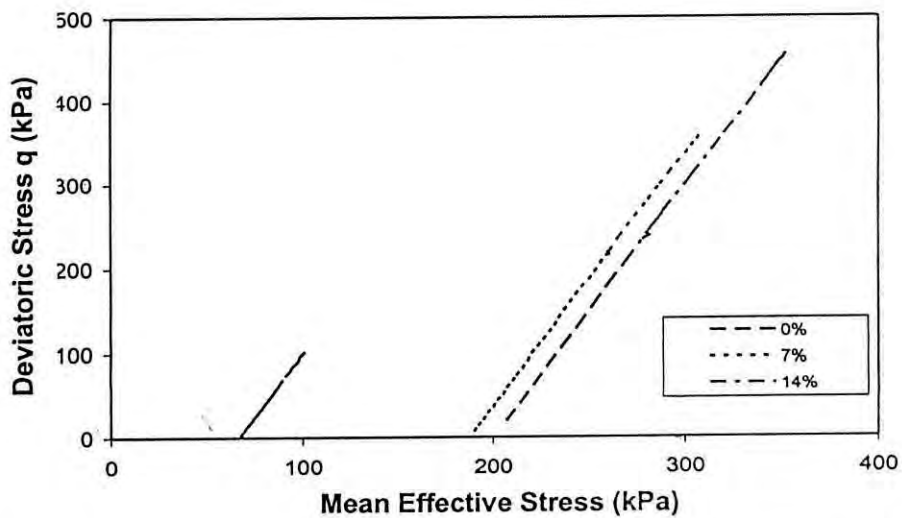


Figure 6.26 MCC predictions of drained stress path of low overconsolidated (OCR=2) remolded Savar clay for varying degrees of cementation

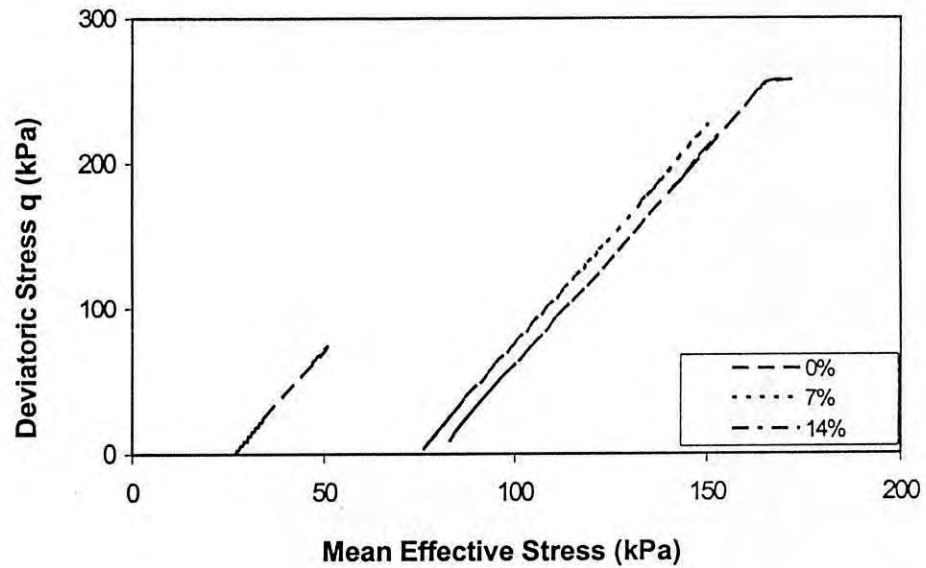


Figure 6.27 MCC prediction of drained stress path of moderately overconsolidated (OCR=5) remolded Savar clay for varying degrees of cementation

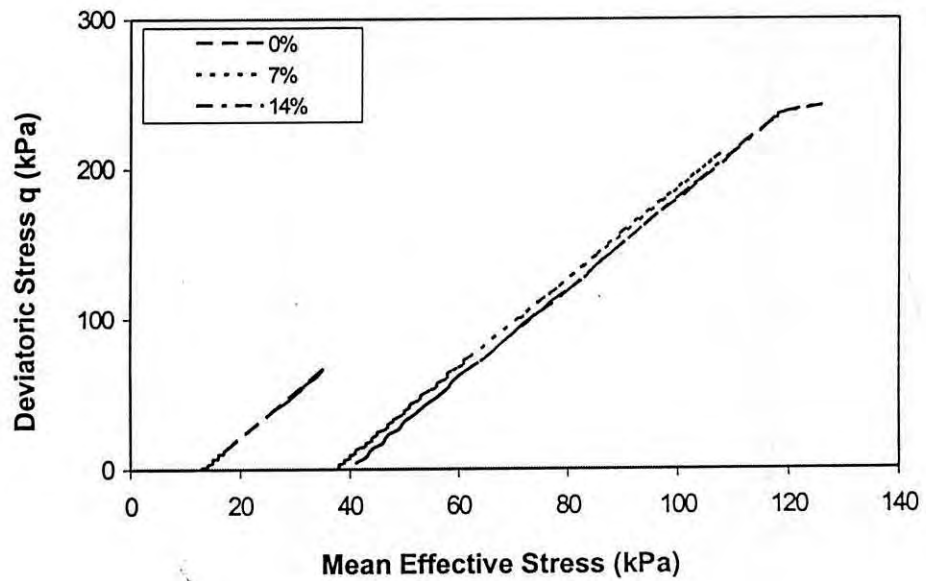


Figure 6.28 MCC prediction of drained stress path of highly overconsolidated (OCR=10) remolded Savar clay for varying degrees of cementation

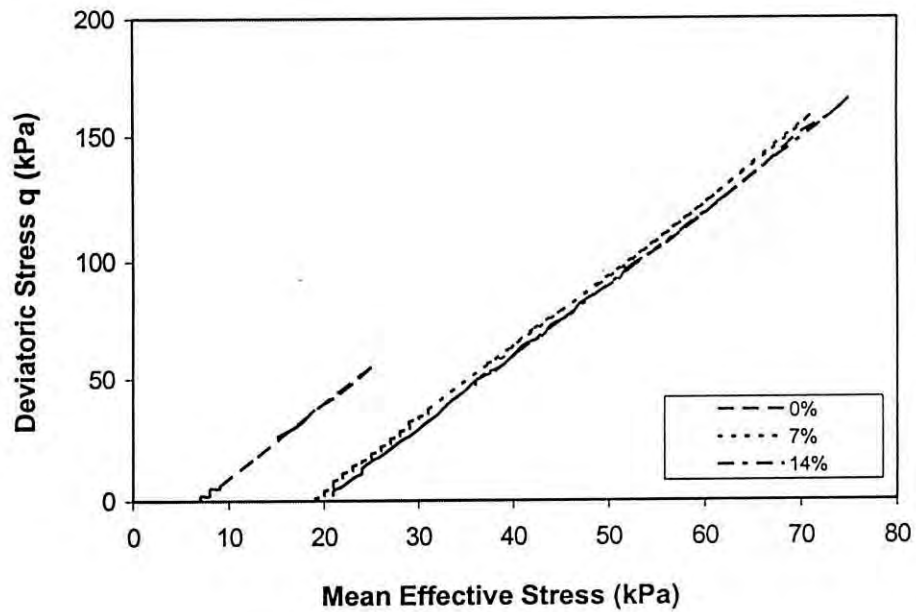


Figure 6.29 MCC prediction of drained stress path of highly overconsolidated (OCR=20) remolded Savar clay for varying degrees of cementation

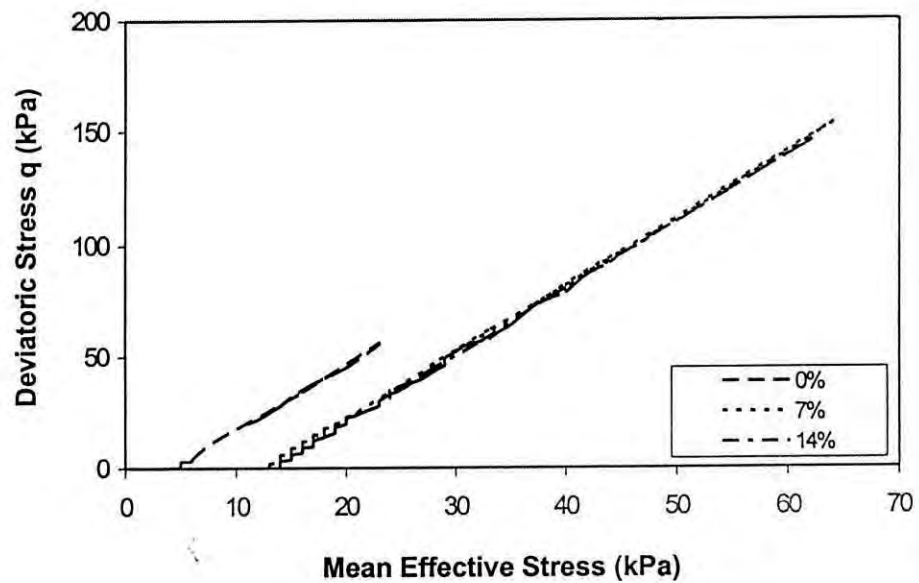


Figure 6.30 MCC prediction of drained stress path of highly overconsolidated (OCR=30) remolded Savar clay for varying degrees of cementation.

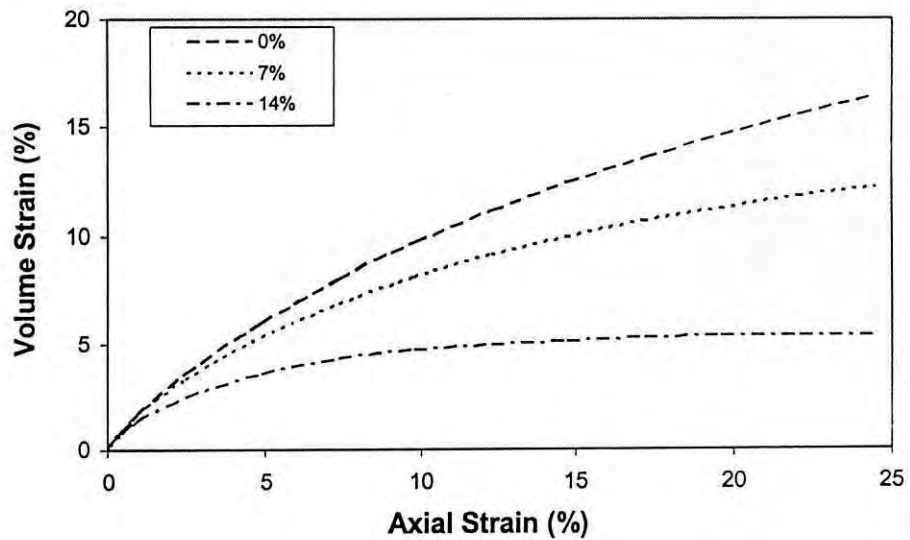


Figure 6.31 MCC predictions of volume change response of normally consolidated (OCR=1) remolded Savar clay for varying degrees of cementation

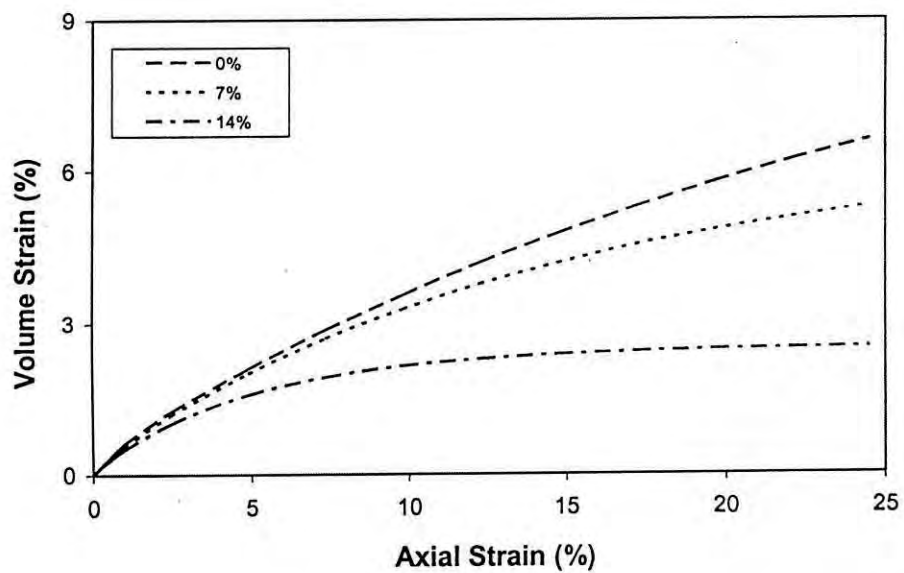


Figure 6.32 MCC predictions of volume change response of low overconsolidated (OCR=2) remolded Savar clay for varying degrees of cementation

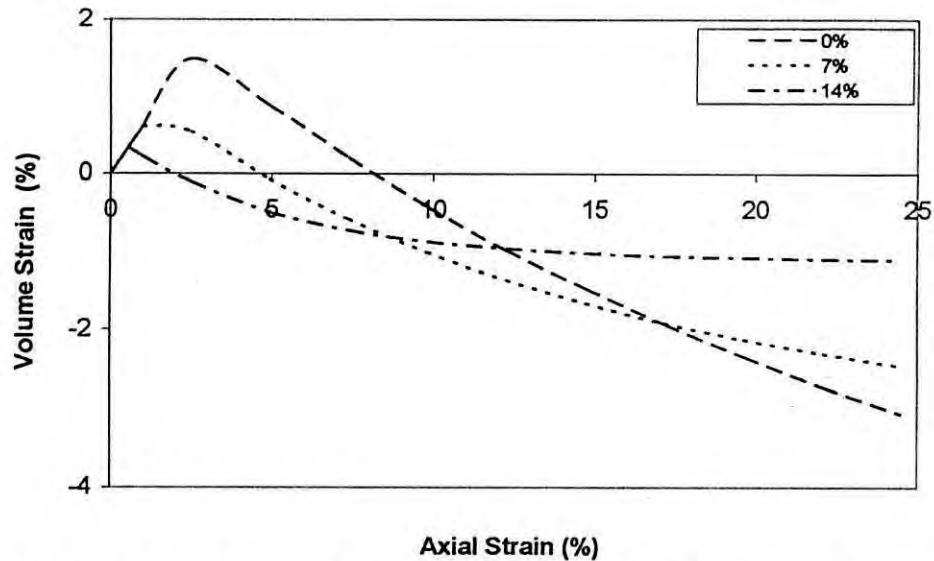


Figure 6.33 MCC predictions of volume change response of moderately overconsolidated (OCR=5) remolded Savar clay for varying degrees of cementation

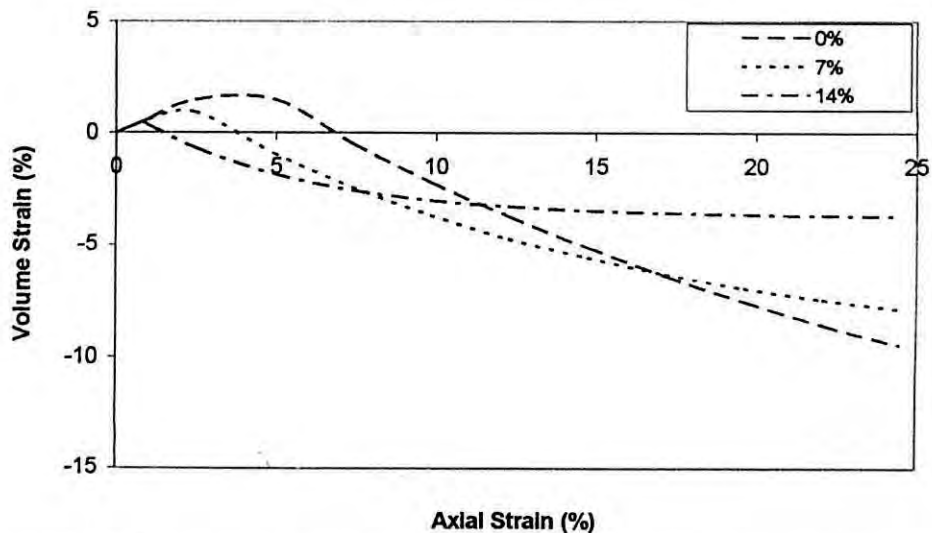


Figure 6.34 MCC predictions of volume change response of highly overconsolidated (OCR=10) remolded Savar clay for varying degrees of cementation

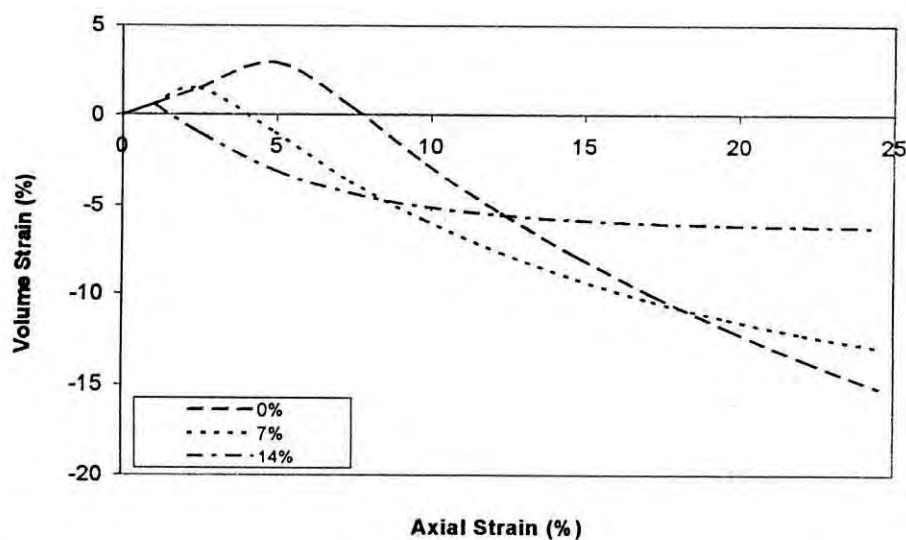


Figure 6.35 MCC predictions of volume change response of highly overconsolidated (OCR=20) remolded Savar clay for varying degrees of cementation

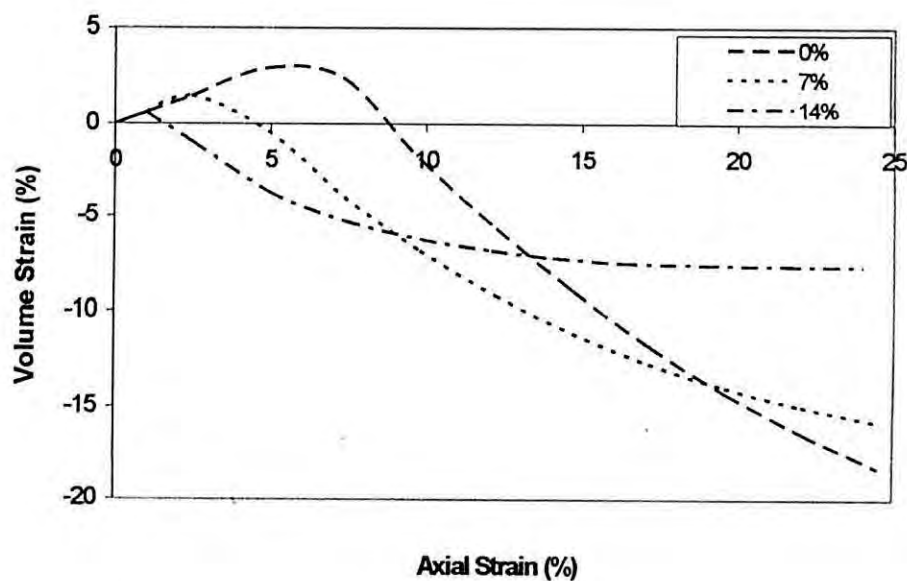


Figure 6.36 MCC predictions of volume change response of highly overconsolidated (OCR=30) remolded Savar clay for varying degrees of cementation

## CHAPTER 7

### MODIFIED MODIFIED CAM CLAY MODEL (MMCC MODEL)

#### 7.1 Introduction:

In the previous chapters, the stress-strain behaviour of remolded Savar clays, with and without cementation, was modeled using the MCC Model. However, the tensile strength that develops in clays as a result of cementation was not incorporated in these models. This chapter discusses a variation of the MCC model which incorporates tensile strength as a model parameter. The predicted drained and undrained stress-strain response of remolded Savar clays, with and without cementation, is discussed in this chapter.

#### 7.2 Modified Modified Cam Clay (MMCC) Model

A variant of the MCC model which incorporates tensile strength as a model parameter is discussed here as the Modified Modified Cam Clay (MMCC) model. The various aspects of the MMCC model are discussed in detail in the following subsections as given below.

##### 7.2.1 The MMCC Yield Locus and Plastic Flow Rule

Cement treatment of clays gives it the ability to resist tensile forces. This is termed as tensile or cementation strength. The tensile strength is explicitly incorporated in the MMCC yield locus as follows

$$\left\{ \frac{q}{M(p' + p'_i)} \right\}^2 = \frac{p'_o + p'_i}{p' + p'_i} - 1 \quad (7.1)$$



Where

$$p' = \frac{\sigma'_1 + \sigma'_2 + \sigma'_3}{3} \quad (7.2)$$

$$q = \sqrt{\frac{(\sigma'_1 - \sigma'_2)^2 + (\sigma'_2 - \sigma'_3)^2 + (\sigma'_1 - \sigma'_3)^2}{2}} \quad (7.3)$$

$$M = \frac{q}{p' + p'_i} \quad (7.4)$$

In the above equations,  $\sigma'_1, \sigma'_2, \sigma'_3$  are the principal effective stress components,  $p'_i$  is the tensile strength and  $p'_o$  is the preconsolidation pressure of the soil.

The MMCC model is assumed to obey the associated flow rule. Thus the MMCC model plastic potential function is identical to the MMCC yield locus equation given by equation (7.3). The plastic flow rule of the MMCC model is identical to that of the plastic flow rule of the MCC model and is given as below:

$$\frac{d\varepsilon_v^p}{d\varepsilon_q^p} = \frac{M^2 - \eta^2}{2\eta} \quad (7.5)$$

However, the  $\eta$  term in the above equation is defined in the MMCC model as follows:

$$\eta = \frac{q}{p' + p'_i} \quad (7.6)$$

### 7.2.2 Tensile Strength and Unconfined Compression Strength

When tensile strength is explicitly incorporated in the MCC model, it is termed as the MMCC model. The tensile strength of clay may be obtained from its unconfined compression strength by a procedure which is described as below.

The undrained shear strength of the soil at zero cell pressure or zero mean effective pressure may be termed as the unconfined compression strength of the soil. Thus substituting  $p' = 0$  and  $q = q_u$  in equation (7.1), the MMCC yield equation may be rewritten as below:

$$\left\{ \frac{q_u}{M(0 + p'_i)} \right\}^2 = \frac{p'_o + p'_i}{0 + p'_i} - 1 \quad (7.7)$$

From equation (7.7) the relationship between tensile strength and unconfined compression strength may be obtained as below:

$$\frac{q_u^2}{M^2 p_i'^2} = \frac{p_o'}{p_i'} \quad (7.8)$$

$$p_i' = \frac{q_u^2}{M^2 p_o'} \quad (7.9)$$

Equation (7.7) relates the tensile strength  $p'_i$  of cemented clay with its unconfined compression strength  $q_u$ ,  $M$  and  $p'_o$  are the critical stress ratio and preconsolidation pressure of the cemented soil.

### 7.3 Prediction of Drained Response Using MCC and MMCC

#### 7.3.1 Model Parameters

The MCC model parameters for 7% and 14% cementation of remolded Savar clays are given in Table 5.1. Additionally, Table 7.1 includes the tensile strength parameter computed using equation (7.8) from the value of unconfined compression strength  $q_u$ , preconsolidation pressure  $p'_o$  and critical state ratio  $M$ . These model parameters were used in the MMCC model to compute the stress-strain, volume strain and pore pressure change characteristics of the remolded Savar clay, with and without cementation.

Table 7.1 The MMCC model parameters

Modified Modified Cam Clay Parameters	7% Cemented Clay	14% Cemented Clay
$\lambda$	.2	.1
$\kappa$	0.03	0.01
M	1.25	1.3
$p'_o$	375	400
$p_{to}$	213	509

#### 7.3.2 Stress-Strain

Figures 7.1 through 7.12 show the stress-strain response of Savar clays, with and without cementation, using the MMCC model for different OCR values. For normally consolidated clays and clays with low overconsolidation ratio, it is observed that initial shear stiffness of Savar clays using the MMCC model are predicted to be significantly higher than that predicted using the MCC model. This is reasonable, as cemented clays

are generally expected to have more initial shear stiffness than uncemented clays. The deviator stress is observed to increase with increasing axial strain.

Similar behavior is observed in case of high OCR clays also. It is observed that for clays with high overconsolidation ratio (OCR values of 10, 20 and 30), the predicted initial shear stiffness of clays using the MMCC model, is higher than that using the MCC model. The predicted deviator stress ultimately attains a constant with continuous shearing. This implies that the critical state is reached. It is also observed that the increase of initial shear stiffness is higher for clays with higher value of OCR's.

### 7.3.3 Stress Path

Figures 7.13 through 7.24 show the predicted drained stress paths of cemented Savar clays, using the MMCC model at different OCR values. During triaxial shear under drained conditions, the drained total and effective stress paths are identical, and the stress path is independent of the soil model used, as described in the previous chapters.

### 7.3.4 Volume Change Response

Figures 7.25 through 7.36 show the predicted drained volume change response of cemented remolded Savar clays, using both the MCC and MMCC model, for different OCR values. It is observed that for normally consolidated Savar clays, positive volume change response is predicted using either the MCC or MMCC model. However, higher volume change response is predicted for remolded Savar clays, when using the MCC model than the MMCC model, for the 7% cemented sample. However, in general, for low OCR (OCR equals 2) Savar clays with 7% and 14% cementation and at OCRs equals to 1 and 2. Higher positive volume change responses are predicted by the MMCC model relative to the MCC model. This is expected, because the computed overconsolidation ratio using the MMCC model will, in general, be lower than that computed using the

MCC model. As the computed OCR by the MMCC model is lower for a given preconsolidation pressure, the relative positive volume change response using that model is predicted to be higher.

At OCR value of 5 and for different percentages of cementation (7% and 14%), positive volume change response is predicted using the MMCC model. Negative volume change response is predicted in this case when using the MCC model.

The predicted positive volume change response decrease and reach either zero or negative for remolded Savar clays when using the MMCC model for higher OCR values (OCR values of 10, 20 and 30). However, the predicted negative volume change response increases with higher OCR values when using the MCC model.

## **7.4 Prediction of Undrained Response Using MMCC and MCC**

### **7.4.1 Model Parameters**

The MMCC model parameters for undrained prediction are obtained in a similar way as discussed in drained analysis. The MMCC model parameters used for undrained analysis are identical to those given in Table A7.1. The undrained analysis using the MMCC model was used to predict the stress-strain, stress path and pore pressure response of remolded Savar clays, with and without cementation.

### **7.4.2 Stress-Strain**

Figures 7.37 through 7.48 show the stress –strain response for uncemented and cemented Savar clays with different degrees of cementation (7% and 14%) using MMCC and MCC model. The predictions were made for different OCR values. It was observed that similar

to drained predictions, the predicted initial shear stiffness is higher for remolded Savar clays using MMCC model compared to the predictions of the MCC model. The predicted value of deviator stress is observed to decrease with increasing OCR, both in case of the MMCC and the MCC model. The predicted deviatoric stress becomes constant with continuous shearing. This indicates that the critical state condition has been reached. This is predicted both by the MCC and MMCC model.

#### 7.4.3 Stress Path

Figures 7.49 through 7.60 show the predicted undrained stress paths for remolded Savar clays using the MMCC and MCC model for different values of OCR. Decreasing effective stresses and positive pore pressures are predicted for normally consolidated Savar clays. In case of 7% cementation with low overconsolidation ratio (OCR equals 2), similar stress paths are predicted both for the MMCC and MCC model. These stress paths are observed to be vertical in  $p' - q$  space initially. Subsequently, constant deviator stresses with increasing mean pressure are predicted. Similar observations are predicted for clays of low overconsolidation ratios having 14% cementations. For moderately and highly overconsolidated clays, increasing mean effective stresses along with increasing deviator stresses are predicted. The stress paths predicted by both the MMCC and MCC model are straight vertical lines initially in  $p' - q$  space. Thus both the MMCC and MCC model simulates elastic behavior prior to yielding, in case of high OCR clays.

#### 7.4.4 Pore Pressure Response

Figures 7.61 through 7.72 show the excess pore pressure response for remolded Savar clays with and without cementation using the MCC and MMCC model for various OCR values.

For an OCR value of 1, excess positive pore pressures are predicted for all degrees of cementation. The predicted excess pore pressure is higher for the MMCC model relative to the MCC model. For an OCR value of 2 and 7% cementation, the predicted excess pore pressures are either zero or close to zero for the MCC model. However, negative excess pore pressure is predicted in this case when using the MMCC model. However, for OCR value of 2 and 14% cementation, positive excess pore pressure responses are predicted by the MMCC model.

For OCR values of 5, 10, 20 and 30, excess negative pore pressures are predicted for 7% cemented remolded Savar clay both by the MMCC and MCC model. However, the predicted excess pore pressures for 14% cementation are zero for MMCC model and negative for the MCC model. Negative excess pore pressures are predicted for higher OCR values (OCR values of 10, 20 and 30) both for MMCC and MCC model. However, higher negative excess pore pressures are predicted using the MCC model than using the MMCC model.

## 7.5 Summary and Conclusion

In this chapter, numerical predictions were made using the Modified Modified Cam Clay model for remolded Savar clays, with and without cementation. The drained predictions for stress-strain and volume change response of the MMCC model were compared with the corresponding predictions of the MCC model. Differences were observed in the predictions of initial shear stiffness, stress-strain, volume change and excess pore pressure response for remolded Savar clays, with and without cementation, and for various degrees of overconsolidation ratios. The results of the study in this chapter clearly show that a simple variation of the MCC model which incorporates tensile strength arising from cementation of clays significantly change the numerical predictions for stress-strain, volume change and excess pore pressure response for artificially cemented remolded Savar clays.

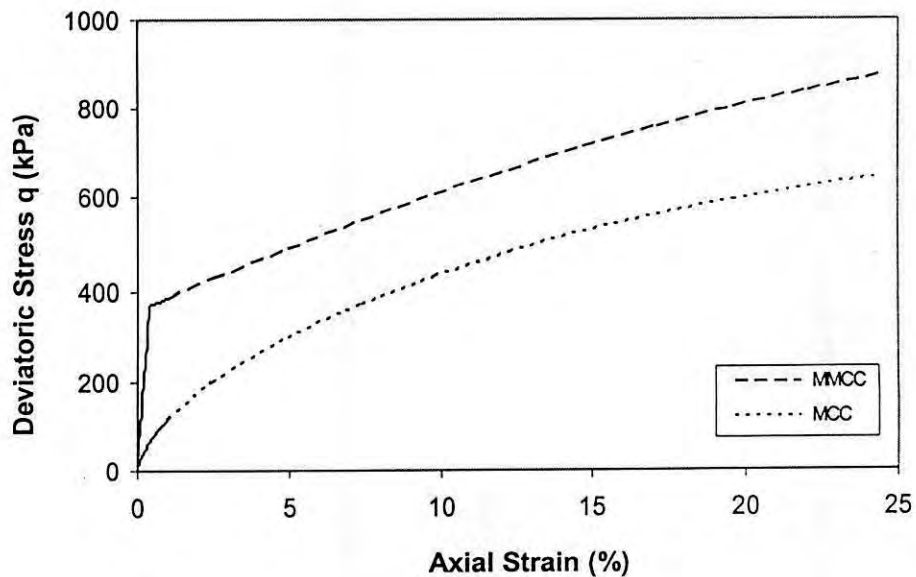


Figure 7.1 MCC and MMCC prediction of drained stress-strain response of 7% cemented Savar clay (OCR=1)

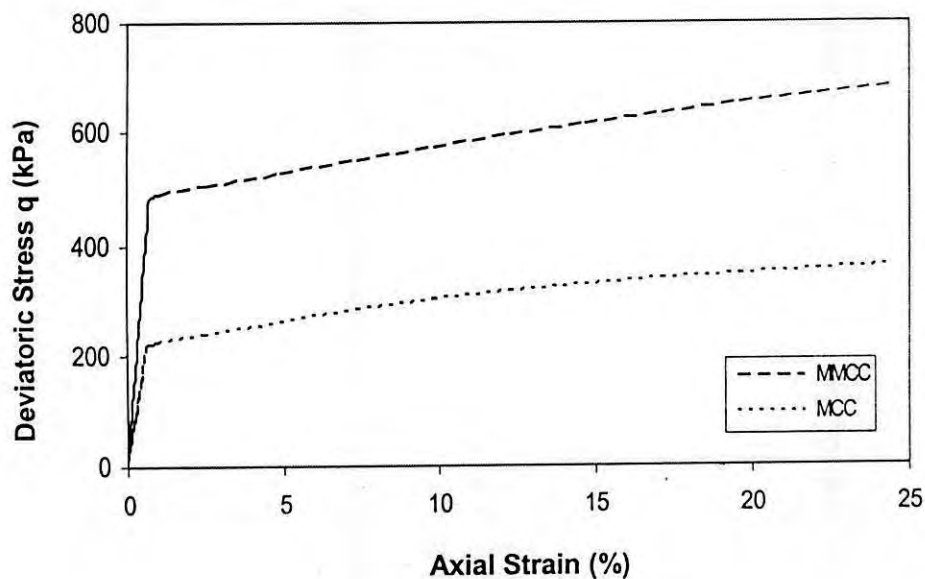


Figure 7.2 MCC and MMCC prediction of drained stress-strain response of 7% cemented Savar clay (OCR=2)



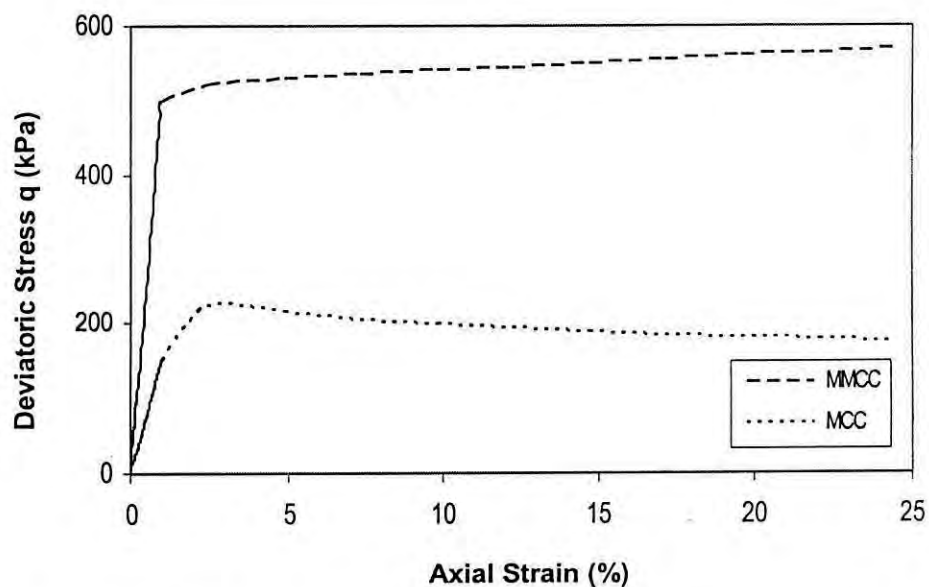


Figure 7.3 MCC and MMCC prediction of drained stress-strain response of 7% cemented Savar clay (OCR=5)

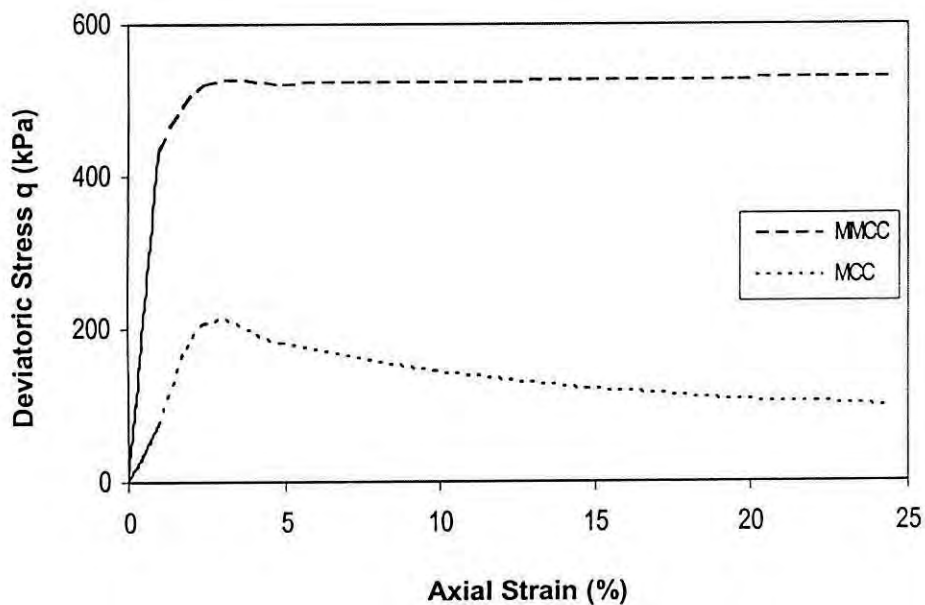


Figure 7.4 MCC and MMCC prediction of drained stress-strain response of 7% cemented Savar clay (OCR=10)

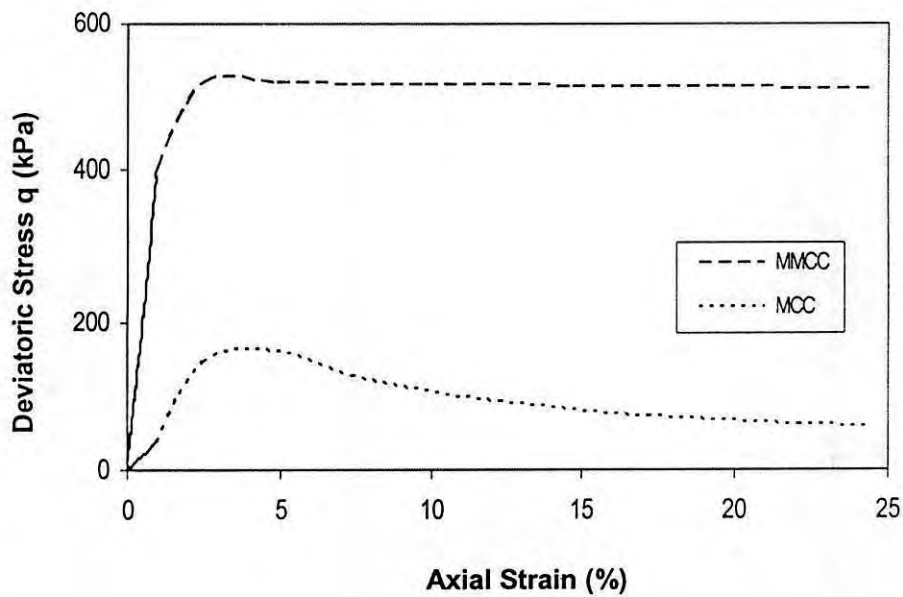


Figure 7.5 MCC and MMCC prediction of drained stress-strain response of 7% cemented Savar clay (OCR=20)

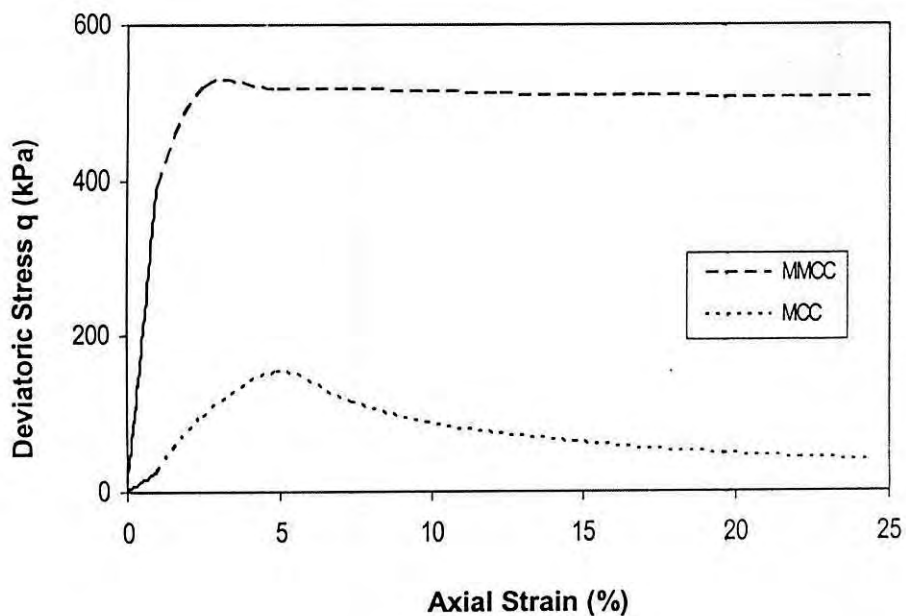


Figure 7.6 MCC and MMCC prediction of drained stress-strain response of 7% cemented Savar clay (OCR=30)

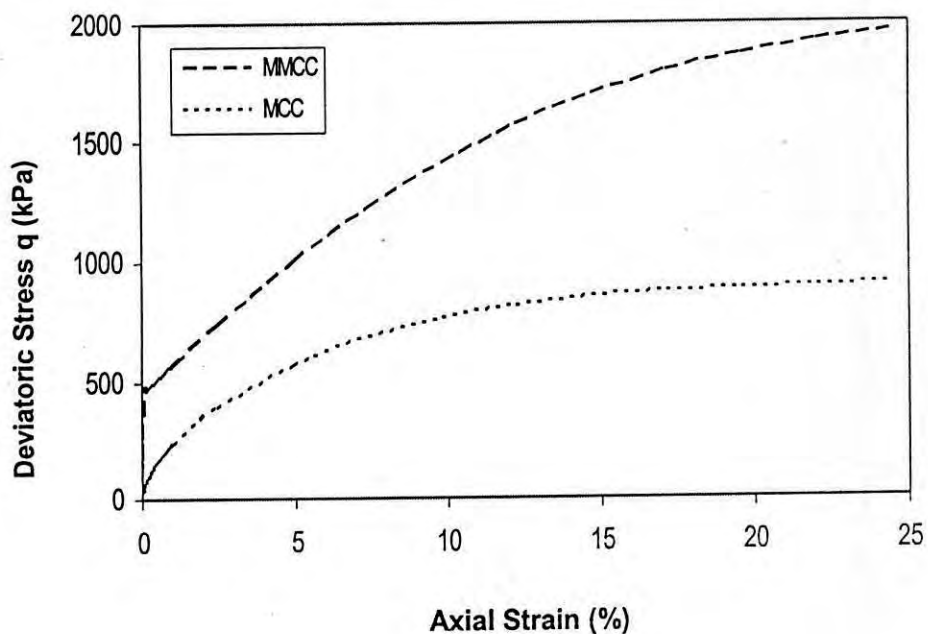


Figure 7.7 MCC and MMCC prediction of drained stress-strain response of 14% cemented Savar clay (OCR=1)

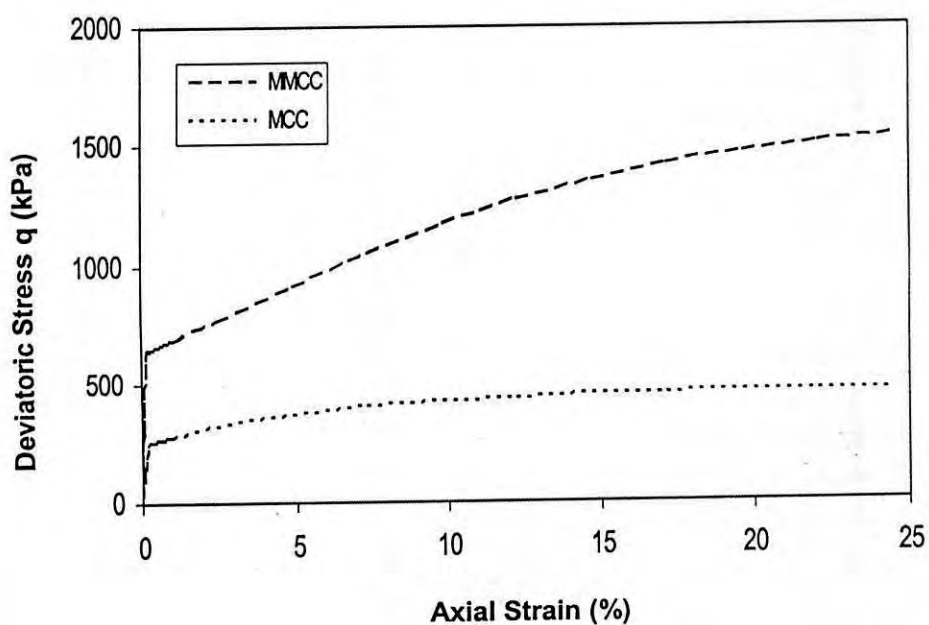


Figure 7.8 MCC and MMCC prediction of drained stress-strain response of 14% cemented Savar clay (OCR=2)

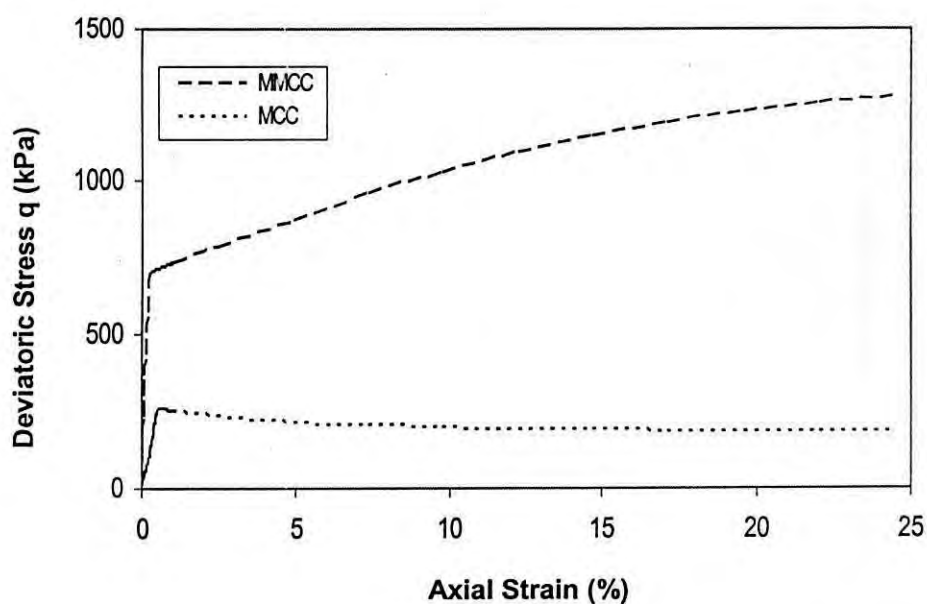


Figure 7.9 MCC and MMCC prediction of drained stress-strain response of 14% cemented Savar clay (OCR=5)

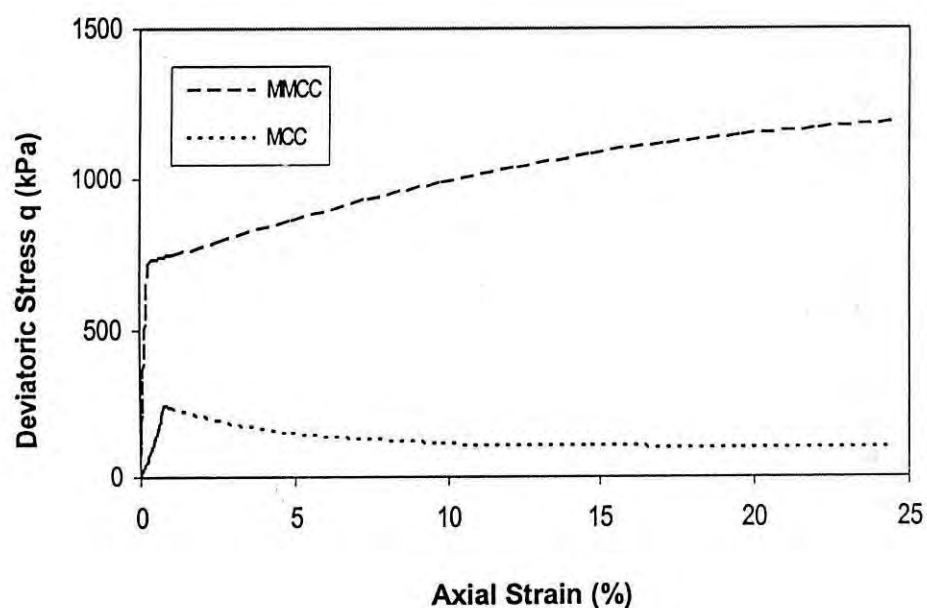


Figure 7.10 MCC and MMCC prediction of drained stress-strain response of 14% cemented Savar clay (OCR=10)

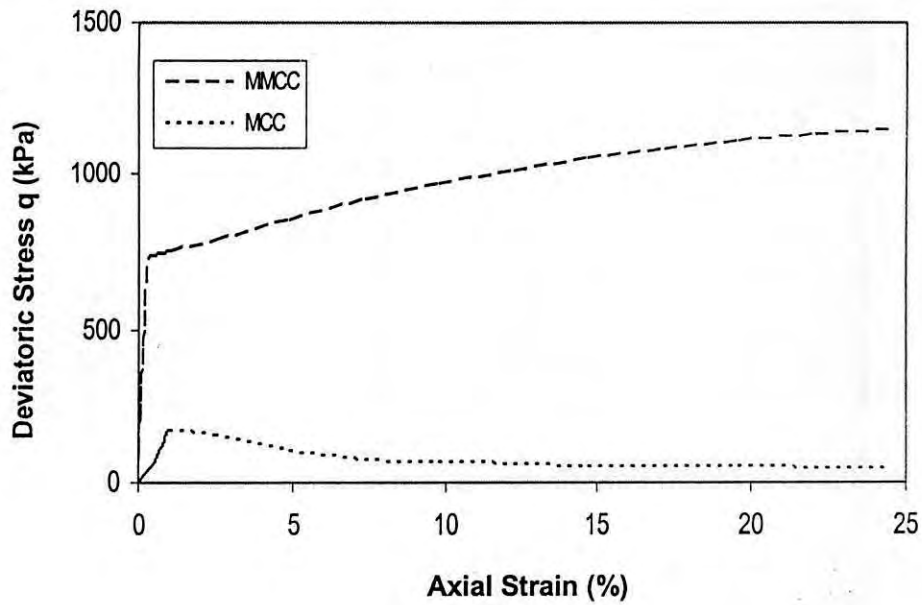


Figure 7.11 MCC and MMCC prediction of drained stress-strain response of 14% cemented Savar clay (OCR=20)

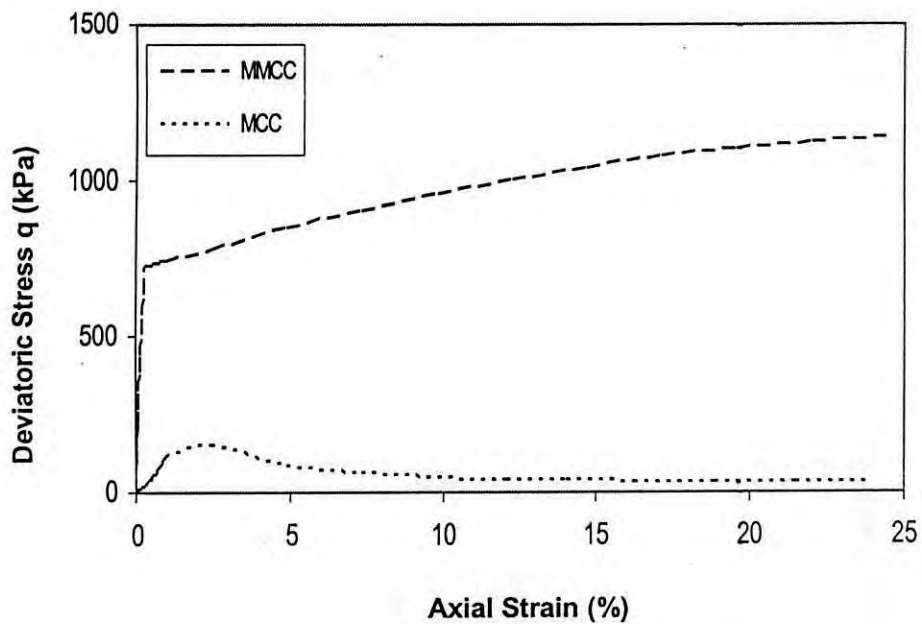


Figure 7.12 MCC and MMCC prediction of drained stress-strain response of 14% cemented Savar clay (OCR=30)

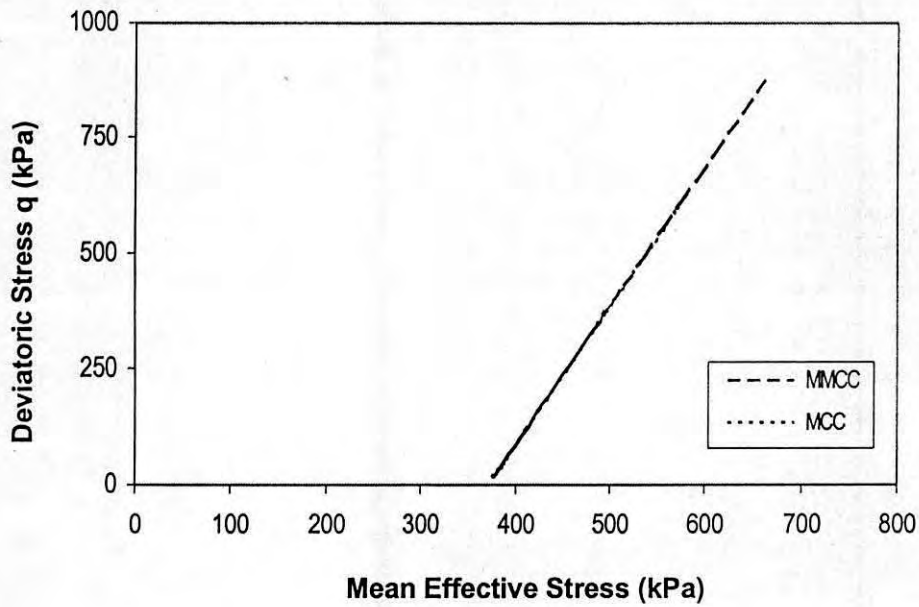


Figure 7.13 MCC and MMCC prediction of drained triaxial stress path for 7% cemented Savar clay (OCR=1)

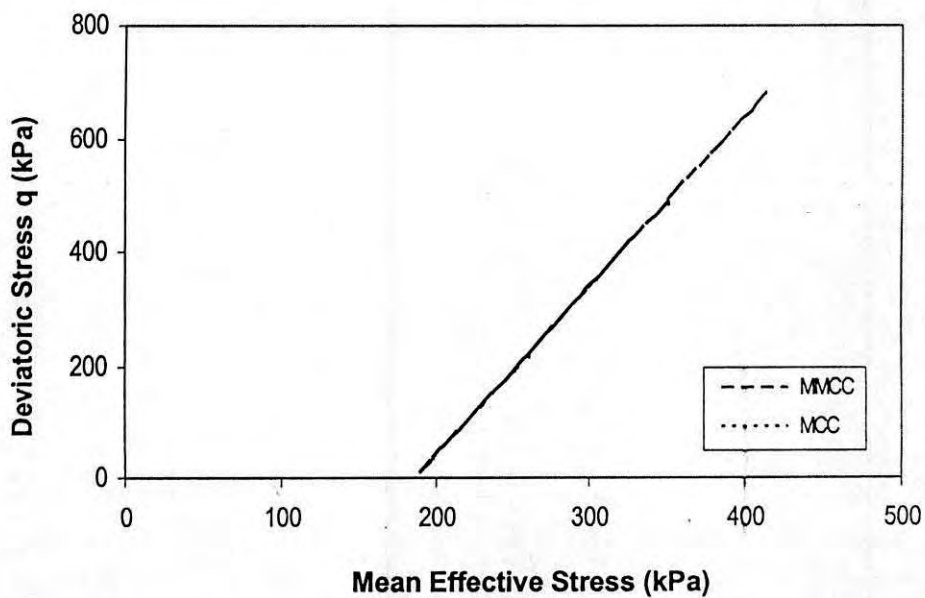


Figure 7.14 MCC and MMCC prediction of drained triaxial stress path for 7% cemented Savar clay (OCR=2)

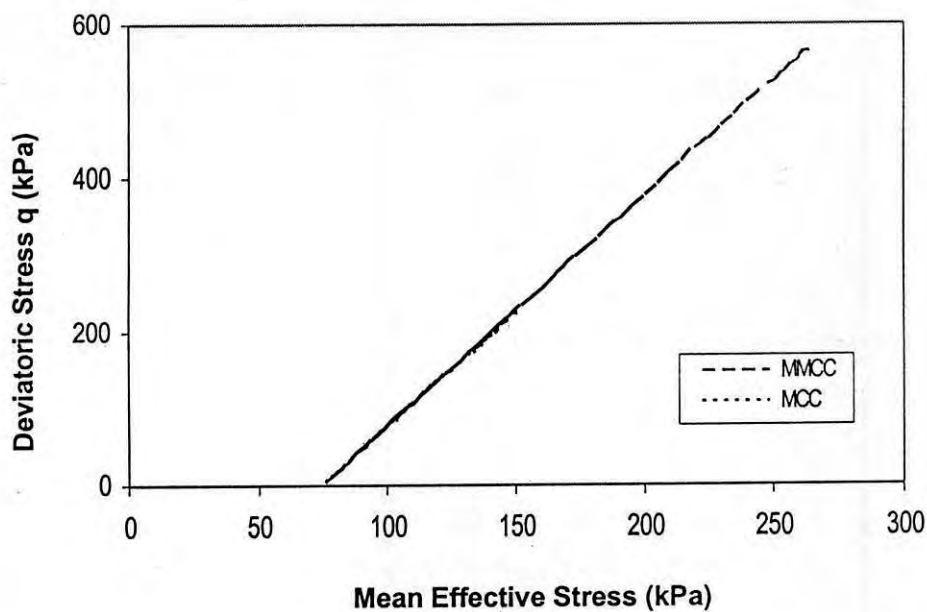


Figure 7.15 MCC and MMCC prediction of drained triaxial stress path for 7% cemented Savar clay (OCR=5)

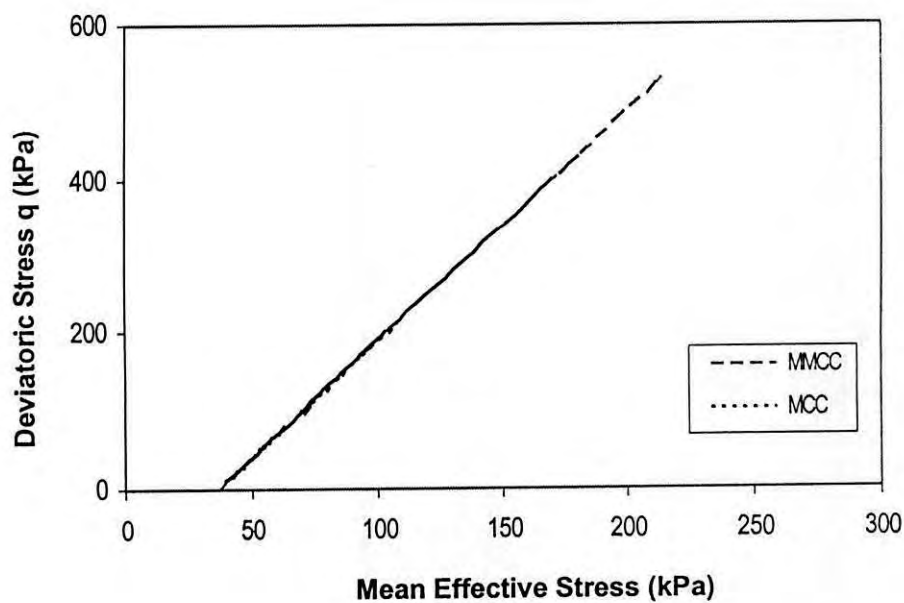


Figure 7.16 MCC and MMCC prediction of drained triaxial stress path for 7% cemented Savar clay (OCR=10)

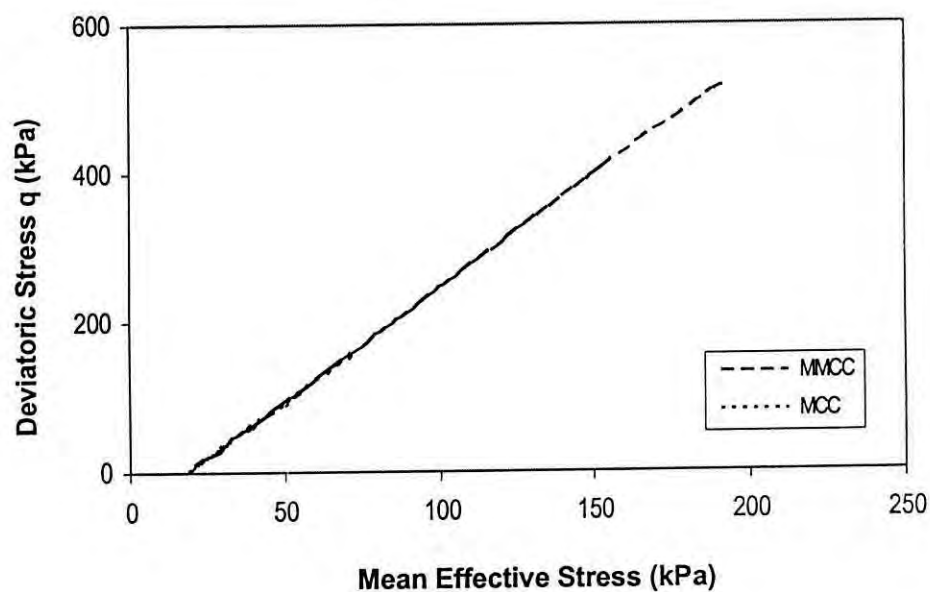


Figure 7.17 MCC and MMCC prediction of drained triaxial stress path for 7% cemented Savar clay (OCR=20)

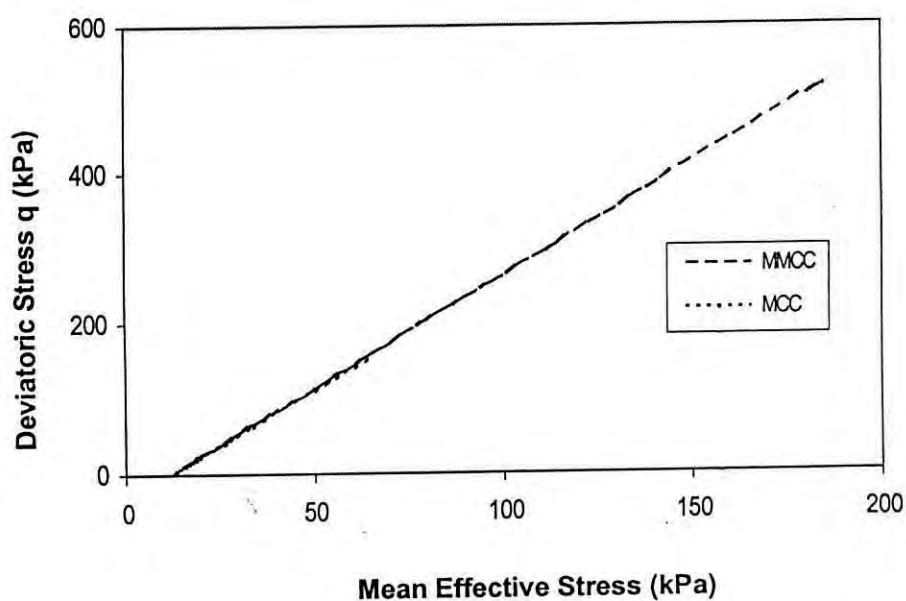


Figure 7.18 MCC and MMCC prediction of drained triaxial stress path for 7% cemented Savar clay (OCR=30)



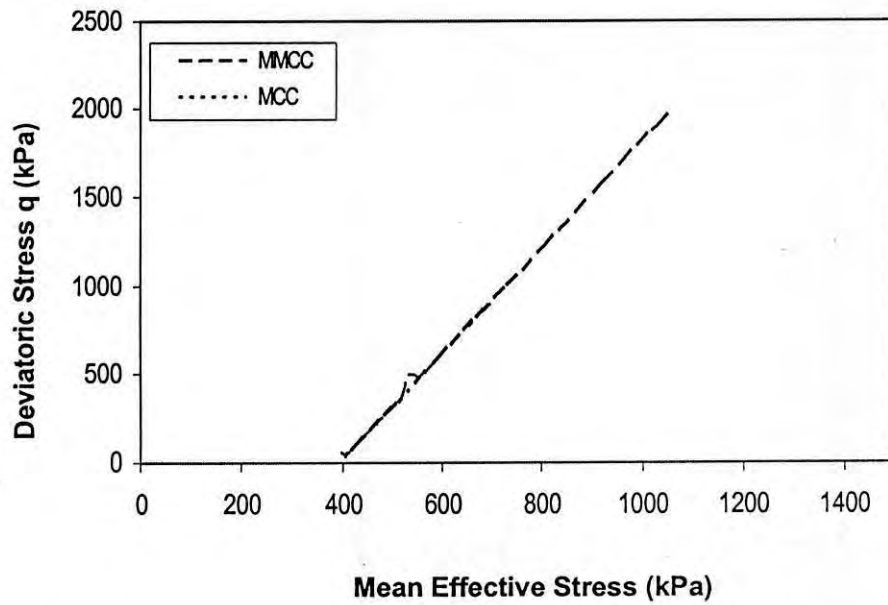


Figure 7.19 MCC and MMCC prediction of drained triaxial stress path for 14% cemented Savar clay (OCR=1)

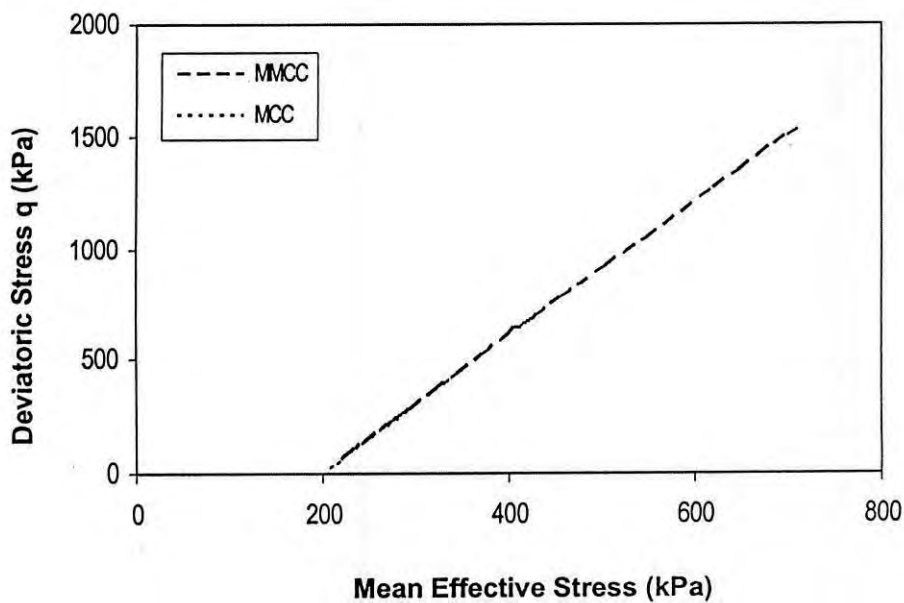


Figure 7.20 MCC and MMCC prediction of drained triaxial stress path for 14% cemented Savar clay (OCR=2)

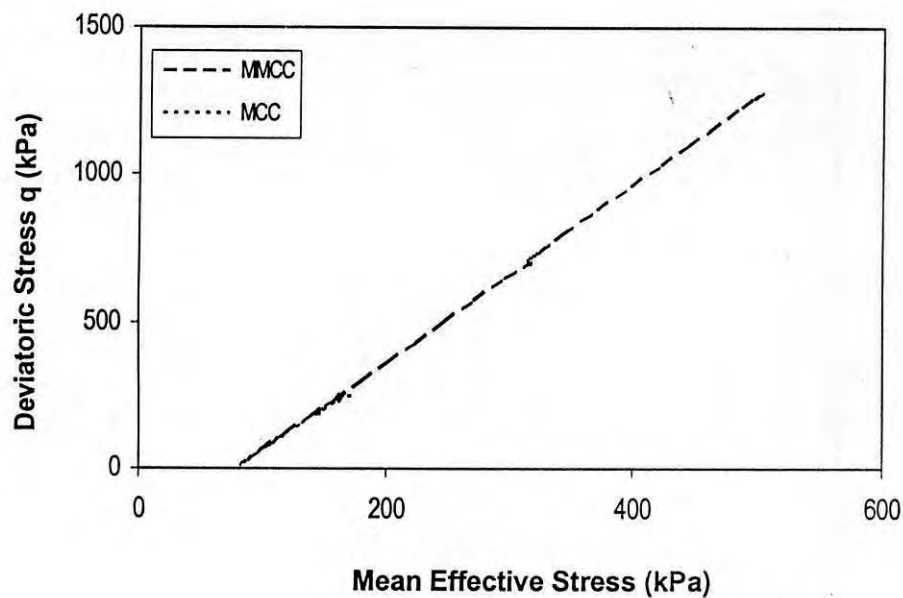


Figure 7.21 MCC and MMCC prediction of drained triaxial stress path for 14% cemented Savar clay (OCR=5)

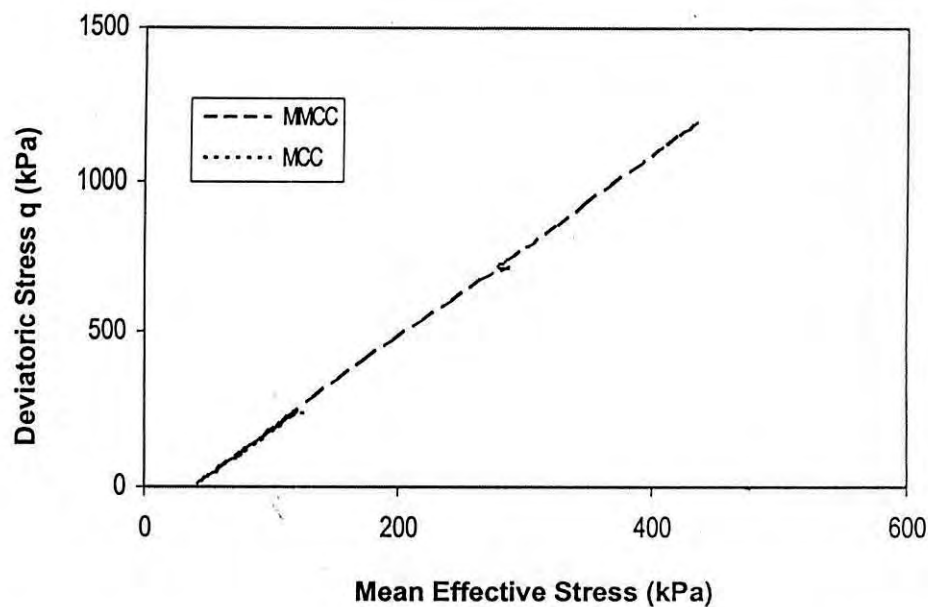


Figure 7.22 MCC and MMCC prediction of drained triaxial stress path for 14% cemented Savar clay (OCR=10)

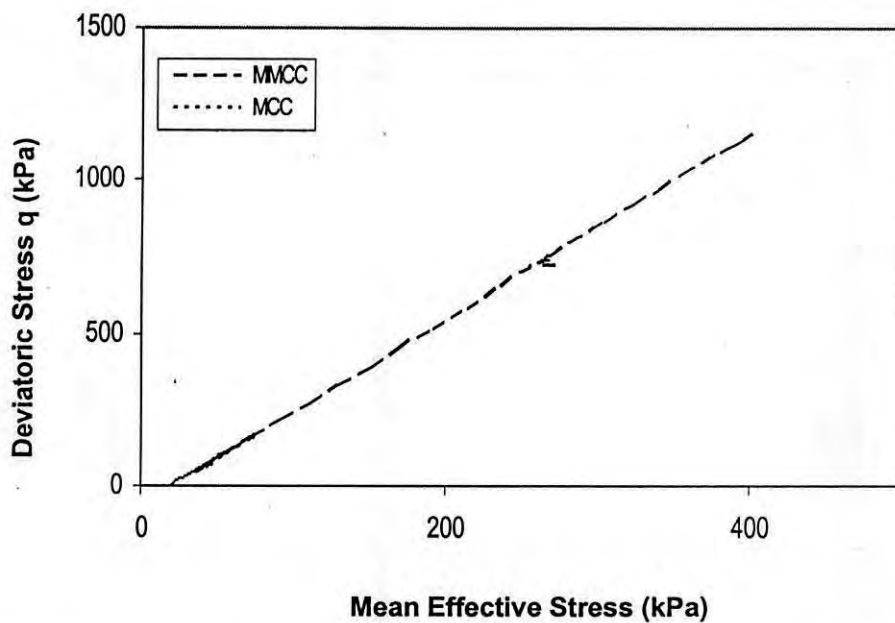


Figure 7.23 MCC and MMCC prediction of drained triaxial stress path for 14% cemented Savar clay (OCR=20)

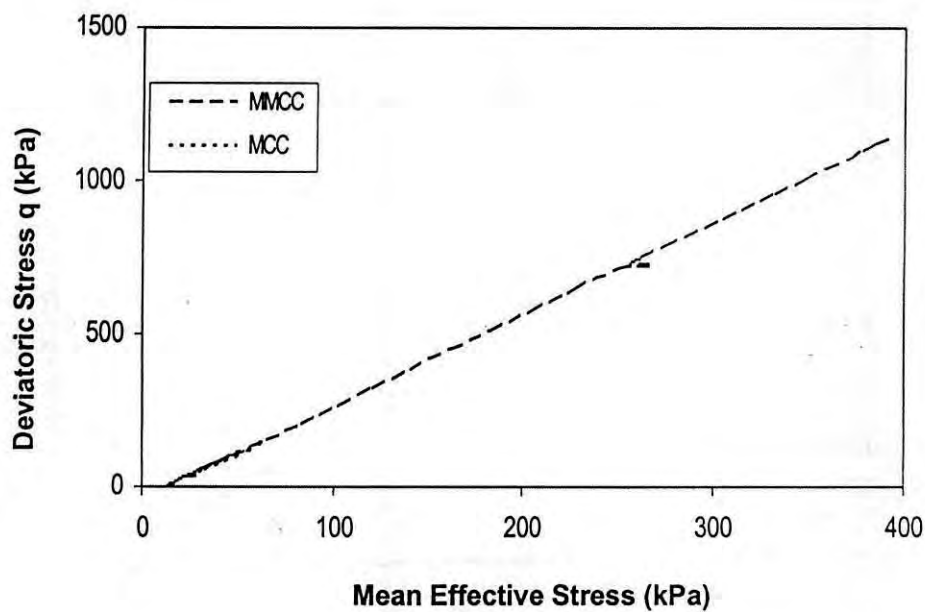


Figure 7.24 MCC and MMCC prediction of drained triaxial stress path for 14% cemented Savar clay (OCR=30)

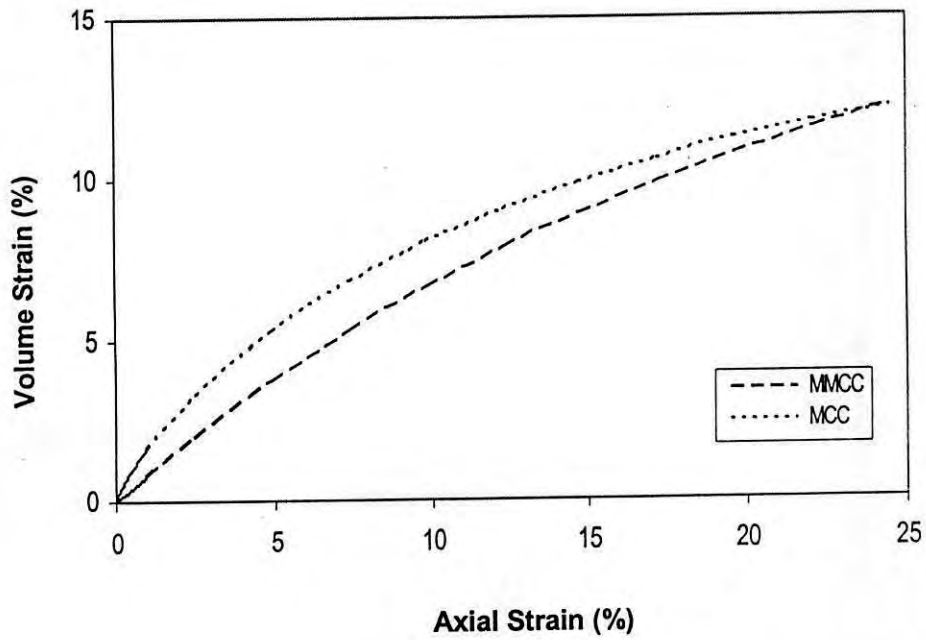


Figure 7.25 MCC and MMCC prediction of volume change response for 7% cemented Savar clay (OCR=1)

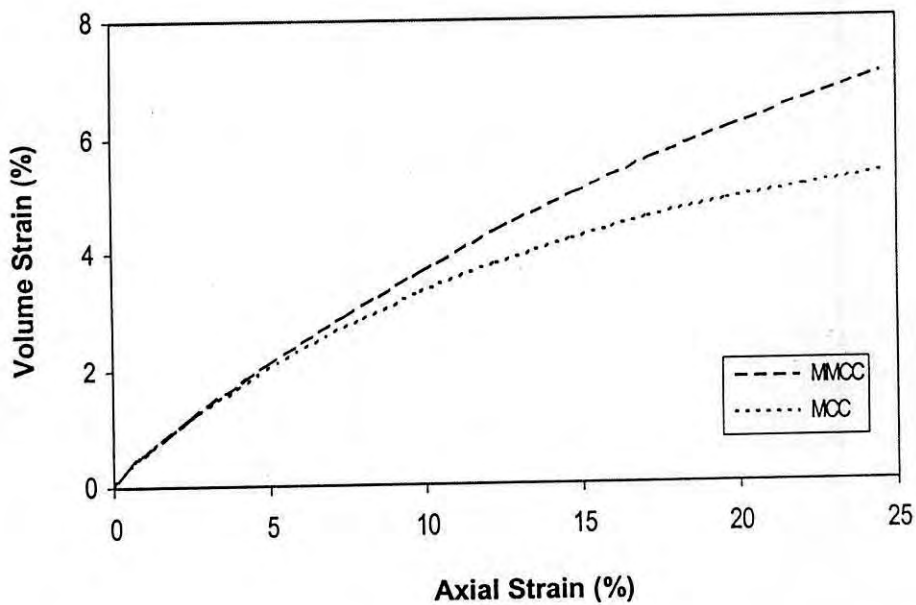


Figure 7.26 MCC and MMCC prediction of volume change response for 7% cemented Savar clay (OCR=2)

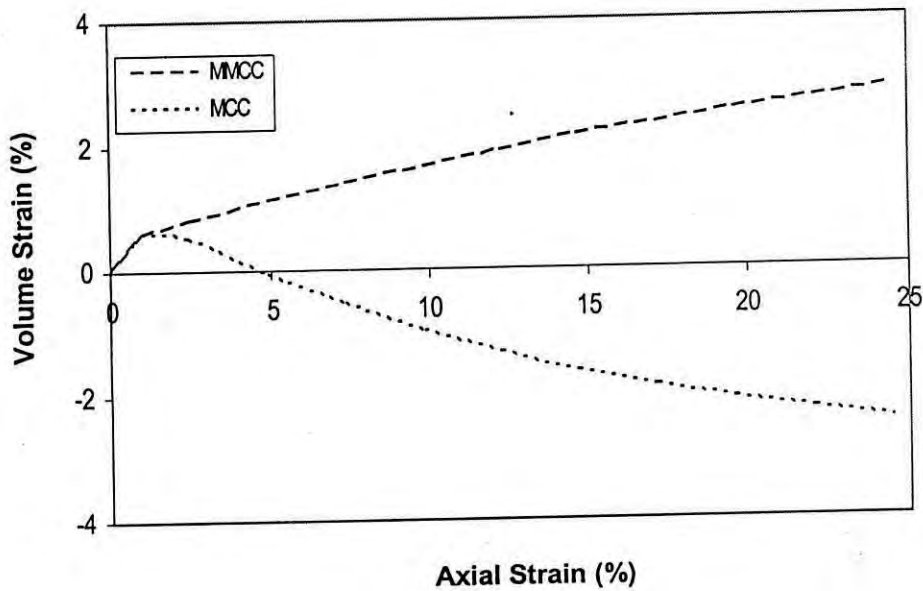


Figure 7.27 MCC and MMCC prediction of volume change response for 7% cemented Savar clay (OCR=5)

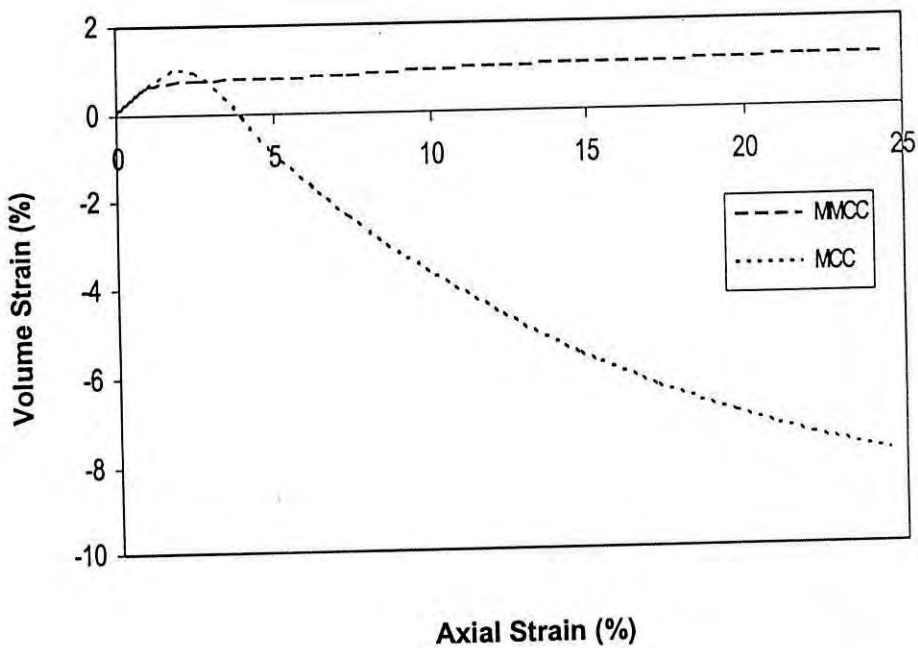


Figure 7.28 MCC and MMCC prediction of volume change response for 7% cemented Savar clay (OCR=10)

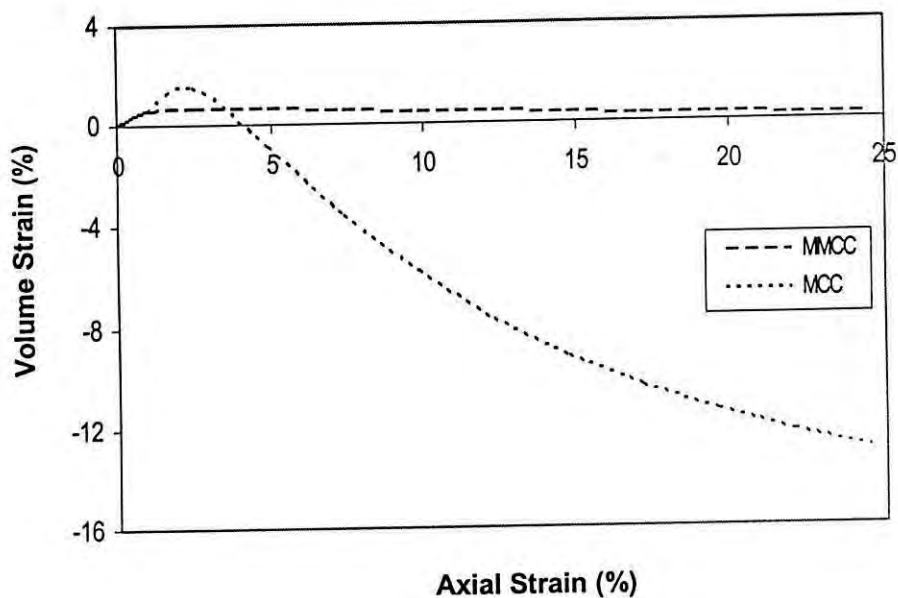


Figure 7.29 MCC and MMCC prediction of volume change response for 7% cemented Savar clay (OCR=20)

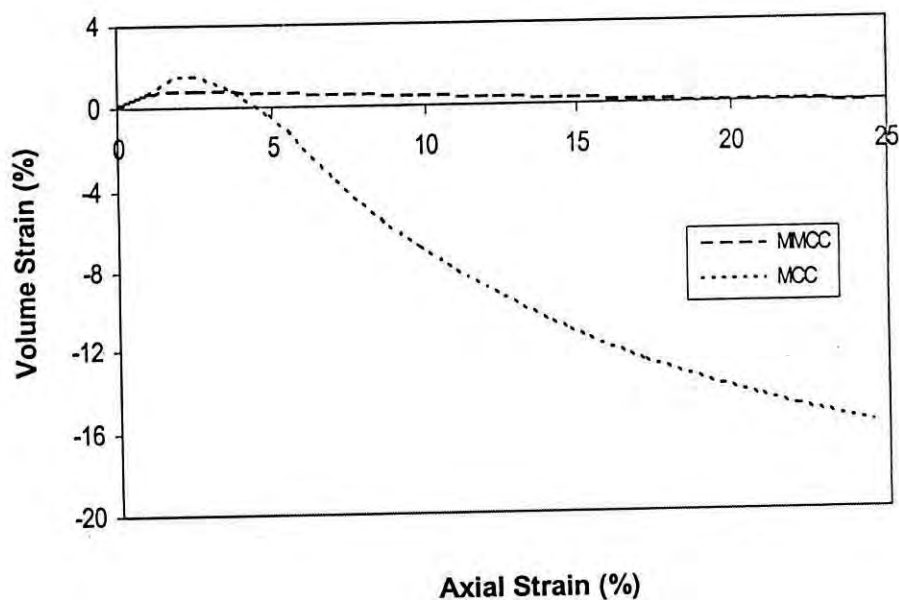


Figure 7.30 MCC and MMCC prediction of volume change response for 7% cemented Savar clay (OCR=30)

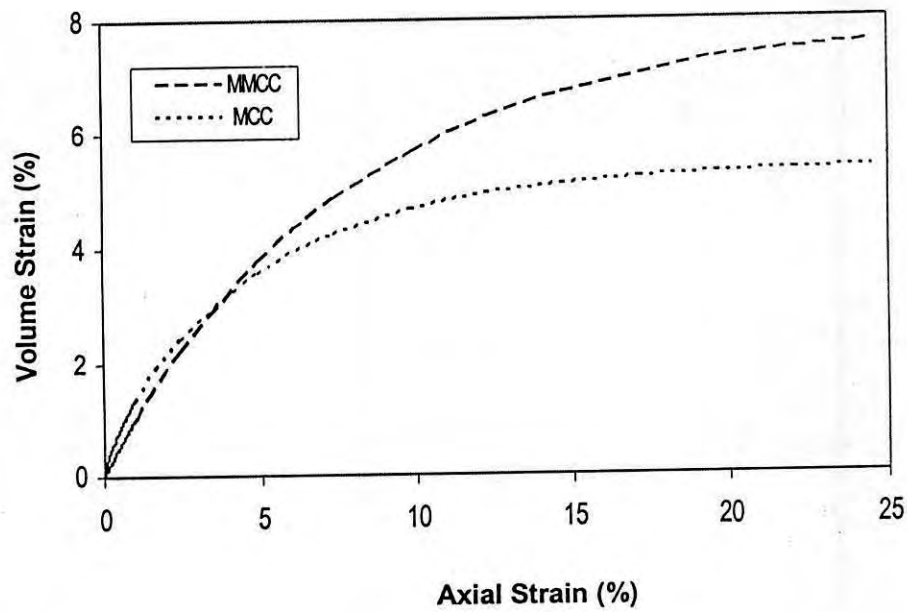


Figure 7.31 MCC and MMCC prediction of volume change response for 14% cemented Savar clay (OCR=1)

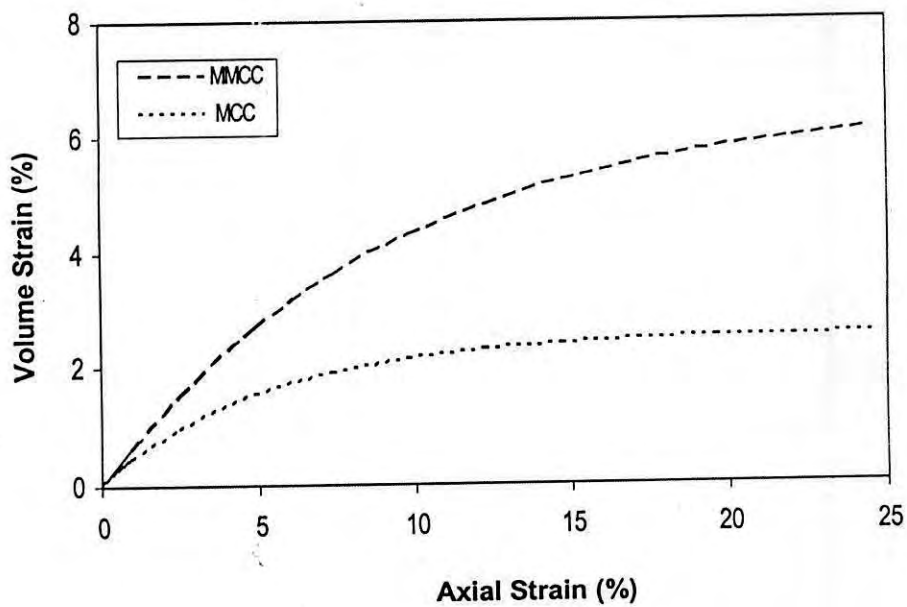


Figure 7.32 MCC and MMCC prediction of volume change response for 14% cemented Savar clay (OCR=2)

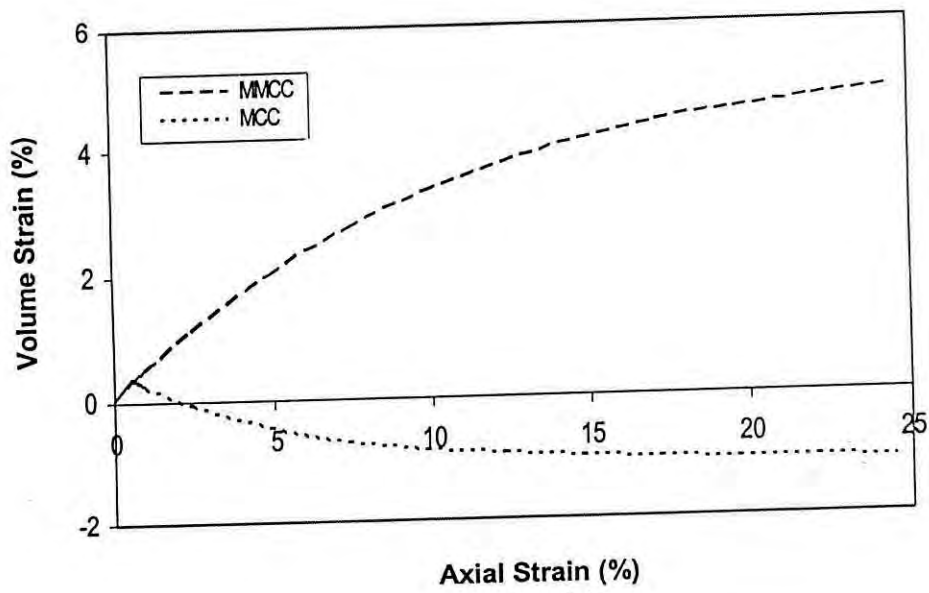


Figure 7.33 MCC and MMCC prediction of volume change response for 14% cemented Savar clay (OCR=5)

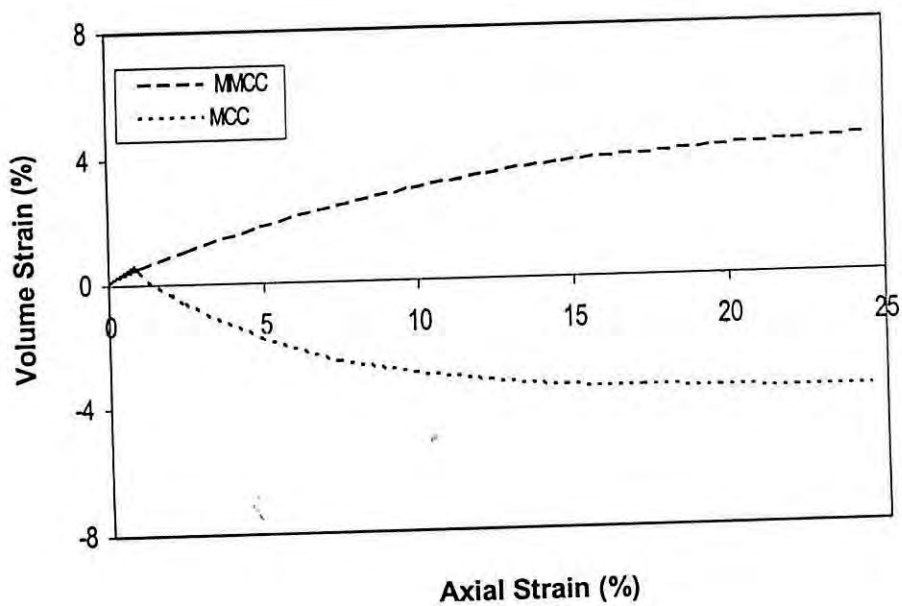


Figure 7.34 MCC and MMCC prediction of volume change response for 14% cemented Savar clay (OCR=10)



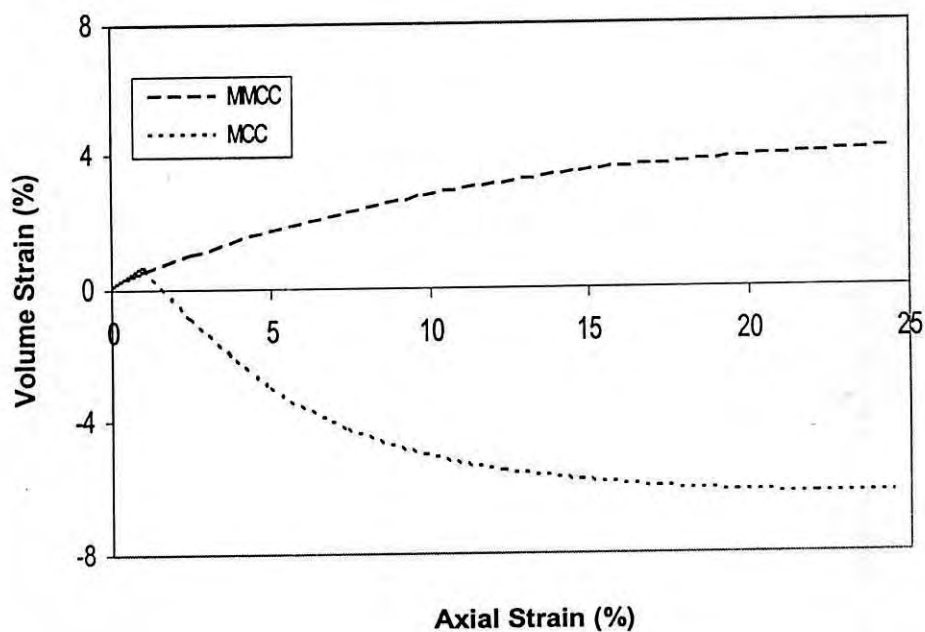


Figure 7.35 MCC and MMCC prediction of volume change response for 14% cemented Savar clay (OCR=20)

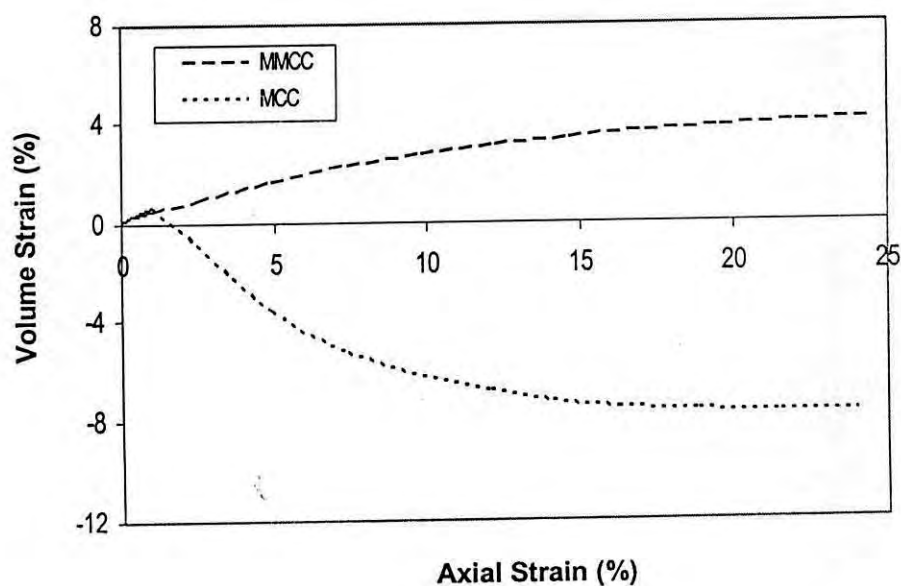


Figure 7.36 MCC and MMCC prediction of volume change response for 14% cemented Savar clay (OCR=30)

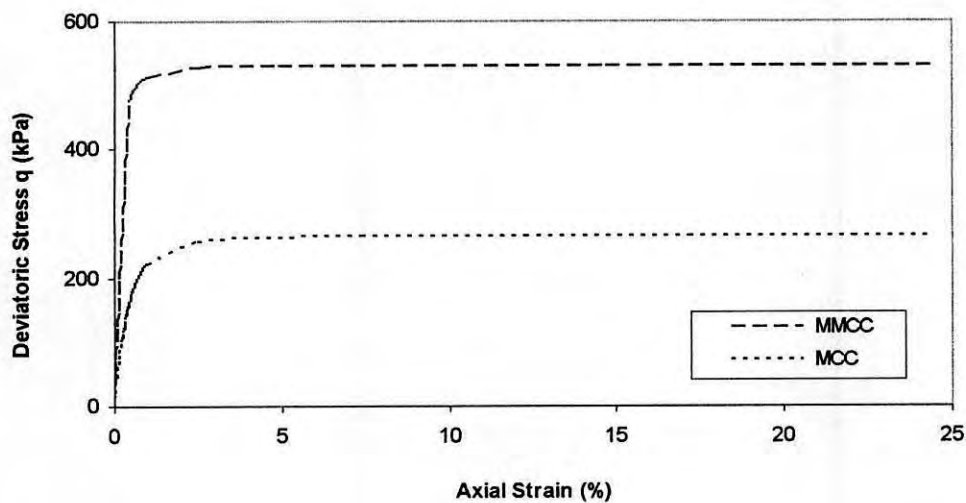


Figure 7.37 MCC and MMCC prediction of undrained stress-strain response for 7% cemented Savar clay (OCR=1)

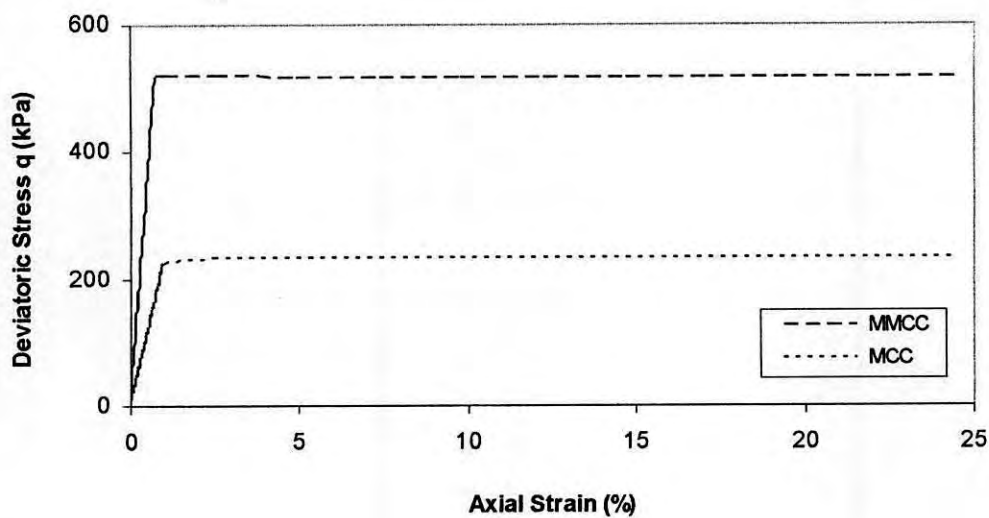


Figure 7.38 MCC and MMCC prediction of undrained stress-strain response for 7% cemented Savar clay (OCR=2)

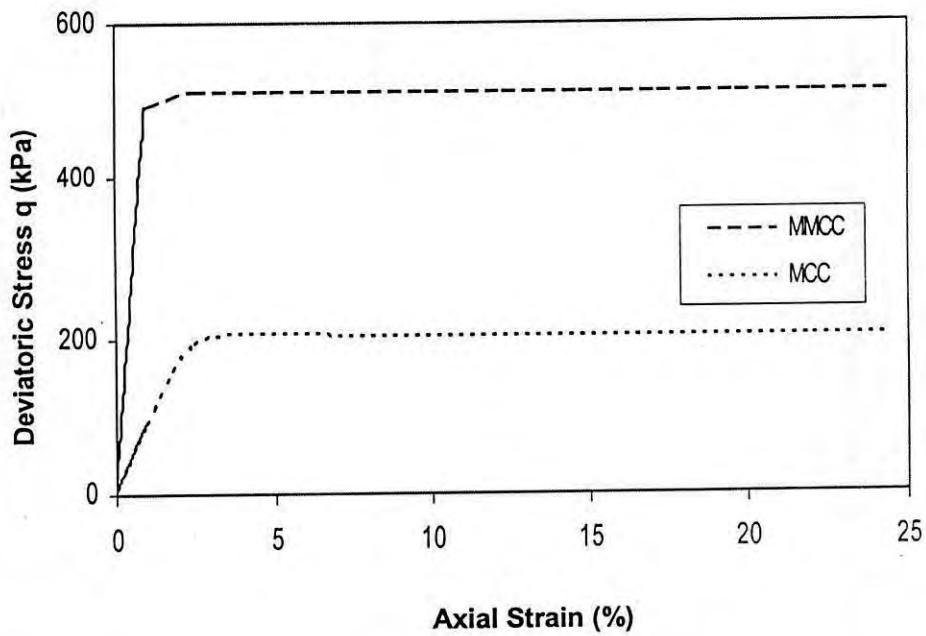


Figure 7.39 MCC and MMCC prediction of undrained stress-strain response for 7% cemented Savar clay (OCR=5)

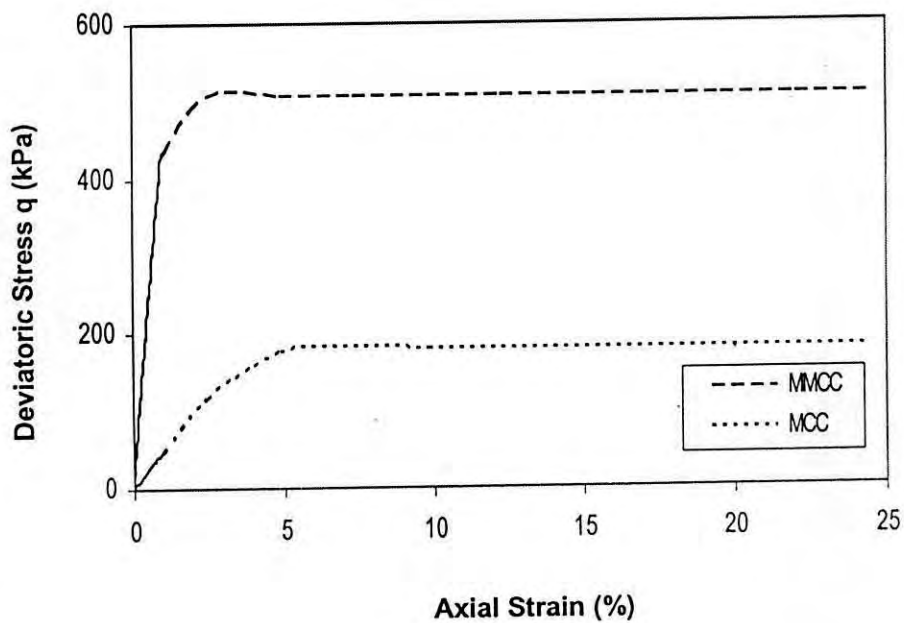


Figure 7.40 MCC and MMCC prediction of undrained stress-strain response for 7% cemented Savar clay (OCR=10)

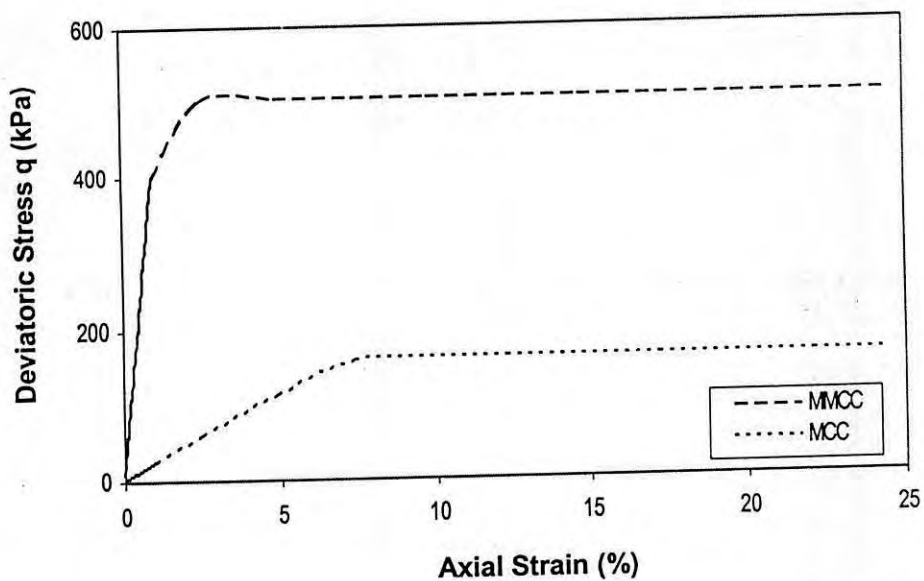


Figure 7.41 MCC and MMCC prediction of undrained stress-strain response for 7% cemented Savar clay (OCR=20)

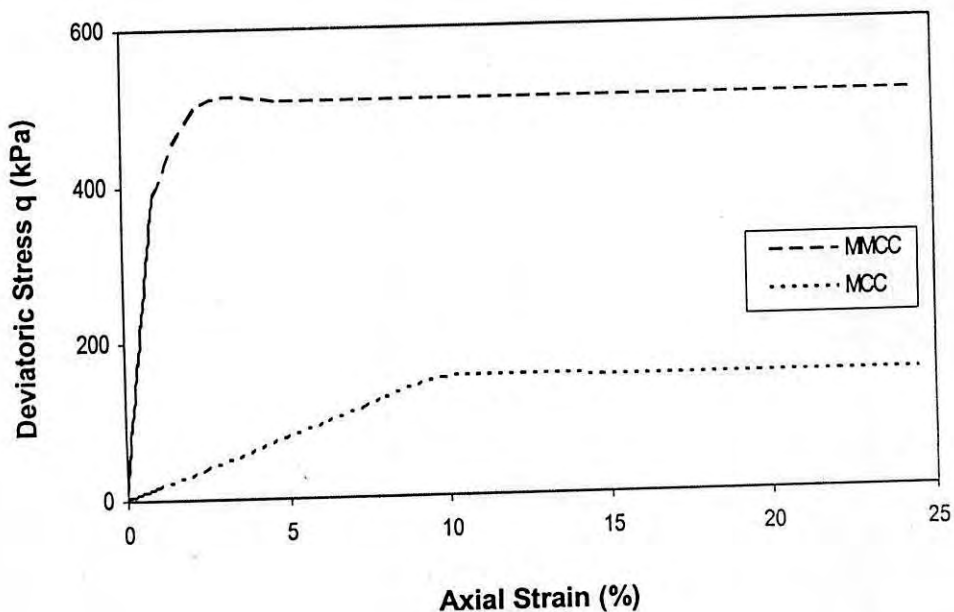


Figure 7.42 MCC and MMCC prediction of undrained stress-strain response for 7% cemented Savar clay (OCR=30)

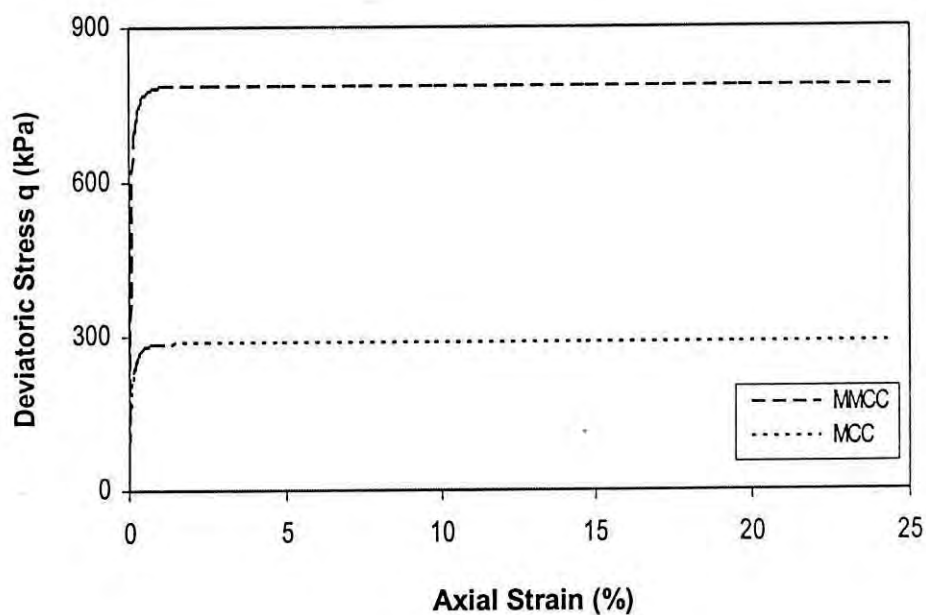


Figure 7.43 MCC and MMCC prediction of undrained stress-strain response for 14% cemented Savar clay (OCR=1)

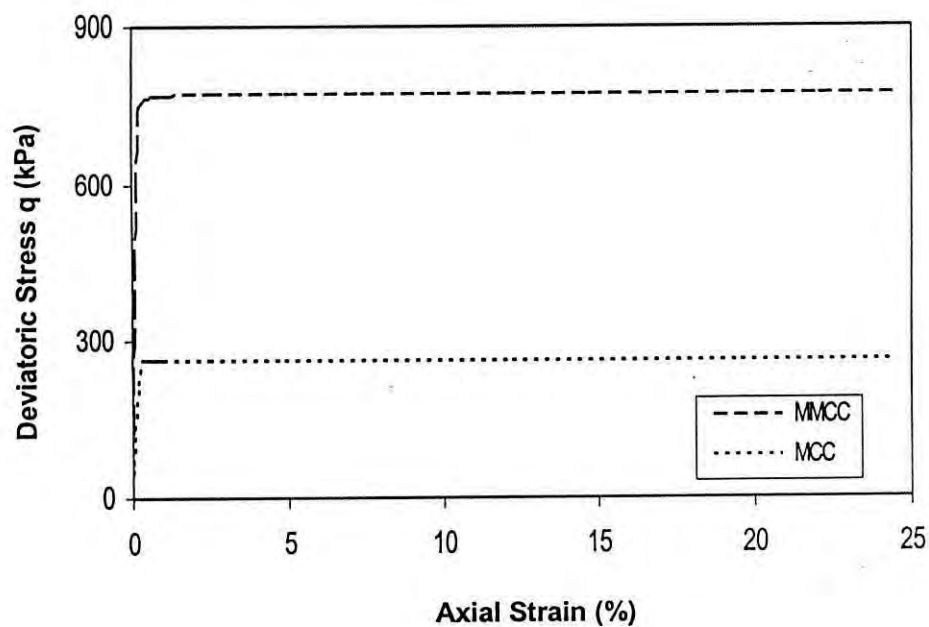


Figure 7.44 MCC and MMCC prediction of undrained stress-strain response for 14% cemented Savar clay (OCR=2)

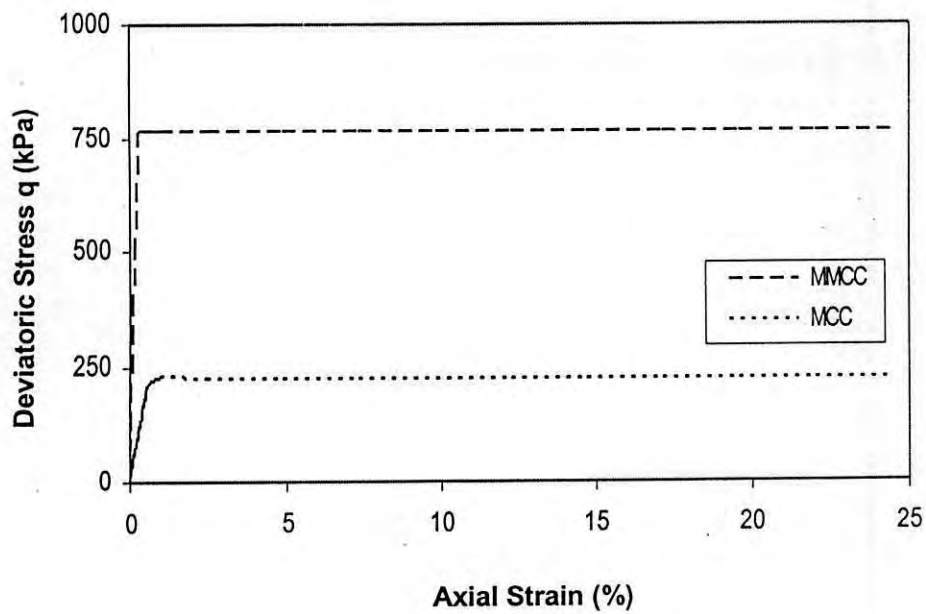


Figure 7.45 MCC and MMCC prediction of undrained stress-strain response for 14% cemented Savar clay (OCR=5)

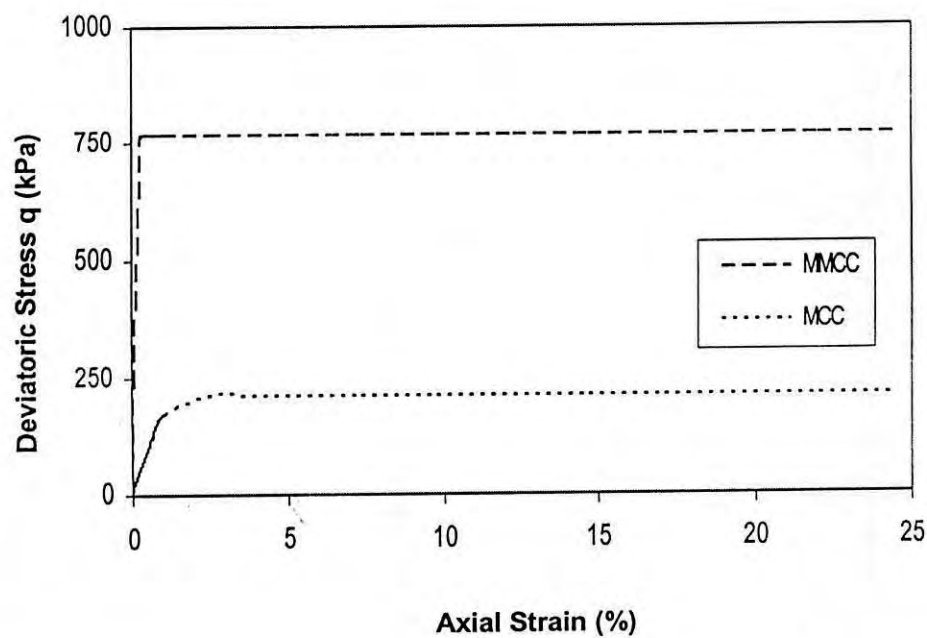


Figure 7.46 MCC and MMCC prediction of undrained stress-strain response for 14% cemented Savar clay (OCR=10)

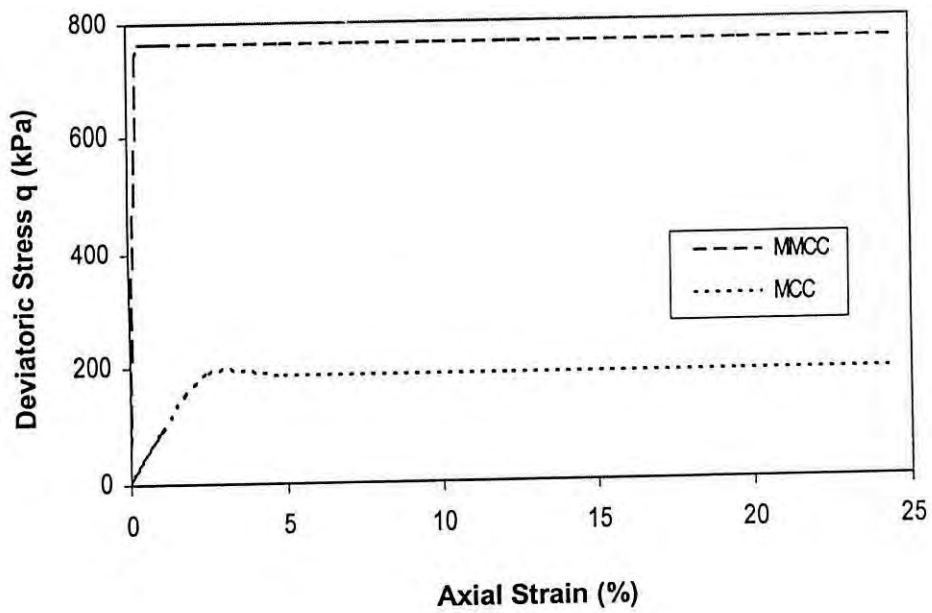


Figure 7.47 MCC and MMCC prediction of undrained stress-strain response for 14% cemented Savar clay (OCR=20)

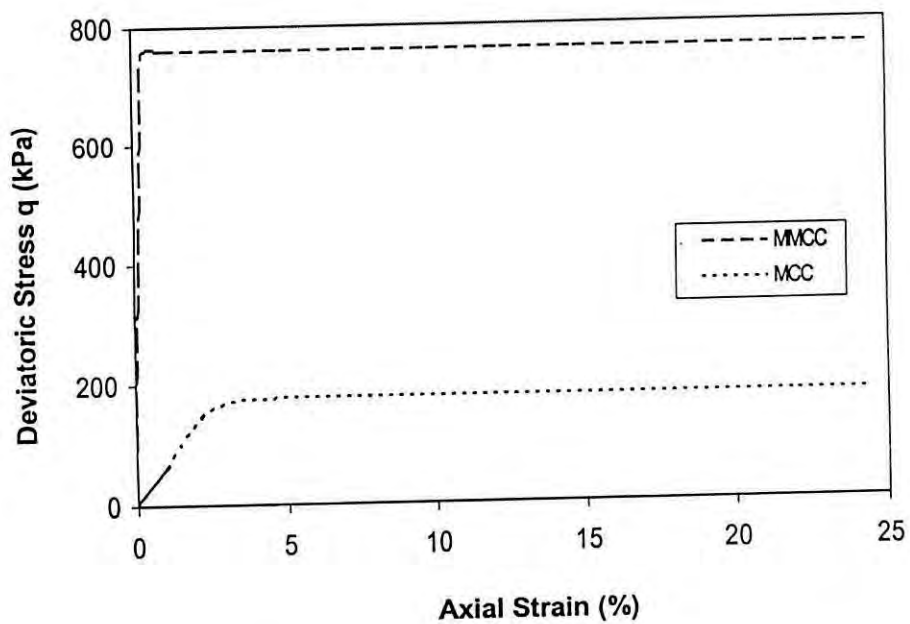


Figure 7.48 MCC and MMCC prediction of undrained stress-strain response for 14% cemented Savar clay (OCR=30)

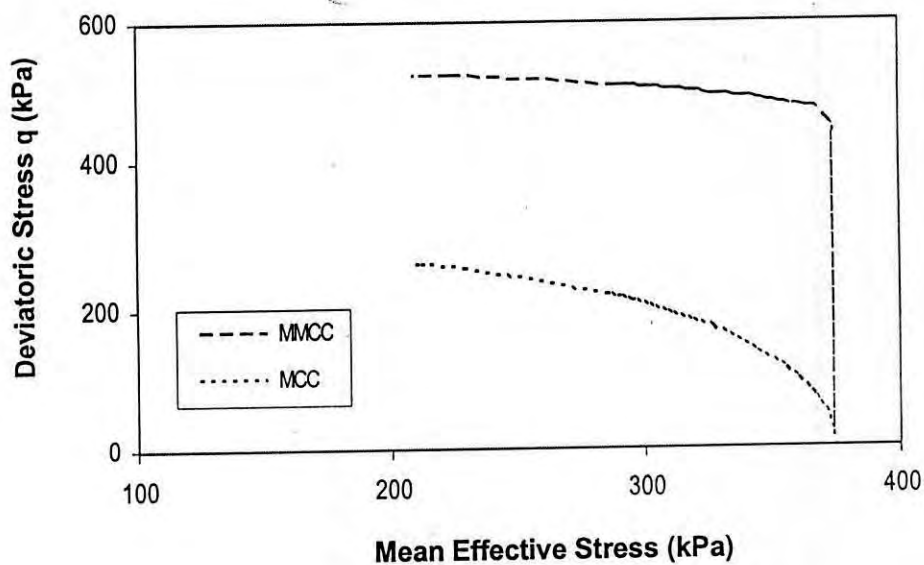


Figure 7.49 MCC and MMCC prediction of undrained triaxial stress path for 7% cemented Savar clay (OCR=1)

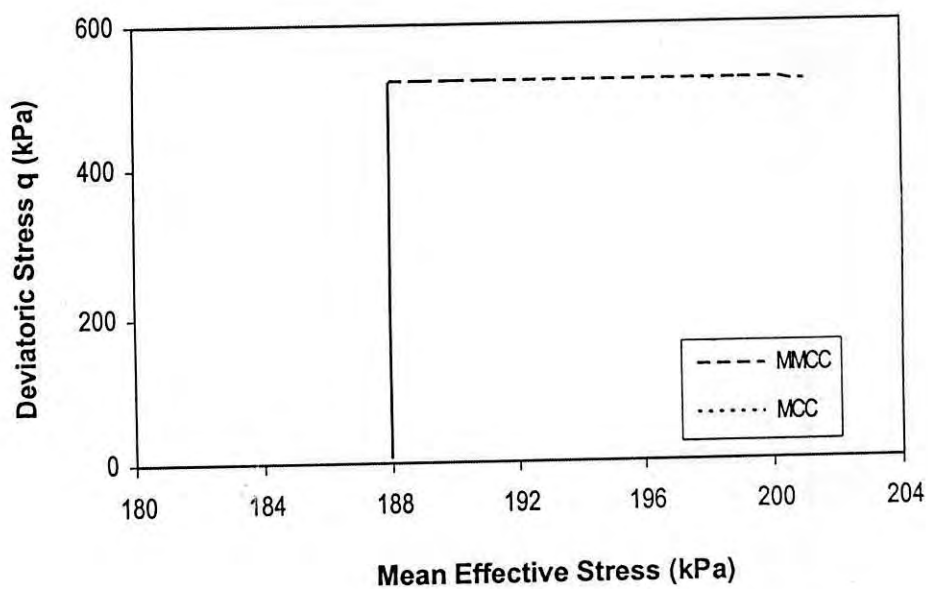


Figure 7.50 MCC and MMCC prediction of undrained triaxial stress path for 7% cemented Savar clay (OCR=2)



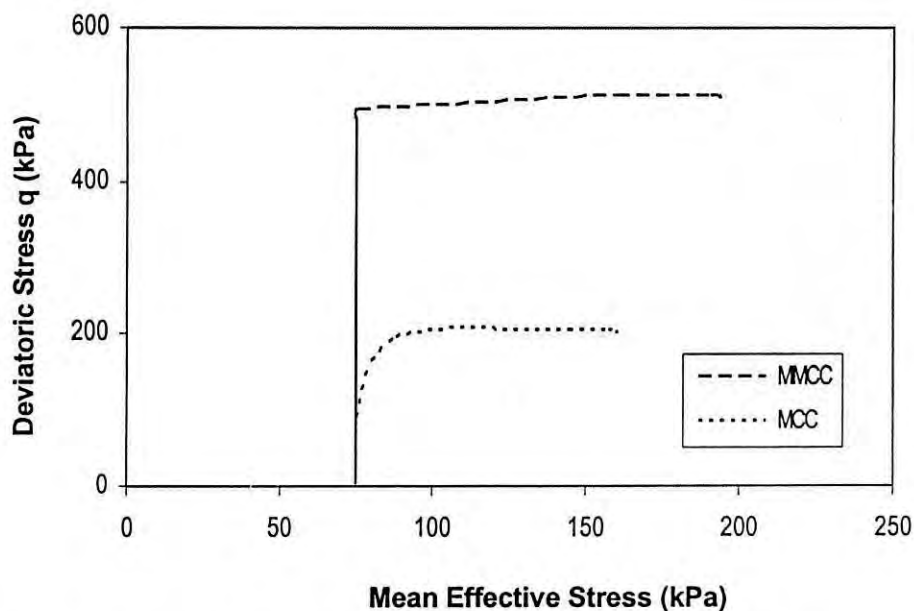


Figure 7.51 MCC and MMCC prediction of undrained triaxial stress path for 7% cemented Savar clay (OCR=5)

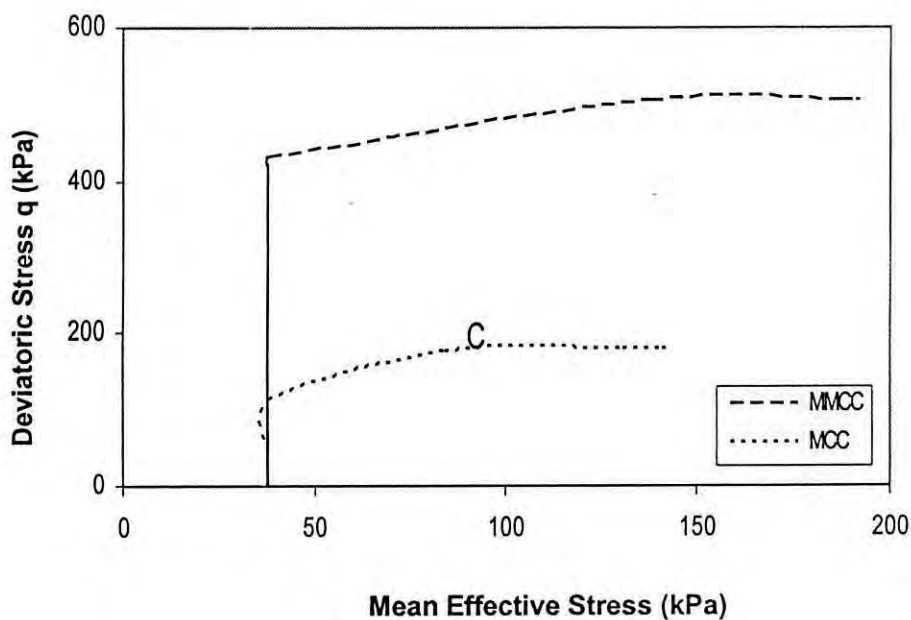


Figure 7.52 MCC and MMCC prediction of undrained triaxial stress path for 7% cemented Savar clay (OCR=10)

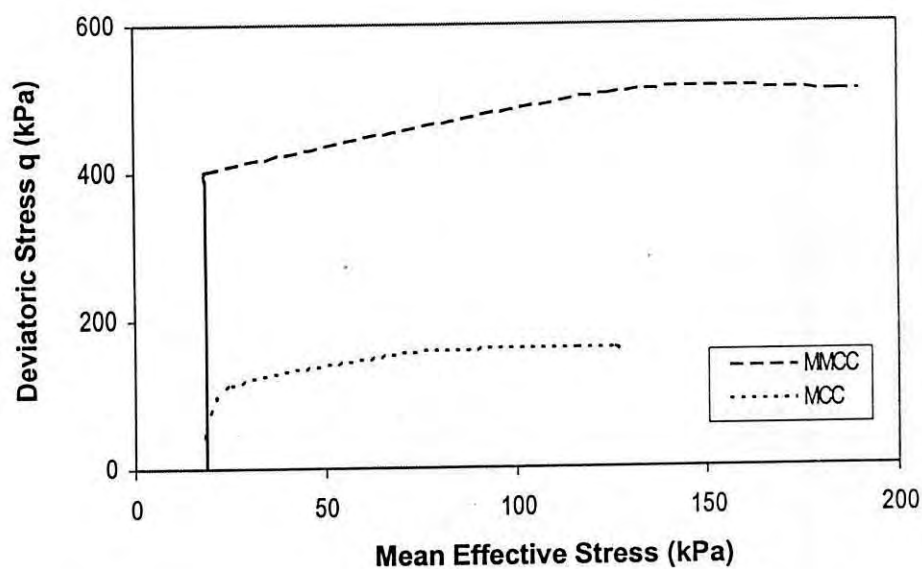


Figure 7.53 MCC and MMCC prediction of undrained triaxial stress path for 7% cemented Savar clay (OCR=20)

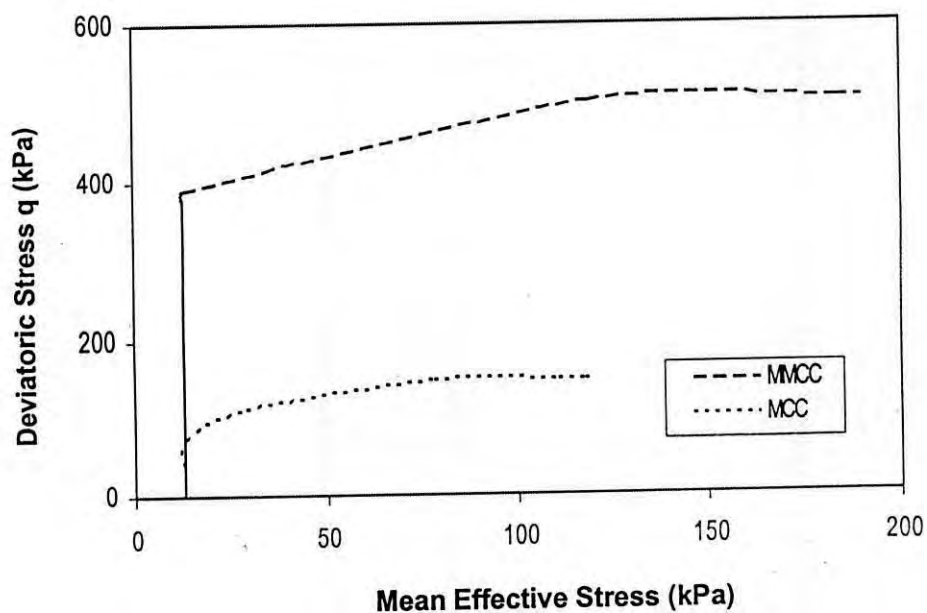


Figure 7.54 MCC and MMCC prediction of undrained triaxial stress path for 7% cemented Savar clay (OCR=30)

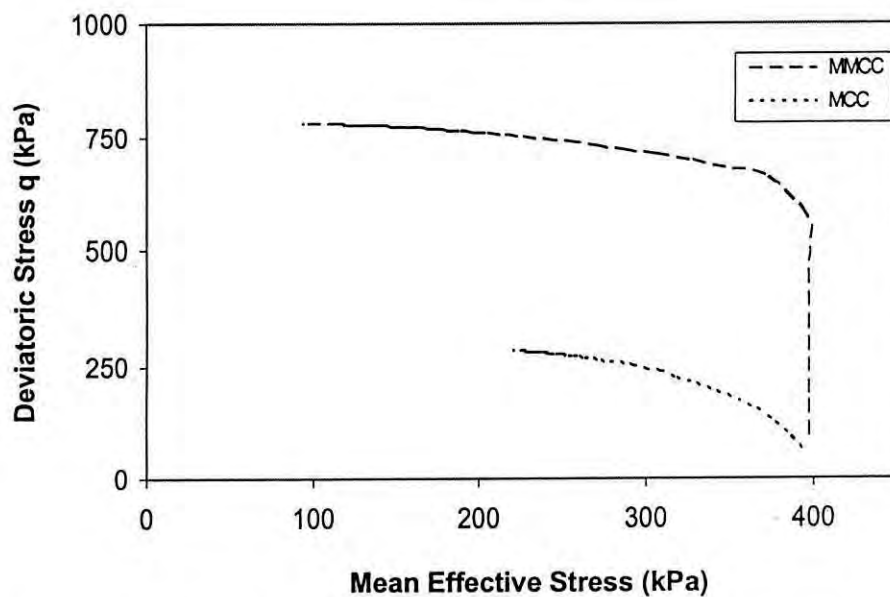


Figure 7.55 MCC and MMCC prediction of undrained triaxial stress path for 14% cemented Savar clay (OCR=1)

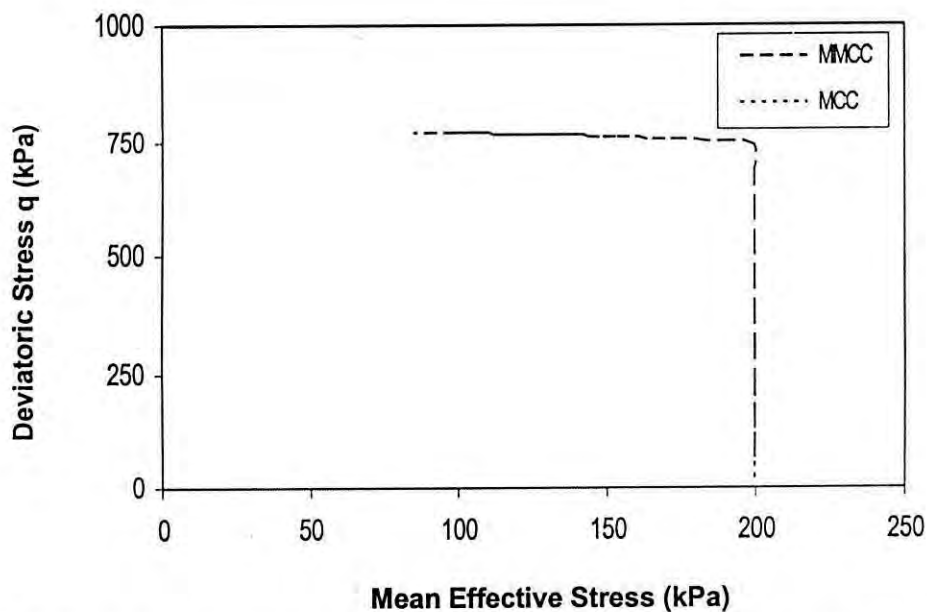


Figure 7.56 MCC and MMCC prediction of undrained triaxial stress path for 14% cemented Savar clay (OCR=2)

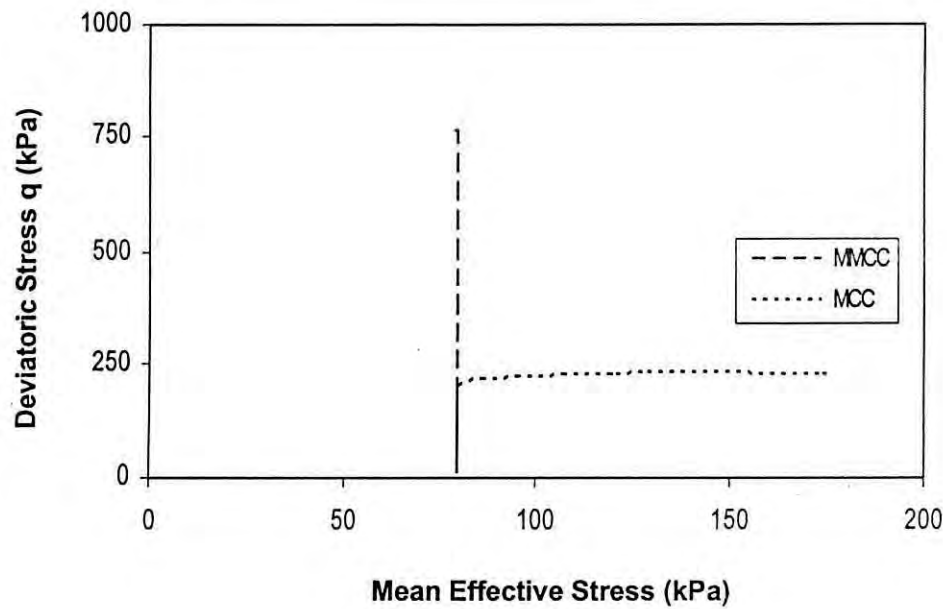


Figure 7.57 MCC and MMCC prediction of undrained triaxial stress path for 14% cemented Savar clay (OCR=5)

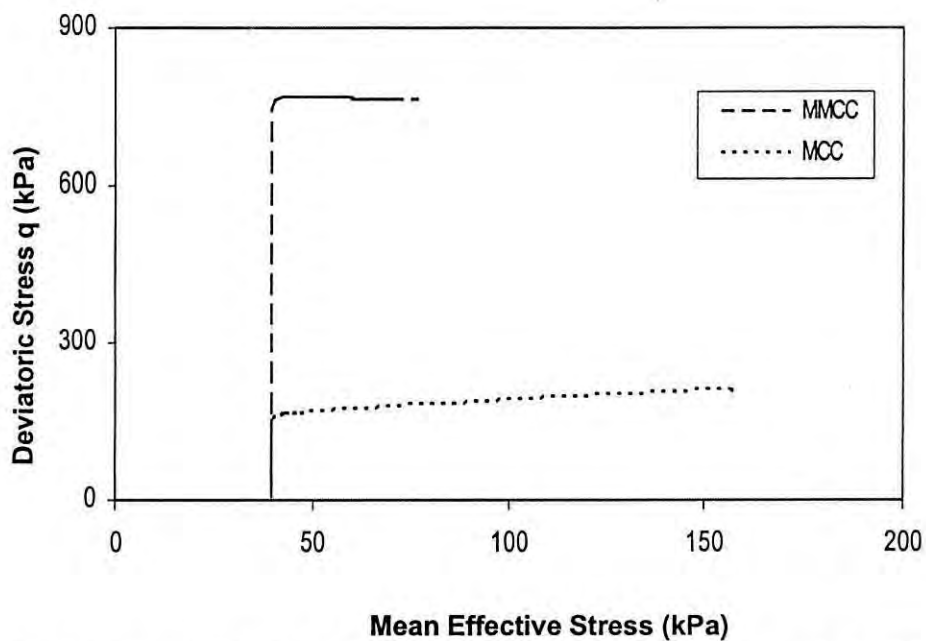


Figure 7.58 MCC and MMCC prediction of undrained triaxial stress path for 14% cemented Savar clay (OCR=10)

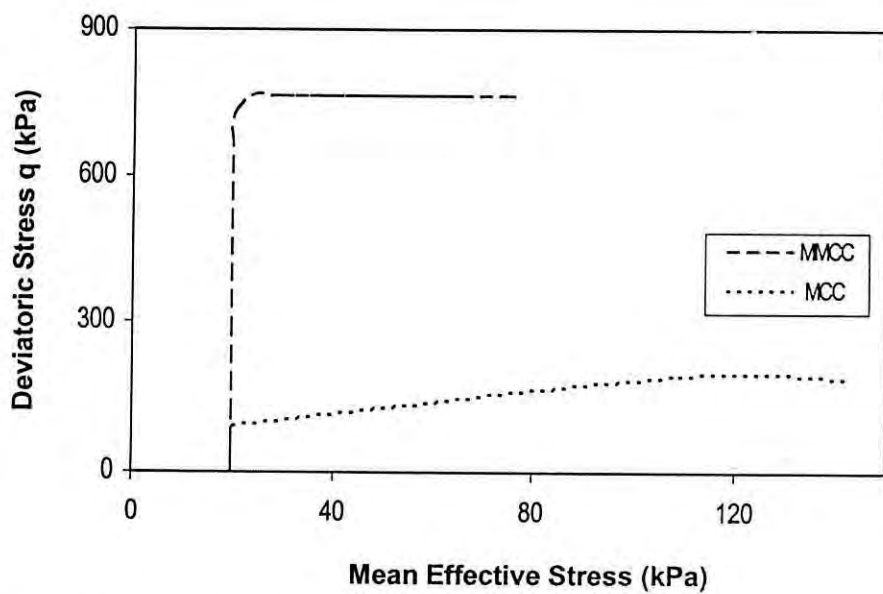


Figure 7.59 MCC and MMCC prediction of undrained triaxial stress path for 14% cemented Savar clay (OCR=20)

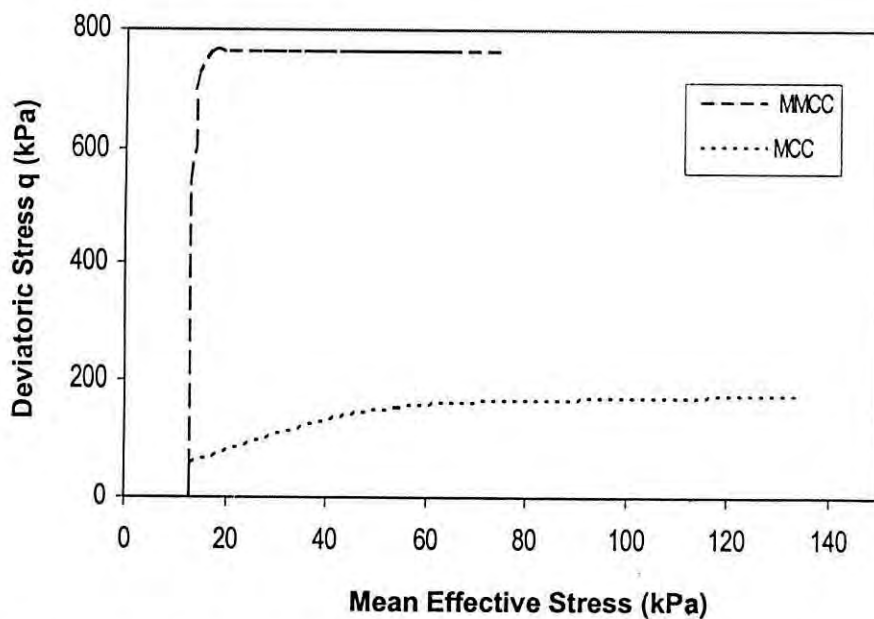


Figure 7.60 MCC and MMCC prediction of undrained triaxial stress path for 14% cemented Savar clay (OCR=30)

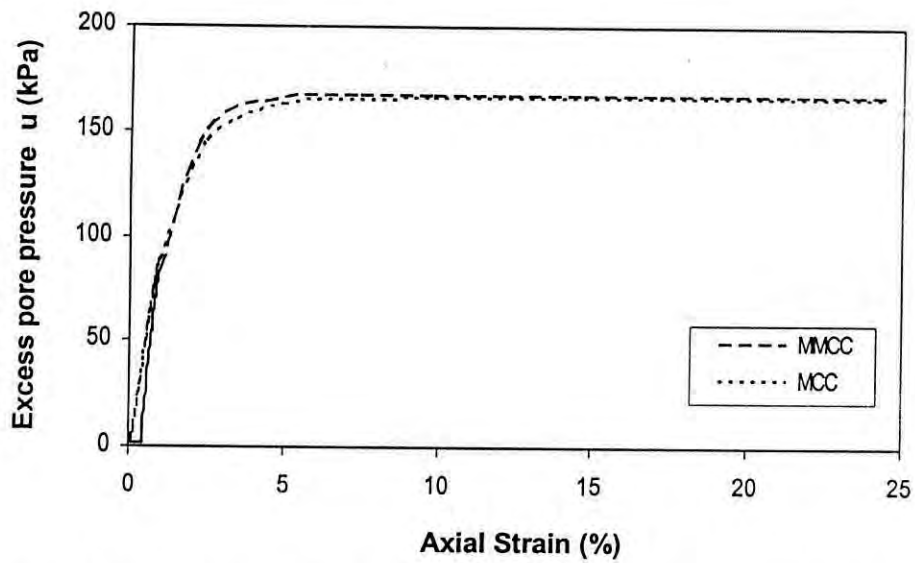


Figure 7.61 MCC and MMCC prediction of excess pore pressure response for 7% cemented Savar clay (OCR=1)

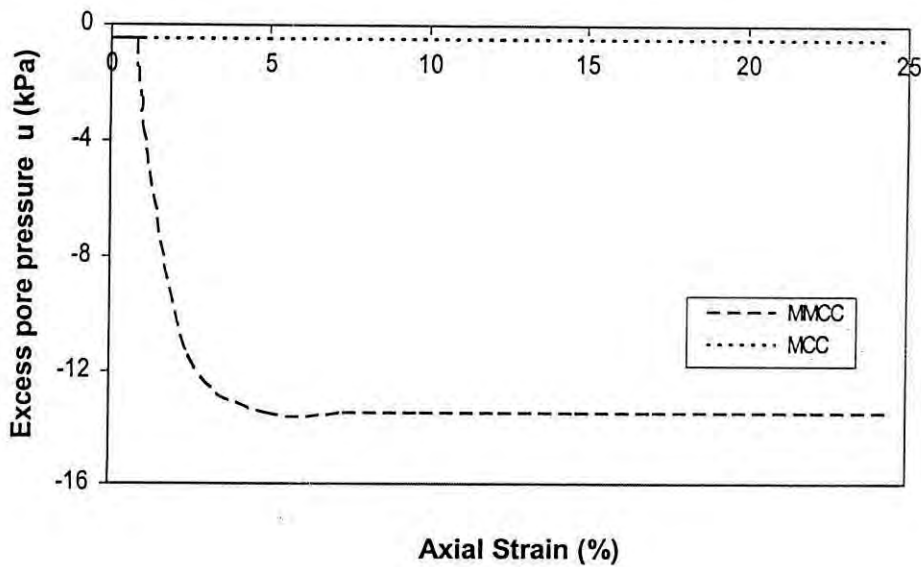


Figure 7.62 MCC and MMCC prediction of excess pore pressure response for 7% cemented Savar clay (OCR=2)

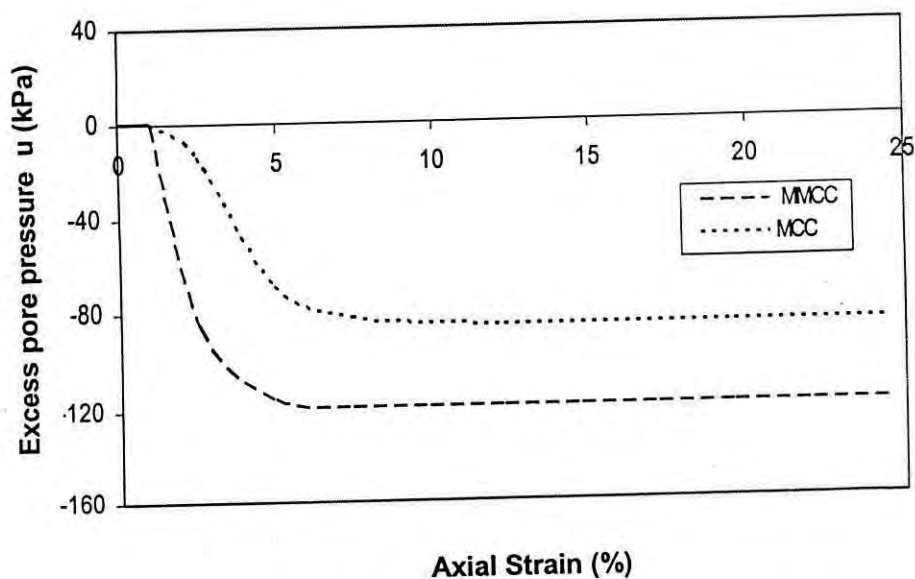


Figure 7.63 MCC and MMCC prediction of excess pore pressure response for 7% cemented Savar clay (OCR=5)

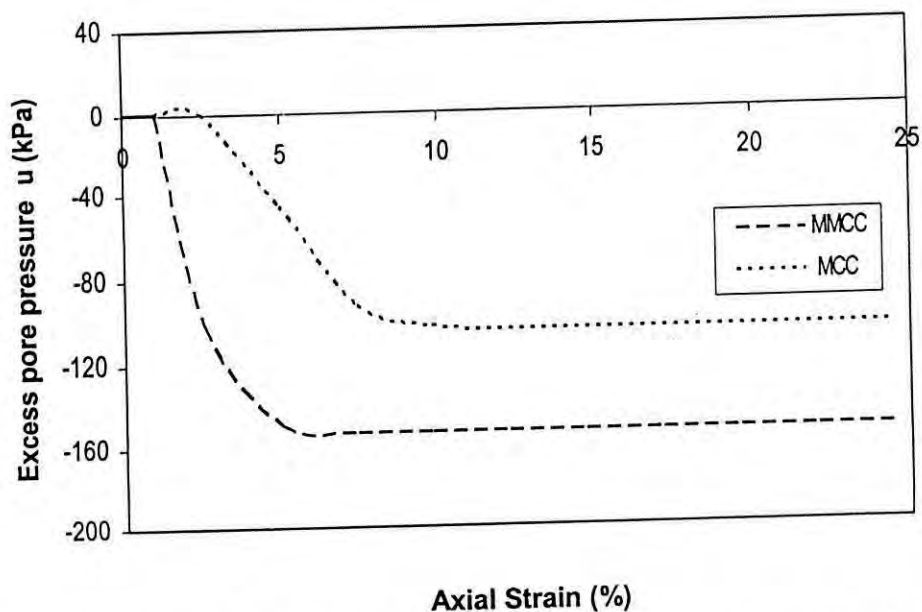


Figure 7.64 MCC and MMCC prediction of excess pore pressure response for 7% cemented Savar clay (OCR=10)

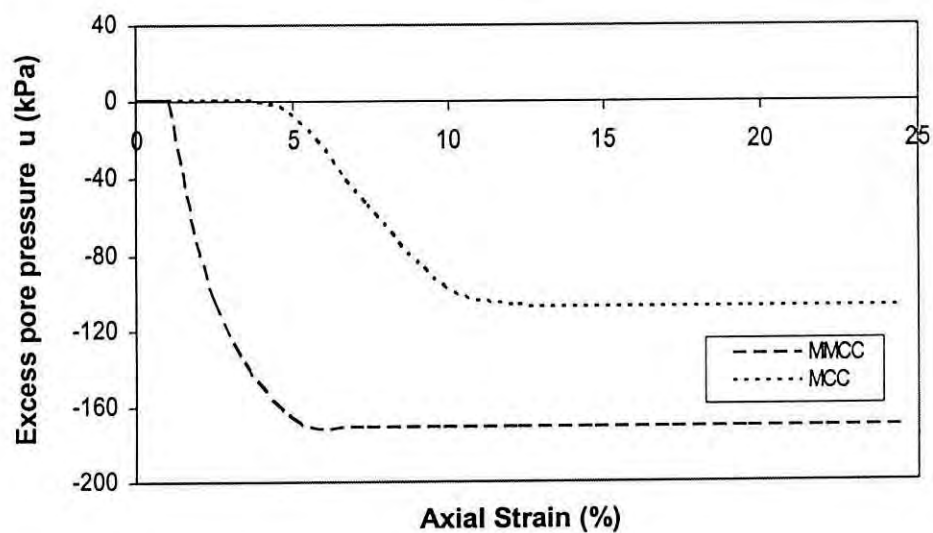


Figure 7.65 MCC and MMCC prediction of excess pore pressure response for 7% cemented Savar clay (OCR=20)

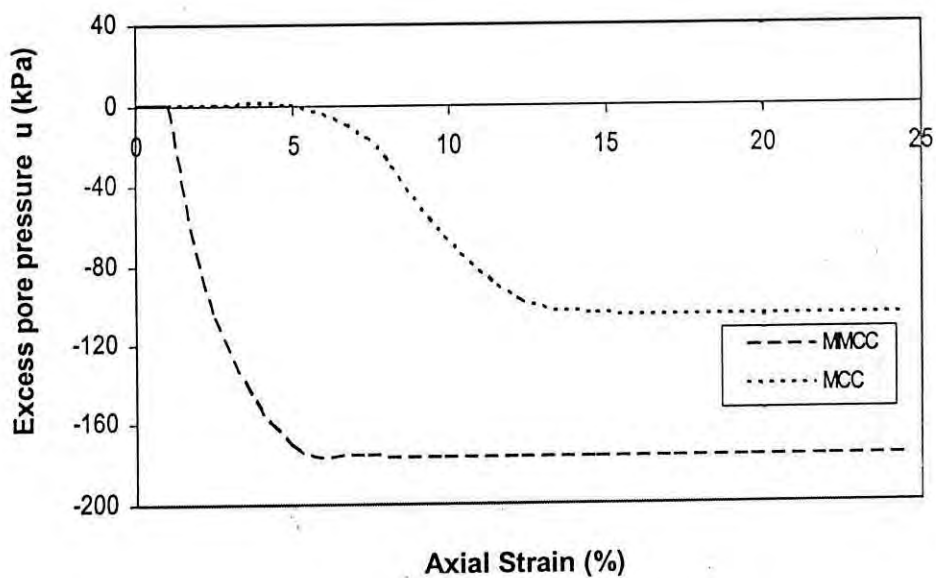


Figure 7.66 MCC and MMCC prediction of excess pore pressure response for 7% cemented Savar clay (OCR=30)



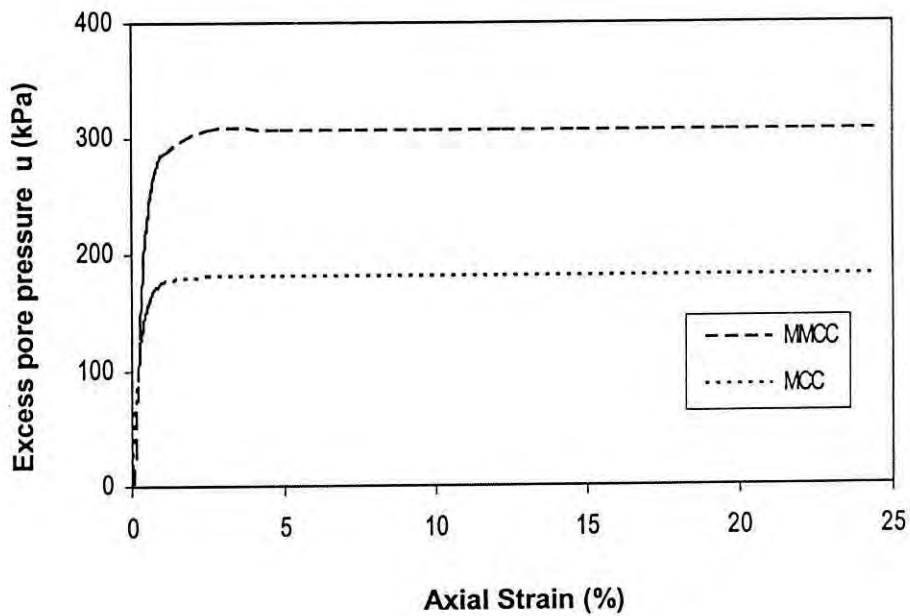


Figure 7.67 MCC and MMCC prediction of excess pore pressure response for 14% cemented Savar clay (OCR=1)

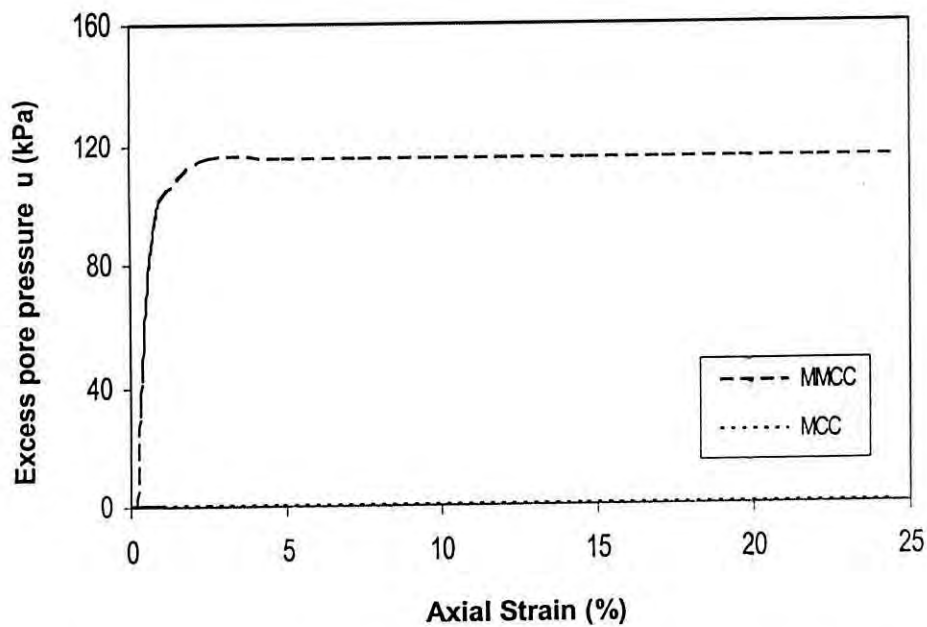


Figure 7.68 MCC and MMCC prediction of excess pore pressure response for 14% cemented Savar clay (OCR=2)

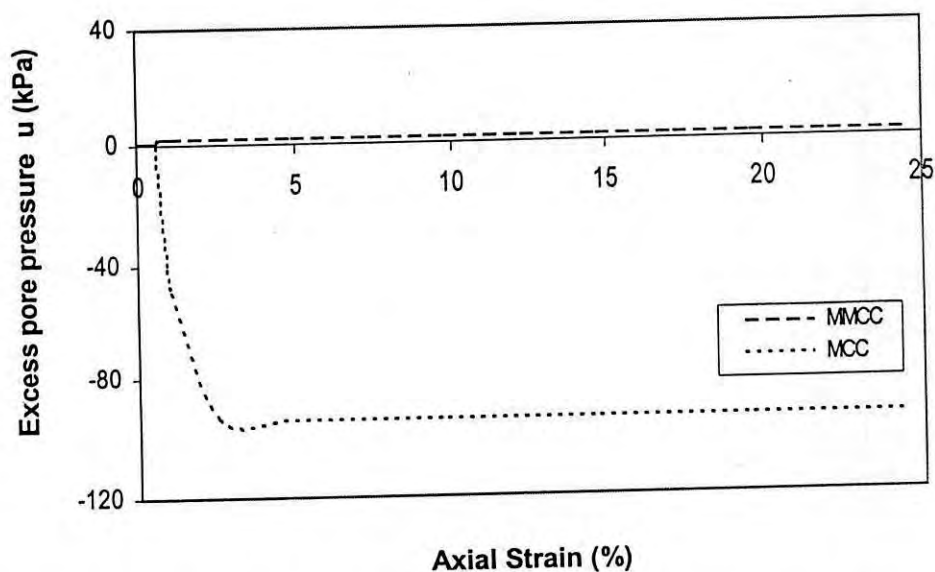


Figure 7.69 MCC and MMCC prediction of excess pore pressure response for 14% cemented Savar clay (OCR=5)

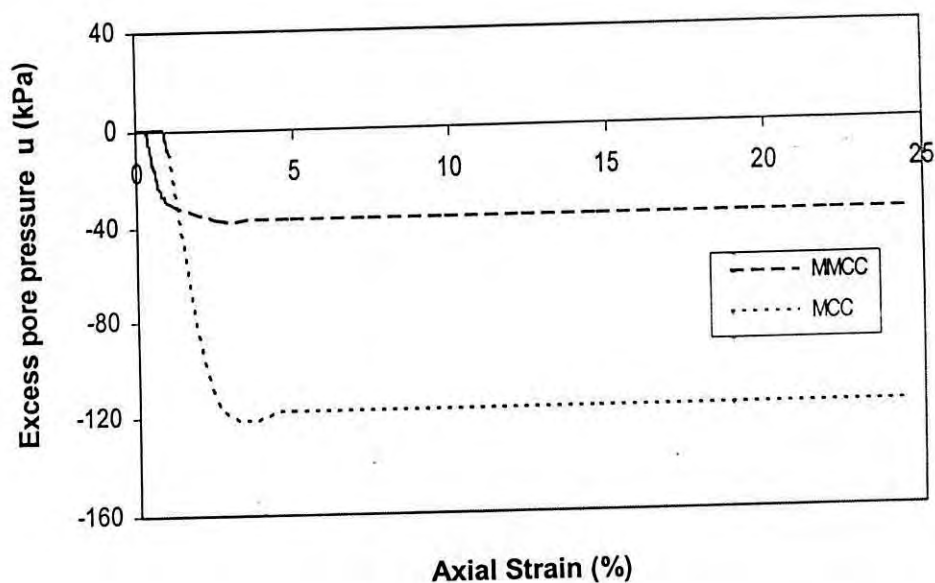


Figure 7.70 MCC and MMCC prediction of excess pore pressure response for 14% cemented Savar clay (OCR=10)

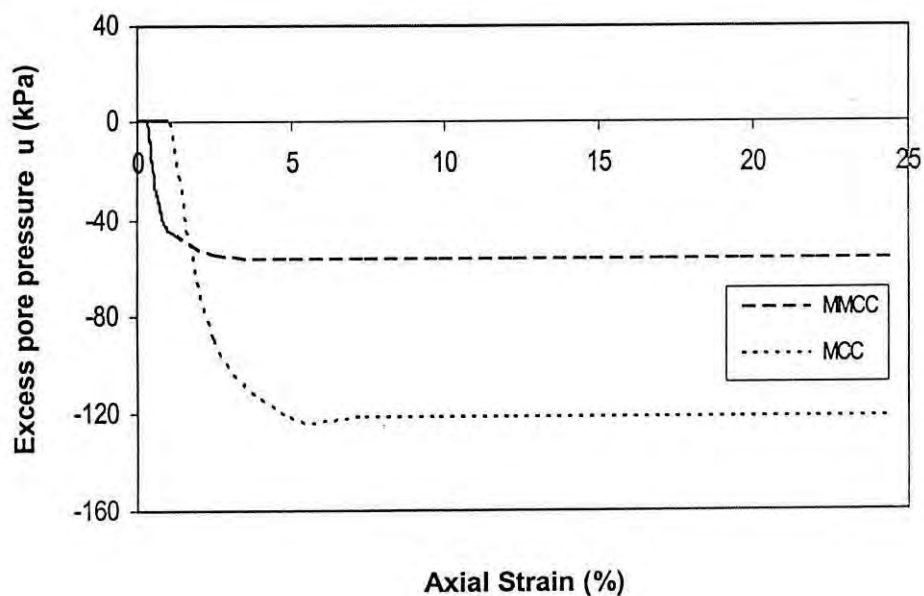


Figure 7.71 MCC and MMCC prediction of excess pore pressure response for 14% cemented Savar clay (OCR=20)

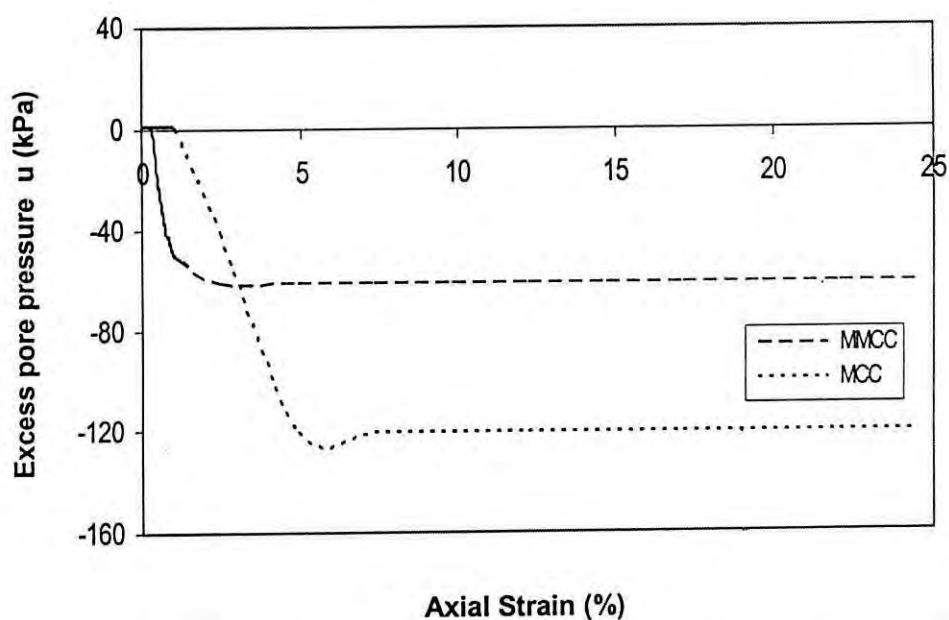


Figure 7.72 MCC and MMCC prediction of excess pore pressure response for 14% cemented Savar clay (OCR=30)

## CHAPTER -8

### EMMCC MODEL INCORPORATING CEMENTATION BREAKDOWN

#### 8.1 Introduction

The Modified Modified Cam Clay (MMCC) model incorporated the tensile strength of artificially cemented remolded Savar clays as a model parameter. However, it is quite natural to expect that with increasing shearing strain and volume change of soil, cohesion or cementation force i.e. the tensile strength of the clay will gradually breakdown. This is expected to result in a decrease of the predicted shear strength of the clay with increase of stress and strain. Currently, certain critical state soil models employ equations to simulate cementation or tensile strength breakdown to simulate the effect of such breakdown on the shear behavior of cemented soils. Such a cementation breakdown assumption may be incorporated in the MCC or the MMCC model discussed in previous chapters. The model may then be used to predict the stress-strain, volume change and excess pore pressure response for remolded Savar clays, with and without cementation, and for various degrees of overconsolidation and for various values of the cementation breakdown parameter. The following chapter discusses in detail the various aspects of an extended MMCC model incorporating the cementation breakdown assumption.

#### 8.2 Extended MMCC (EMMCC) Model

As a result of cementation of clays, both the consolidation and tensile strength of the clay increases. Both these components of cementation components may be distinctly incorporated in the MCC model, along with separate breakdown effects for each of these

components. In Chapter 7, only tensile strength component of cementation was incorporated in the MCC model. This was termed as the MMCC model. The resulting model is termed here as the MCC model with cementation breakdown assumption. Various aspects of both the MCC and MMCC model has been discussed in the previous chapters. In the following subsections, the incorporation of the consolidation and tensile strength component as a result of cementation in the MCC model is discussed. The process of incorporating cementation breakdown effects in the MCC model is also discussed in the following subsections.

### 8.2.1 Tensile Strength Breakdown

It is assumed in the EMMCC model that the tensile strength degrades with the accumulation of the absolute value of plastic volumetric strain. The equation used to simulate the breakdown of tensile strength with plastic volumetric strain is as given below:

$$p'_t = p'_{t0} \exp[-\rho_t(\varepsilon^d)] \quad (8.1)$$

Where

$$\varepsilon^d = \int |d\varepsilon_v^p| \quad (8.2)$$

In the above equation,  $\rho_t$  is the degradation parameter for tensile strength,  $p'_{t0}$  is the tensile strength of reconstituted cemented Savar clay. Generally a large positive number greater than 1.0 is used to effectively simulate a realistic cementation breakdown effect. Zero value is assumed for  $\rho_t$  in the case of no break down assumption.

### 8.2.2 Consolidation Strength Breakdown

It is assumed in the EMMCC model that the increment of consolidation strength as a result of cementation degrades with the accumulation of the absolute value of plastic volumetric strain. The equation that is used to simulate the breakdown of increment of consolidation strength (as a result of cementation) with volumetric strain is as given below:

$$p_m = p_{m0} \exp\left[-\rho_m (\varepsilon^d)^3\right] \quad (8.3)$$

$$\text{Where } \varepsilon^d = \int |d\varepsilon_v^p| \quad (8.4)$$

In the above equation,  $\rho_m$  is the degradation parameter for the increment of consolidation strength  $p_{m0}$  of reconstituted cemented Savar clay. As discussed before, generally a large positive number greater than 1.0 is used for  $\rho_m$  to realistically simulate the breakdown effects. Zero value is assumed for  $\rho_m$  for no break down assumption. *It is to be noted that in the numerical predictions presented in this chapter using the EMMCC model, it was assumed that there is no breakdown of the increment of consolidation strength component occurring as a result of cementation. The above cementation breakdown equations given in this section are presented here only for the purpose of completeness.*

### 8.2.3 Yield Locus and Flow Rule

The yield locus of the EMMCC model is given as follows:

$$\left\{ \frac{q}{M(p' + p'_i)} \right\}^2 = \frac{p'_o + p'_i + p'_m}{p' + p'_i} - 1 \quad (8.5)$$

Where

$$p = \frac{\sigma'_1 + \sigma'_2 + \sigma'_3}{3} \quad (8.6)$$

$$q = \sqrt{\frac{(\sigma'_1 - \sigma'_2)^2 + (\sigma'_2 - \sigma'_3)^2 + (\sigma'_1 - \sigma'_3)^2}{2}} \quad (8.7)$$

$$M = \frac{q}{p' + p'_i} \quad (8.8)$$

In the above equations,  $\sigma'_1, \sigma'_2, \sigma'_3$  are the principal effective stress components,  $p'_i$  is the tensile strength due to cementation or cohesion,  $p'_m$  is the increment of consolidation strength due to cementation and  $p'_o$  is the pre-consolidation pressure of the remolded Savar clay without any cementation effects.

The EMMCC model is assumed to obey the associated flow rule. Thus the EMMCC model plastic potential function is identical to the EMMCC yield locus equation. The plastic flow rule for the EMMCC model in its incremental form is identical to that of the plastic flow rule of MCC model as given below:

$$\frac{d\varepsilon_v^p}{d\varepsilon_q^p} = \frac{M^2 - \eta^2}{2\eta} \quad (8.9)$$

However, the  $\eta$  term in the above equation is defined in the EMMCC model as follows:

$$\eta = \frac{q}{p + p_i} \quad (8.10)$$

The remaining aspects of the EMMCC model are identical to the MCC and MMCC model described previously in chapters 6 and 7 respectively.

### 8.3 Prediction of Drained Response

#### 8.3.1 Drained Model Parameters

The MMCC model parameters for different percentages of cement (7% and 14%) for artificially cemented remolded Savar clays have been previously given in Table A7.1. Additionally, Table 8.1 includes the tensile strength parameter  $p_{to}$  and the parameter  $p'_{mo}$  which gives increment of consolidation strength of soil as a result of cementation. The tensile strength  $p_t$  of the cemented clay is computed from the value of unconfined compression strength, pre-consolidation pressure ( $p'_o + p'_{mo}$ ) and the critical state ratio  $M$  as given in equation 5.10. The increment of consolidation strength parameter  $p_{mo}$  as a result of cementation may be computed as the difference between the pre-consolidation pressure of the cemented Savar clay and that of the remolded Savar clay without cementation. Numerical predictions using EMMCC model were obtained for values of the cementation breakdown parameter  $\rho_t$  by assuming the values of  $\rho_t$  to be 1, 10 and 100 respectively. A value 1, 10 and 100 of the tensile strength parameter  $\rho_t$  may be assumed to correspond to mild, moderate and severe rates of breakdown of the tensile strength component  $p_{to}$  of the cemented Savar clay.



Table 8.1 The EMMCC model parameters

Modified Modified Cam Clay Parameters	7% Cemented Clay	14% Cemented Clay
$\lambda$	0.197	0.1
$\kappa$	0.03	0.01
M	1.25	1.3
$P'_o$	375	400
$P_{to}$	213	509
$P_{mo}$	242	267

### 8.3.2 Stress-Strain

Values of 1, 10, and 100 were used for the EMMCC model parameter  $\rho_i$  to get the prediction of stress-strain response for cemented Savar clays (7% and 14%) for different OCR values. Figures 8.1 through 8.6 give the model predictions for 7% cemented Savar clay. Figures 8.7 through 8.12 give similar model predictions for 14% cemented Savar clay. Similar trends were observed for 7% and 14% cemented Savar clays. These are discussed in the following paragraphs. Deviator stress was observed to increase with increasing OCR value both for 7% and 14% cemented Savar clays in all cases.

For normally consolidated and clays with low overconsolidation ratios, and for 7% and 14% cemented Savar clays, it was observed that initial shear stiffness is unaffected by the value of cementation breakdown parameter  $\rho_i$ . A higher value of the cementation breakdown parameter  $\rho_i$  predicts a relatively lower increase of deviator stress with axial strain both for 7% and 14% cemented Savar clays.

For a high OCR value of 10 and 7% cemented Savar clay,  $\rho_i$  appears to have no effect on the mobilized deviator stress. For very high OCR values of 20 and 30 respectively, a  $\rho_i$  value equal to 100 results in a sharp decrease of the deviator stress as observed in the case of numerical predictions for 7% cemented Savar clay.

### 8.3.3 Stress Path

Figures 8.13 through 8.24 show the predicted drained stress paths of cemented Savar clays, for different values of the cementation breakdown parameter  $\rho_i$  (values of 1, 10 and 100) and at different OCR values (OCR values of 1, 2, 5, 10, 20 and 30). During triaxial shear under drained condition, the drained total and effective stress paths are identical, and the stress path is independent of the soil model used as described previous chapter.

### 8.3.4 Volume Change Response

The drained volume change response of cemented Savar clays as predicted by the EMMCC model are shown in Figures 8.25 through 8.36 for 7% and 14% cementation, and for different values of OCR. A value of 1, 10 and 100 of  $\rho_i$  was assumed and the corresponding predictions were compared. In case of 7% cementation, it was observed that for OCR values of 1, 2, 5 and 10 and all values of  $\rho_i$ , a positive volume change response is predicted. However, a higher value of break down parameter  $\rho_i$  lowers the predicted positive volume change response. The positive volume change responses are also observed to decrease with increasing OCR values.

It is also observed that for clays with overconsolidation ratio values equal to 20 and 30 respectively, and for 7% cementation, volume change response is either zero or negative for values of 1 and 10 of the cementation breakdown parameter  $\rho_i$ . Negative volume

change response was also predicted for a value of  $\rho_i$  equals 100. For 14% cementation, positive volume change response is predicted for different values of cementation breakdown parameter  $\rho_i$  in all cases. The positive volume change response was observed to decrease with increasing OCR value. It was also observed that an increase in the value of the cementation breakdown parameter  $\rho_i$  results in a decrease in the predicted positive volume change response.

## 8.4 Prediction of Undrained Response

### 8.4.1 Model Parameters

For undrained predictions, model parameters used for the EMMCC model are identical to that used for drained predictions. However, minor adjustments were made to the value of  $\lambda$  which is the slope of the normal consolidation line, and to the value of  $\kappa$ , which is the slope of the elastic rebound line. This was done, as some numerical instability was observed when obtaining undrained predictions using the exact values of the parameters  $\lambda$  and  $\kappa$ . EMMCC model was used with these parameter values to obtain the stress-strain, stress path and pore pressure response of cemented Savar clays.

### 8.4.2 Stress-Strain

The EMMCC model with different values for the tensile strength breakdown parameter  $\rho_i$  (values of 1, 10, and 100) was used to predict the stress-strain response for cemented Savar clays (7% and 14% cementation) for different OCR values. Figures 8.37 through 8.42 show the model predictions for 7% cemented Savar clay. Figures 8.43 through 8.48 shows the model predictions for 14% cemented Savar clay. These cases are discussed in the following paragraphs.

For normally consolidated clays and for clays with low overconsolidation ratios, and for 7% and 14% cementation, it was observed that the initial shear stiffness is unaffected by

the value of the parameter  $\rho_c$ . A higher value of the cementation break down parameter  $\rho_c$  predicted a relatively lower increase of deviator stress with axial strain, both for 7% and 14% cemented Savar clays.

However, constant deviator stress with continuous shearing are predicted for all cases after a certain value of axial strain is reached. A higher value of the cementation break down parameter  $\rho_c$  predicts a relatively lower increase of deviator stress with axial strain. For lower values of the break down parameters  $\rho_c$  (values are 1 and 10), no or insignificant effect was observed in the predicted deviator stress for 7% cementation and for all OCR values. However, the differences in the predicted deviator stresses were observable for very high values of the parameter  $\rho_c$  (100). Similar observations were made in case prediction for 14% cementation and for all OCR values. It is also observed that deviator stress increases with increasing OCR values both for 7 % and 14% cemented Savar clays.

#### 8.4.3 Stress Path

Figures 8.49 through 8.60 show the predicted undrained stress paths for cemented Savar clay for different values of the cementation break down parameter  $\rho_c$  and for different values of OCR. The effect of OCR on stress path as predicted by the EMMCC model was observed to be similar to that of the MMCC model as given in the relevant section in chapter 7. For low values of the cementation break down parameter  $\rho_c$  (values of 1 and 10), no observable deviation of the predicted effective stress path could be detected. This was observed to be the case for effective stress paths for 7% cemented Savar clays i.e. for clays with low degree of cementation, at all values of OCR. For significantly higher values of the cementation breakdown parameter  $\rho_c$ , the predicted effective stress path was observably lower than those predicted for low or zero value of  $\rho_c$ . For 14% cemented Savar clay and for OCR values of 1, 2, 20 and 30 respectively, trends in the effective

stress path were similar to those for 7% cemented Savar clay for low, medium and high values of the cementation breakdown parameter  $\rho_t$ . For OCR values of 5 and 10 and for 14% cemented Savar clay, no change in the effective stress path was predicted by the EMMCC model irrespective of the value of the cementation breakdown parameter  $\rho_t$ .

#### 8.4.4 Pore Pressure Response

Figures 8.61 through 8.72 show the predicted excess pore pressure response for cemented Savar clays with different values of cementation break down parameter  $\rho_t$  and for various values of OCR.

For OCR value of 1, and for 7% cemented Savar clay and for OCR values of 1 and 2 and 14% cemented Savar clay, excess positive pore pressures are predicted. The predicted excess positive pore pressures were observed to be higher for lower values of the cementation break down parameter  $\rho_t$ .

For OCR values of 2, 5, 10, 20 and 30 and for 7% cemented Savar clay, the predicted excess pore pressures were observed to be negative in all cases. For higher values of the breakdown parameter  $\rho_t$ , higher excess negative pore pressures are predicted. The predicted excess negative pore pressures were observed to increase with increasing values of OCR. For OCR values of 5 and for 14% cemented Savar clay, the predicted excess pore pressures were positive. There was no observable effect of the value of the cementation breakdown parameter  $\rho_t$  on the predicted values of excess positive pore pressure response in this case. For OCR values of 10, 20, and 30 and for 14% cemented Savar clay, negative excess pore pressures were predicted in all cases. Higher values of the cementation breakdown parameter  $\rho_t$ , predicted a higher excess negative pore pressure response in each case.

## 8.5 Summary and Conclusion

An extended form of the MMCC model termed as the EMMCC model was used to predict the stress-strain, volume change and excess pore pressure response and effective stress path for cemented Savar clays. It was observed that cementation breakdown has a well defined effect on the predicted stress-strain behavior of cemented Savar clays, as would be normally expected. The effect of the rate of cementation breakdown on the predicted stress-strain response of cemented Savar clays was also studied. It could be concluded from this study that only high rates of cementation breakdown predict a significant effect the stress-strain response of cemented Savar clays. Moderate or low rates of cementation breakdown show little or insignificant effect on the stress-strain response of cemented Savar clays. The effect of cementation breakdown on the stress-strain response of cemented Savar clays was observed to be more pronounced for strongly cemented clays, with higher rates of cementation breakdown. The effect of cementation breakdown was observed to be different for different values of OCR. In general, the EMMCC model incorporating cementation breakdown effect gives a qualitative view of the possible effect of the rate of cementation breakdown and the degree of cementation on the stress-strain response of cemented clays in general and cemented Savar clays in particular.

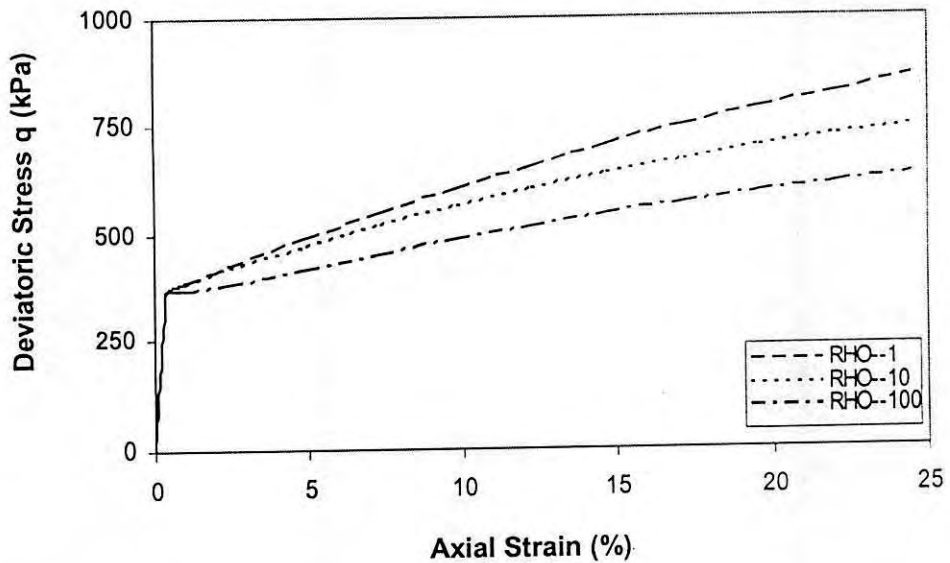


Figure 8.1 EMMCC model prediction of drained triaxial stress-strain response of 7% cemented Savar clay (OCR=1)

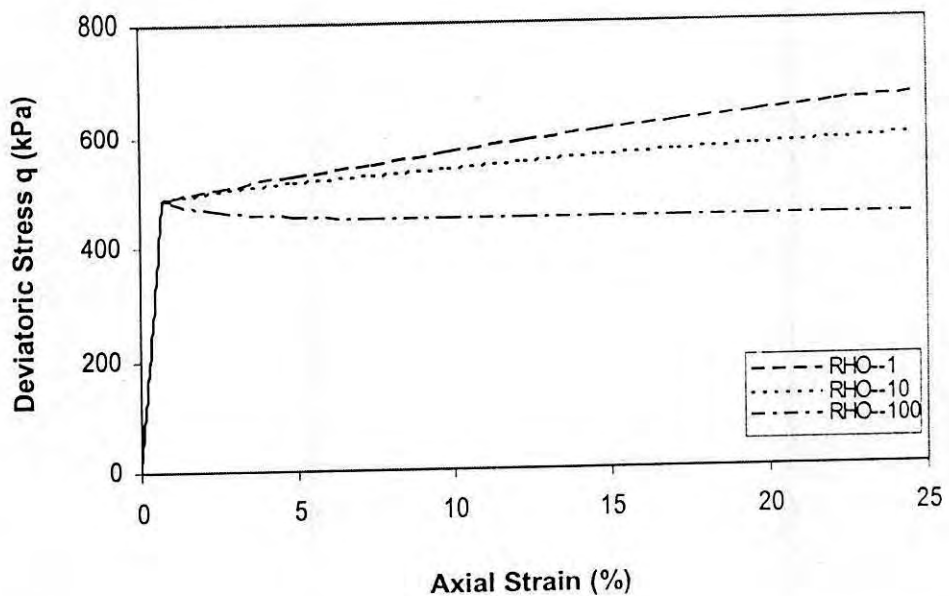


Figure 8.2 EMMCC model prediction of drained triaxial stress-strain response of 7% cemented Savar clay (OCR=2)

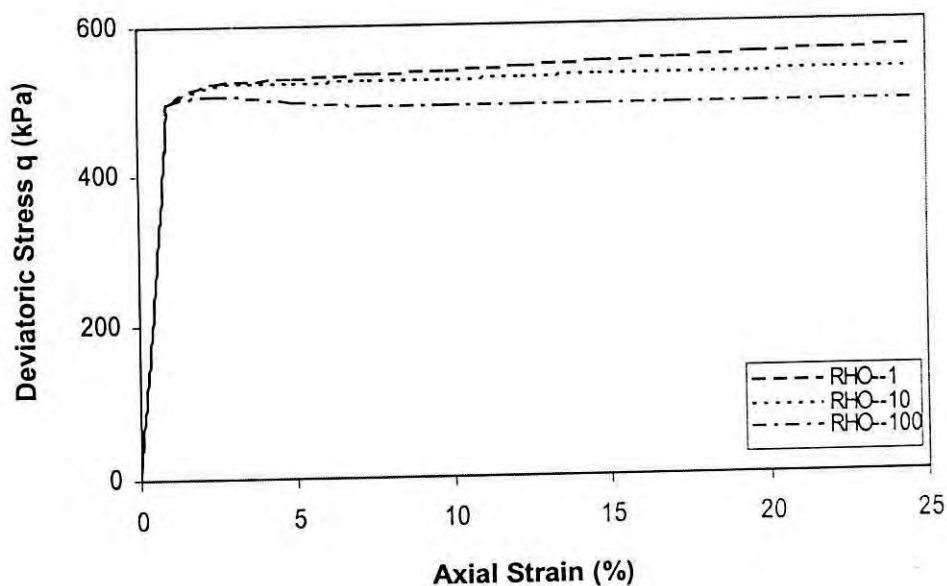


Figure 8.3 EMMCC model prediction of drained triaxial stress-strain response of 7% cemented Savar clay (OCR=5)

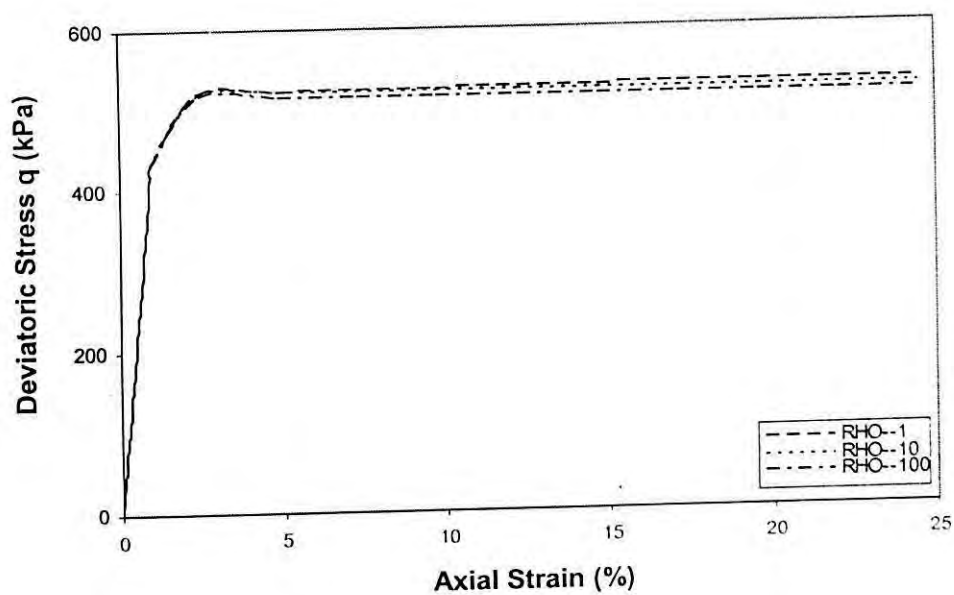


Figure 8.4 EMMCC model prediction of drained triaxial stress-strain response of 7% cemented Savar clay (OCR=10)



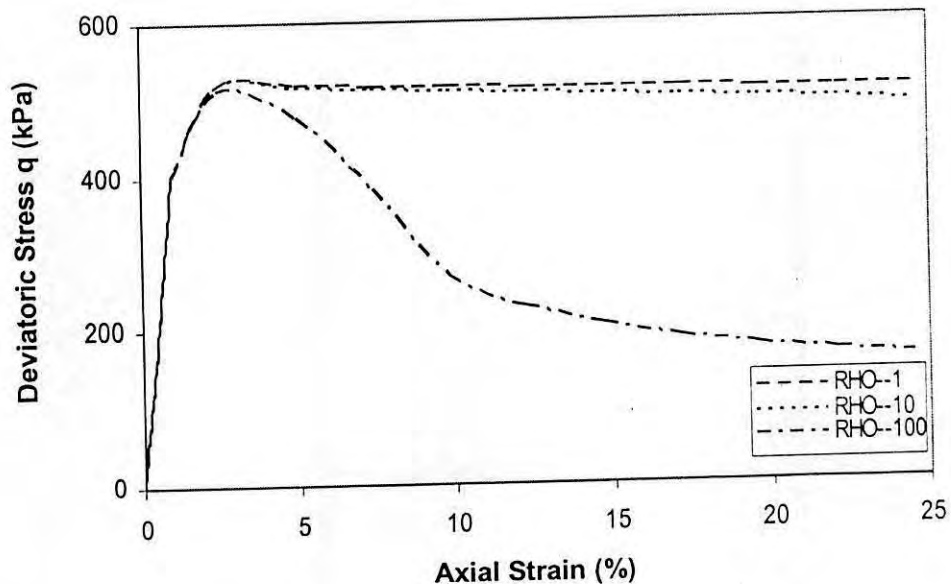


Figure 8.5 EMMCC model prediction of drained triaxial stress-strain response of 7% cemented Savar clay (OCR=20)

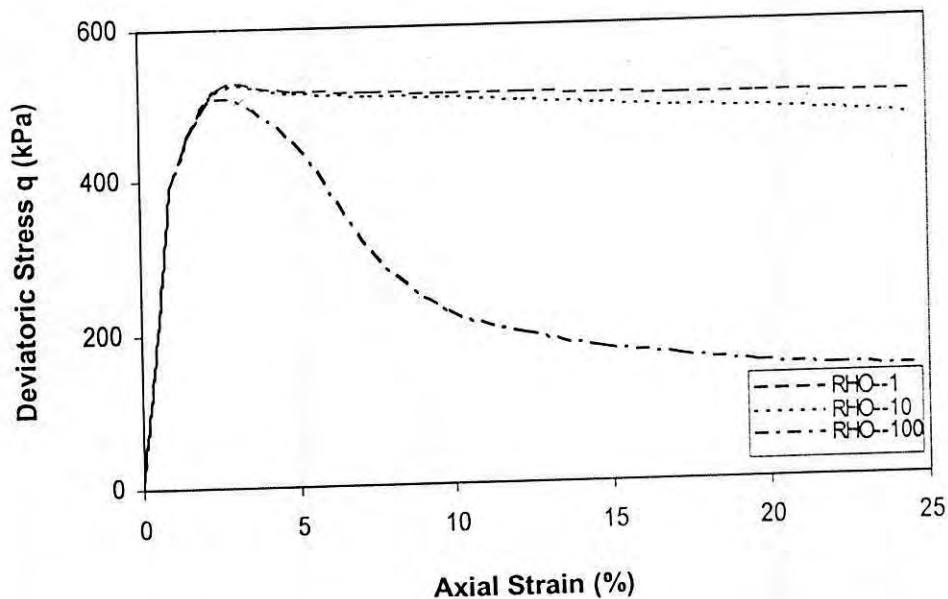


Figure 8.6 EMMCC model prediction of drained triaxial stress-strain response of 7% cemented Savar clay (OCR=30)

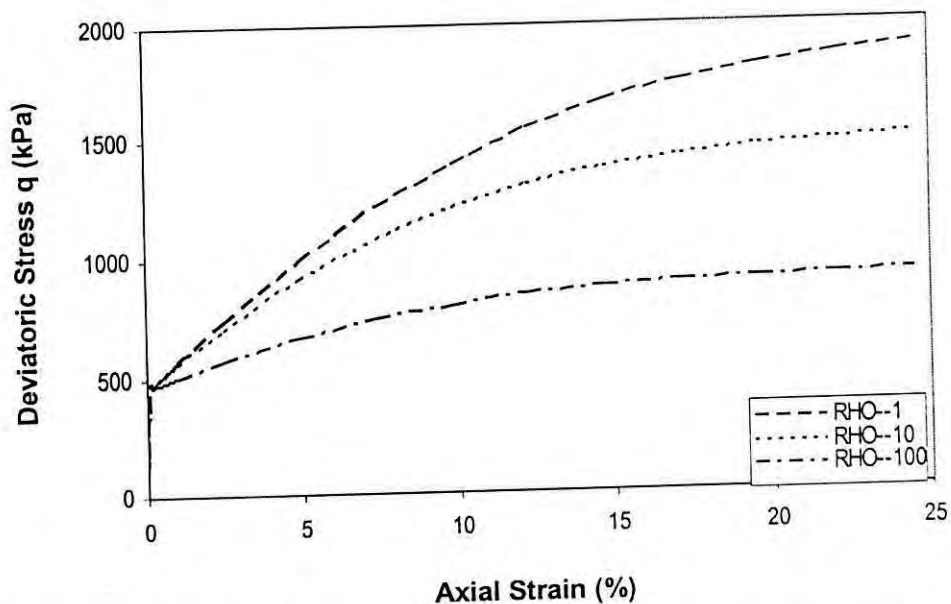


Figure 8.7 EMMCC model prediction of drained volume-strain response of 14% cemented Savar clay (OCR=1)

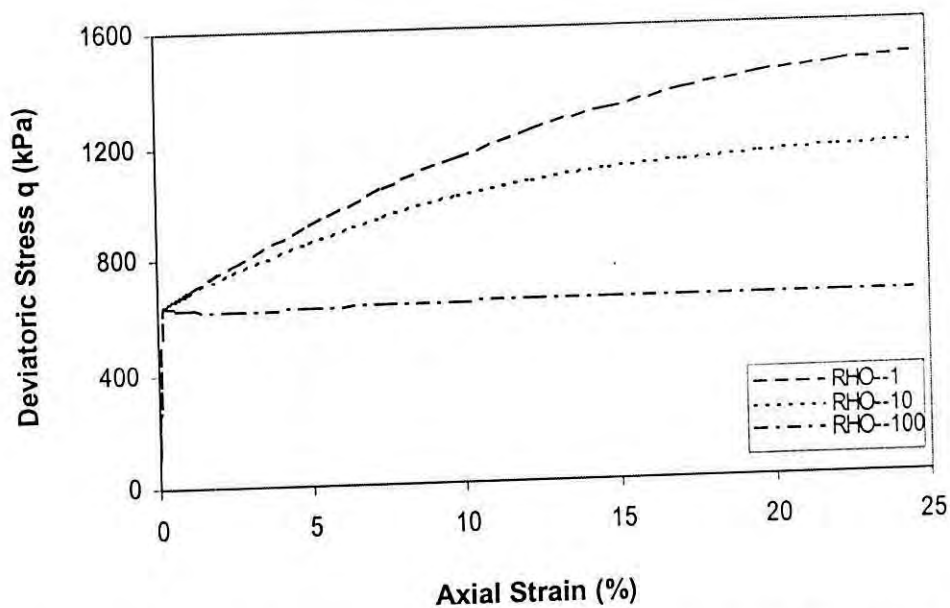


Figure 8.8 EMMCC model prediction of drained triaxial stress-strain response of 14% cemented Savar clay (OCR=2)

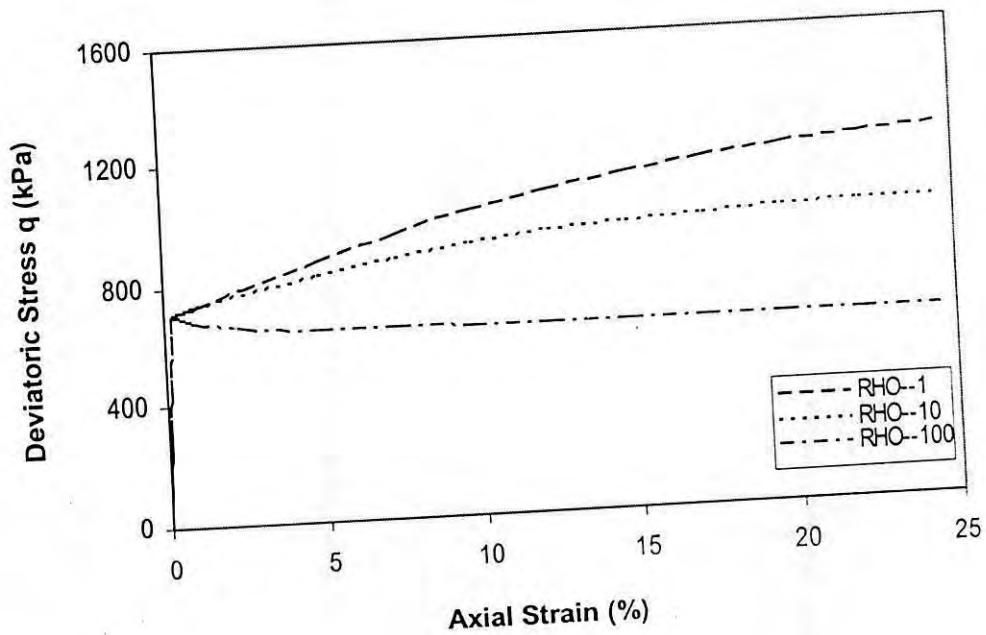


Figure 8.9 EMMCC model prediction of drained triaxial stress-strain response of 14% cemented Savar clay (OCR=5)

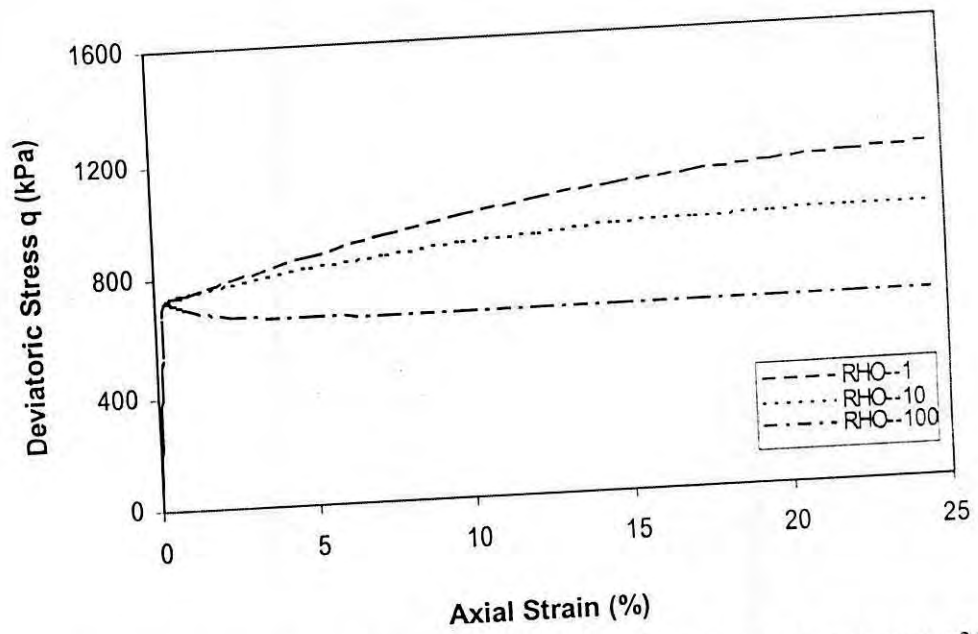


Figure 8.10 EMMCC model prediction of drained triaxial stress-strain response of 14% cemented Savar clay (OCR=10)

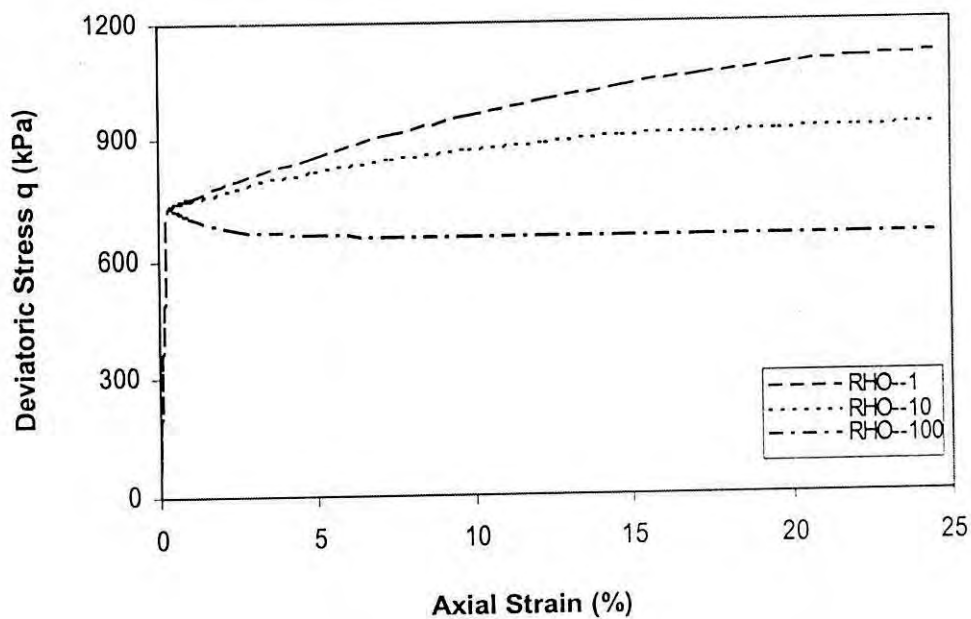


Figure 8.11 EMMCC model prediction of drained triaxial stress-strain response of 14% cemented Savar clay (OCR=20)

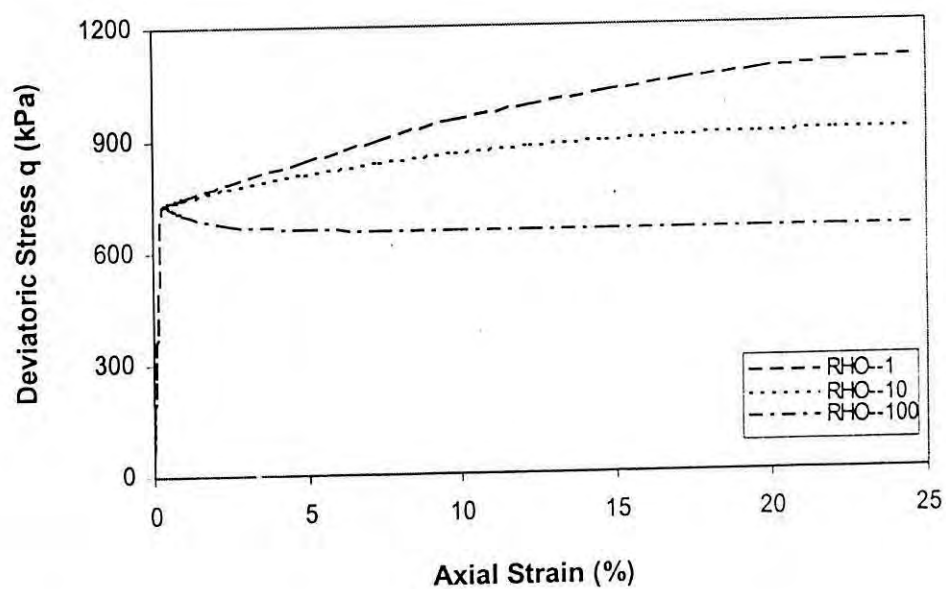


Figure 8.12 EMMCC model prediction of drained triaxial stress-strain response of 14% cemented Savar clay (OCR=30)

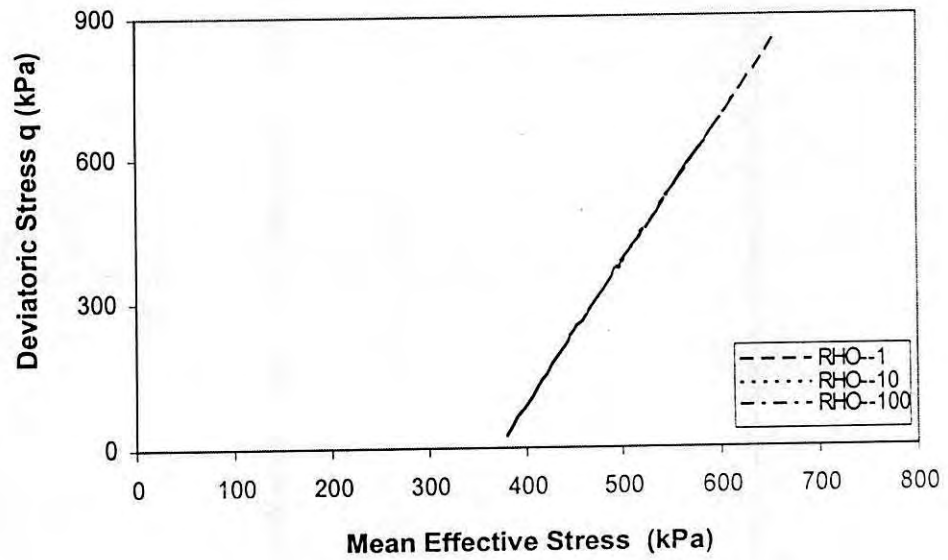


Figure 8.13 EMMCC model prediction of drained triaxial stress path of 7% cemented Savar clay (OCR=1)

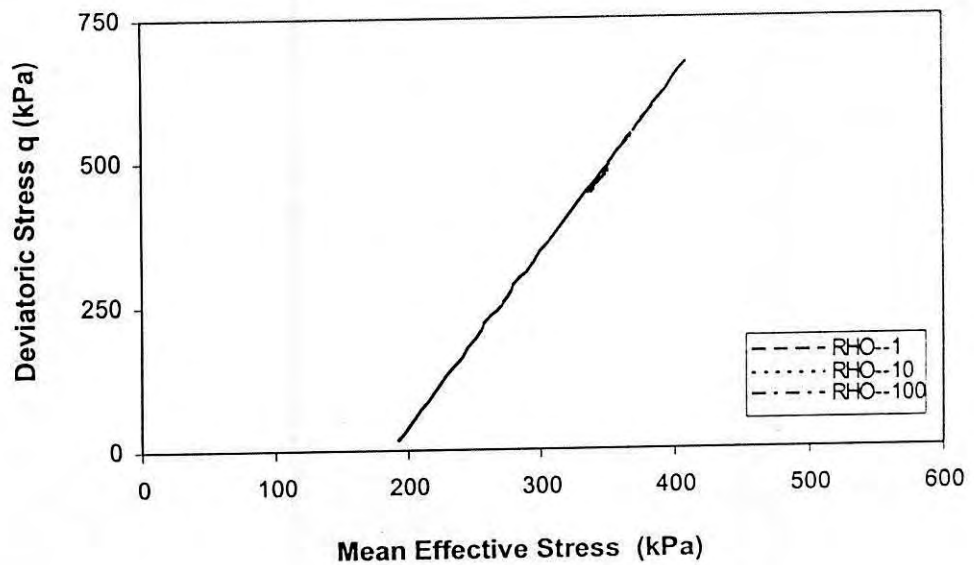


Figure 8.14 EMMCC model prediction of drained triaxial stress path of 7% cemented Savar clay (OCR=2)

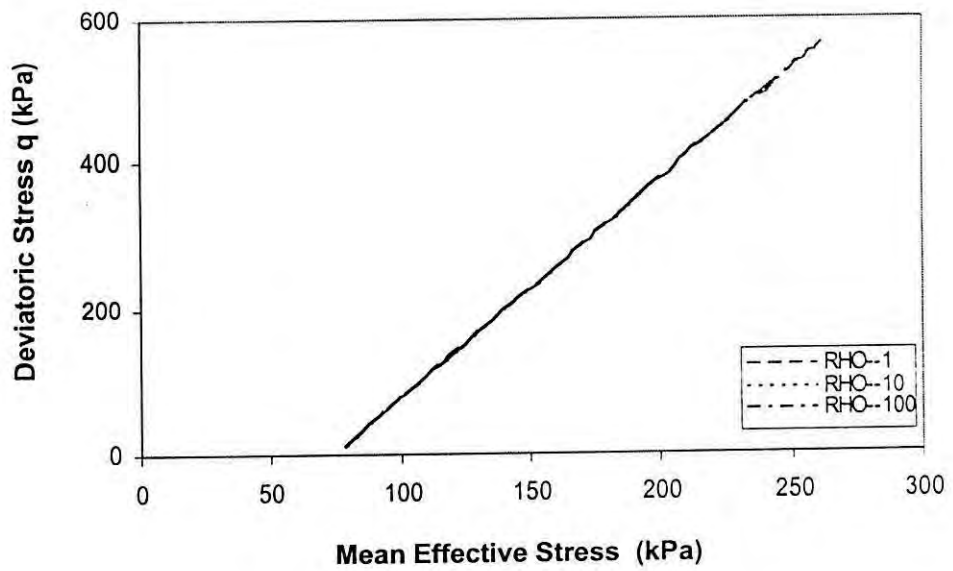


Figure 8.15 EMMCC model prediction of drained triaxial stress path of 7% cemented Savar clay (OCR=5)

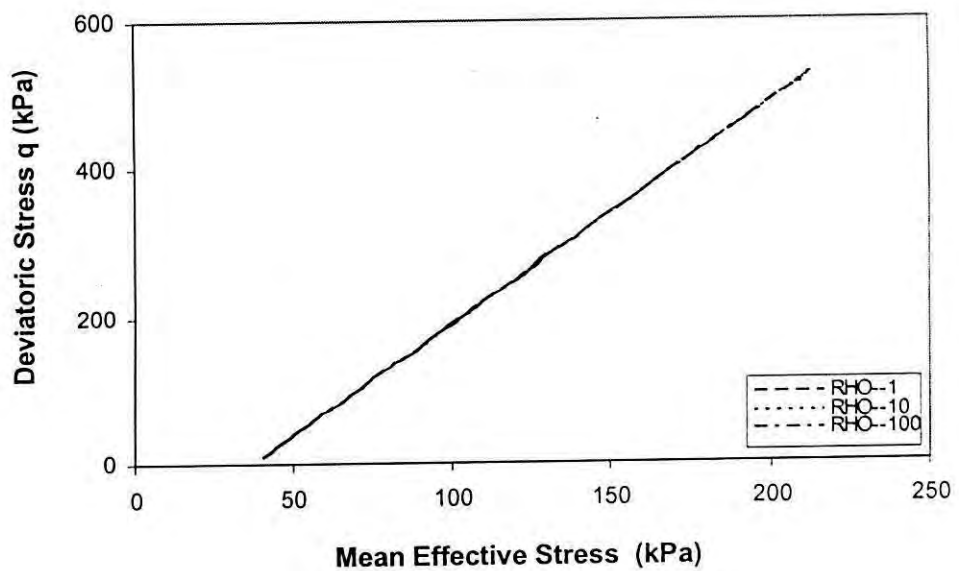


Figure 8.16 EMMCC model prediction of drained triaxial stress path of 7% cemented Savar clay (OCR=10)

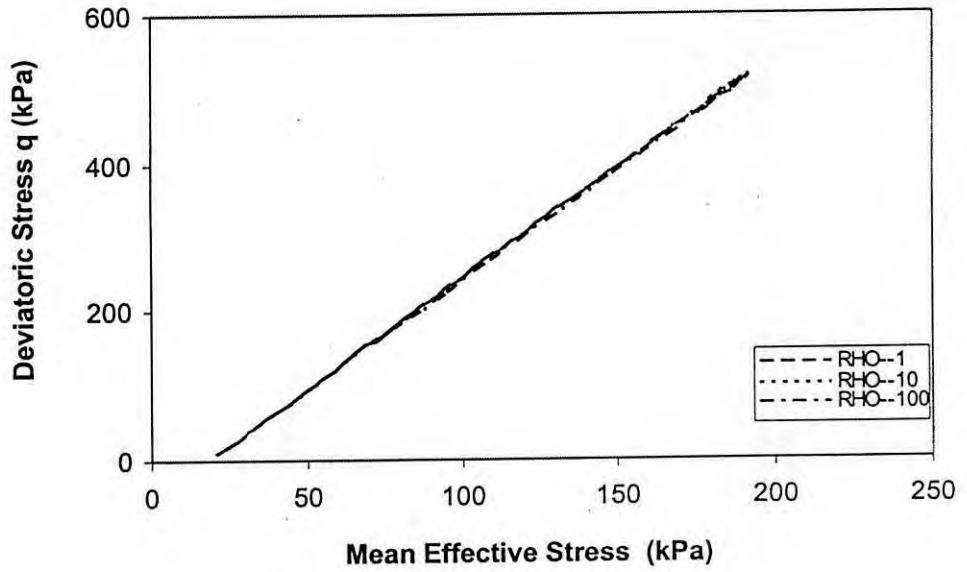


Figure 8.17 EMMCC model prediction of drained triaxial stress path of 7% cemented Savar clay (OCR=20)

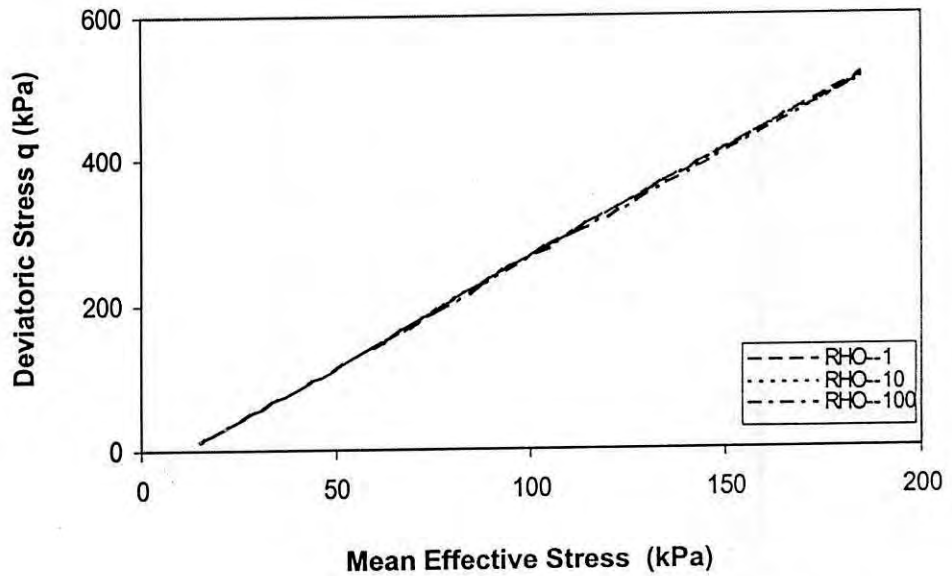


Figure 8.18 EMMCC model prediction of drained triaxial stress path of 7% cemented Savar clay (OCR=30)

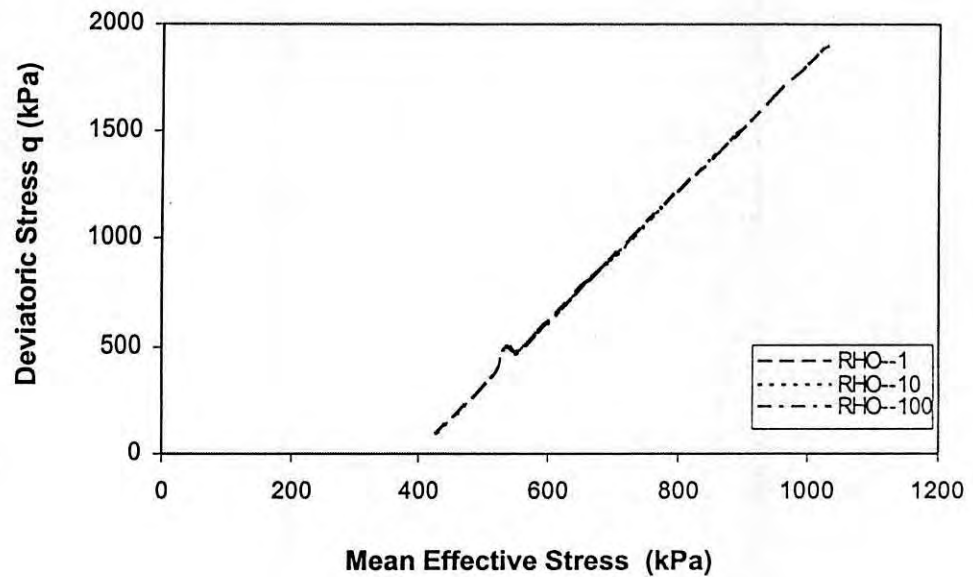


Figure 8.19 EMMCC model prediction of drained triaxial stress path of 14% cemented Savar clay (OCR=1)

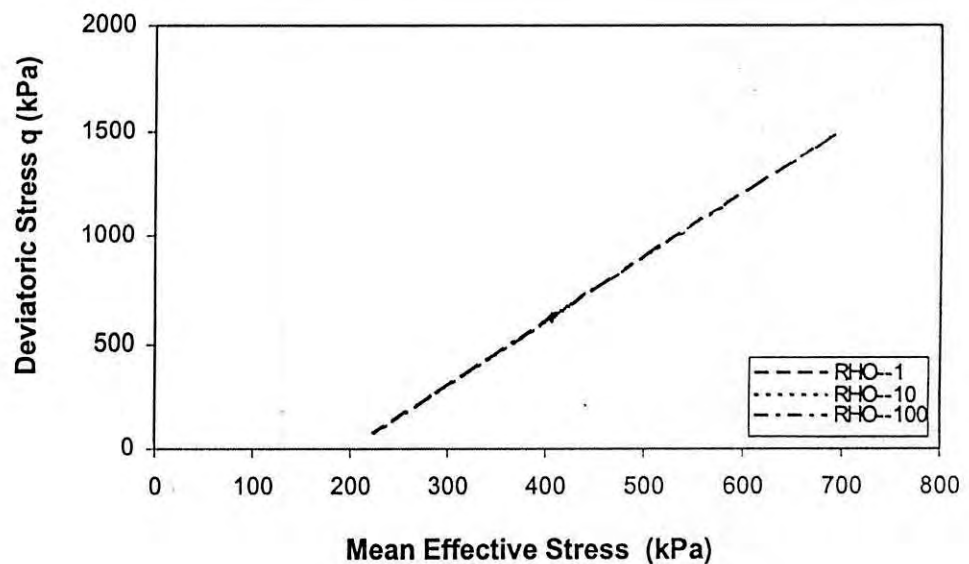


Figure 8.20 EMMCC model prediction of drained triaxial stress path of 14% cemented Savar clay (OCR=2)



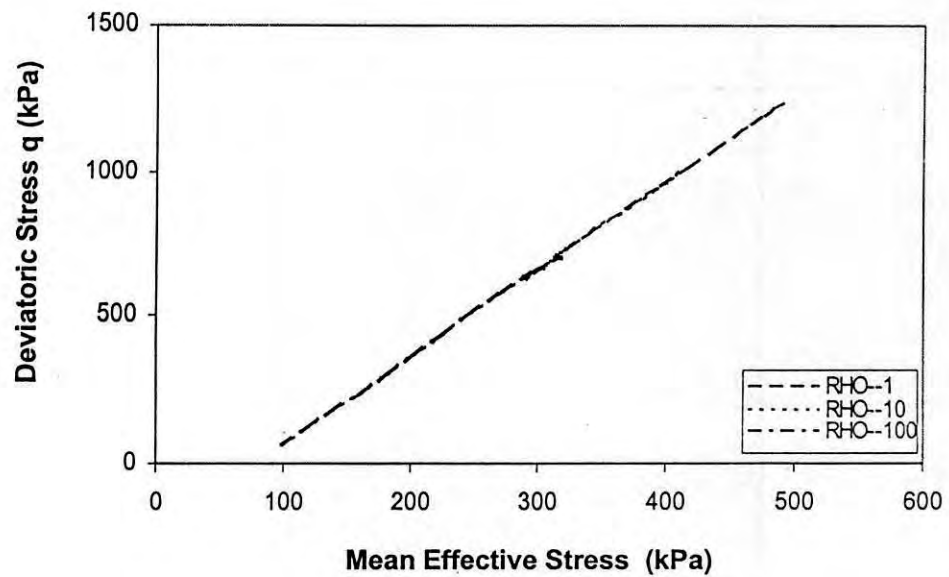


Figure 8.21 EMMCC model prediction of drained triaxial stress path of 14% cemented Savar clay (OCR=5)

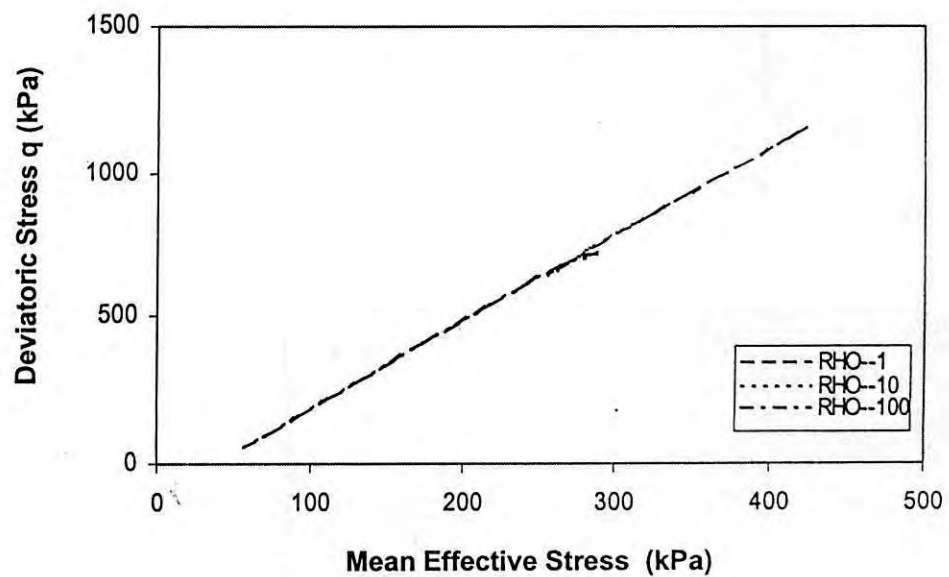


Figure 8.22 EMMCC model prediction of drained triaxial stress path of 14% cemented Savar clay (OCR=10)

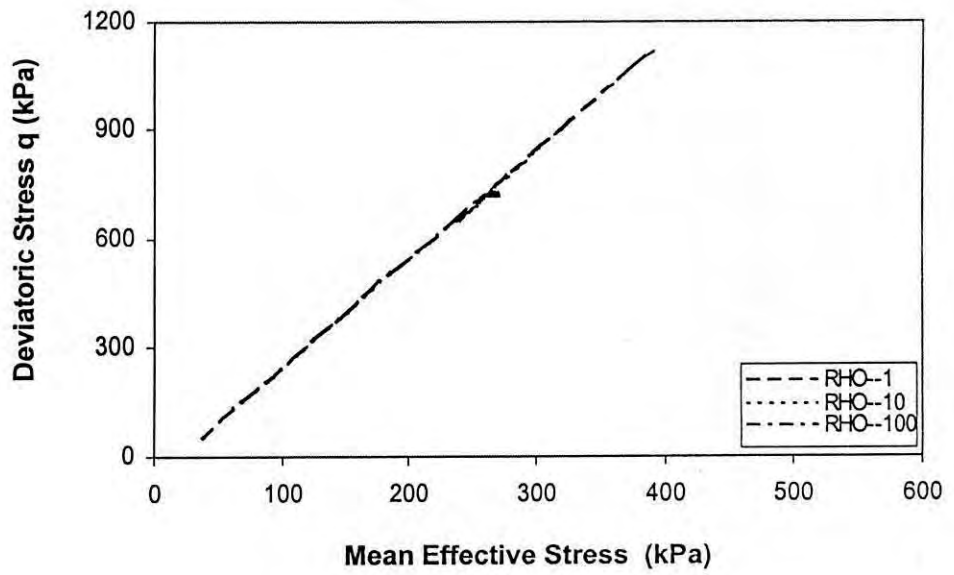


Figure 8.23 EMMCC model prediction of drained triaxial stress path of 14% cemented Savar clay (OCR=20)

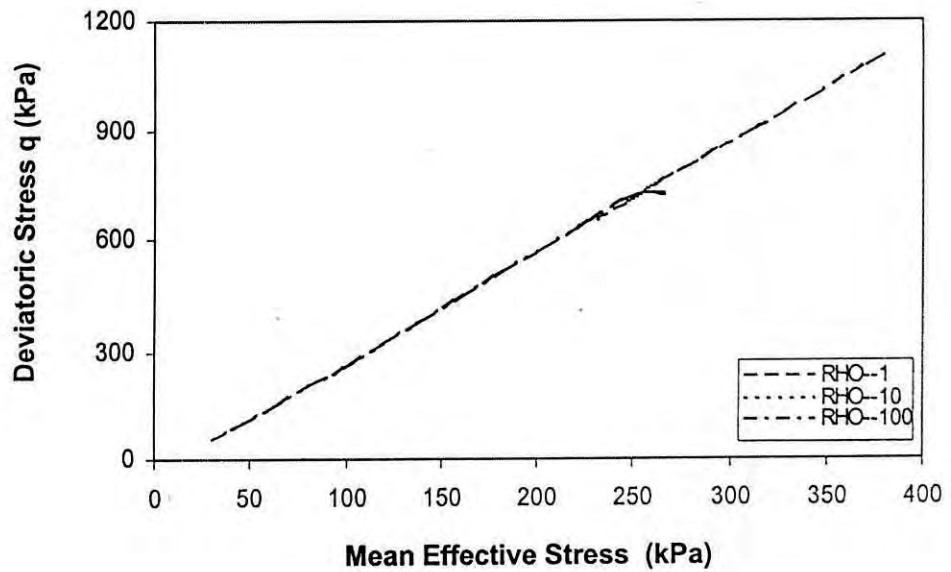


Figure 8.24 EMMCC model prediction of drained triaxial stress path of 14% cemented Savar clay (OCR=30)

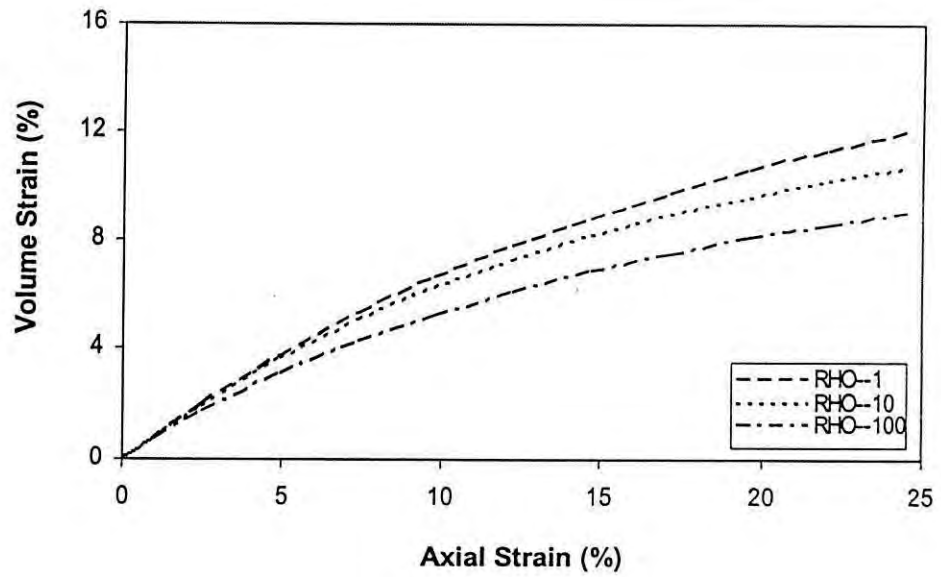


Figure 8.25 EMMCC model prediction of drained volume-strain response of 7% cemented Savar clay (OCR=1)

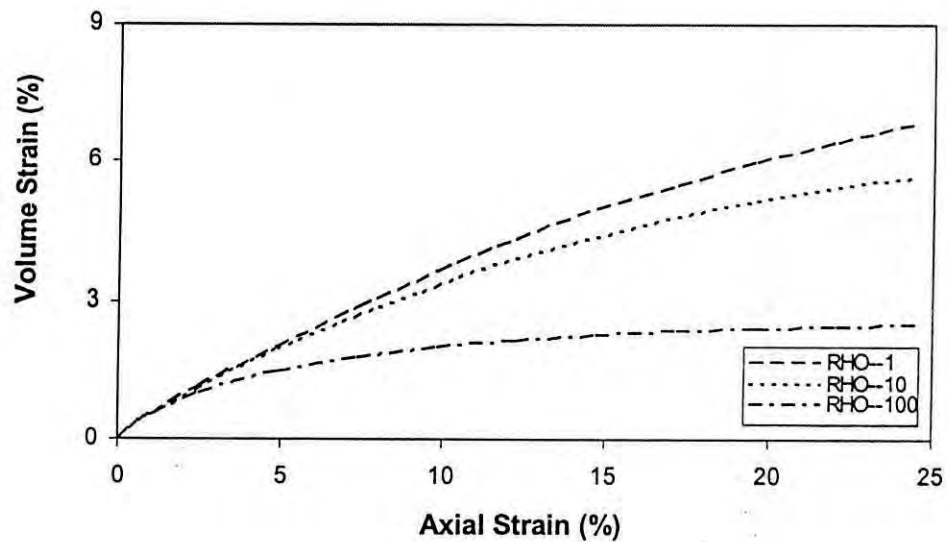


Figure 8.26 EMMCC model prediction of drained volume-strain response of 7% cemented Savar clay (OCR=2)

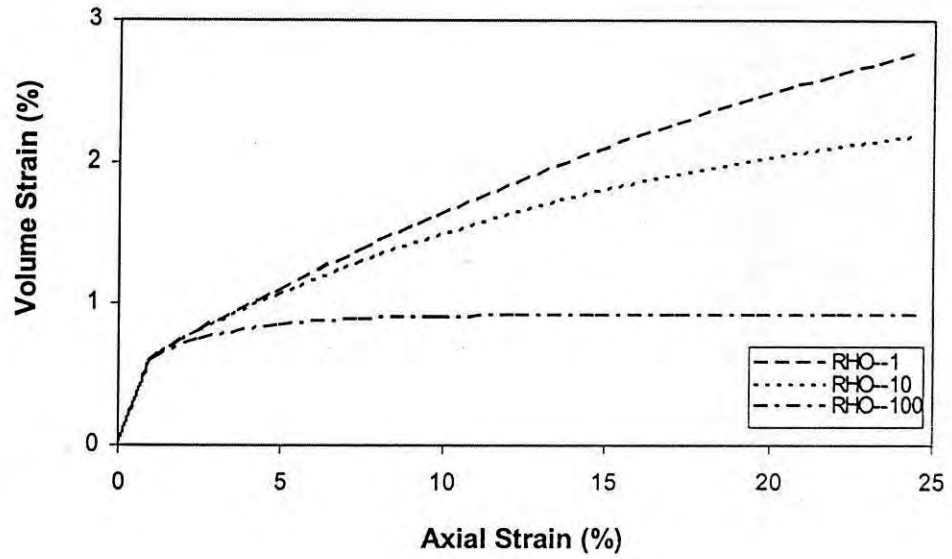


Figure 8.27 EMMCC model prediction of drained volume-strain response of 7% cemented Savar clay (OCR=5)

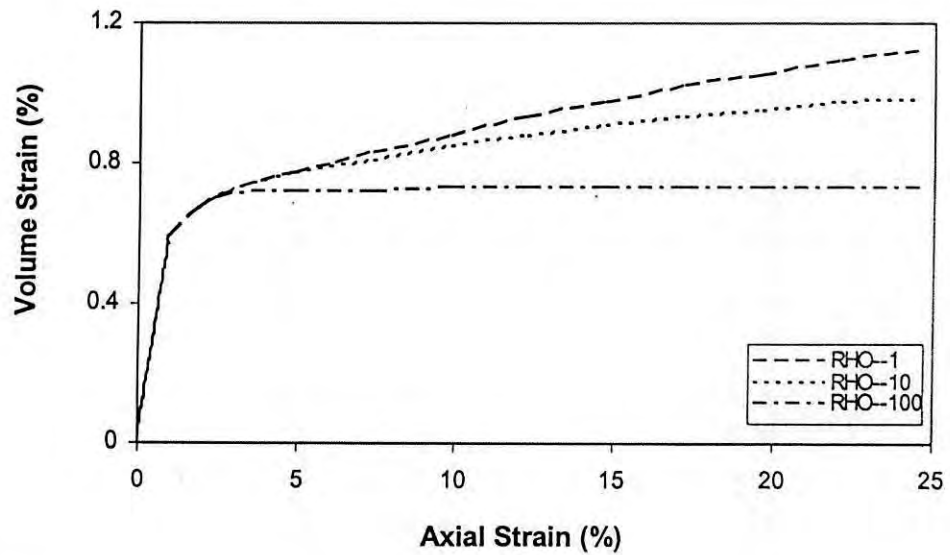


Figure 8.28 EMMCC model prediction of drained volume-strain response of 7% cemented Savar clay (OCR=10)

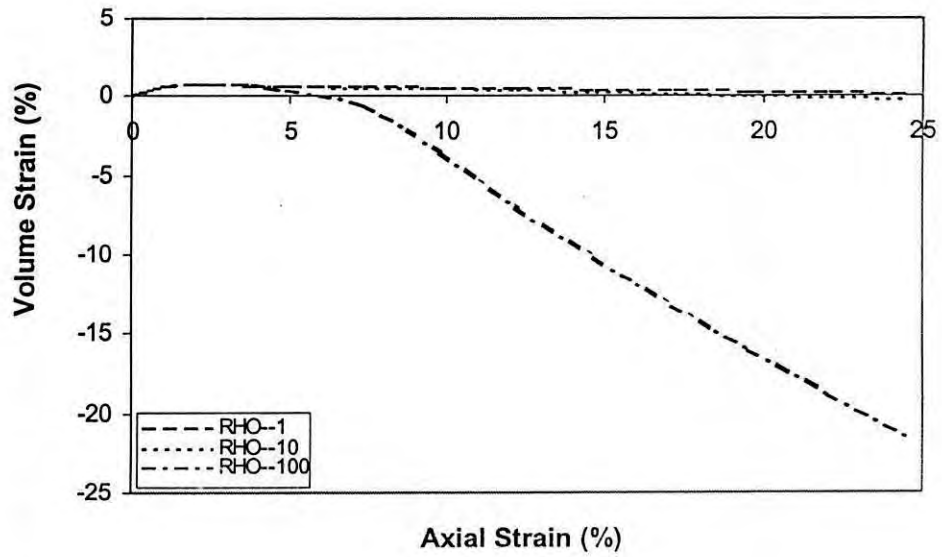


Figure 8.29 EMMCC model prediction of drained volume-strain response of 7% cemented Savar clay (OCR=20)

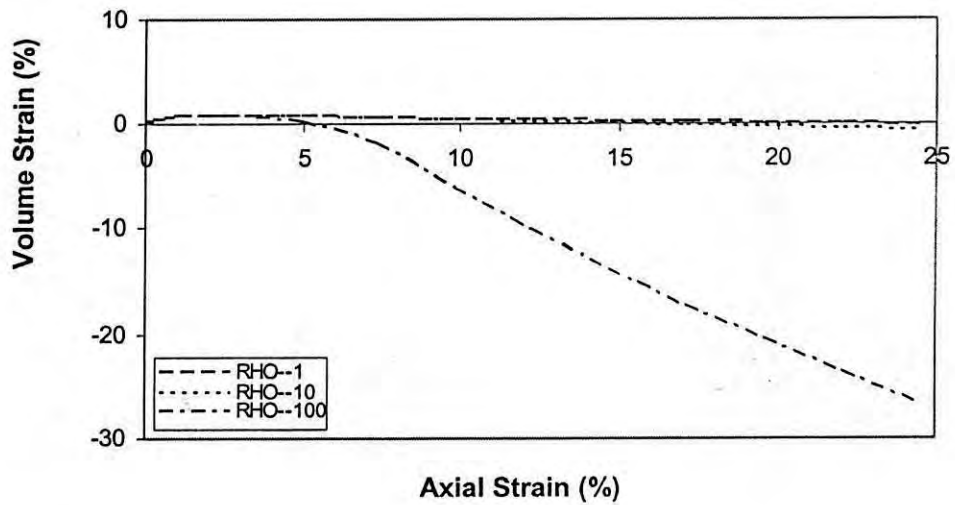


Figure 8.30 EMMCC model prediction of drained volume-strain response of 7% cemented Savar clay (OCR=30)

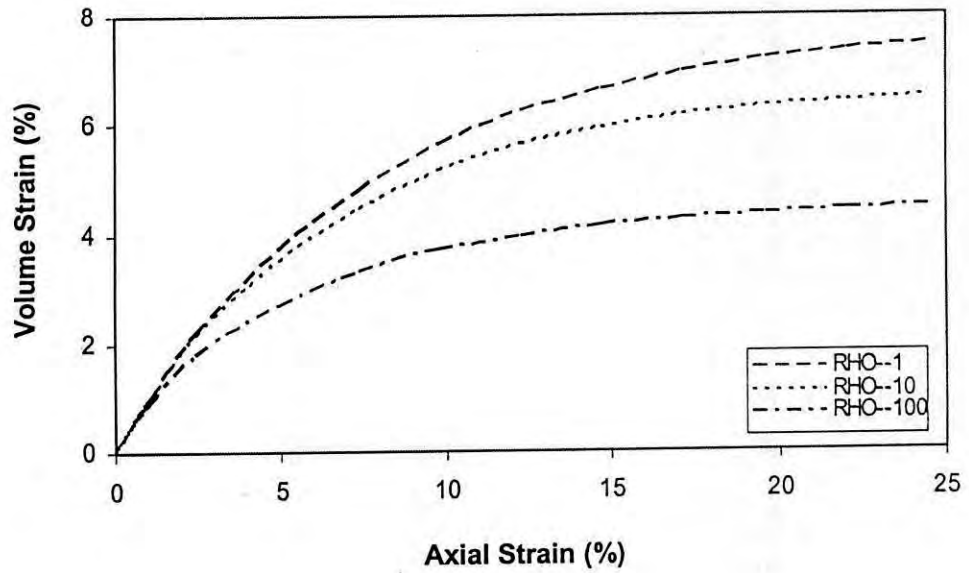


Figure 8.31 EMMCC model prediction of drained volume-strain response of 14% cemented Savar clay (OCR=1)

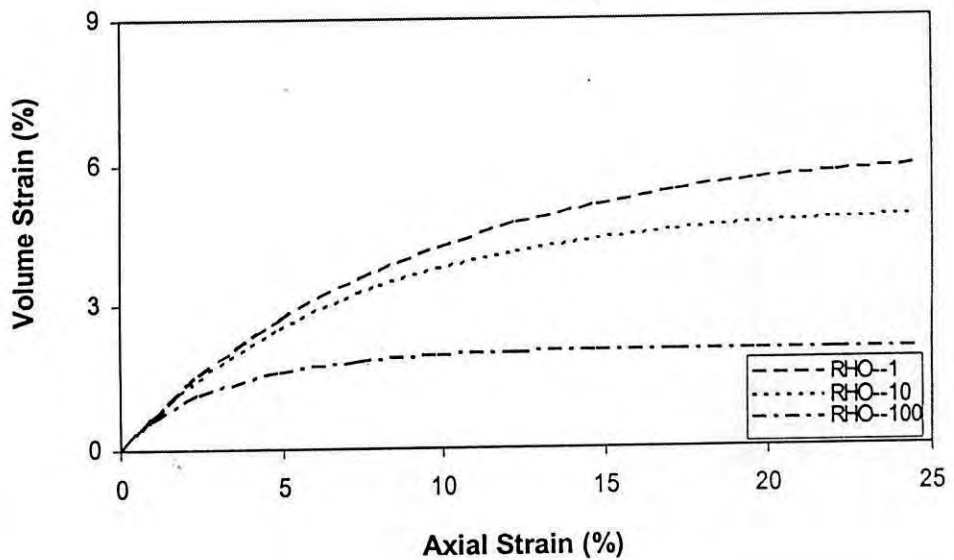


Figure 8.32 EMMCC model prediction of drained volume-strain response of 14% cemented Savar clay (OCR=2)

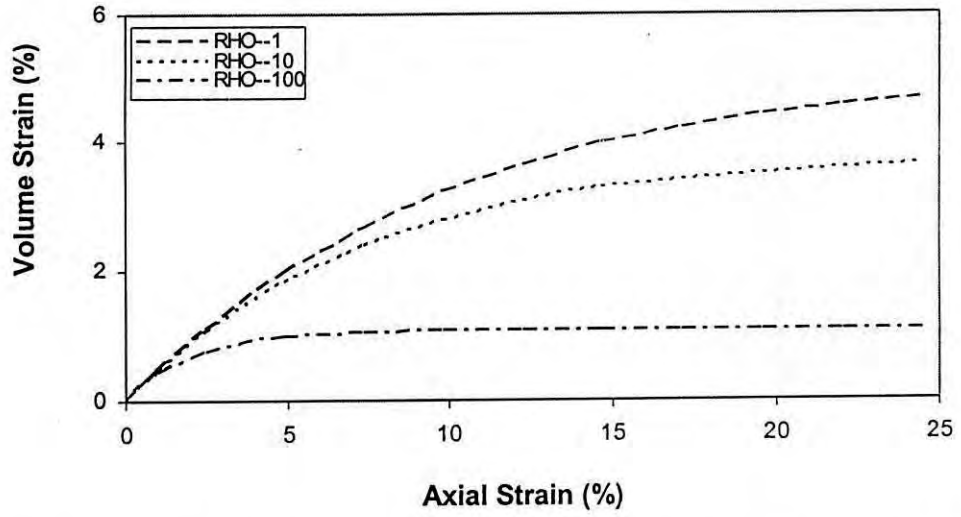


Figure 8.33 EMMCC model prediction of drained volume-strain response of 14% cemented Savar clay (OCR=5)

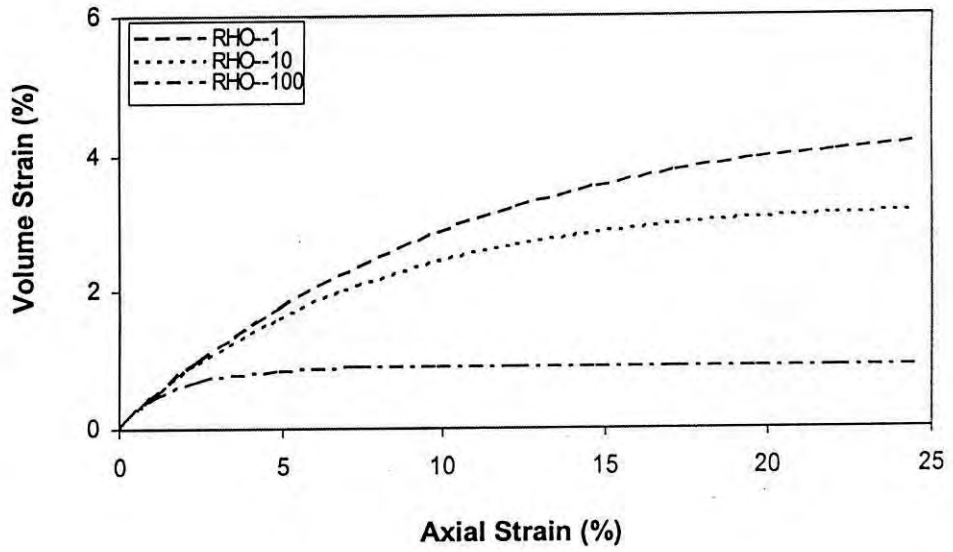


Figure 8.34 EMMCC model prediction of drained volume-strain response of 14% cemented Savar clay (OCR=10)

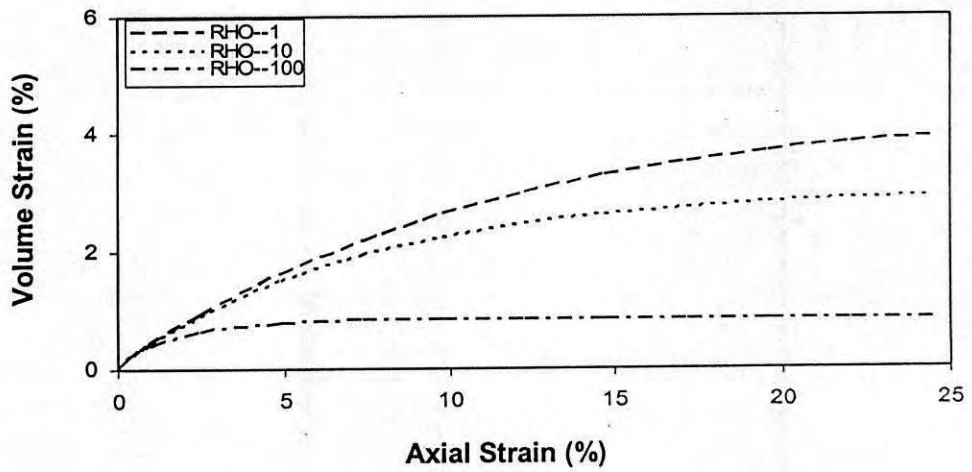


Figure 8.35 EMMCC model prediction of drained volume-strain response of 14% cemented Savar clay (OCR=20)

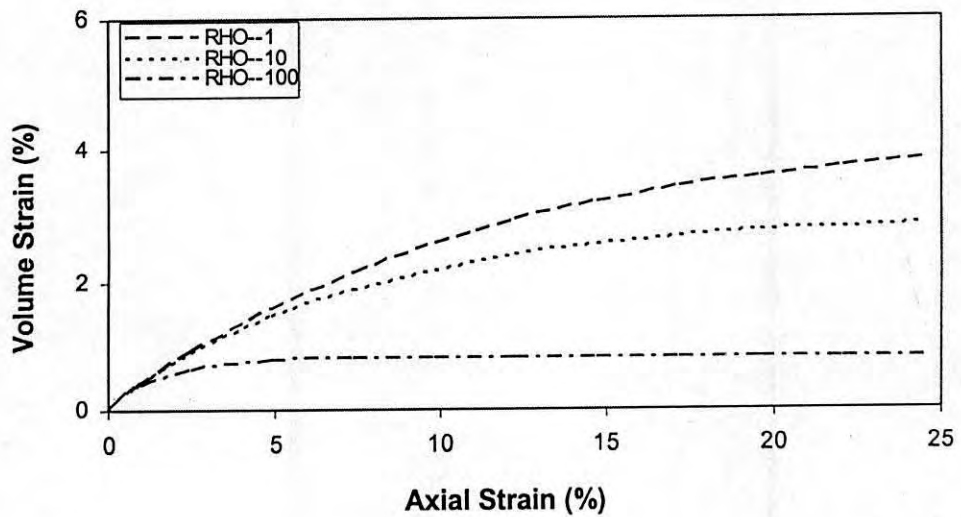


Figure 8.36 EMMCC model prediction of drained volume-strain response of 14% cemented Savar clay (OCR=30)



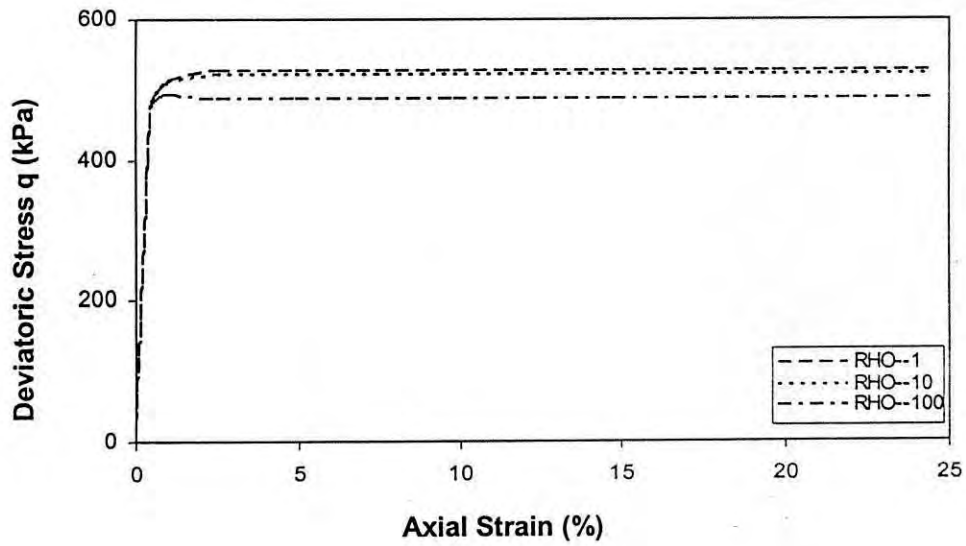


Figure 8.37 EMMCC model prediction of undrained triaxial stress-strain response of 7% cemented Savar clay (OCR=1)

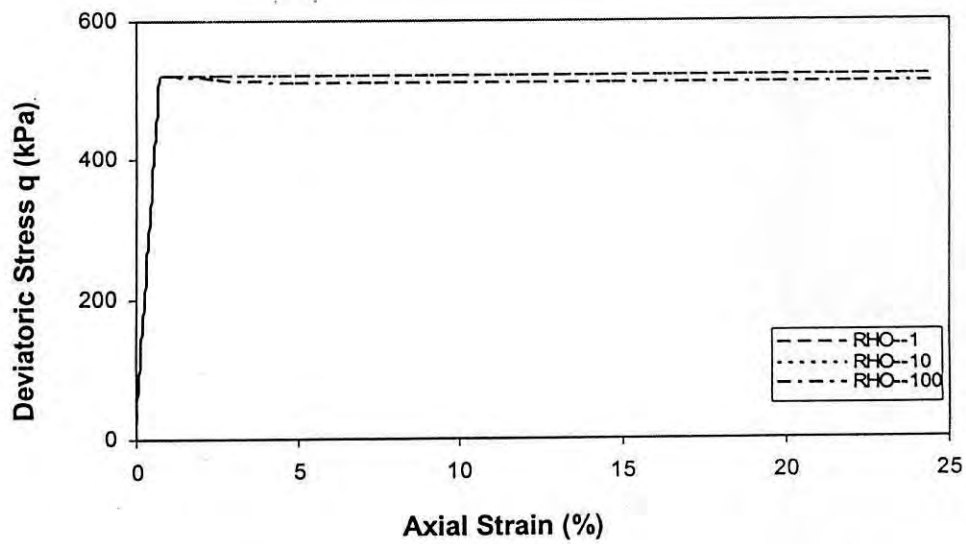


Figure 8.38 EMMCC model prediction of undrained triaxial stress-strain response of 7% cemented Savar clay (OCR=2)

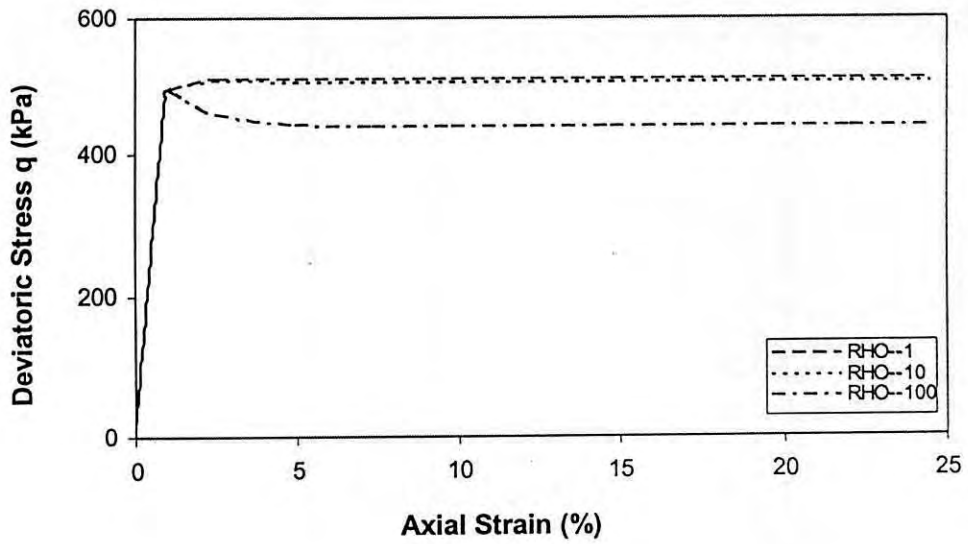


Figure 8.39 EMMCC model prediction of undrained triaxial stress-strain response of 7% cemented Savar clay (OCR=5)

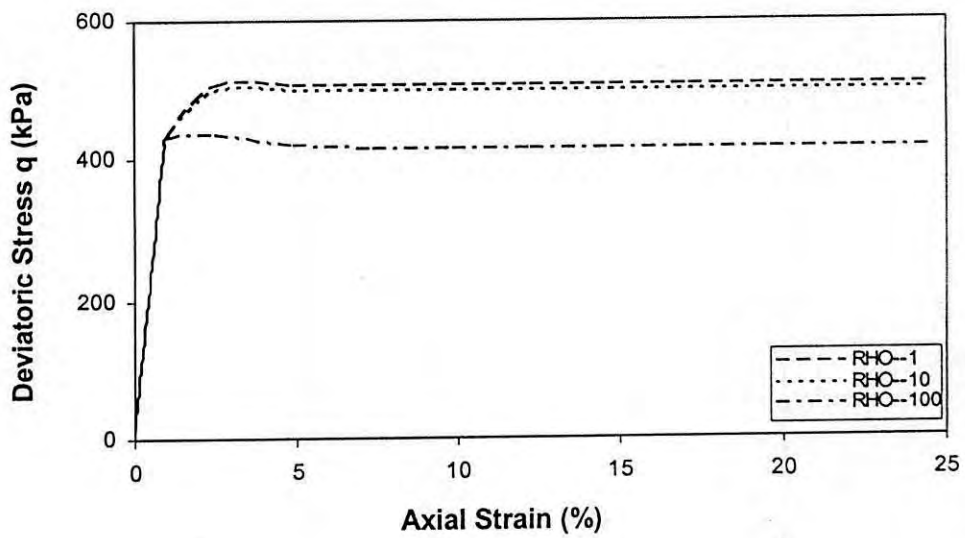


Figure 8.40 EMMCC model prediction of undrained triaxial stress-strain response of 7% cemented Savar clay (OCR=10)

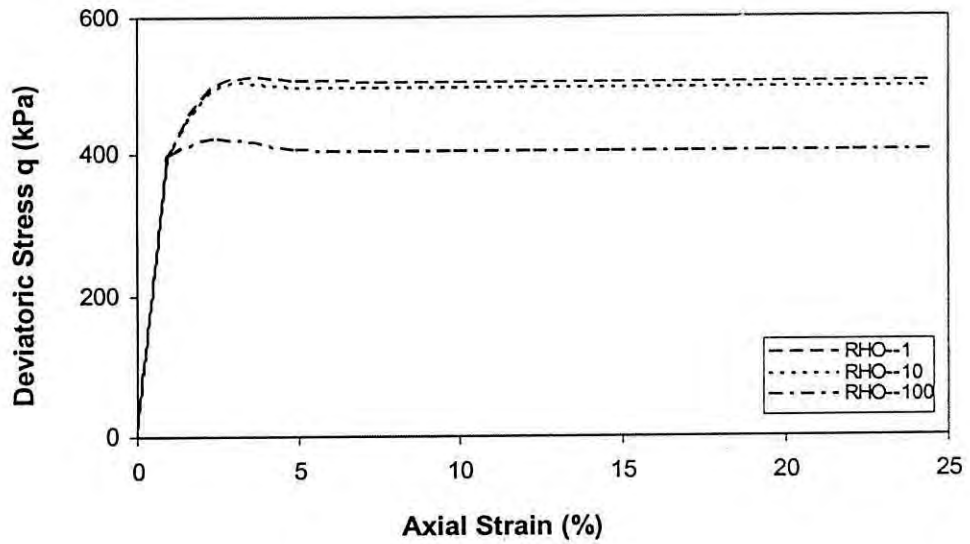


Figure 8.41 EMMCC model prediction of undrained triaxial stress-strain response of 7% cemented Savar clay (OCR=20)

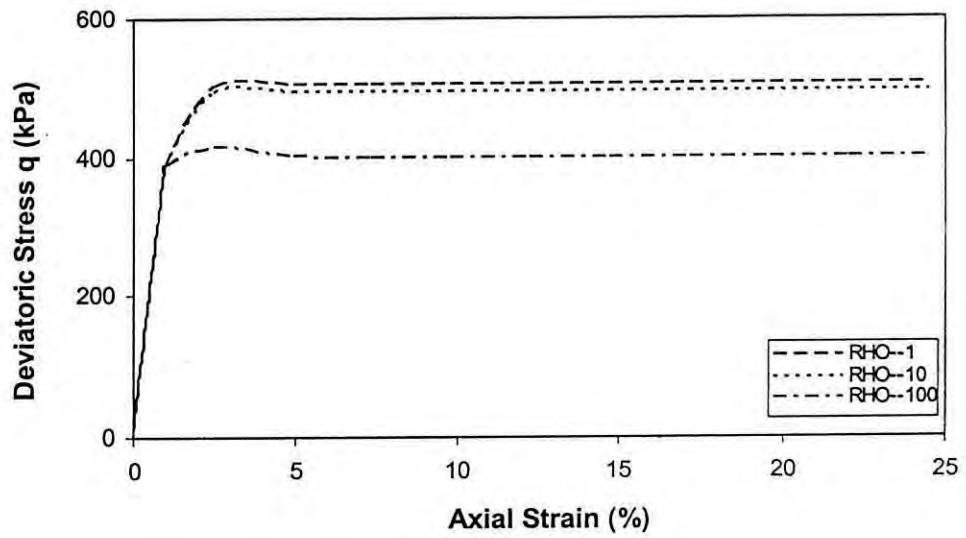


Figure 8.42 EMMCC model prediction of undrained triaxial stress-strain response of 7% cemented Savar clay (OCR=30)

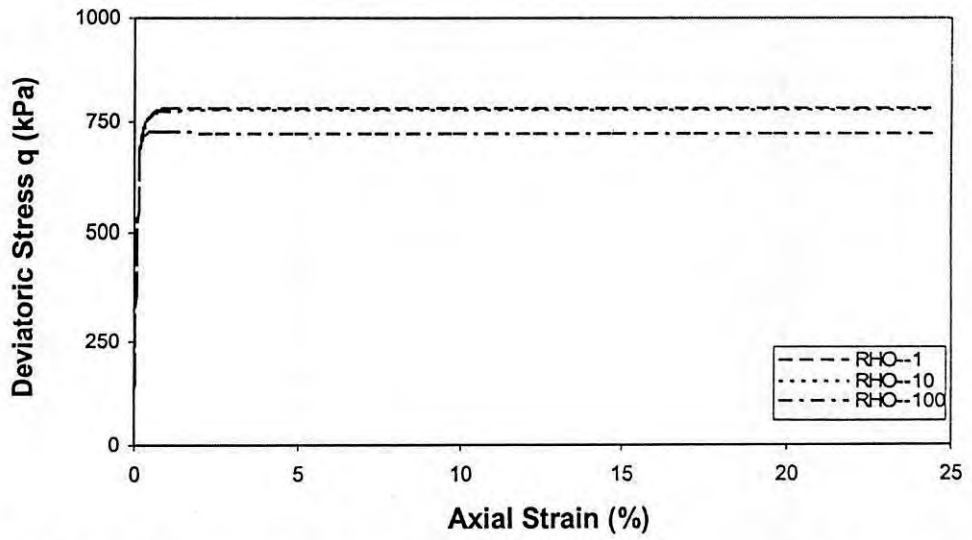


Figure 8.43 EMMCC model prediction of undrained triaxial stress-strain response of 14% cemented Savar clay (OCR=1)

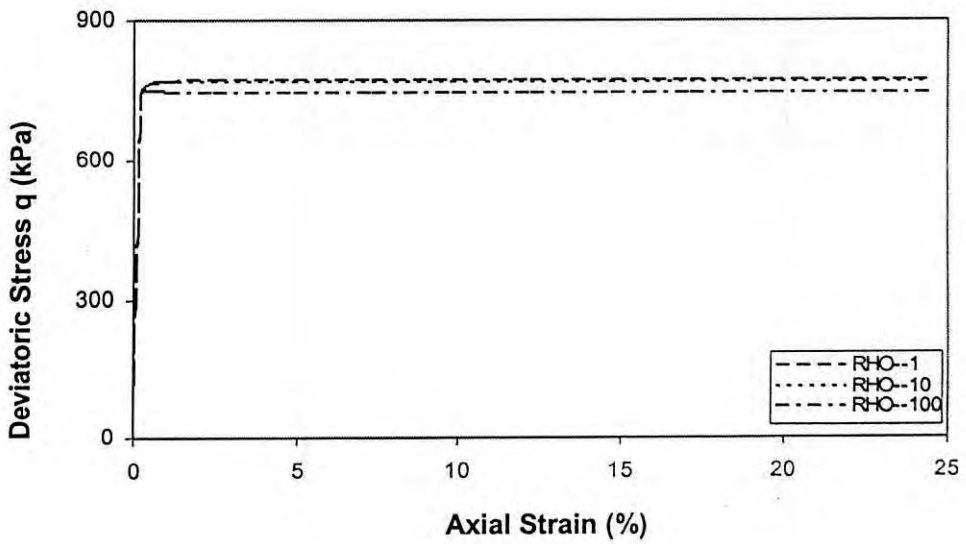


Figure 8.44 EMMCC model prediction of undrained triaxial stress-strain response of 14% cemented Savar clay (OCR=2)

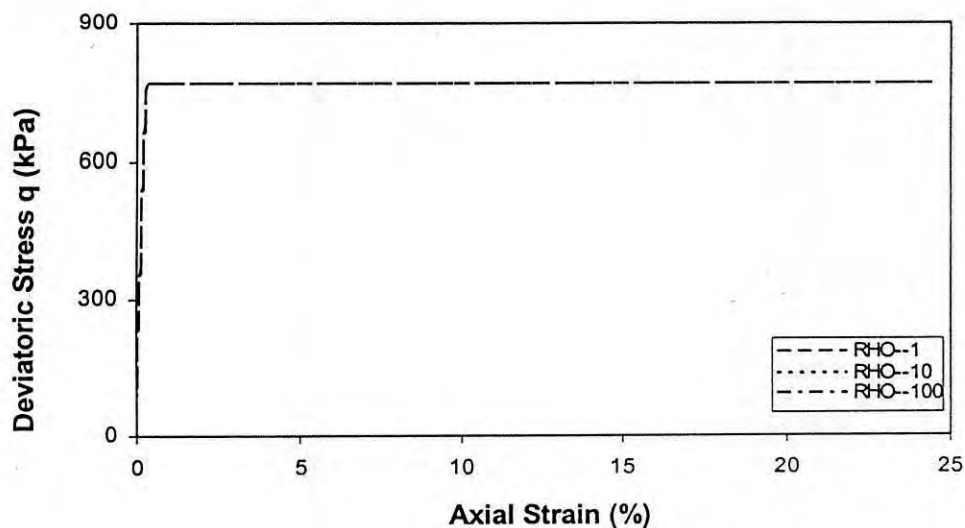


Figure 8.45 EMMCC model prediction of undrained triaxial stress-strain response of 14% cemented Savar clay (OCR=5)

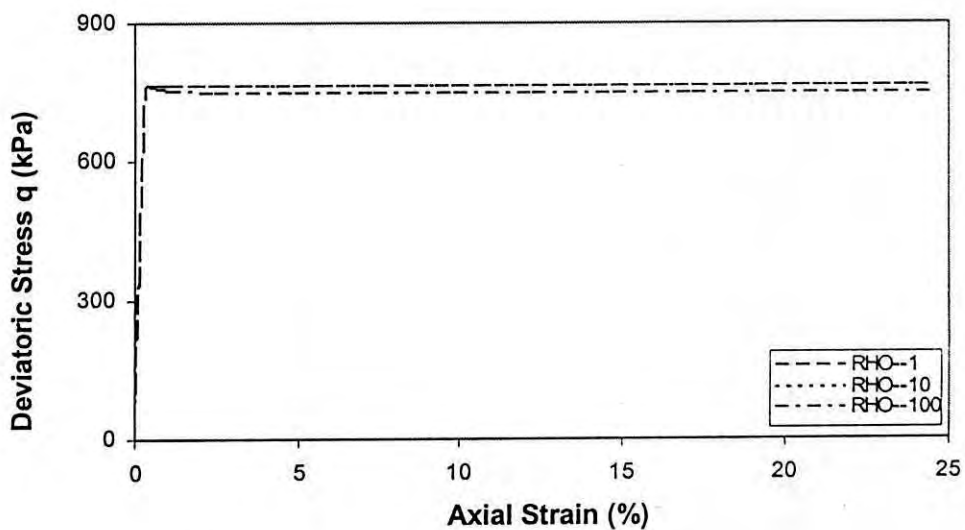


Figure 8.46 EMMCC model prediction of undrained triaxial stress-strain response of 14% cemented Savar clay (OCR=10)

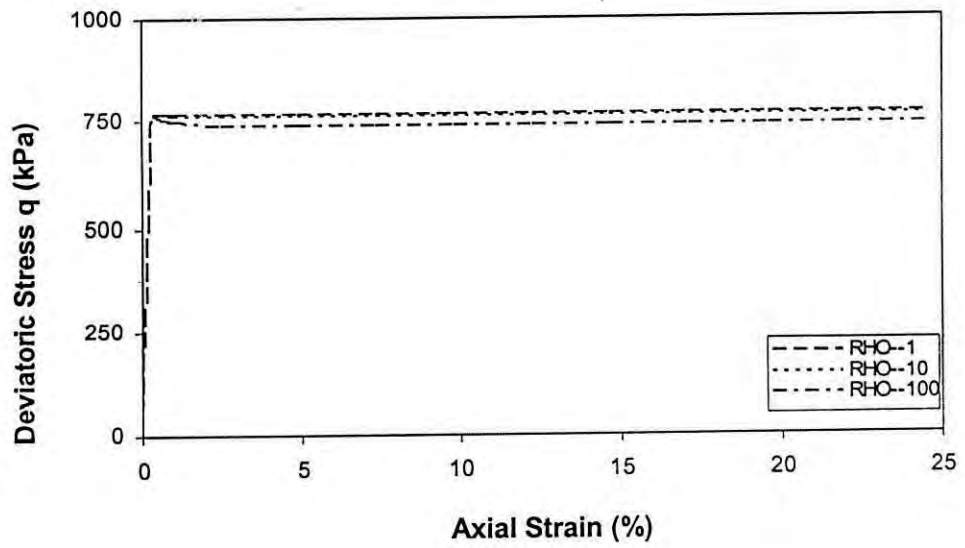


Figure 8.47 EMMCC model prediction of undrained triaxial stress-strain response of 14% cemented Savar clay (OCR=20)

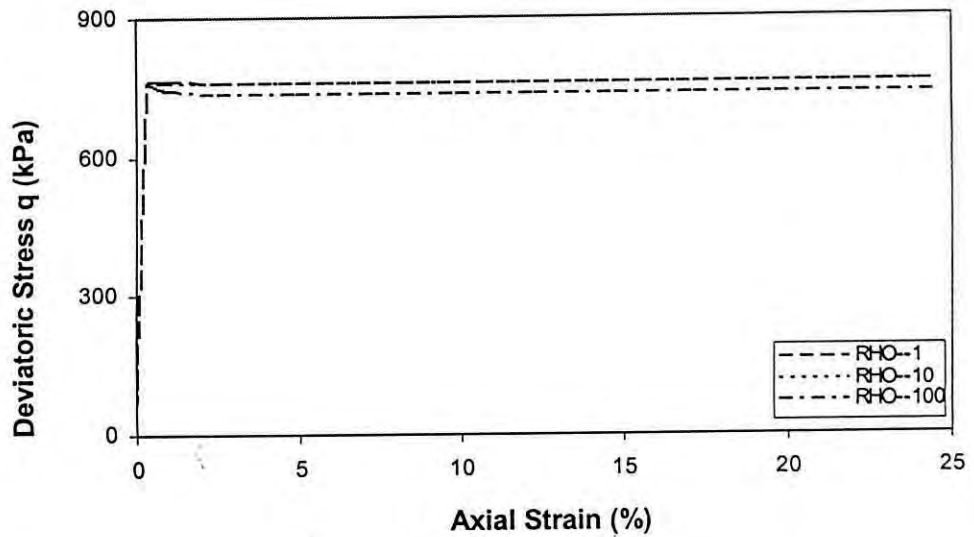


Figure 8.48 EMMCC model prediction of undrained triaxial stress-strain response of 14% cemented Savar clay (OCR=30)

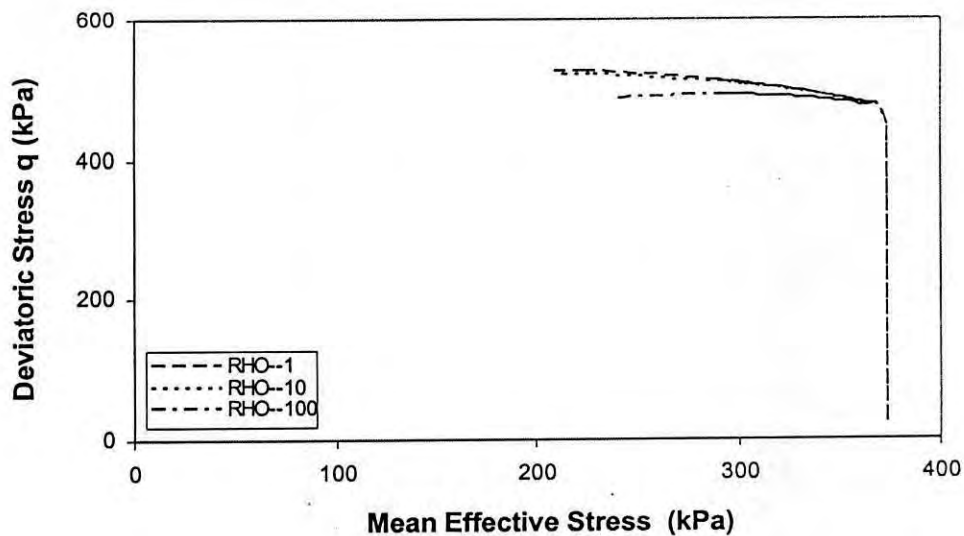


Figure 8.49 EMMCC model prediction of undrained triaxial stress path of 7% cemented Savar clay (OCR=1)

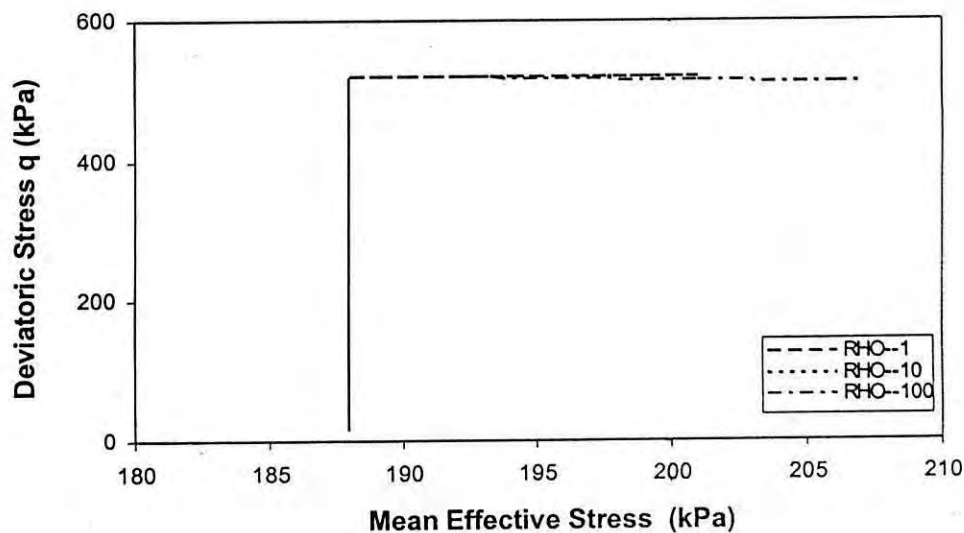


Figure 8.50 EMMCC model prediction of undrained triaxial stress path of 7% cemented Savar clay (OCR=2)

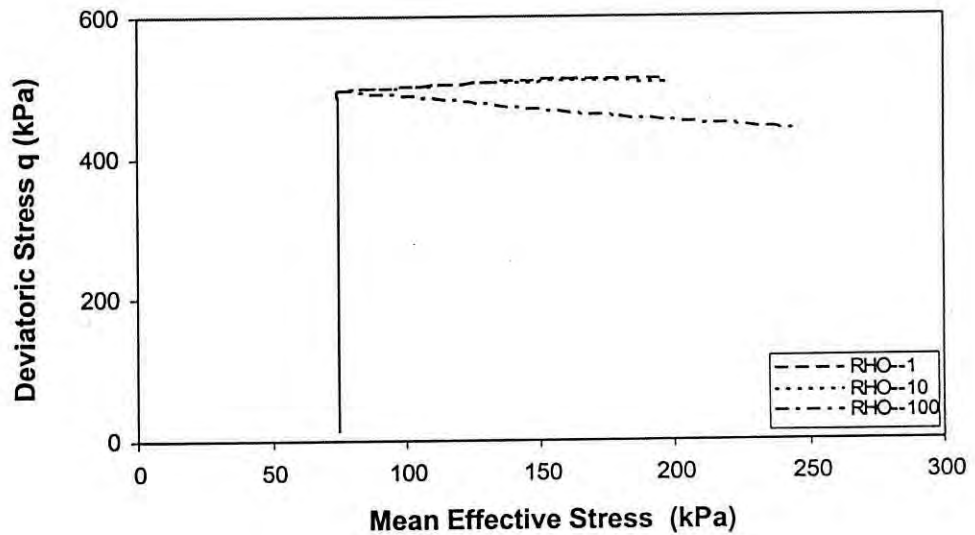


Figure 8.51 EMMCC model prediction of undrained triaxial stress path of 7% cemented Savar clay (OCR=5)

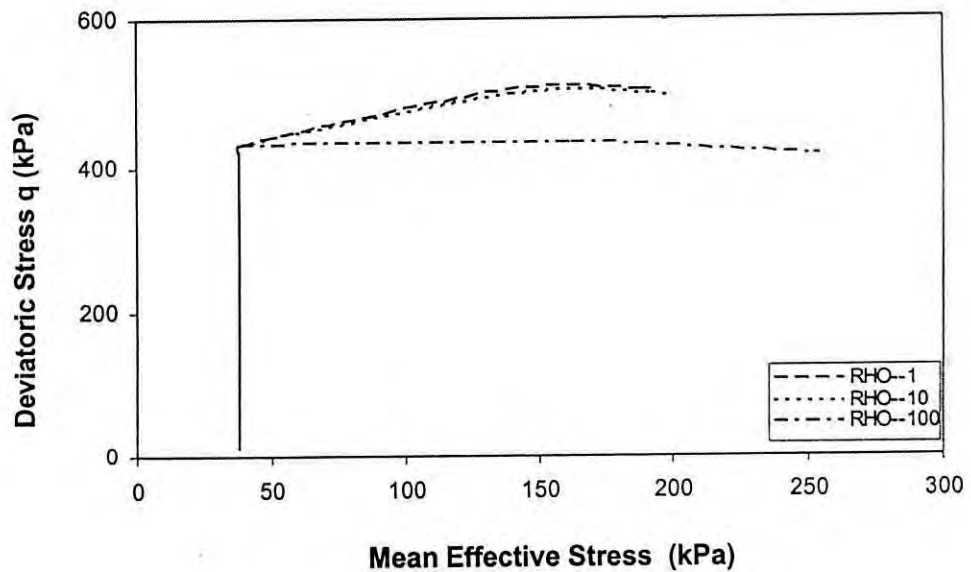


Figure 8.52 EMMCC model prediction of undrained triaxial stress path of 7% cemented Savar clay (OCR=10)



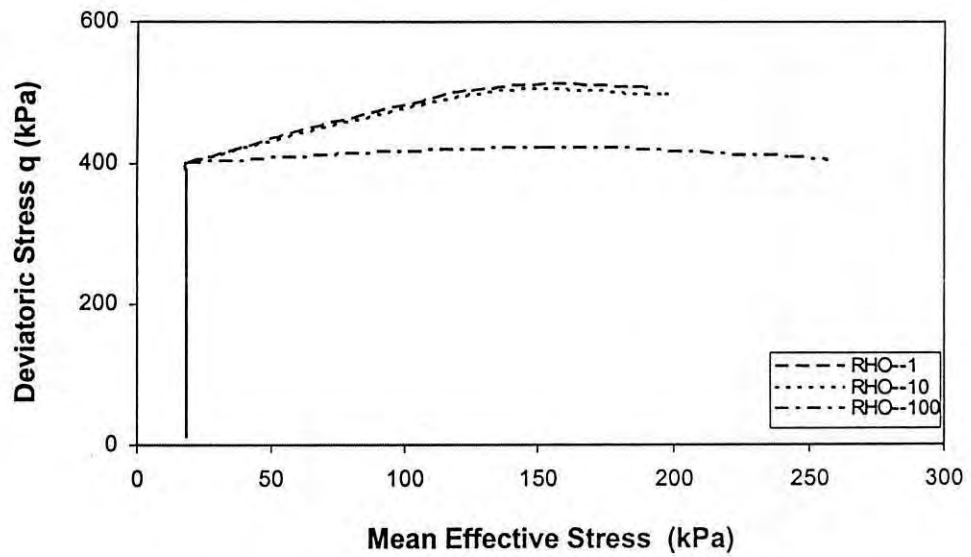


Figure 8.53 EMMCC model prediction of undrained triaxial stress path of 7% cemented Savar clay (OCR=20)

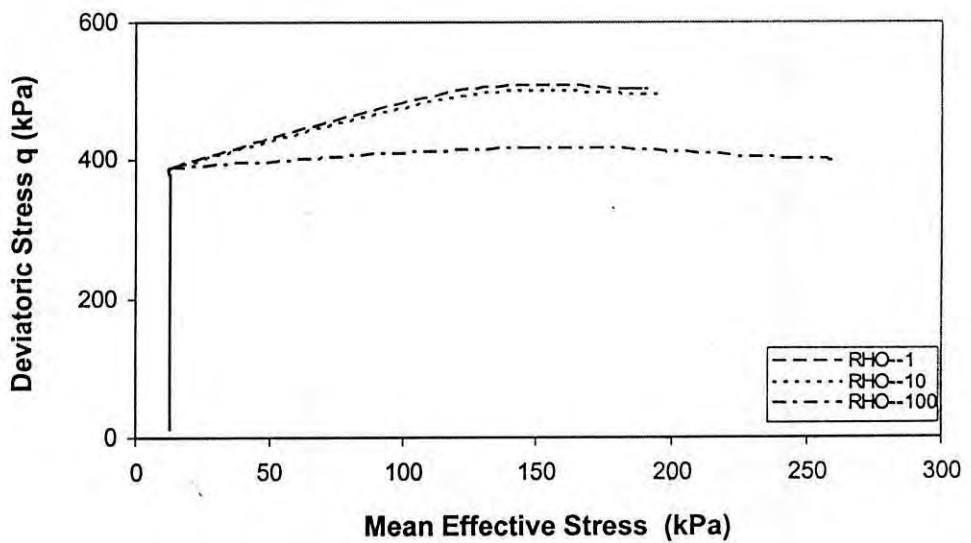


Figure 8.54 EMMCC model prediction of undrained triaxial stress path of 7% cemented Savar clay (OCR=30)

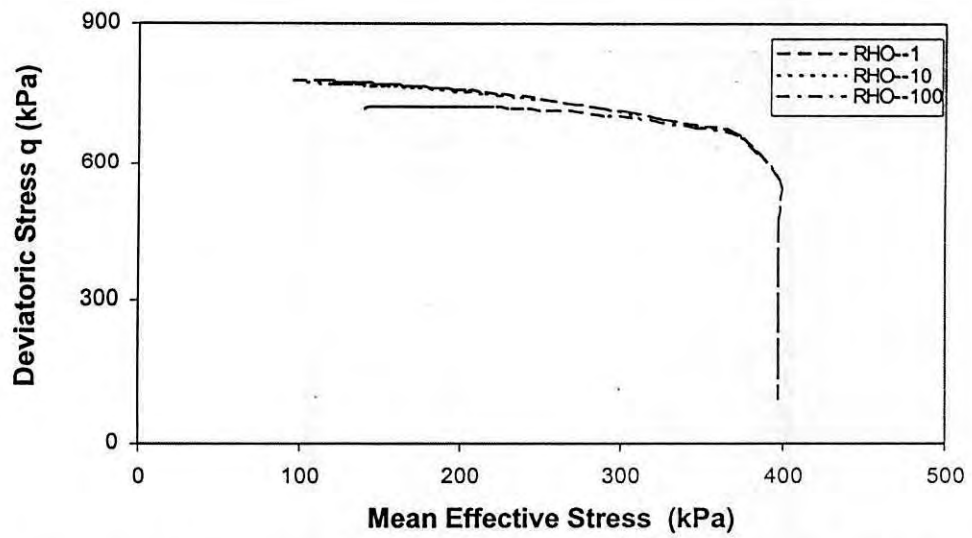


Figure 8.55 EMMCC model prediction of undrained triaxial stress path of 14% cemented Savar clay (OCR=1)

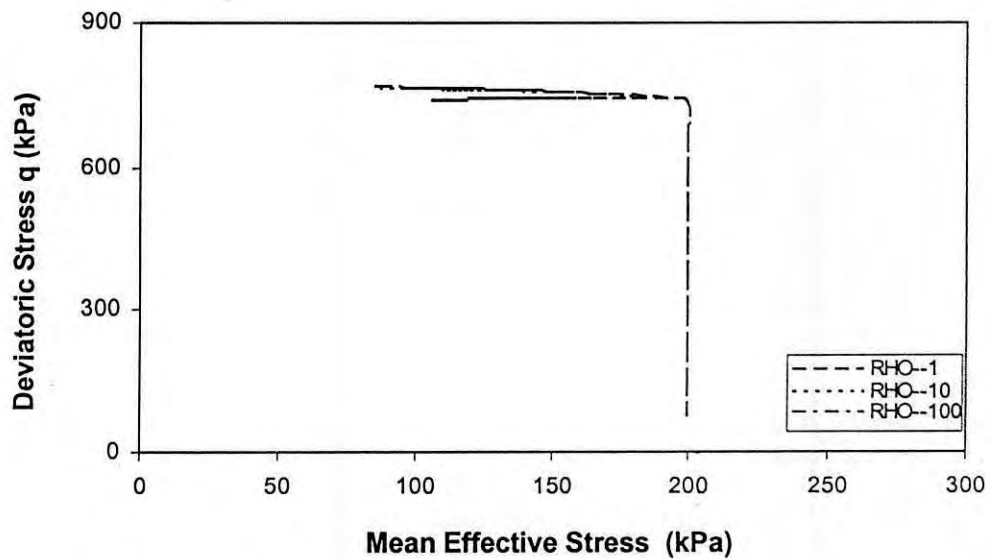


Figure 8.56 EMMCC model prediction of undrained triaxial stress path of 14% cemented Savar clay (OCR=2)

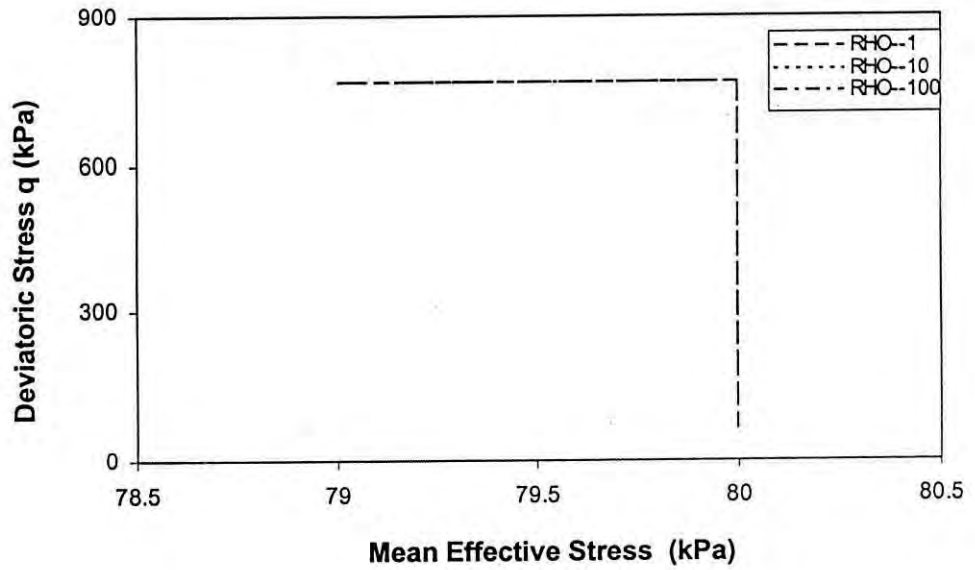


Figure 8.57 EMMCC model prediction of undrained triaxial stress path of 14% cemented Savar clay (OCR=5)

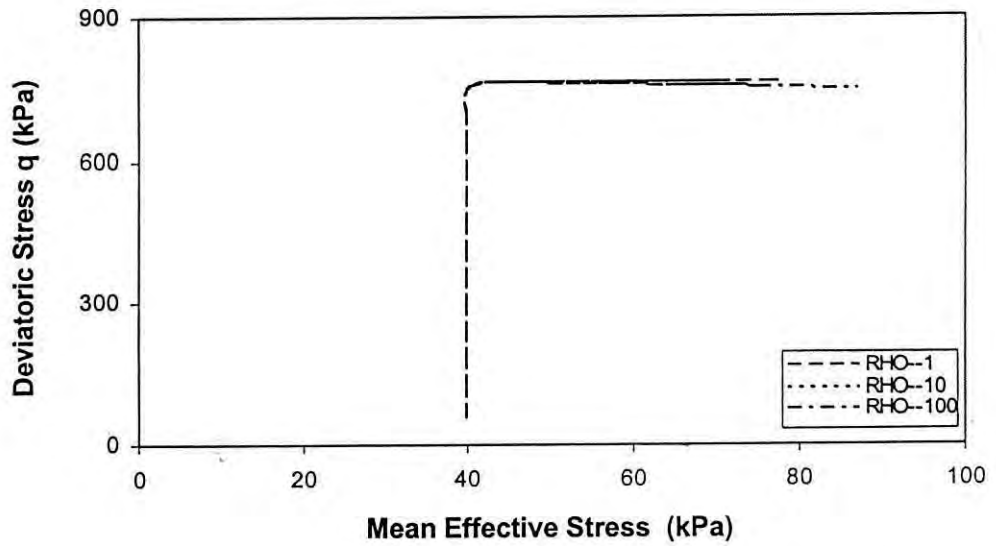


Figure 8.58 EMMCC model prediction of undrained triaxial stress path of 14% cemented Savar clay (OCR=10)

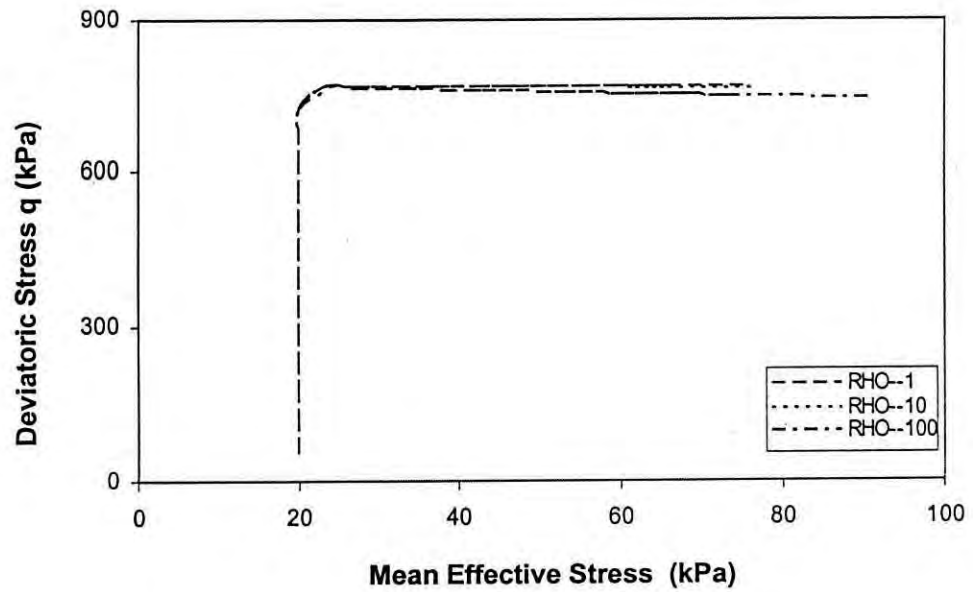


Figure 8.59 EMMCC model prediction of undrained triaxial stress path of 14% cemented Savar clay (OCR=20)

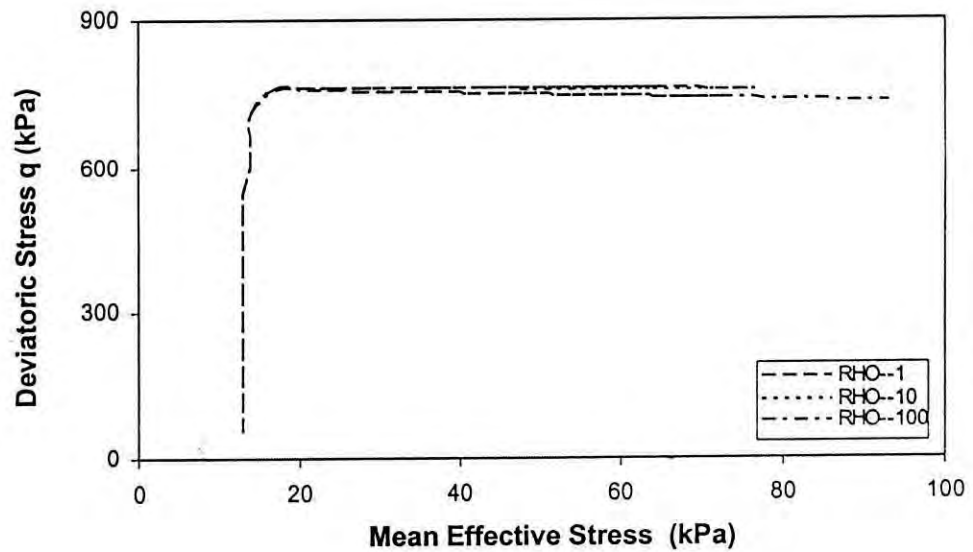


Figure 8.60 EMMCC model prediction of undrained triaxial stress path of 14% cemented Savar clay (OCR=30)

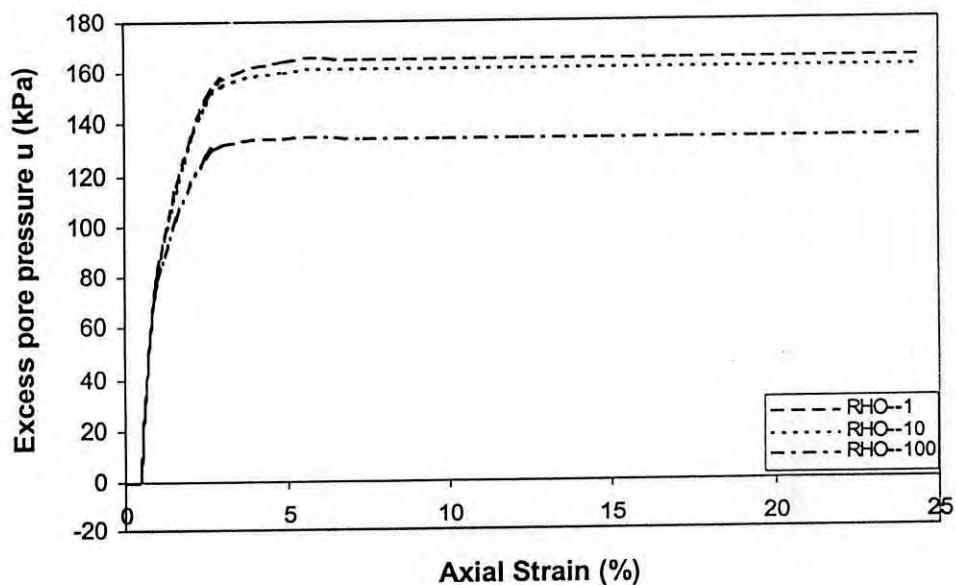


Figure 8.61 EMMCC model prediction of excess pore pressure response of 7% cemented Savar clay (OCR=1)

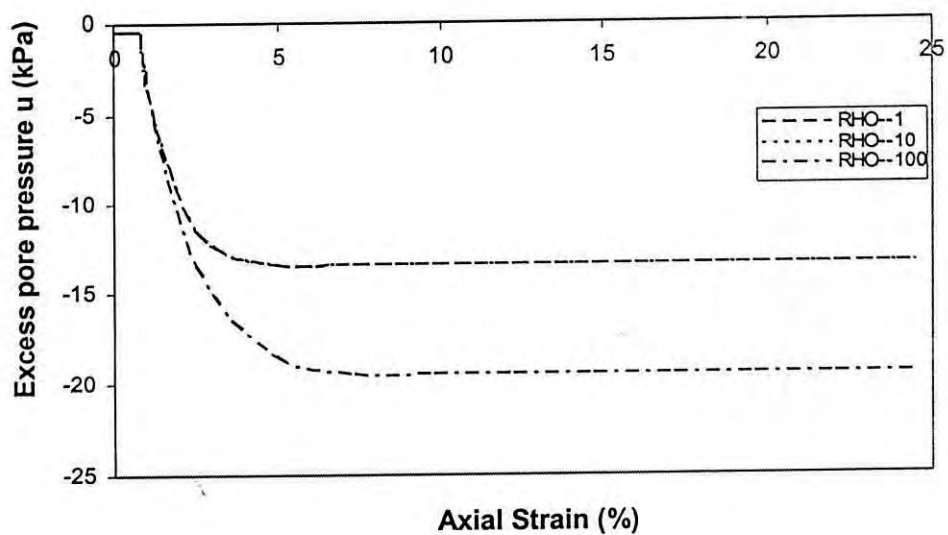


Figure 8.62 EMMCC model prediction of excess pore pressure response of 7% cemented Savar clay (OCR=2)

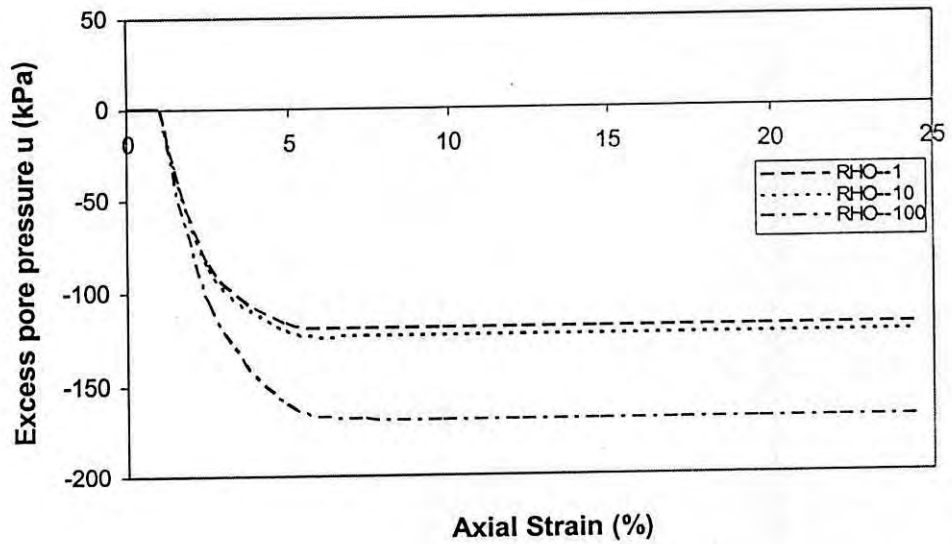


Figure 8.63 EMMCC model prediction of excess pore pressure response of 7% cemented Savar clay (OCR=5)

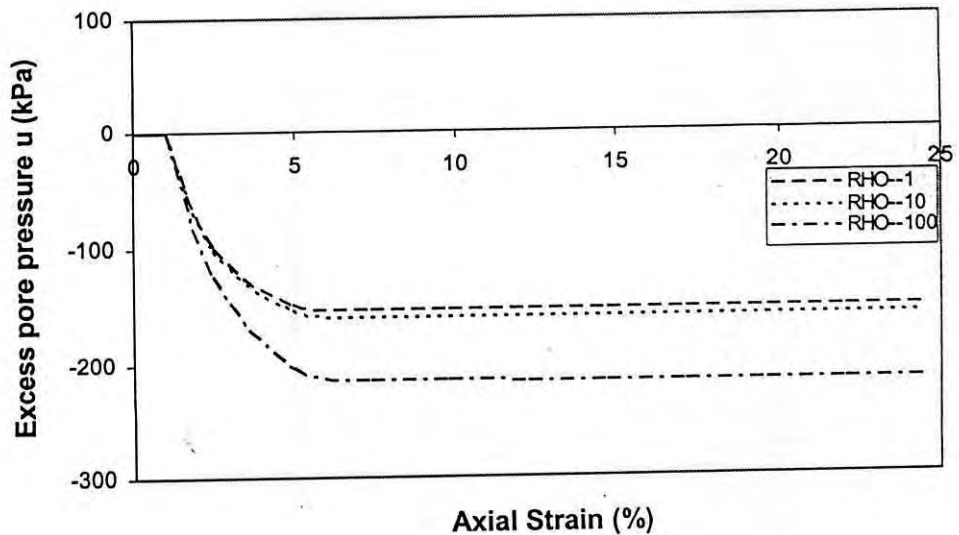


Figure 8.64 EMMCC model prediction of excess pore pressure response of 7% cemented Savar clay (OCR=10)

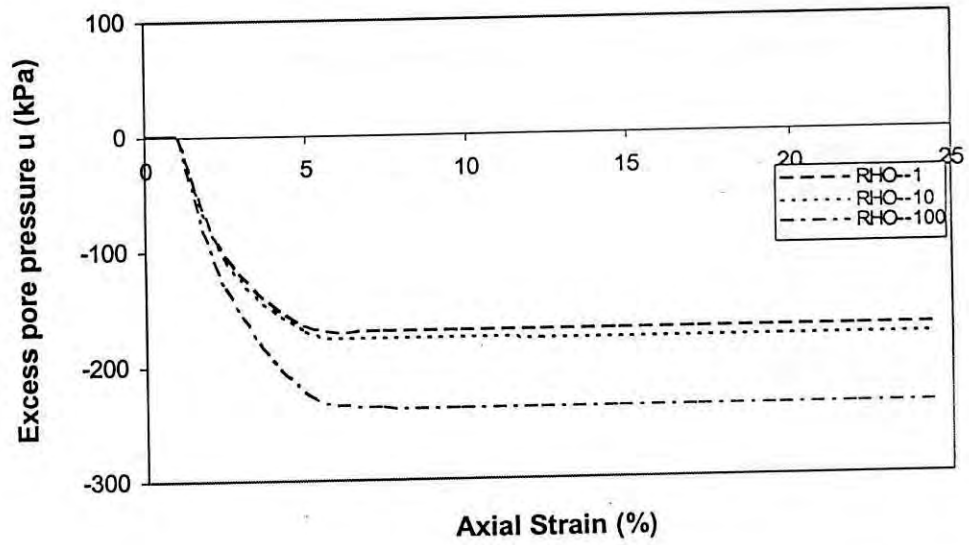


Figure 8.65 EMMCC model prediction of excess pore pressure response of 7% cemented Savar clay (OCR=20)

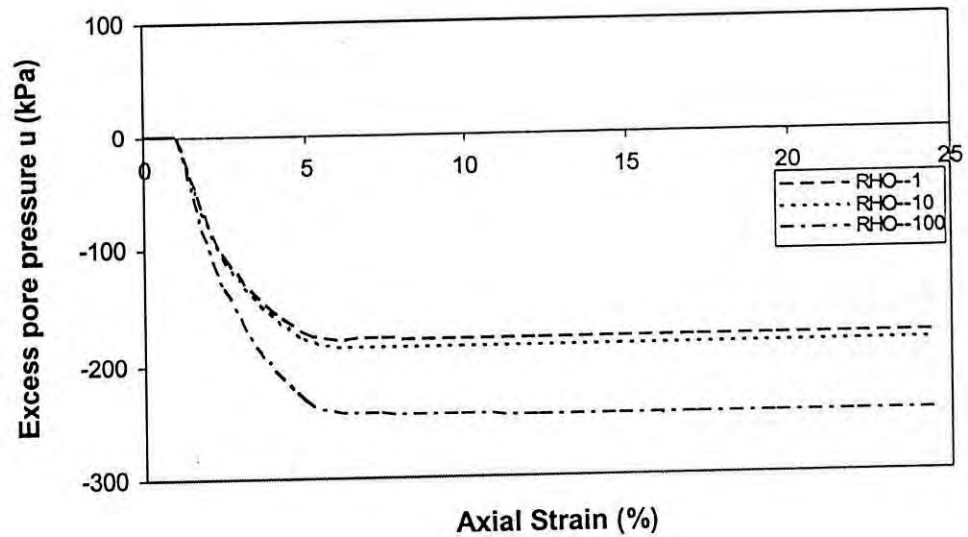


Figure 8.66 EMMCC model prediction of excess pore pressure response of 7% cemented Savar clay (OCR=30)

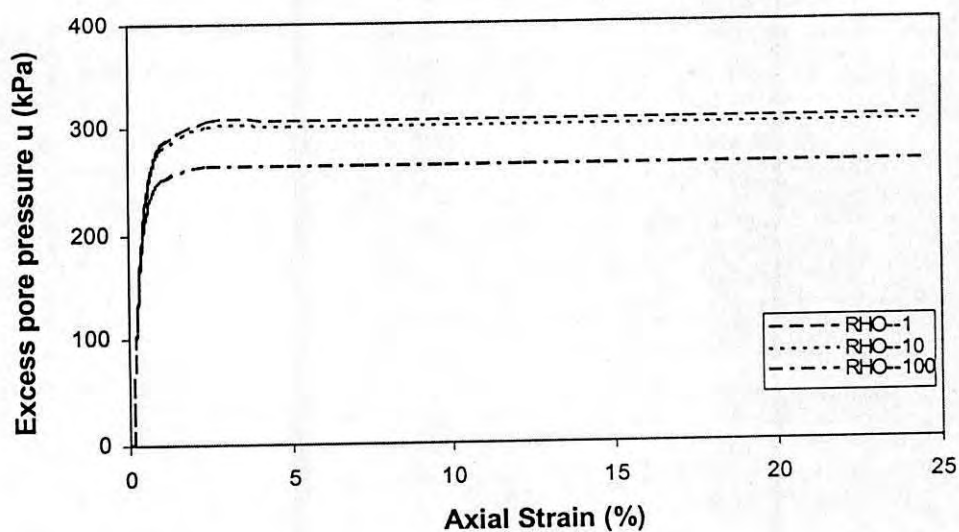


Figure 8.67 EMMCC model prediction of excess pore pressure response of 14% cemented Savar clay (OCR=1)

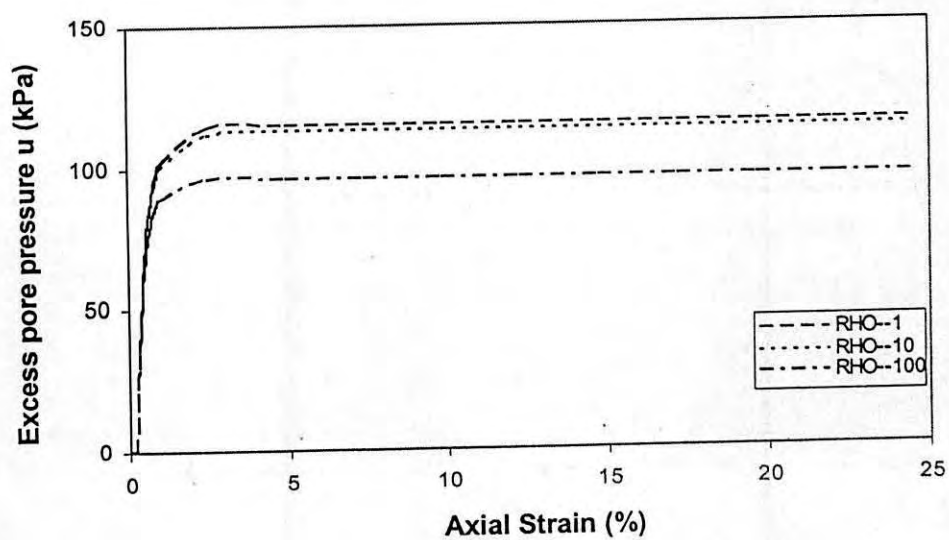


Figure 8.68 EMMCC model prediction of excess pore pressure response of 14% cemented Savar clay (OCR=2)



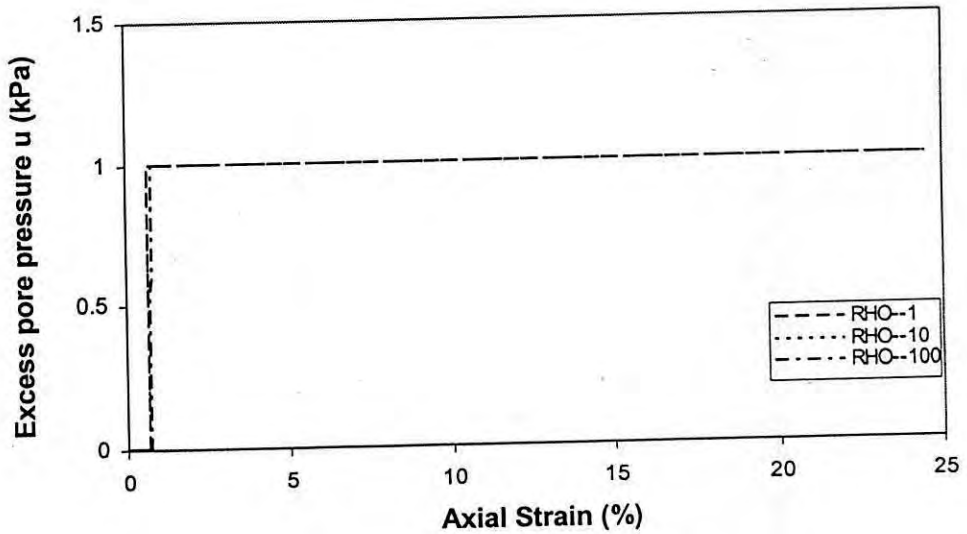


Figure 8.69 EMMCC model prediction of excess pore pressure response of 14% cemented Savar clay (OCR=5)

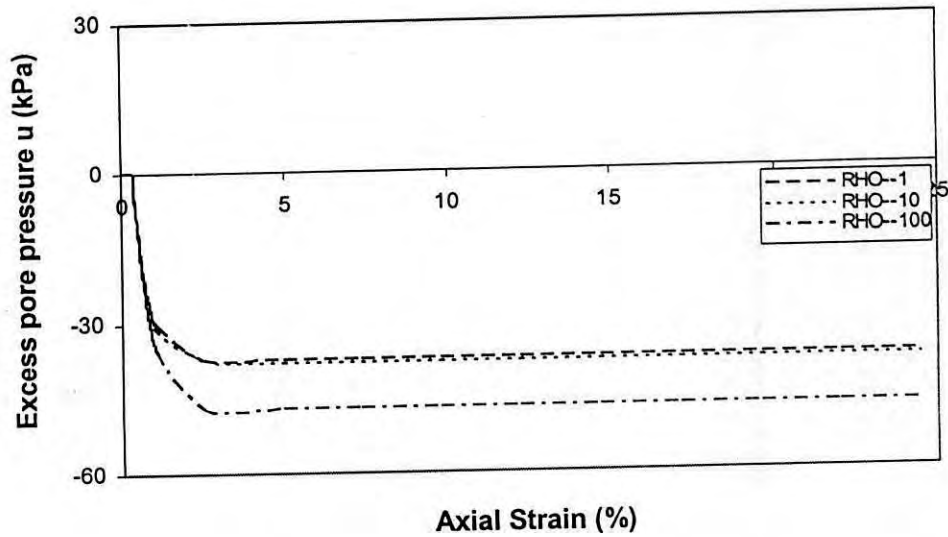


Figure 8.70 EMMCC model prediction of excess pore pressure response of 14% cemented Savar clay (OCR=10)

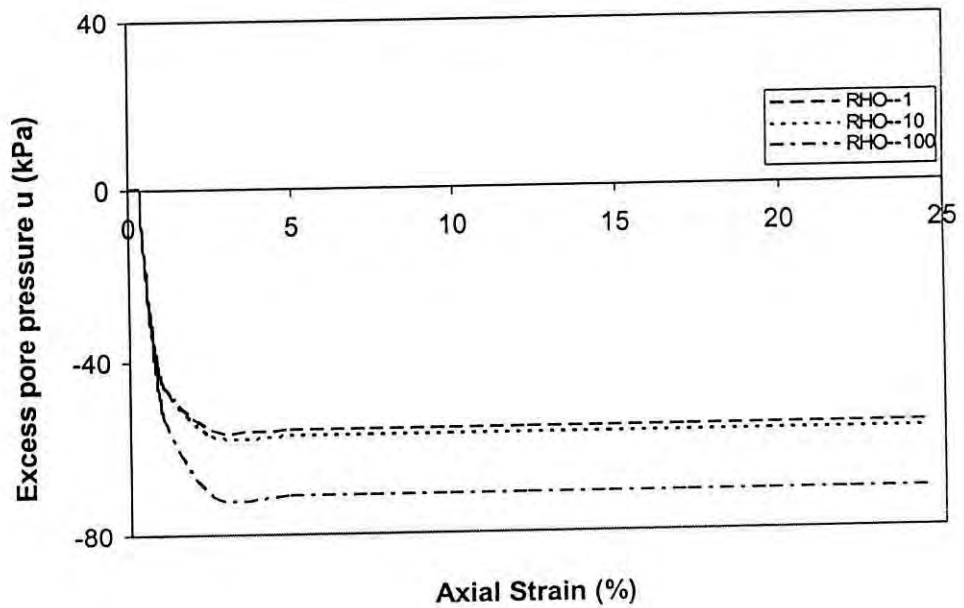


Figure 8.71 EMMCC model prediction of excess pore pressure response of 14% cemented Savar clay (OCR=20)

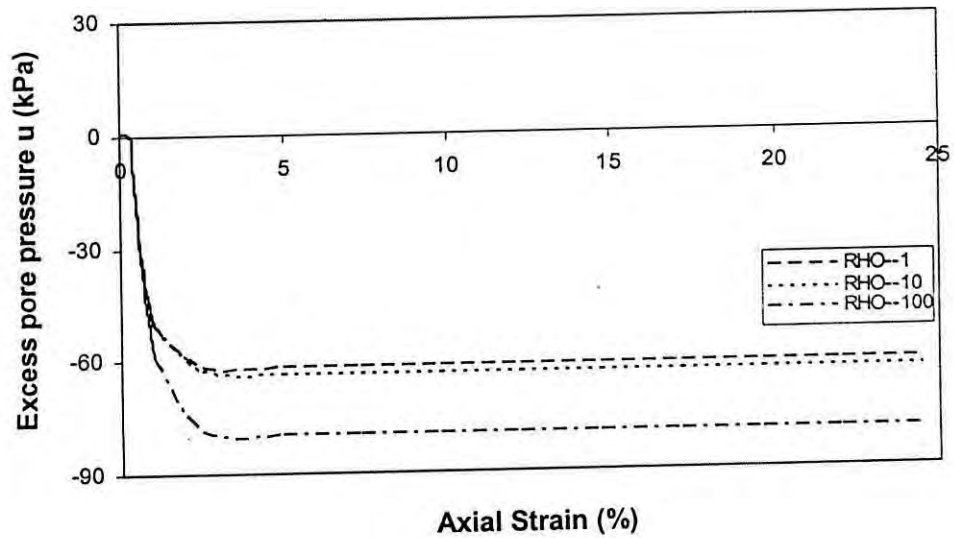


Figure 8.72 EMMCC model prediction of excess pore pressure response of 14% cemented Savar clay (OCR=30)

## CHAPTER 9

### EXPERIMENTAL AND NUMERICAL INVESTIGATION OF MODEL SCALE FOOTINGS AND PILES

#### 9.1 Introduction

A numerical and experimental investigation of the bearing capacity of model scale footings and piles resting on remolded Savar clays, with and without cementation, was carried out as part of this research investigation. An elasto-plastic finite element analysis was done to numerically simulate the load-displacement response of model scale footings and piles resting on remolded Savar clays, with and without cementation, and using the Modified Cam Clay (MCC) model and Modified Modified Cam Clay (MMCC) model. The results of the numerical analysis were compared with the experimental data.

#### 9.2 Sample Preparation

The collected sample of Savar clay was dried in air. It was then pulverized using a grinding machine. The pulverized soil was then sieved through a sieve of size 40. The soil passing sieved 40 sample was thoroughly mixed with water. The water content used was approximately 1.5 times the Liquid Limit (L.L) of the soil, which was determined in the laboratory. The water was mixed with the soil by hand kneading initially. Subsequently, the soil and water was further mixed in a Hobart rotary laboratory mixer for about 30 minutes. The homogeneous soil slurry then prepared was placed in a cylindrical consolidation cell and subjected to  $K_0$  consolidation. The cylindrical consolidation cell was 210 mm in diameter and 180 mm in height. A thick perforated steel disc covered with a filter paper was placed on top and bottom of the cell consolidated to ensure adequate drainage during consolidation.

The soil slurry was for consolidated by self weight for the first 24 hours. Subsequently, the computed target consolidation load of 50 kPa and 150 kPa was

gradually applied on the slurry sample in 10 equal increments. Each increment of load was applied for 24 hours. A loading frame was used for the load application and a proving ring was used for measuring the load. The consolidation was generally maintained until the load displacement curve indicated the end of primary consolidation of the slurry sample. After the completion of consolidation of the remolded soil sample in the cylindrical mold was used to conduct model scale footing and pile tests

### 9.3 Experimental Setup

The model scale footing and pile test was conducted using the same cylindrical mold that was used for consolidation of the soil slurry. A model scale circular steel footing 10 mm in thickness and 25 mm in diameter was made. The footing had a long column at the centre for application of the load. This column was 10mm diameter and 50 mm in length. The top of the column was given a conical depression. The circular steel footing was placed at the centre of the consolidation mold on the surface of the consolidated clay. The column at the top of the circular footing was brought in contact with the centre of the proving ring. The footing was then axially loaded in ten equal increments of load using the proving ring and the loading frame. The applied load was measured from the displacement of the proving ring as measured by a dial gauge placed inside it. This displacement was multiplied by the proving ring constant to compute the axial load applied to the footing at each increment. The displacement of the footing for each loading increment was measured by another dial gauge placed in contact with the surface of the circular steel footing.

For the pile test, a 100 mm long column (model pile) with 10 mm diameter was added to the bottom of the circular steel footing manufactured for the footing test. The 100 mm long column or pile was then pushed into the consolidated soil sample at the centre of the consolidation mold. This was construed as a single steel pile with a 25 mm diameter and 5 mm thick circular steel pile cap. The 50 mm long and 10 mm diameter column at the top of the pile cap was used to axially load the pile in ten equal load increments. The displacement of the steel pile was measured as the axial

vertical displacement of the steel pile cap using a separate dial gauge attached to the pile cap. Figures 9.1 and 9.2 shows a model scale footing test being carried out in the cylindrical consolidation mold using the model scale steel footing, proving ring and the loading frame.

#### 9.4 Finite Element Modeling

The model scale footing and pile test was numerically simulated using the finite element method. The model scale footing test domain geometry was generated using a total of 114, 8-noded quadrilateral elements, with a total of 387 nodes. The steel footing was simulated using 4, 8-noded quadrilateral elements. For the model scale pile, 112, 8-noded quadrilateral elements with a total of 383 nodes and reduced numerical integration (2x2) were used. The 100 mm long and 10 mm diameter steel pile was geometrically modelled using 14, 8-noded quadrilateral elements at the centre of the mold and embedded within the cylindrical soil domain. Figure 9.3 shows the typical mesh geometry used in the finite element analysis to simulate the model scale footing and pile using 8-noded quadrilateral elements. Figure 9.4 shows a typical isoparametric 8-noded quadrilateral element.

The distance of the cylindrical domain boundary from the edge of the circular footing was approximately 10 times the diameter of the footing. This distance generally considered adequate to preclude any boundary effects on the footing. The vertical boundary of the footing was restrained from movement in the horizontal direction. However, it was free to move in the vertically downward direction. The bottom boundary of the cylindrical domain was at a depth of approximately 10 times the footing diameter from the surface of load application. This precludes any boundary effect of the bottom boundary on the footing. The bottom boundary was restrained from moving both in the vertical and horizontal direction. The soil was modeled using the Modified Cam Clay (MCC) and Modified Modified Cam Clay (MMCC) model. Axisymmetric, finite element analysis was done with appropriate soil parameters for each model. The load-displacement data of the centre of the footing was plotted for

each of the two model scale footing tests and the single model scale pile test using the MCC and MMCC model.

The soil parameter values used for the elasto-plastic finite element analysis are those given in Tables A5.1 and A7.1. The soil was assumed to be  $K_0$  consolidated with value of approximately 0.5.

### 9.5 Comparison of Numerical Predictions with Experimental Data

In this section, the experimental and numerical mobilised bearing pressure curves obtained for uncemented and cemented Savar clay for model scale footings and piles are presented and compared. The pressure-displacement relationship obtained by numerical analysis for the centre of the model scale footing and pile by elasto-plastic finite element analysis using the MCC and MMCC was plotted for uncemented and cemented Savar clays. Figures 9.5 and 9.6 show that reasonable qualitative agreement of the plots with experimental data obtained for model scale footings and piles.

### 9.6 Comparison of MCC and MMCC Model Predictions

From load-displacement curve shown in Figures 9.7 through 9.10, it is apparent that the MMCC Model which incorporates tensile strength predicts higher loads at a given displacement, than the MCC model. However, the qualitative nature of the load displacement curves for both models appear to be similar. The nature of the predicted load-displacement curves for 14% cemented Savar clay using the MMCC and MCC Model were observed to be similar to those for 7% cementation.

The numerical predictions of the load-displacement response of model scale footings resting on 7% and 14% cemented Savar clay respectively and using the MMCC model are shown in Figures 9.11 and 9.12. Bearing capacity predictions of footings resting on 14% cemented sample were significantly higher than those for 7% cemented sample, which is reasonable. The MMCC model appears to be a better predictor of the load-displacement response of model scale footings and pile.

## 9.7 Conclusions

The load-displacement response of a model scale footing and pile in uncemented and artificially cemented remolded Savar clays was obtained, both experimentally as well as numerically. It was observed that both the MCC and MMCC model give a reasonable qualitative approximation of the experimental load-displacement response obtained for model scale footings and piles resting on remolded Savar clays, with and without cementation. More model scale and prototype footing and pile tests, as well as more detailed numerical analysis, need to be conducted to validate the results of the experimental and numerical investigations of the current research.



Fig. 9.1 Model scale footing on consolidation mold



Fig. 9.2 Model scale footing on consolidation mold





Fig. 9.1 Model scale footing on consolidation mold



Fig. 9.2 Model scale footing on consolidation mold

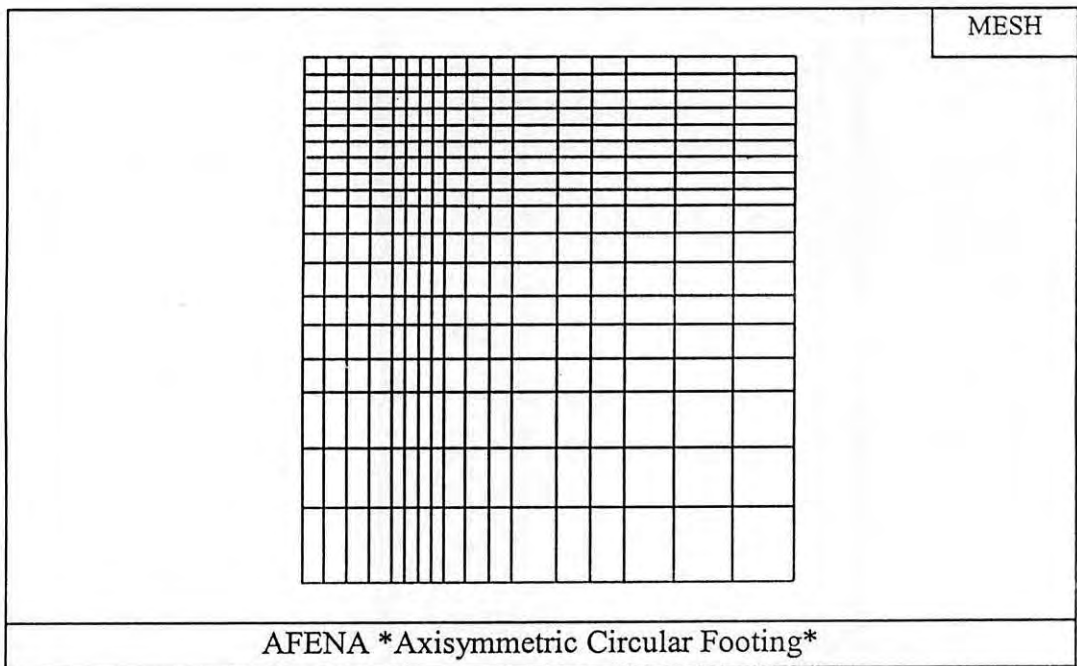


Figure 9.3 Finite element mesh for model footing using 8-noded quadrilateral elements

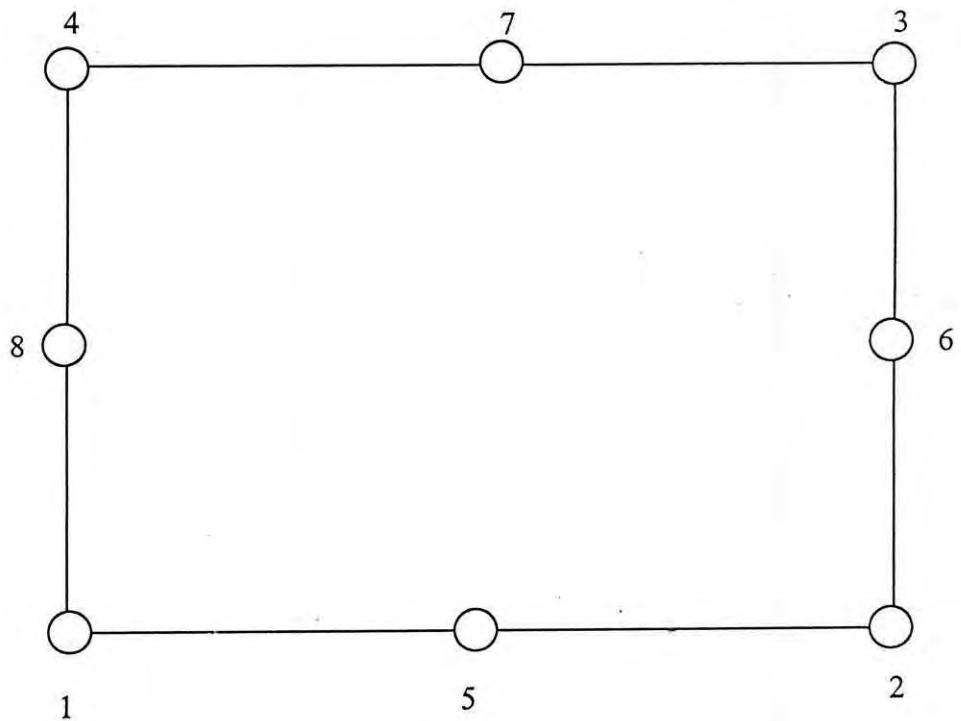


Figure 9.4 An 8-noded quadrilateral elements

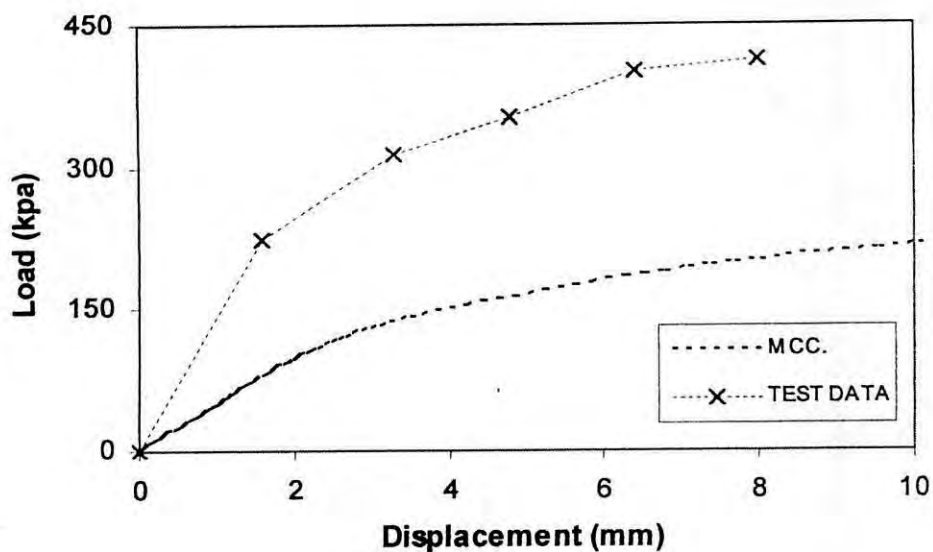


Figure 9.5 Comparison of MCC model predictions with the test data (T.D) of model scale footing on uncemented Savar clay

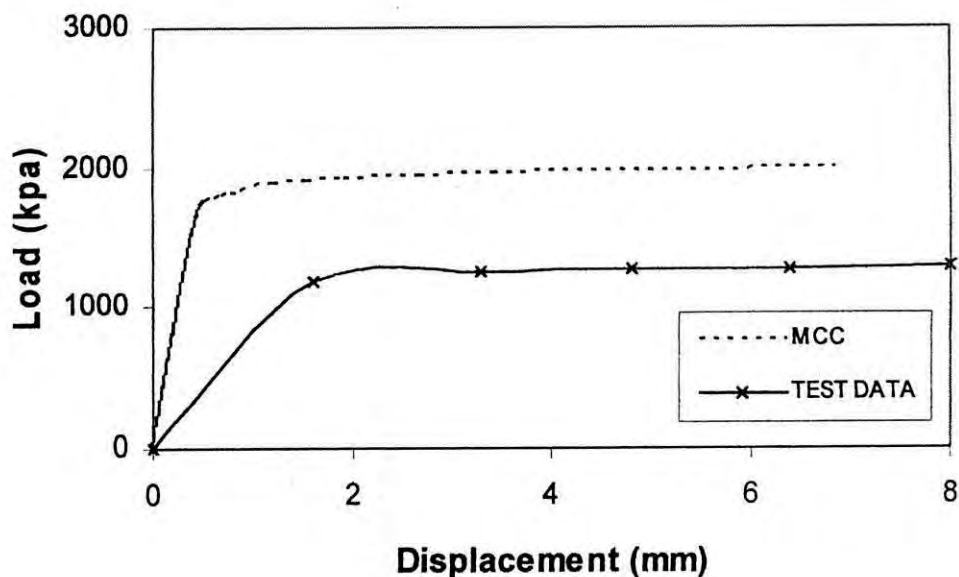


Figure 9.6 Comparison of MCC model predictions with the test data (T.D) of model scale piles on uncemented Savar clay

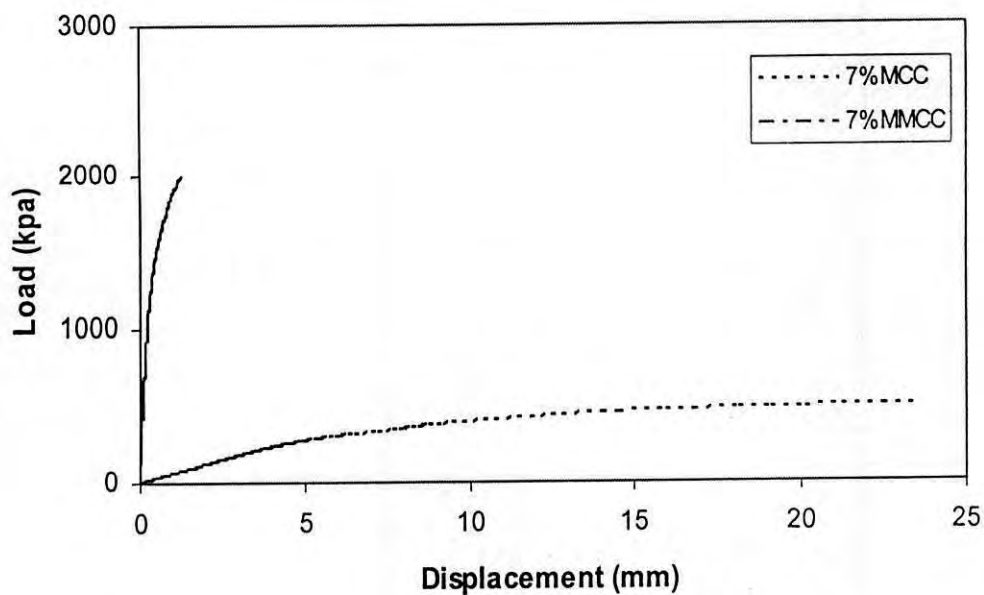


Figure 9.7 Comparison of MCC & MMCC model prediction for model scale footing resting on 7% cemented remolded Savar clay

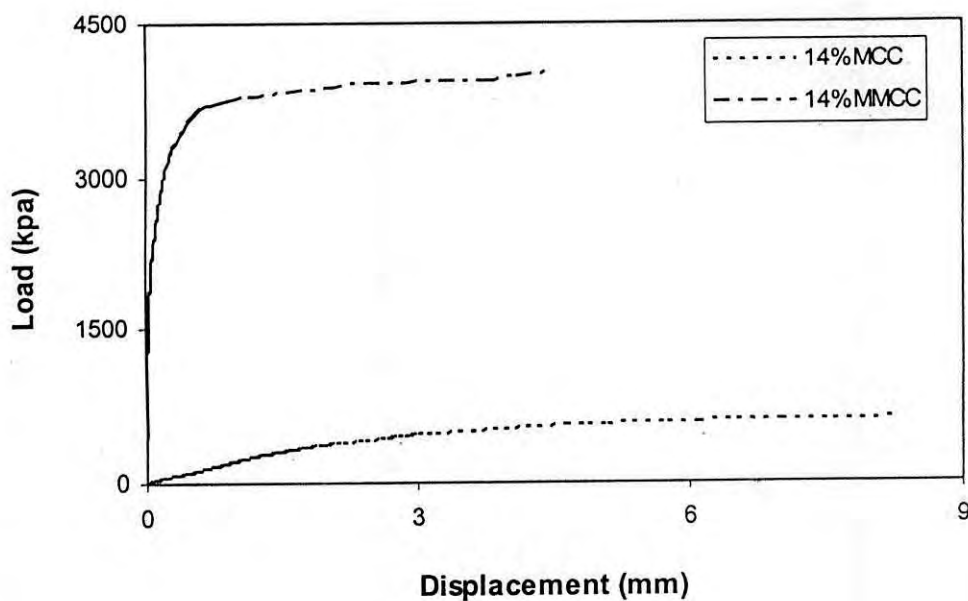


Figure 9.8 Comparison of MCC & MMCC model prediction for model scale footing resting on 14% cemented remolded Savar clay

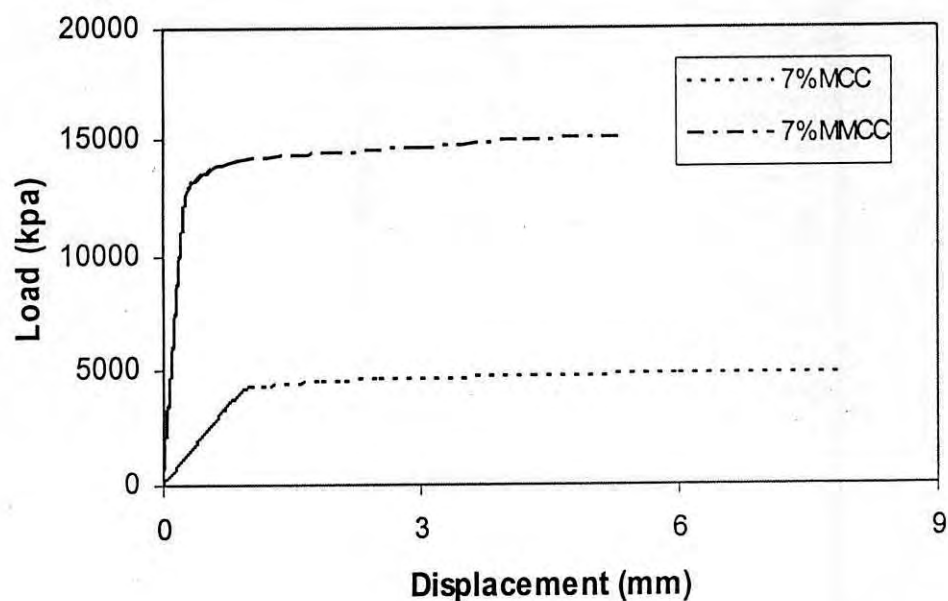


Figure 9.9 Comparison of MCC & MMCC model prediction for model scale pile test on 7% cemented remolded Savar clay

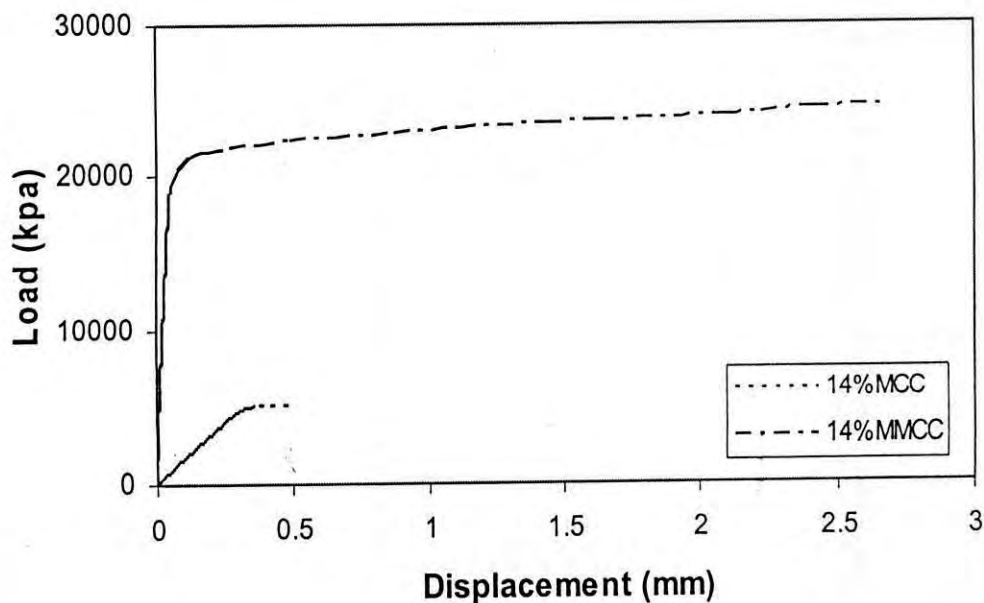


Figure 9.10 Comparison of MCC & MMCC model prediction for model scale pile test on 14% cemented remolded Savar clay

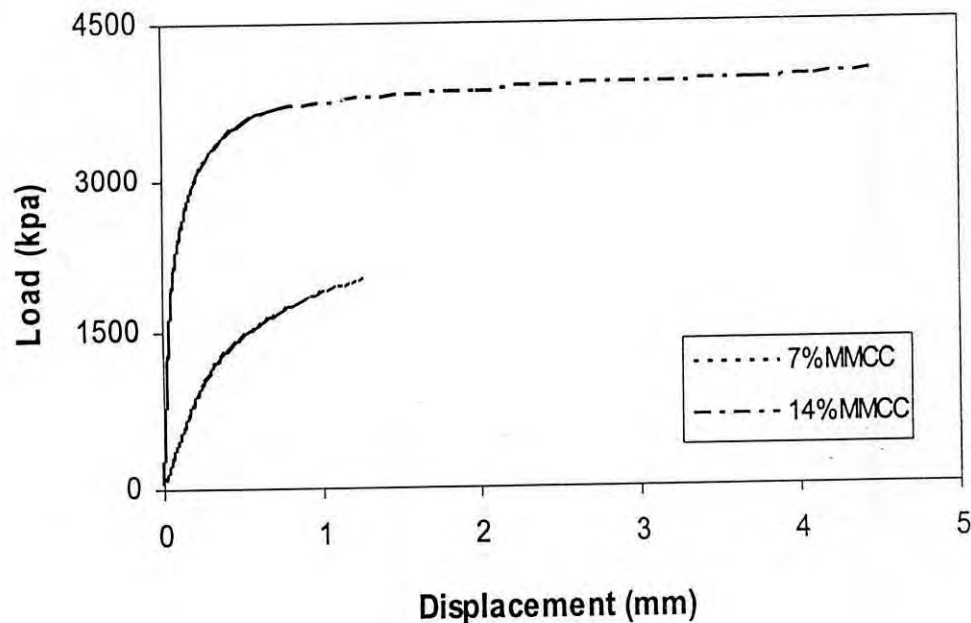


Figure 9.11 Comparison of MMCC model prediction of load-displacement response of model scale footings resting on 7% & 14% cemented remolded Savar clay

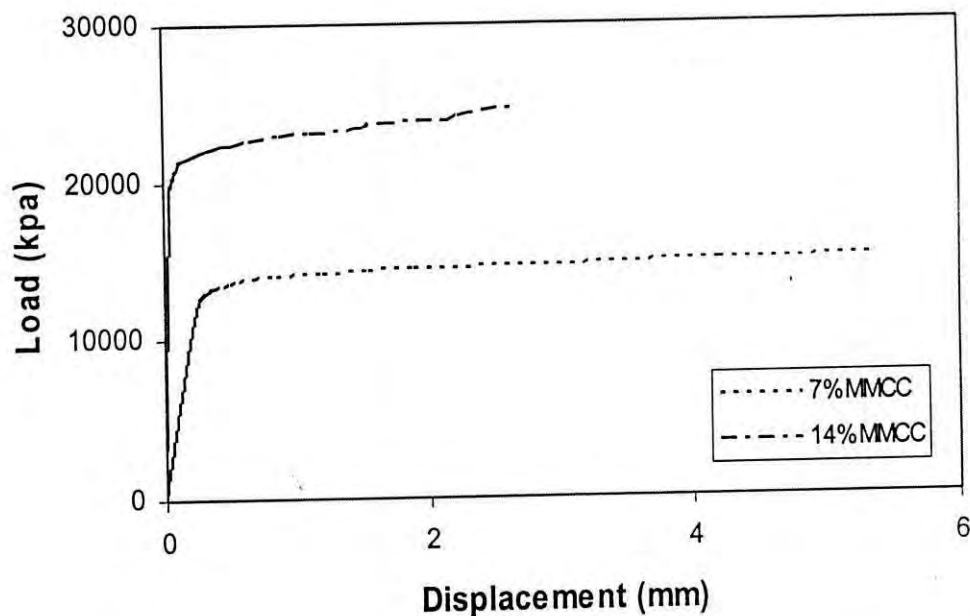


Figure 9.12 Comparison of MMCC model prediction of load-displacement response of model scale piles resting on 7% & 14% cemented remolded Savar clay

## CHAPTER 10

### CONCLUSIONS AND RECOMMENDATIONS

#### 10.1 Introduction

A limited research investigation was carried out for numerical prediction of the stress-strain behavior of Savar area clays, with and without cementation. Three advanced critical state constitutive models, namely the Modified Cam Clay (MCC) model, the Modified Modified Cam Clay (MMCC) model, and the extended MMCC model or EMMCC model, were used to simulate the triaxial stress-strain response of remolded Savar area clays, with and without cementation, both for drained and undrained conditions. An experimental study of the load-displacement response of model scale circular footings and piles resting on remolded Savar clays was also undertaken. The MCC model was used in an elasto-plastic finite element procedure to simulate the experimentally obtained load-displacement response for model scale circular footings and piles resting on remolded Savar area clays.

The results of the numerical analysis and experimental work, observations and conclusions, recommendations made and propositions for further investigation are discussed in this chapter.

#### 10.2 Concluding Observations

Simulation of the numerical behavior of Savar area clays was carried out using three constitutive models. The MCC model, and its two variants, the MMCC and EMMCC model, were used to predict the stress-strain, excess pore pressure and effective stress path of reconstituted Savar clays, without cementation and with 7% and 14% cementation, for various OCR values, and under drained and undrained conditions. Experimental results and numerical predictions using the MCC and MMCC model were obtained for model scale footings and piles resting on remolded Savar clays, with and without cementation. Specifically, the following conclusions and

observations may be made regarding the capabilities of the MCC model and its variations, the MMCC and EMMCC model, to predict the stress-strain behavior of remolded Savar clays, with and without cementation.

- The MCC model is a good predictor of the undrained stress-strain behaviour of remolded Savar clays.
- The MCC model predicts increased undrained shear strength for increased percentage of cementation in Savar clays. The rate of increase of shear strength decreases with increase in the percentage of cementation.
- The MCC model predicts an initial stiff elastic stress-strain response both for overconsolidated and cemented clays.
- The MCC model incorporating tensile or cementation strength, termed in this thesis as the MMCC model, predict higher undrained shear strength for cemented clays than the MCC model. The MMCC model appears to be an improvement over the MCC model for prediction of the undrained shear strength of cemented clays.
- The drained stress-strain responses predicted for remolded Savar clays, with and without cementation, are significantly higher than the corresponding undrained stress-strain predictions, using the MCC, MMCC and the EMMCC model.
- The EMMCC model, incorporating cementation strength and its breakdown effects, appear to have relatively smaller influence on the predicted stress-strain response of remolded Savar clays, with and without cementation.
- The MCC and MMCC model provides reasonable qualitative predictions of the mobilised load-displacement response of model scale footings and piles resting on remolded Savar clays, with and without cementation.



### 10.3 Recommendations for Further Research

Detailed experimental investigation of the triaxial stress-strain response of remolded Savay clays, with and without cementation, for various OCRs, and for drained and undrained conditions, need to be carried out. These experimental results may then be compared with the numerical predictions presented in this work. This will help to identify the strengths and limitations of various components of each of the models presented in this thesis.

A more detailed experimental investigation of the load- displacement response of model footings and piles on resting on remolded and artificially cemented clays may also be undertaken. This will give greater understanding of the effect of cementation of clays on the bearing pressure mobilised by footings and piles resting on such clays. The behavior of footings and piles underlain by layered materials, with alternating cemented and uncemented clay layers of various thicknesses, may also be carried out, both numerically and experimentally. This is likely to provide valuable insights on the load-displacement response of footings and piles under realistic field conditions.

## REFERENCES

1. Ameen, S.F. and Safiullah, A.M.M., 1986 Undrained shear strength characteristics of Dhaka clay, *Journal of the Institution of Engineers, Bangladesh*, 14, 4, pp. 1-8.
2. Siddiquee, A.K.M.A.R, 2006, Experimental & Numerical study of coastal clays of Bangladesh, M.Sc. thesis, department of Civil Engineering, Bangladesh University of Engineering and Technology, Dhaka, Bangladesh
3. Atkinson, J.H. and Bransby, P.L., 1978. *The mechanics of soils-An introduction to critical state soil mechanics*, McGraw Hill, New York, NY, pp.375
4. Balasubramaniam, A.S., 1969, some factors influencing the stress-strain behaviour of clay, PhD. Thesis, Cambridge University
5. Barden, L. and Monkton, M.F., 1970. Test on model pile groups on soft clay. *Geotechnique*, 20: 94-96
6. Barden, L., 1969. Time dependent deformation of normally consolidated clays and peats. *J. soil Mech. Found. Div., ASCE*, 95(SM1): 1-31
7. Bashar, M.A., 2002, Stress-deformation characteristics of selected coastal soils of Bangladesh and their sampling effects, PhD. thesis, department of Civil Engineering, Bangladesh University of Engineering and Technology, Dhaka, Bangladesh
8. Biot, M.A., 1941. General theory of three dimensional consolidations, *J. Applied Physics*, 12: 155-164.
9. Bishop A.W. and Henkel, D. J., 1962. *The measurement of soil properties in the triaxial test*. Edward Arnold, London, 2<sup>nd</sup> ed, 228 pp

10. Bjerrum, L., 1955. Stability of natural slopes in quick clay. *Geotechnique*, 5: 101-110
11. Bjerrum, L., 1954a. Geotechnical properties of Norwegian marine clays, *geotechnique*, Vol. 4, p. 49
12. Bjerrum, L., 1954b. Theoretical and Experimental Investigation on the shear strength of soils, Norwegian Geotechnical Institute Publication No. 5, Oslo, 113pp.
13. Bjerrum, L., and Landva A., 1966. Direct Simple-Shear tests on a Norwegian quick clay, *geotechnique*, Vol 16, No 1, pp. 1-20.
14. Carter, J.P. and Balaam, N.P. 1995. AFENA-A Finite Element Numerical Algorithm, User's Manual, Centre for Geotechnical Research, University of Sydney
15. Casagrande, A., 1932a. Research on the Atterberg limits of soils. *Public Roads*, 13(8):121-130
16. Cadling, L. and Odenstad, S., 1958. The vane borer. An apparatus for determining the shear strength of clay soils directly in the ground, Swedish Geotechnical Institute Proc, No. 2, 88pp
17. Casagrande, A., 1944. Cooperative research on stress-deformation and strength characteristics, Harvard University, Seventh Progress Report, 142 pp.
18. Casagrande, A., 1948. Classification and identification of soils, *Trans ACSE*, Vol. 113, p.901.
19. Casagrande, A., and Fadum, R.E., 1944 Application of soil mechanics in designing building foundations, *Trans ASCE*, Vol 109, p. 383

20. Casagrade, A. and Wilson, S.D., 1949. Investigation of the effect of long-time loading on the strength of clays and shales at constant water content, Harvard Univ, Report to U.S. waterway Experiment Station, 77 pp.
21. Chellis, R. D., 1962. Pile Foundations, Chapter 7, Foundation Engineering, G.A. Leonards (ed.) McGraw Hill, New York
22. Chen, W.F. and Mizuno, E., 1990. Non-linear analysis in soil mechanics, Elsevier Science Publishers, B.V., New York, USA
23. de Borst, R. and Vermeer, P.A., 1984. Possibilities and limitations of finite elements for limit analysis, *Geotechnique* 34, No 2, pp. 199-210.
24. Dimaggio, F.L, and Sandler, I. S., 1971. Material model for granular soils, *Journal of Engineering Mechanics Division, ASCE*, 97 (EM3), pp. 935-950.
25. Drucker, D.C. and Prager, W., 1952. Soil mechanics and plasticity analysis or limit state design. *Quart. Appl. Math*, 10(2): pp. 157-175
26. Foster, C.R., 1962. Field Problems: Compaction, Foundation Engineering, G. A. Leonards (ed.), McGraw-Hill, New York.
27. Gens, A. and Potts, D.M., 1988. Critical state models in computational geomechanics, *Engineering computations*, Vol 5, pp. 178-197.
28. Glossop, R. 1968. The rise of geotechnology and its influence on engineering practice. *Geotechnique*, 18: 105-150.
29. Griffiths, D.V., 1982. Elastoplastic analysis of deep foundations in cohesive soils, *International Journal for Numerical and Analytical Methods in Geomechanics*, Vol. 6, pp. 211-218.

30. Ingles, O.G. and Metcalf, J. B., 1972. Soil Stabilization, Principles and Practice, Butterworths Pty Ltd, Melbourne.
31. Islam, M.J., 2003. A comparative study on engineering properties of block and tube samples of Dhaka clay, M. Engg. Thesis, BUET, Dhaka
32. Hanna, A.M. and Meyerhoff, C.G., 1981. Experimental evaluation of bearing capacity of footings subjected to inclined loads, Canadian Geotechnical Journal, Vol. 18, pp. 599-603.
33. Hasan, K.A., 2002. A study on cement and lime stabilization on soils of selected reclaimed sites of Dhaka city, MSc. Engg. Thesis, BUET, Dhaka
34. Henkel, D. J., 1960. The relationship between effective stresses and water content in saturated clays, Geotechnique, Vol. 10, p. 41.
35. Henkel, D. J., 1959. The relationship between strength, pore-water pressure, and volume change characteristics of saturated clays, Geotechnique, Vol. IX, p. 119.
36. Henkel, D. J., 1956. The effect of overconsolidation on the behaviour of clays during shear, geotechnique, Vol. 6, p. 139.
37. Kamon, M. & Bergado, D.T., 1992. Ground improvement techniques, 9<sup>th</sup> Asian geotechnical conference, Bangkok, Vol 2, pp. 526-546.
38. Kamaluddin, M., 1990, Compressibility and shear strength of remoulded Dhaka clay, MSc. Engg. Thesis, BUET, Dhaka
39. Kamaluddin, M., 2004. Advanced Ground improvement Technique by Cement and Lime treatment, IAT, BUET, Dhaka, Vol 1, p.117

40. Kerisel, J. L., 1967. Vertical and horizontal bearing capacity of deep foundations in clay, Proc. symposium on bearing capacity and settlement of foundations, Duke Univ, Durham, N.C., p. 45
41. Ladd, C.C., 1973. Settlement analysis for cohesive soils. Res. Rep. R71-2, Soils Publ. 272, Dept. of civil Engineering, Mass Inst of Technology, Cambridge, Mass, 115 pp. (revised 1973)
42. Lade, P.V. and Duncan, J.M., 1975. Elastoplastic stress-strain theory for cohesionless soil. J. geotech. Engg. Div., ASCE, 101(GT10), pp. 1037-1053
43. Lambe, T.W. 1964. Methods of estimating settlement. J. Soil Mech. Found. Div., ASCE, 90(SM5):43-67
44. Lambe, T.W. and Martin, R.T., 1953-1957 Composition and engineering properties of soils. Proc. Highway. Res. Board, (5 papers), 32: 576-590, 33: 515-532, 34: 566-582, 35: 661-677, 36:693-702.
45. Lambe, T.W. 1951. Soil Testing for Engineers, Wiley, New York, 165pp.
46. Lagioia, R. and Nova, R., 1993. A constitutive model for soft rocks. Geotechnical Engineering of Hard Soils-Soft Rocks, Anagnostopoulos et al (eds.), Balkema, Rotterdam, pp. 6235-632.
47. Leonards, G. A., 1962. Foundation Engineering, McGraw-Hill, New York
48. Meyerhoff, G. G., 1951a. The ultimate bearing capacity of foundations, Geotechnique, Vol 2, pp. 301-332.
49. Mitchell, R. J., 1970. On the yielding and mechanical strength of Leda clays, Can. Geotech. J., 7: 297-312

50. Mitchell, R.J. and Gardener, W.S., 1975. In situ measurement of volume change characteristics, Proc Spec Conf. In Situ Measurement of Soil properties, Raleigh, N.C., 2: 279-345.
51. Nadarajah, V., 1973. Stress-strain properties of lightly overconsolidated clays. Ph.D. Thesis, Cambridge University.
52. Newland, P.L. and Alley, B.H., 1960. A study of the consolidation characteristics of clay. *Geotechnique*, 10:62-74.
53. O'Neill, H. M. 1962. Direct shear test for effective strength parameters, Proc ASCE, Vol 88, No SM4, pp. 109-137
54. Rahman, M.M., 2000. Effects of sampling disturbance on mechanical properties of reconstituted normally consolidated and overconsolidated Dhaka clay, MSc. Engg. Thesis, BUET, Dhaka
55. Roscoe, K.H. and Burland, J.B., 1968. On the generalized stress-strain behaviour of 'wet' clay. In: *Engineering Plasticity*, Ed. J. Heyman & F.A. Leckie, pp.535-609. Cambridge Univ. Press, London.
56. Roscoe, K.H. and Schofield, A. N., 1963. Mechanical behaviour of an idealized 'Wet-clay', Proc. 2<sup>nd</sup> European Conf. Soil Mech. Found Eng., Wiesbaden, 1: 47-54
57. Schofield, A. and Wroth, C.P., 1968. *Critical state soil mechanics*, McGraw-Hill, London.
58. Siddique, A. and Safiullah, A.M.M., 1995. Permeability characteristics of Dhaka clay, *Journal of the Civil Engineering Division*, The Institution of Engineers, Bangladesh, Vol. CE 23, No. 1, pp. 103-115.

59. Siddique, A. and Sarker, J.K., 1998. Effect of stress reconsolidation on shear characteristics of reconstituted soft Dhaka clay, *The Indian Engineer Journal*, India, Vol 40, No 11, pp. 3-13.
60. Skempton, A.W., 1948. The  $\phi=0$  analysis for stability and its theoretical basis, *Proc 2<sup>nd</sup> Int Conf Soil Mech and Found Engg. (Rotterdam)*, Vol 1, p. 72.
61. Skempton, A.W. and Golder, H. Q., 1948. Practical examples of the  $\phi=0$  analysis for stability of clays, *Proc 2<sup>nd</sup> Int Conf Soil Mech and Found Engg. (Rotterdam)*, Vol 1, p. 63.
62. Skempton, A. W. 1942. An investigation of the bearing capacity of soft clay soil, *J. Inst. Civil Engrs*, Vol. 18, p. 307
63. Smith, I.M., 1982. *Programming the finite element method*, New York: Wiley.
64. Sowers, G.F., 1963. *Shallow Foundations, Foundation Engineering*, G.A. Leonards (ed.), McGraw-Hill, New York
65. Tate, A.P.K. 1963. Model behaviour of pile groups in clay. *Proc. 2<sup>nd</sup> Panama Conf. Soil Mech. Found. Eng.*, Brazil, 2: 235-253.
66. Tavenas, F.A. 1975a. In site measurement of initial stresses and deformation characteristics. *Proc Spec. Conf. In-Situ Measurement of Soil Properties*, Raleigh, N.C., 2: 263-270.
67. Terzaghi, K., 1943. *Theoretical Soil Mechanics*, Wiley, New York, 510 pp.
68. Tschebotarioff, G.P., 1951. *Soil Mechanics, Foundations and Earth Structures*, McGraw-Hill, New York 655pp.
69. Uddin, M.K., 2001. Intrinsic compressibility, shear properties and some strength models for Dhaka clay, *The Journal of Civil Engineering*, The Institution of Engineers, Bangladesh (IEB), Dhaka, Bangladesh, Vol CE 27, No. 2.



70. Uddin, M.K. & Buensuceso, B. R., 2002. Lime treated clay: salient engineering properties and a conceptual model, *Journal of Soils and Foundations*, The Japanese Geotechnical Society, Tokyo Japan, Vol. 42, No. 5, pp. 79-89.
71. Uddin, M.K. & Buensuceso, B. R., 2001. Engineering properties and a conceptual model for lime treated clay, *The Journal of Civil Engineering*, The Institution of Engineers, Bangladesh (IEB), Dhaka, Bangladesh., Vol CE 28, No. 2
72. van Weele, A.F. 1957. A method of separating the bearing capacity of a test pile into skin friction and point resistance. *Proc. 4<sup>th</sup> Int. Conf. Soil mech. Found. Eng.*, London 3: 76:80.
73. Wagner, A.A., 1957. The use of the unified classification system in the Bureau of Reclamation, *Proc. 4<sup>th</sup> Inter Conf Soil Mech. Found. Eng. (London)*, Vol I, p. 125
74. Wissa, A.E.Z, Ladd, C.C. and Lambe, T.W., 1965. Effective stress-strength parameters of stabilized soils, *Proc. 6<sup>th</sup> ICSMFE*, Montreal, pp. 412-416.
75. Wroth, C.P. 1977. The predicted performance of soft clay under a trial embankment loading based on the Cam-clay model. In: *Finite elements in geomechanics*, Ed. G. Gudehus, pp. 191-208, Wiley, London
76. Yu, H.S., 1995. A unified constitutive model for clay and sand, research Report No. 112.08.1995, department of Civil Engineering and Surveying, University of Newcastle
77. Zienkiewicz, D.C. and Naylor, D.J., 1971. The adaptation of critical state soil mechanics theory for use in finite elements, *Proc. Roscoe Memorial Symp. Stress-Strain Behaviour of Soils*, Cambridge, England, pp. 537-547.

## APPENDIX I

### GEOTECHNICAL PARAMETERS OF UNCEMENTED AND CEMENTED DHAKA CLAY

**Table A1.1 Index and other properties of Dhaka Clay (Uddin, 1990)**

Sl. No	Properties	Range
1	Liquid limit	39% to 50%
2	Plastic limit	18% to 25%
3	Plasticity index	18 to 29
4	Clay content (less than 2 micron)	15% to 35%
5	Sand content	0% to 11%
6	Silt content	65% to 85%
7	Water content	17% to 37%
8	Co-efficient of consolidation	.14 to .34
9	Soil classification under unified classification system	CL and CH

**Table A1.2 Geotechnical parameter of Dhaka Clay (Ameen, 1985)**

Sl. No	Parameter	Value
1	Isotropic compression index[ $C_c$ (iso)]	.27
2	Isotropic swelling index	.04- .01
3	$K_o$ compression index [ $C_c$ ( $K_o$ )]	.27
4	$K_o$ swelling index	.02- .005
5	$K_o$ value at normally loaded state	.46
6	$K_o$ value at preloaded state(OCR=1.2 to 12)	.512 to 3.23
7	$S (S_u / \sigma_v')$ for $K_o$ consolidated soil	.19
8	$S (S_u / \sigma_v')$ for isotropically consolidated soil	.30

**Table A1.3 Effect of Cement Treatment on engineering properties of the Clay (Uddin, 2004)**

Properties	General Effect in comparison to the Untreated Clay	Effect of increasing Cement Content	Effect of increasing Curing Time
Specific gravity	Decrease significantly	Reduces significantly in the case of higher cement content	Generally, decrease with time but remain almost constant at 2.61-2.62 after 8-12 weeks time
Water content	Immediate decrease in water content by about 5% to 10%	Reduces significantly with higher cement content	Reduces substantially at longer curing time
Plastic limit	Increases	Increases at higher cement content	Increases in the case of longer curing time
Liquid limit	Small reduction	Insignificant change but some samples show little reduction of liquid limit with an increase of cement content	Slight reduction of liquid limit occurs at longer curing time
Plasticity index	Reduces	Reduces in the case of higher cement content	Decreases at longer curing time. Effect of curing time is more than that of cement content
Unit weight	Increases	Increases in the case of higher cement content	Increases at longer curing time
Void ratio	Decreases	Reduces in the case of higher cement content	Reduces in the case of longer curing time
Degree of saturation	Increases	Increases with higher cement content	Increases in the case of longer curing time

**Table A1.4 Index and shrinkage properties of Cement-treated Dhaka Clay (Hasan, 2002)**

Index and shrinkage Properties	Cement content (%)				
	0	1	3	5	7
Liquid limit	52	51	48	46.5	45.5
Plastic limit	23	25	30	31.5	32
Plasticity index	29	26	18	15	13.5
Shrinkage limit	22	21.5	20	19	18

**Table A1.5 Index and shrinkage properties of Lime-treated Dhaka Clay (Hasan, 2002)**

Index and shrinkage Properties	Cement content (%)				
	0	1	3	5	7
Liquid limit	52	50.5	49	48	46.5
Plastic limit	23	23.5	24	25	25.5
Plasticity index	29	27.5	25	23	22.5
Shrinkage limit	14	15	15.5	16	17

**Table A1.6 Unconfined compressive strength test result of untreated and cement treated Dhaka Clay (Hasan, 2002)**

Cement content (%)	Curing Age (Days)	Q <sub>u</sub> (kPa)
0	-	380
1	7	482
	14	653
	28	1020
3	7	946
	14	1636
	28	2464
5	7	2188
	14	2551
	28	3075
7	7	2671
	14	2892
	28	3588

**Table A1.7 Unconfined compressive strength test result of untreated and lime treated Dhaka Clay (Hasan, 2002)**

Lime content (%)	Curing Age (Days)	Q <sub>u</sub> (kPa)
0	-	380
1	7	470
	14	775
	28	984
3	7	1020
	14	1381
	28	2015
5	7	1877
	14	2192
	28	2385
7	7	2173
	14	2304
	28	2678

## APPENDIX II

INDEX PROPERTIES AND DIFFERENT PARAMETRS OF  
UNCEMENTED AND CEMENTED SAVAR CLAY



Table A2.1 Index properties and classification of uncemented remolded Savar area clay.

Specific Gravity Gs	Liquid Limit, LL	Plastic Limit, LL	Plasticity Index, PI	Grain Size Distribution			USCS Symbol
				% Sand	% Silt	% Clay	
2.68	43	17	26	10	62	28	CL

Table A2.2 Index properties of the cemented Savar area clay.

% Of Cement Content	Specific Gravity Gs	Liquid Limit, LL	Plastic Limit, PL	Plasticity Index, PI
7 %	2.64	43	22	21
14 %	2.6	42	24	18

Table A2.3 Unconfined compression strength and elastic modulus of uncemented and 7% and 14% cemented reconstituted Savar clay.

Sample Designation	$q_u$ (KN/m <sup>2</sup> )	$E_i$ (KN/m <sup>2</sup> )
Remolded Savar clay	110	18230
Savar clay with 7 % cement	354	22125
Savar clay with 14 % cement	587	28765

Table A2.4 Unconsolidated Quick Direct Shear test result of uncemented and 7% and 14% cemented reconstituted Savar clay.

Sample Designation	Undrained Shear Stress, (KN/m <sup>2</sup> )	Shear Displacement (mm)
Remolded Savar clay	37	4.4
Savar clay with 7 % cement	186	4.2
Savar clay with 14 % cement	280	4.06

Table A2.5 the critical state parameters from consolidation test of uncemented and 7% and 14% cemented reconstituted Savar clay.

Sample Designation	Parameters	
	$\lambda$	$\kappa$
Remolded Savar clay	.290	.0332
Savar clay with 7 % cement	.197	.1
Savar clay with 14 % cement	.03	.01

## APPENDIX I I I

COMPARISON OF EXPERIMENTAL DATA OF MODEL  
SCALE FOOTING TEST WITH NUMERICAL  
PREDICIONS USING THE MCC AND MOHR-COULOMB  
MODEL ON COASTAL CLAYS OF BANGLADESH

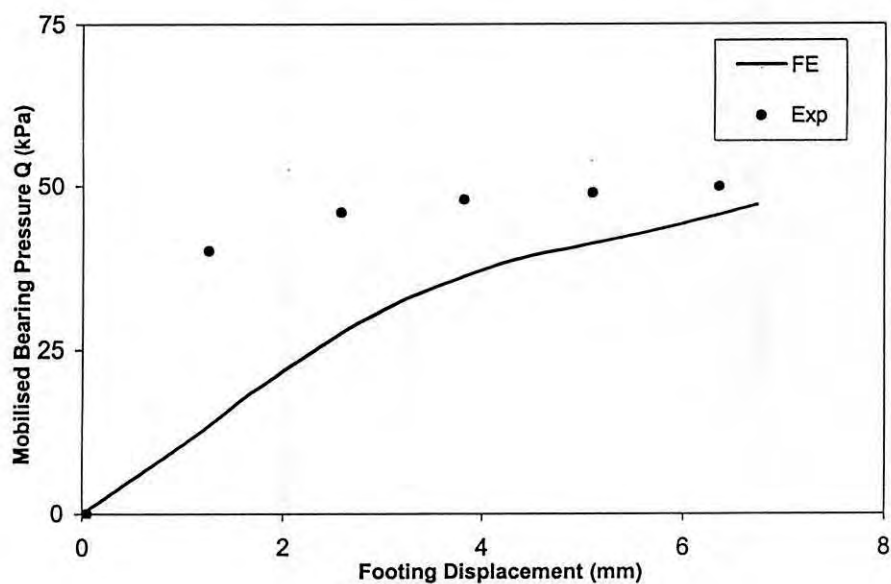


Figure A2.50 Comparison of experimental data of model scale footing test ( $\sigma'_v = 50 \text{ kPa}$ ) with numerical predictions using the Modified Cam Clay model

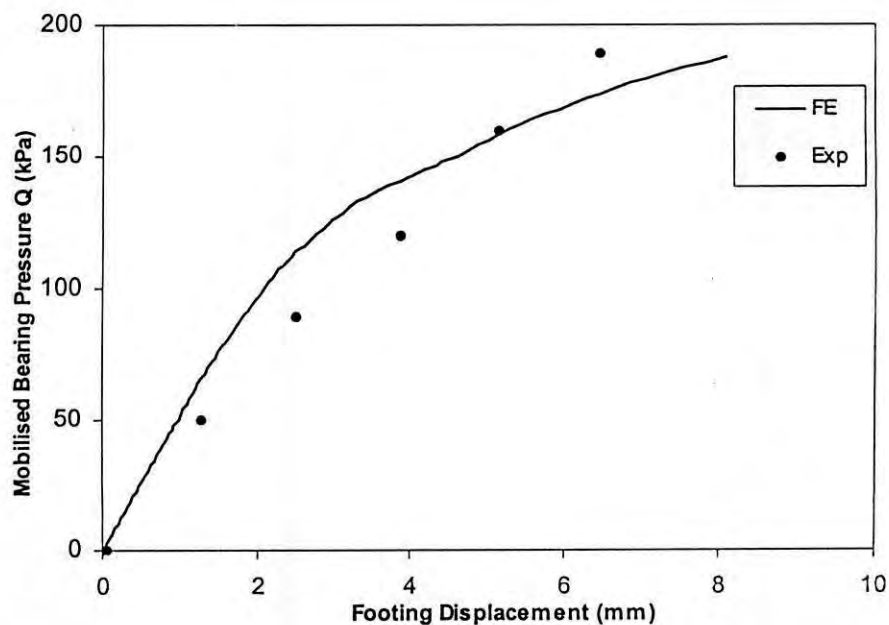


Figure A2.51 Comparison of experimental data of model scale footing test ( $\sigma'_v = 150 \text{ kPa}$ ) with numerical predictions using the Modified Cam Clay model

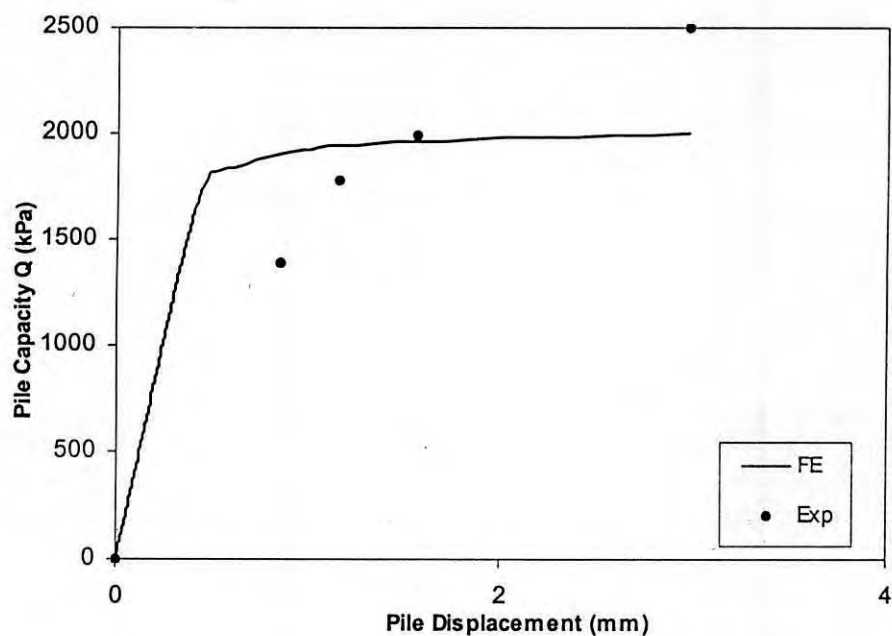


Figure A2.52 Comparison of experimental data of model scale pile test ( $\sigma'_v=150\text{kPa}$ ) with numerical predictions using the Modified Cam Clay model

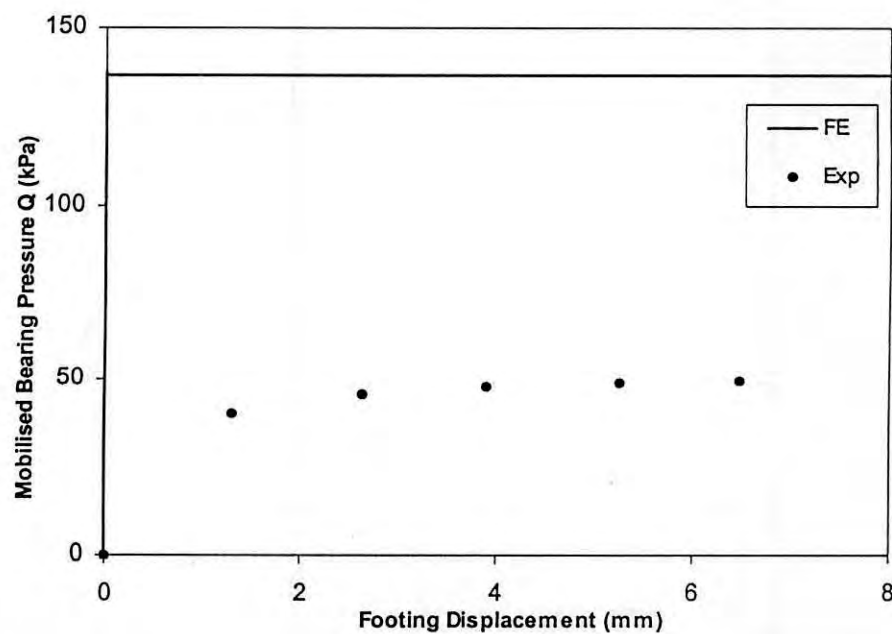


Figure A2.53 Comparison of experimental data of model scale footing test ( $\sigma'_v=50\text{kPa}$ ) with numerical predictions using the Mohr-Coulomb model

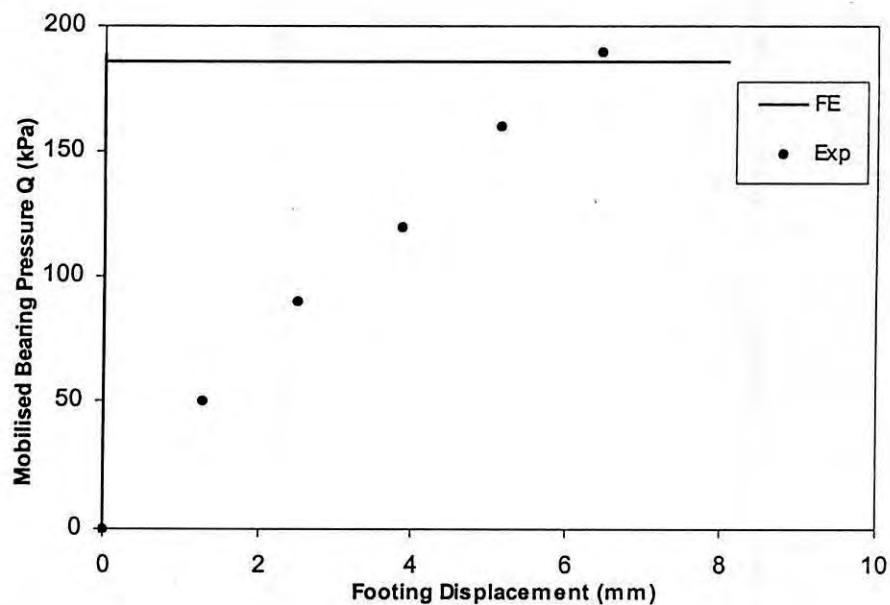


Figure A2.54 Comparison of experimental data of model scale footing test ( $\sigma'_v=150\text{kPa}$ ) with numerical predictions using the Mohr-Coulomb model

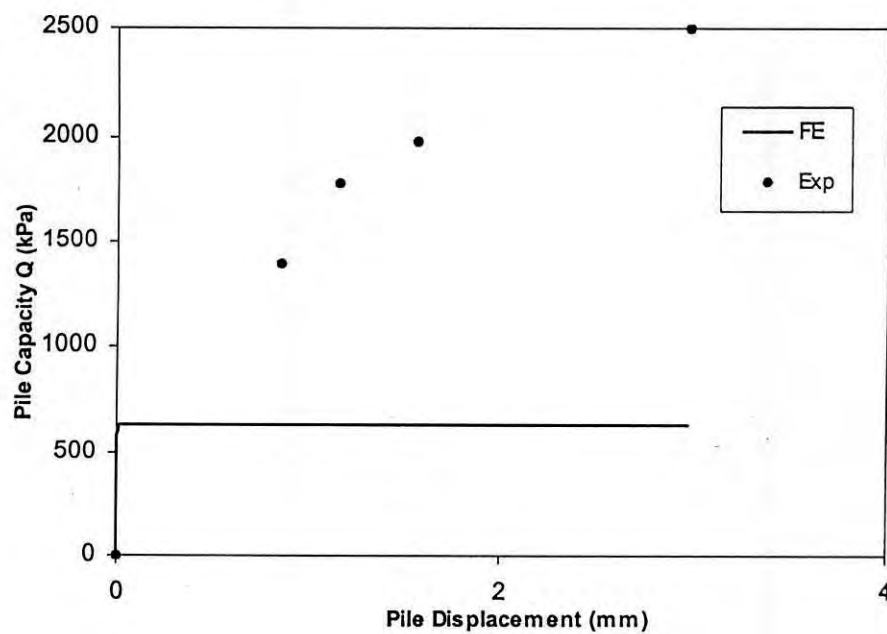


Figure A2.55 Comparison of experimental data of model scale pile test ( $\sigma'_v=150\text{kPa}$ ) with numerical predictions using the Mohr-Coulomb model

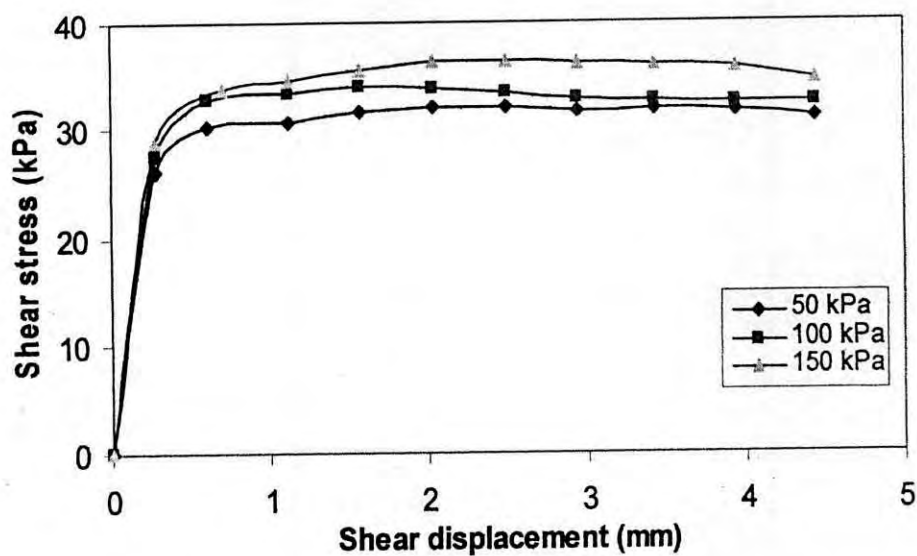


Figure A4.10 Shear stress vs shear displacement curve of uncemented Savar clay

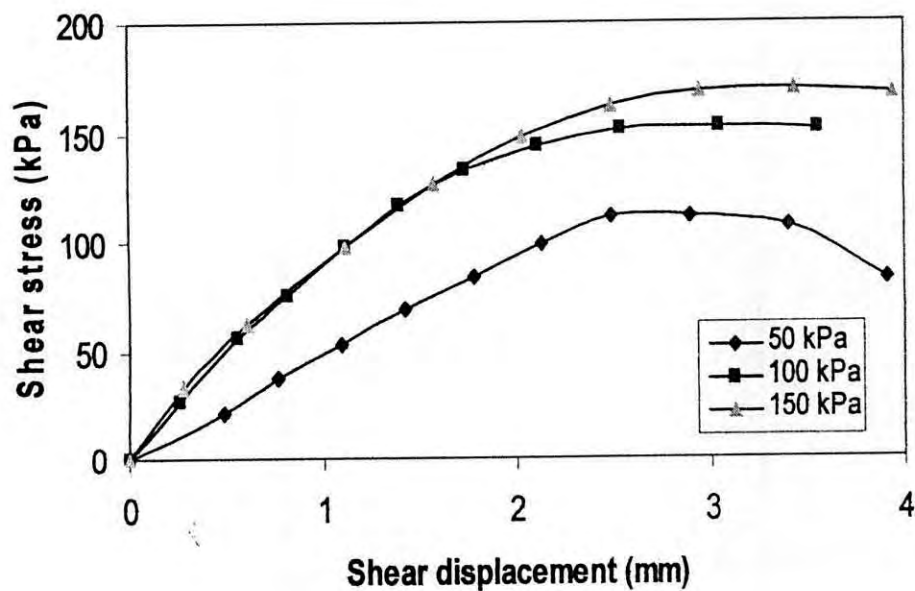


Figure A4.11 Shear stress vs shear displacement curve of 7% cemented Savar clay

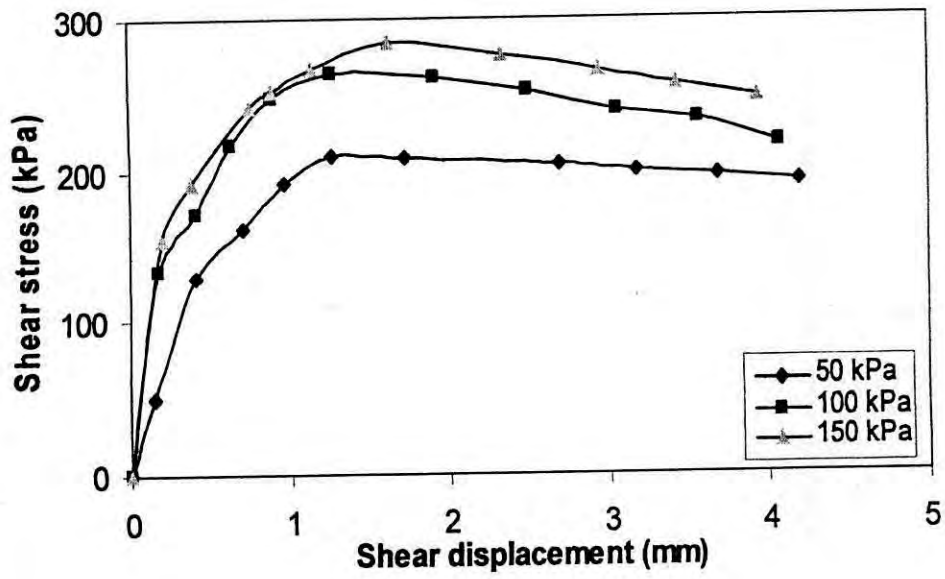


Figure A4.12 Shear stress vs shear displacement curve of 14 % cemented Savar clay

